Stable isotope and whole rock geochemical study of the Cretaceous Koegel Fontein Complex: magma characterisation, evidence for fluid–rock interaction and source constraints for low–δ^{18}O magmas

Catherine Curtis

Dissertation presented for the degree of Master of Science
In the Department of Geological Sciences
University of Cape Town
December 2009

Abstract

The Koegel Fontein Complex is the only known igneous complex associated with rifting between Africa and South America, in northwestern South Africa. The complex consists of syenite and granite plutons and plugs, bostonite, quartz porphyry and mafic dykes. Felsic magmatism at Koegel Fontein occurred in two pulses, one at 144±2Ma and the other at 133.9±1.3Ma. The Mesozoic age of the complex is a recent finding and until 1998 Koegel Fontein was thought to be part of the Proterozoic, Namaqua–Natal metamorphic province and as a result, the complex has remained relatively unstudied.

The syenites, bostonites and Rooivleitjie granite are the oldest rocks at Koegel Fontein. Whole–rock geochemistry and radiogenic isotope data suggest that the three rock types are petrogenetically related. The Rietpoort granite, volumetrically, the main intrusive phase, is associated with a swarm of quartz porphyry dykes which, due to field relations predate the granite. Zircon ages for the Rietpoort granite and quartz porphyry dykes are indistinguishable. Whole–rock geochemistry for the two rock types is also very similar and it is plausible that the quartz porphyries and Rietpoort granite are either petrogenetically related or have a very similar source. The Sr– and Nd–isotope data for the Rietpoort granite suggest that it formed from melting of the crust.

Stable isotope analysis of whole–rock powders, phenocrysts and mineral separates reveal a complex history of high–temperature, fluid–rock interaction. Feldspar is prone to isotopic exchange, often without major or trace element changes or physical affects. Whereas, quartz is relatively inert and preserves its original magmatic signiture (O'Neil and Tayler, 1967). Samples with "normal" δ^{18}O values (>5.7‰) for quartz separates and Low δ^{18}O values for feldspar separates have been hydrothermally altered. Low δ^{18}O values (<5.7) for phenocryst quartz and quartz separates indicate that a rock has crystallized from low–δ^{18}O magmas and is not the result of high–temperature alteration. Quartz and feldspar mineral separates from Koegel Fontein have δ^{18}O values ranging from 0.5 to 9.4‰ and -2.6 to 8.3‰, respectively. Several quartz porphyry dykes, restricted to the centre of the Koegel Fontein complex, have

low–δ^{18}O quartz and quartz phenocrysts and, therefore, crystallized from low–δ^{18}O magmas.

Magmatic δ^{18}O values for the low–δ^{18}O quartz porphyries ranges from -0.5 to 3.5‰. The Rietpoort granite has an average magmatic δ^{18}O value of 6.3±0.5‰. The average δ^{18}O value of the "normal" quartz porphyries (δ^{18}O > +6‰) is 7.7±0.6‰. This suggests that the δ^{18}O value of the Rietpoort granite has been lowered by 1.4‰. The low–δ^{18}O quartz porphyries have an average δ^{18}O value of 1.3±1.2‰.

The δ^{18}O of the hydrothermal fluid was calculated to be -9.9‰ using hydrogen– and oxygen–isotope data from whole–rock powders, mineral separates and quartz veins. This suggests a meteoric source for the hydrothermal fluid. Calculated water/rock (W/R) ratios vary from 0.02 to 1.39, assuming a closed system. When the Koegel Fontein Complex was emplaced, it was relatively close to the ocean, at low altitude and latitude, with a hot and dry climate. Therefore, meteoric water with δ^{18}O values as low as -9.9‰ is unlikely, at the time of emplacement of the complex.

Samples with the lowest δ^{18}O values are restricted to the centre of the Koegel Fontein Complex or along to the coast. These samples tend to be associated with large scale shear zones. The largest of which is in the centre of the complex and coincides with the location of the lowest recorded δ^{18}O value and the low–δ^{18}O magmas.

Assimilation models for O– and Sr–isotopes indicate that assimilation is an unlikely mechanism for producing the low–δ^{18}O magmas. Assimilation can explain the range of isotope ratios recorded for each element, however, when combined the two models contradict one another. Oxygen–isotope assimilation models suggest that the low–δ^{18}O quartz porphyries require the greatest amount of assimilation whereas Sr–isotope assimilation models indicate that the Rietpoort granite requires the largest amount of assimilation.

Trace elements and Pb–isotopes suggest that the source region of the Koegel Fontein Complex was heterogeneous. It is suggested in this study that the low–δ^{18}O magmas are the result of a small amount of partial melting and as such, reflect small scale heterogeneaties in the crust. These heterogeneities where later homogenised by large scale melting which resulted in the emplacement of the Rietpoort granite.

Unpublished oxygen–isotope data indicates that there are areas of hydrothermally altered rocks within the Namaqua Metamorphic Province. This coupled with the low δ^{18}O value calculated for the hydrothermal fluid, trace element and isotope data and the close proximity of the quartz porphyries to large, crustal scale structures suggests that the country rock was altered prior to the emplacement of the Koegel Fontein Complex. It is proposed that altered

Namaqua crust is the protolith for the low–δ^{18}O magmas and that this alteration occurred prior to the emplacement of the Koegel Fontein Complex.

Plagiarism declaration

I know the meaning of plagiarism and declare that all of the work in the document, save for that which is properly acknowledged, is my own.

Contents

List of Figures

List of Tables

Chapter 1

Introduction

The Koegel Fontein Complex, (30° 59'05.5"S; 17° 59'11.24"E) is the only known early Cretaceous igneous complex on the west coast of South Africa (Figure 1.1). Situated 240 km south of the Orange River it intrudes Namaquan metasedimentary rocks and gneisses. The complex has been dated at 133 and 146 Ma (de Beer and Armstrong, 1998; de Beer *et al.*, 2002). Koegel Fontein is, therefore, presumed to have formed during the separation of Africa and South America. It occurs in an area where little igneous activity, related to rifting is preserved onshore and may, therefore, add to our understanding of the relationship between rifting and magmatism during the break-up of Western Gondwana.

1.1 Regional geological setting

Three main events have affected the study area since the mid Proterozoic, 1) the Namaqua–Natal metamorphic event, 2) the Pan African tectono–thermal event and 3) the break-up of Western Gondwana.

Namaqua - Natal metamorphic province

The regional country rock is the Namaqua-Natal Metamorphic Province, 1600–1000Ma, (Figure 1.2) which includes deformation and metamorphism. The Namaqua sector covers 100 000km^2 on the west coast of Southern Africa and can be divided into five domains, the Richtesveld Subprovince, the Bushmanland Terrane, the Kakamas Terrane, the Areachap Terrane and the Kaaien Terrane. The area underwent rifting between 1600 to 1300 million years ago

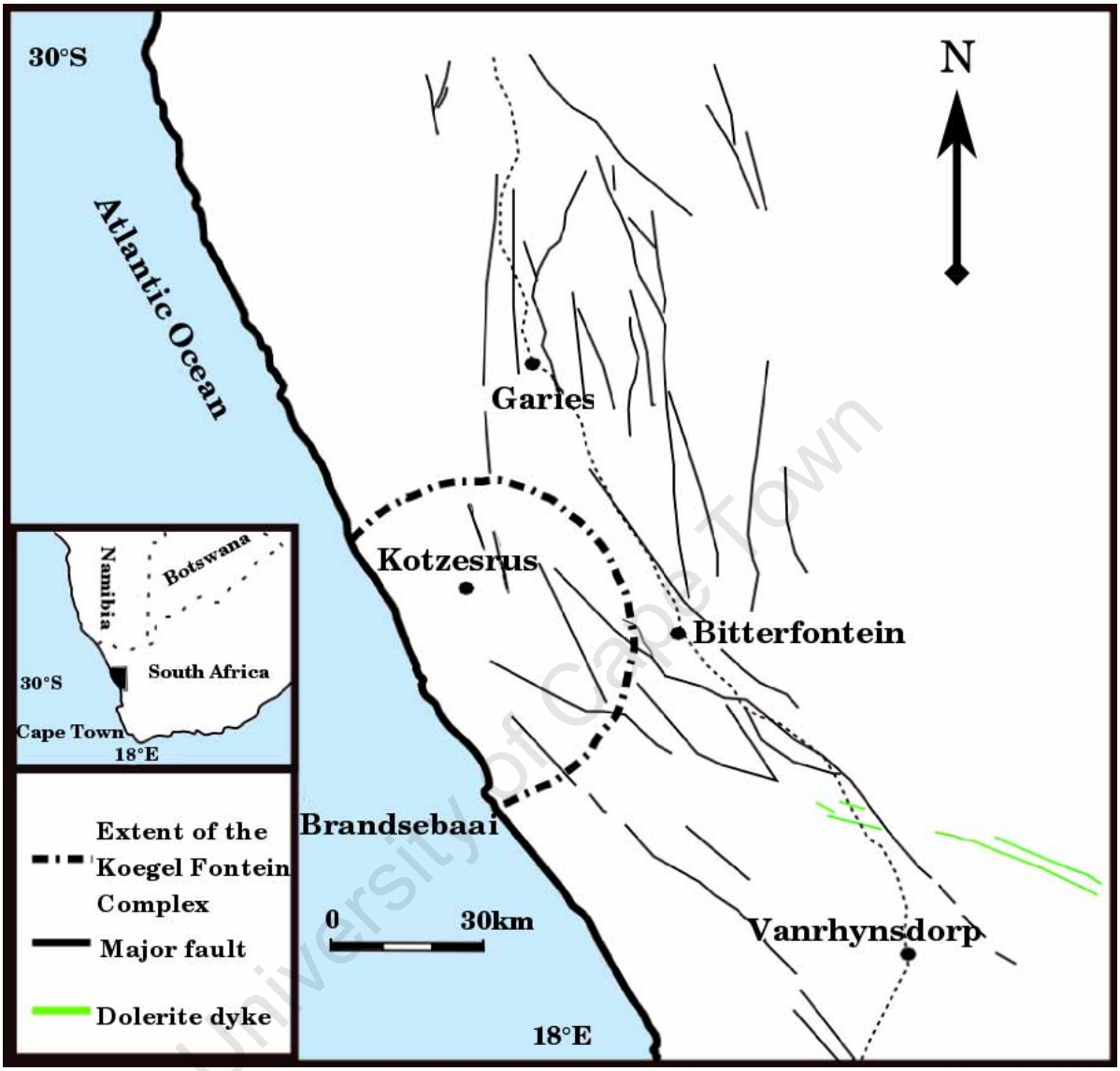

Figure 1.1: Location of the Koegel Fontein Complex. Insert map showing the regional location. Modified from de Beer and Armstrong (1998).

with the formation of the Areachap and Tugela Oceans. Subduction began at 1300 million years along with arc magmatism (1300-1200Ma). The main Namaqua orogenic event (1220-1150Ma) occurred when a crustal block, composed of the Richtesveld Subprovince and rocks from the Bushmanland Terrane, collided with the Kaapvaal–Kheis crustal block during the formation of Rodinia. Finally an oblique strike–slip system developed at 1080 million years along with the emplacement of large volumes of A–type granitoids (Cornell *et al.*, 2006).

The Koegel Fontein Complex intruded the Bushmanland Terrane which is bounded by the Groothoek and Hartbees thrusts and the Wortel Belt. The Terrane is comprised of 2050–

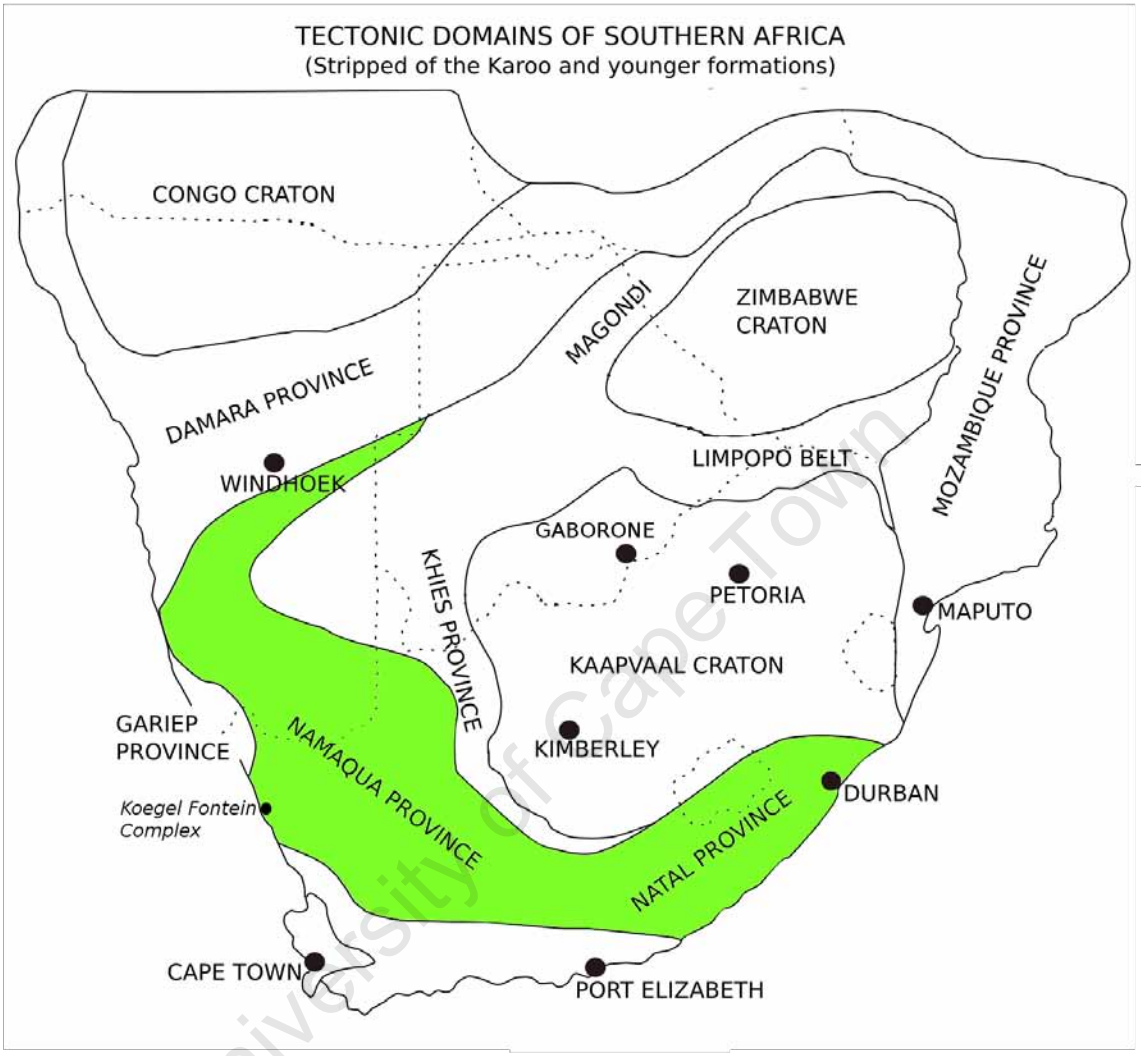

Figure 1.2: Location of the Namaqua–Natal Belt shown in green. After de Beer and Meyer (1984).

1700Ma granitic gneisses, 1600–1200Ma supracrustal rocks metamorphosed to amphibolite and granulite facies and 1200–1000Ma granitoids. The Terrane is thought to be underplated by a 25km thick package of mantle derived rocks (Cornell *et al.*, 2006).

Pan African tectono –thermal event

In 1964 Kennedy described a major tectono–thermal event that occurred around 500Ma in mobile belts throughout Africa which he called the Pan African (Porada, 1989). It is now recognised that Pan African Orogenesis includes a series of Neoproterozoic belts extending

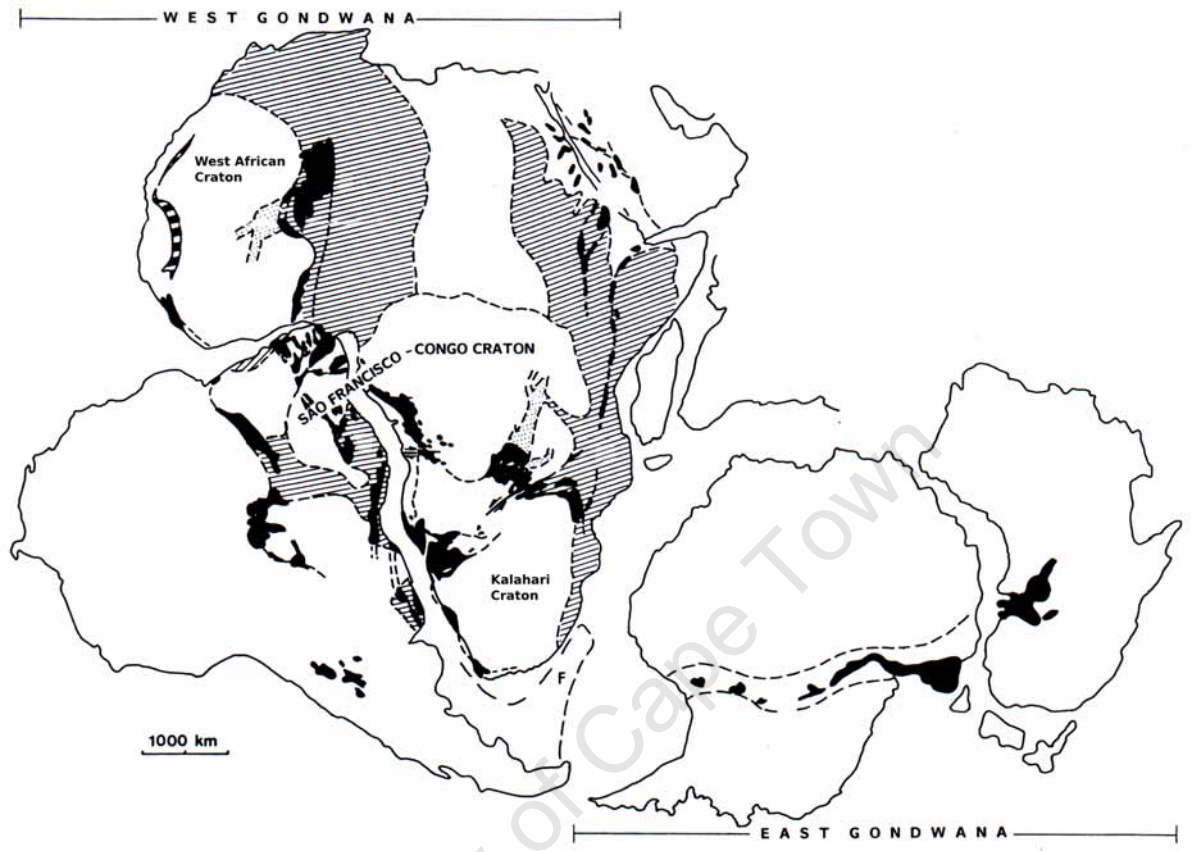

Figure 1.3: Location of the Pan African tectono–thermal event. The black represents juvenile material added during the Pan African while the hatched areas show reworked older crust. From Porada (1989).

into South America, Australia and Antarctica, (Figure 1.3). These mobile belts form sutures between cratons and East and West Gondwana (Porada, 1989; Gresse *et al.*, 2006).

Remnants of the Gariep Belt can be found north of Brandsebaai at the Koegel Fontein Complex. The formation of the Gariep Belt began with the break up of Rodinia and the formation of the Adamastor Ocean at 770Ma (Gresse *et al.*, 2006). The sediments deposited in the Gariep Basin indicate that it evolved from initial rifting (immature terrigenous sediments) to continental drift (marine sediments and ophiolites) before subduction closed the Adamastor Ocean (Porada, 1989; Gresse *et al.*, 2006). Deformation in the Gariep Belt is characterised by crustal scale thrusting to the south east of supracrustal cover sequences and basement gneisses (Porada, 1989; Gresse *et al.*, 2006).

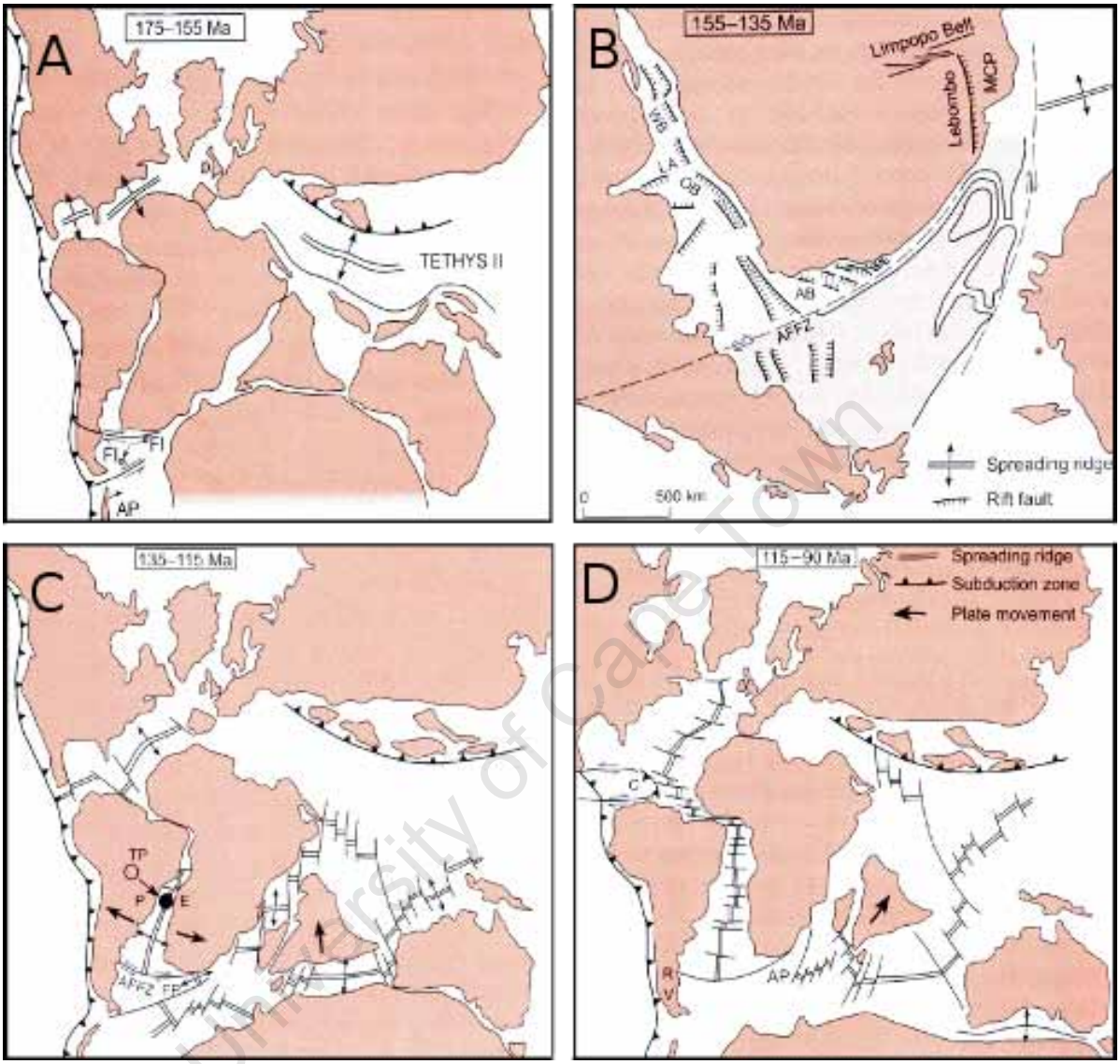

Figure 1.4: Break up of Western Gondwana, after Watkeys (2006). A. Western Gondwana pre-rifting. B. Stage 3. C. Stage 4 showing the configuration of the continents at the time of magmatism at Koegel Fontein and the appearance of the Tristan Plume. D. Stage 5 and the complete fragmentation of Gondwana. AB–Agulhas Bank, AFFZ–Agulhas Falklands Fracture Zone, AP–Agulhas Plateau, C–Caribbean, E–Etendeka, FI–Falklands Islands, FP–Falklands Plateau, GFS–Gastre Fault System, KF–Koegel Fontein Complex, LA–Luderitz Arch, MCP–Mozambique Coastal Plain, OB–Orange River Basin, P–Paraná, RV–Rocas Verdes, TP–Tristan Plume, WB–Walvis Basin.

Break-up of Western Gondwana

The break up of West Gondwana is the most significant event with regards to the Koegel Fontein Complex and occurred between 180–90Ma when the southern supercontinent of Gond-

wana fragmented, (Figure 1.4). Watkeys (2006) divides this fragmentation into five stages starting with incipient rifting in Eastern Gondwana and ending with the final separation of Africa from South America as well as Antarctica from Australia, (Figure 1.4D). Initial rifting and magmatism of Western Gondwana falls into stages three and four, at 155–135Ma and 135–115Ma respectively. During this time the Koegel Fontein Complex was emplaced (146-133Ma, Figure 1.4C).

During stage three, (155–135Ma, Figure 1.4B), movement along the Gastre Fault System and the Agulhas-Faulkland fracture zone may have caused fractures to propagate northwards along pre–existing faults formed during the Namaqua and Pan African orogenic events. Actual rifting did not occur until stage four, (135–115Ma, Figure 1.4C), when the orientation of the plates changed and the Tristan Plume intersected weakened, thinned crust causing the separation of Africa from South America.

1.1.1 Geology of the Koegel Fontein area

The Koegel Fontein Complex is about 35km in diameter and consists of a variety of rock types ranging from quartz syenite to granite, (Figure 1.5). Earlier accounts of the local geology were published in Rogers (1911) and Jansen (1960). The latter produced a detailed map that distinguished the Koegel Fontein Complex from the surrounding gneisses and schists based on its lack of deformation. Joubert (1971) and Jack (1980) confirmed the lack of fabric in the northern extension of the complex. However, Jansen associated Koegel Fontein with the Richtesveld Igneous Complex and ages of 1075Ma and 910Ma for the granitoids obtained by Burger and Coetzee suggested that the correlation was correct, (de Beer and Armstrong, 1998). Although, a post Namaqua age was accepted by earlier workers, it was only after the follow up by McIver (1981) and de Beer and Armstrong (1998) which showed the Jurassic–Cretaceous age of the complex. de Beer and Armstrong (1998) obtained ages of 144±2Ma for the syenite and 133.9±1.3Ma for the granite and associated quartz porphyry dykes.

Little geochemistry on the Koegel Fontein Complex has been published. Initial geochemical analyses was done by the Council for Geoscience when the complex was mapped by de Beer, (between 1992 and 1998) and the mafic and ultramafic rocks were studied by McIver (1981). The dolerite dyke suite along the south west Atlantic coast was analysed by Trumbull *et al.* (2007) as part of a regional study, however, the dolerite dykes at Koegel Fontein were not addressed in detail. There has been almost no geochemistry and radiogenic isotope analysis done on the felsic intrusions and no stable isotope analysis has been done on the Koegel

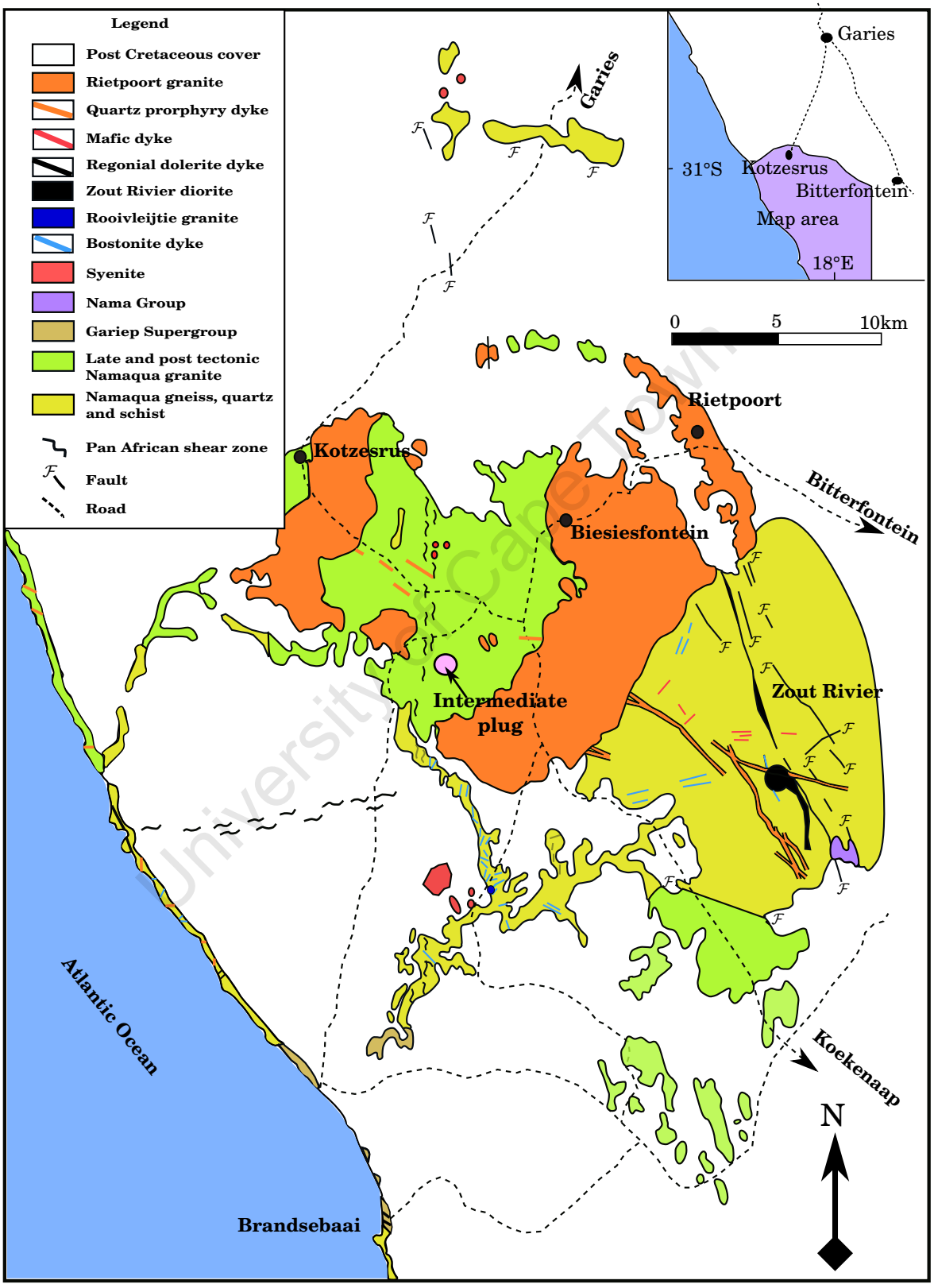

Figure 1.5: Geology of the Koegel Fontein complex, modified from de Beer and Armstrong (1998).

Fontein Complex.

Koegel Fontein was part of a regional aerial magnetic survey. This revealed a magnetic anomaly at the complex. The anomaly resembled magnetic anomalies found at the Messum and Cape Cross Complexes in northern Namibia (Bauer *et al.*, 2003). Messum is thought to represent a differentiated magma chamber as a seismic profile shows a steep velocity anomaly beneath the complex. This is probably due to the presence of a mafic body underlying the granitic rocks at Messum (Bauer *et al.*, 2003). Due to a lack of seismic and gravity data for Koegel Fontein, further geophysical interpretation is not possible. Thus, whether a mafic igneous body underlies the complex is unknown.

Koegel Fontein has proved to be of great interest due to its age, composition, locality and size. These previous studies have shown the complex to have a great diversity of rock types and has a wide compositional range of silica undersaturated and silica oversaturated rocks. This study aims to add to the existing body of information and increase the understanding of processes occurring in the area.

1.1.2 Objectives

There are three objectives for this project, 1) to determine the isotopic composition of the Koegel Fontein Complex 2) to determine crustal and mantle sources involved in magma genesis and determine magma evolution via fractional crystallization and/or assimilation at the Koegel Fontein Complex and 3) to explain the origin of unusually low δ^{18}O and δD values found at the complex. Of specific interest at Koegel Fontein are the following:

1. Stable isotopes can be used to aid whole rock geochemical analysis in understanding the petrogenesis of igneous rocks. Small changes in isotope ratios occur during differentiation processes such as fractional crystallization. These can be used to identify relationships between different rock units or whether material geochemically similar to the magma, has been assimilated, provided the δ^{18}O values are different. Stable isotopes are also a very good indicator of post crystallization alteration. Fluids consisting predominantly of water moving through the rock may not alter the whole rock geochemistry of the rock. Hydrogen is particularly sensitive to this as there is very little hydrogen in rocks and only a small amount of water is required to alter δD (Criss and Taylor Jr., 1986).

2. The southwestern margin of Africa was a volcanic rifted margin during the break–up

of Gondwana. High volumes of magmatic activity, suggested to be plume related, occurred in the north, whereas, low volumes of magmatic activity occurred in the south (Trumbull *et al.*, 2007). The Koegel Fontein Complex is the only known Cretaceous rift–related complex in the southern region of the margin. Ring complexes, associated with the break–up of Western Gondwana, in Northern Namibia are of particular interest as they are anorogenic complexes and therefore, their felsic material should have the same δ^{18}O values as Koegel Fontein. These complexes do not have similar δ^{18}O values to Koegel Fontein and in many instances their δ^{18}O values are higher than expected (Harris, 1995; Trumbull *et al.*, 2004). Due to the age overlap between the Namibian complexes and Koegel Fontein they would have expierence similar climatic conditions and interacted with meteoric water with a similar isotopic composition. Koegel Fontein and the Namibian complexes can, therefore, be used for comparison between processes occurring in the different regions along the margin. The results can then be integrated with the regional studies of magmatic features along the western margin by the Ikaba Ye Africa team (e.g. Trumbull *et al.*, 2007).

3. There is extensive petrographic evidence for alteration of the rocks of the Koegel Fontein Complex, especially in the degree of turbid alteration in feldspar. Initial oxygen isotope results showed that the complex has unusually low O–isotope ratios for igneous rocks and indicate fluid rock interaction at high temperatures. Low δ^{18}O igneous rocks are usually defined as having δ^{18}O values less than that of the mantle (δ^{18}O +5.7 ‰). They are found where rocks have interacted with water at high temperatures, (Taylor, 1977, 1978). Rocks that crystallize from low δ^{18}O magmas form when this previously hydrothermally altered material is assimilated by the magma or remelted. Low δ^{18}O magmas, like unaltered igneous rocks, have a consistent difference between mineral–pair δ^{18}O values indicating equilibrium at magmatic temperatures. Hydrothermally altered rocks show great variation in δ^{18}O values between minerals due to disequillibrium (Criss and Taylor Jr., 1986; Sharp, 2006). The main objective of this thesis is to explain these stable isotope irregularities using O–,H–,Sr–, Nd– and Pb–isotope ratios.

Chapter 2

South Atlantic Magmatism

In the early Cretaceous the South Atlantic was a volcanic rift zone. Magmatism along the coast consists of the Paraná–Etendeka large igneous province (LIP), dykes, plutonic Cretaceous ring complexes and off–shore volcanic rocks. Offshore magmatism associated with rifting includes the Walvis Ridge and Rio Grande Rise. The majority of the magmatism is found in the Paraná and Etendeka basins in eastern Brazil and northern Namibia respectively. Magmatism decreases south of the Paraná–Etendeka and occurs mainly as dolerite dykes. Seaward dipping reflectors, interpreted to have been subaerial volcanics, stretch the entire length of the West Coast and remain the same thickness indicating similar volumes of magmatism along the actual rift. However, plume activity in the north caused the generation of much higher volumes of magma which spread beyond the rift boundaries (Trumbull *et al.*, 2007). The Koegel Fontein Complex is the only known ring complex south of the Orange River.

2.1 Paraná - Etendeka large igneous province.

The Paraná–Etendeka LIP, (Figure 2.1), covers 170 000km^2 with an estimated volume of >800 000km^3 of erupted material, about 10% of which is found in northern Namibia, (Ewart *et al.*, 1998a,b). Volcanism occurred between 138 and 128Ma with the main extrusive event at about 133Ma, (Ewart *et al.*, 1998a; Trumbull *et al.*, 2007) The province consists of basalt, latite and quartz latite or rhyodacite. The Paraná–Etendeka is associated with the Walvis Ridge–Rio Grande Rise, the hot spot track for the Tristan Plume which is thought to have initiated magmatism, (O'Connor and le Roex, 1992; Trumbull *et al.*, 2007). The rocks in the Paraná and Etendeka basins are geochemically and petrographically very similar to each other and are

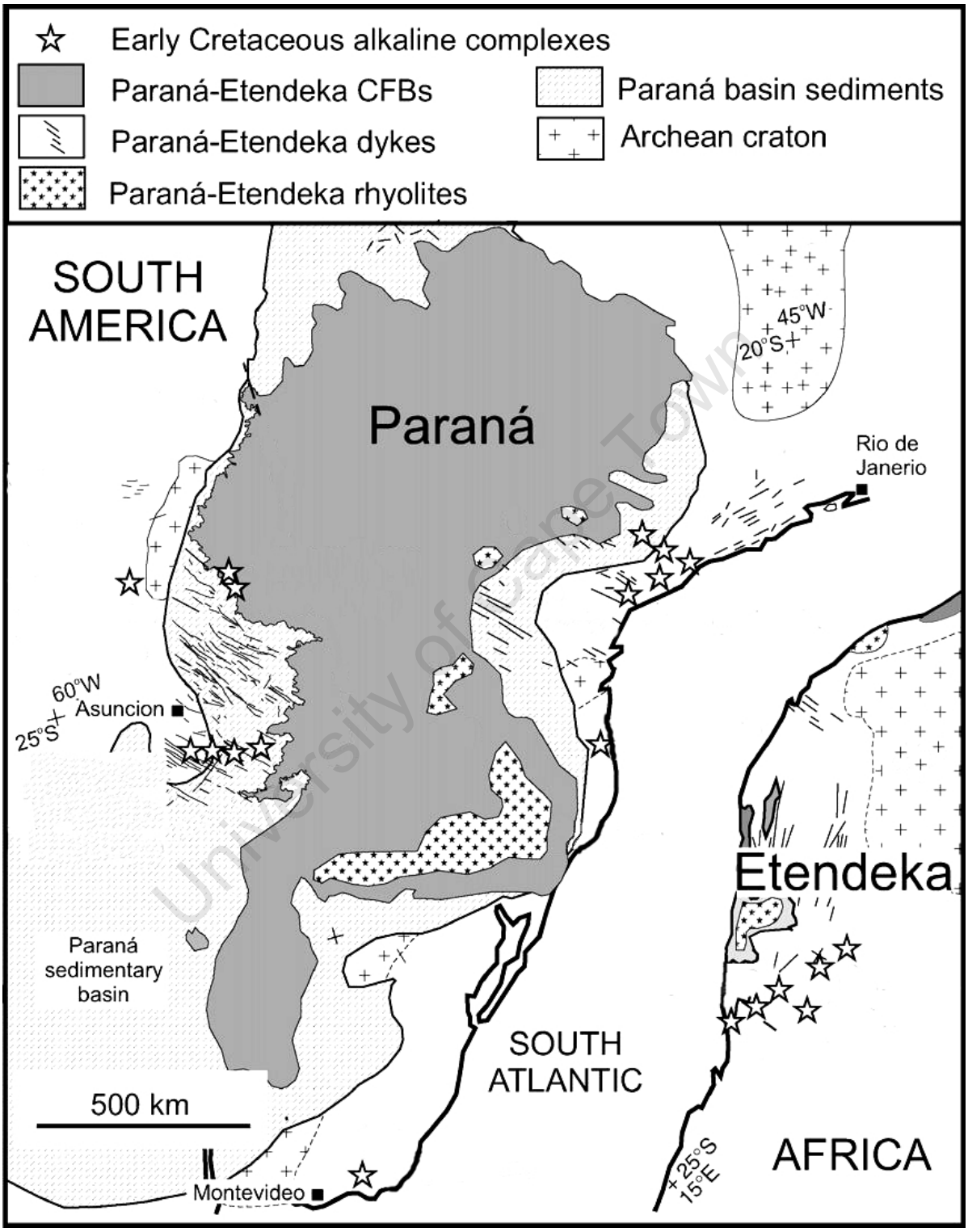

Figure 2.1: Location of the Paranà–Etendeka large igneous province after Gibson *et al.* (2006). Distribution of the volcanics and plate reconstruction at 128Ma prior to continental break–up

considered to have erupted form the same source shortly before the break–up of Gondwana, (Erlank *et al.*, 1984; Harris *et al.*, 1990; Ewart *et al.*, 1998a,b).

The province has two geochemically distinct regions characterised by a low Ti Zr (LTZ) signature in the south and a high Ti Zr (HTZ) signature in the north. These characteristics are seen in both the mafic and felsic volcanic rocks in the province, however, there is no petrogenetic link between the two geochemical groups. Erlank *et al.* (1984); Harris *et al.* (1990); Ewart *et al.* (1998b), attributed the LTZ and HTZ signatures to different crustal sources (felsic rocks) and/or contaminants (mafic rocks) as the southern Etendeka is underlain by rocks from the Proterozoic Damara Belt and the north is underlain by the Archean Congo Craton, (also see Trumbull *et al.* 2004). The Tristan Plume is postulated to be the heat source for melting in the Paraná–Etendeka, although, few rocks in the Etendeka group are consistent with a mantle plume source. The lowermost basalts, the Tafelkop basalts, at the Messum Complex, the alkaline gabbros at the Okenyenya Complex and samples from the Walvis Ridge have a similar geochemical signature to the that of the modern day Tristan Plume, (Milner and le Roex, 1996; Ewart *et al.*, 1998a). The lack of a plume signature in the majority of rocks is attributed to varying amounts of crustal contamination (LTZ), however, contributions from the subcontinental lithospheric mantle (HTZ and LTZ) have been suggested. Although, the latter is still under contention, (Erlank *et al.*, 1984; Harris *et al.*, 1990; Milner and le Roex, 1996; Ewart *et al.*, 1998a,b; Thompson *et al.*, 2001; Peate, 1997).

The Paraná–Etendeka volcanic rocks have no obvious eruptive centre despite there being about 20 subvolcanic ring complexes and numerous dykes associated with the province, (Trumbull *et al.*, 2004). Only one complex, Messum, has been geochemically correlated with any of the felsic units, (Erlank *et al.*, 1984; Ewart *et al.*, 1998a). However, Bauer *et al.* (2003), show that the intrusive structures beneath Messum are not large enough to have erupted all >8600km3 of the felsic material previously attributed to it.

2.2 Damaraland Complexes

There are numerous ring complexes associated with the break–up of Western Gondwana, the majority of which are found in northern Namibia. These are the Damaraland Complexes. They range in age from 125 to 140Ma (Harris, 1995) and are contemporaneous with the Etendeka Group volcanics. The Damaraland Complexes follow a near linear trend from the Cape Cross Complex on the coast (SW) to Okorusu about 350km inland (NE), (Figure 2.2). The complexes range in area from a few km^2 to tens of km^2 (Martin *et al.*, 1960).

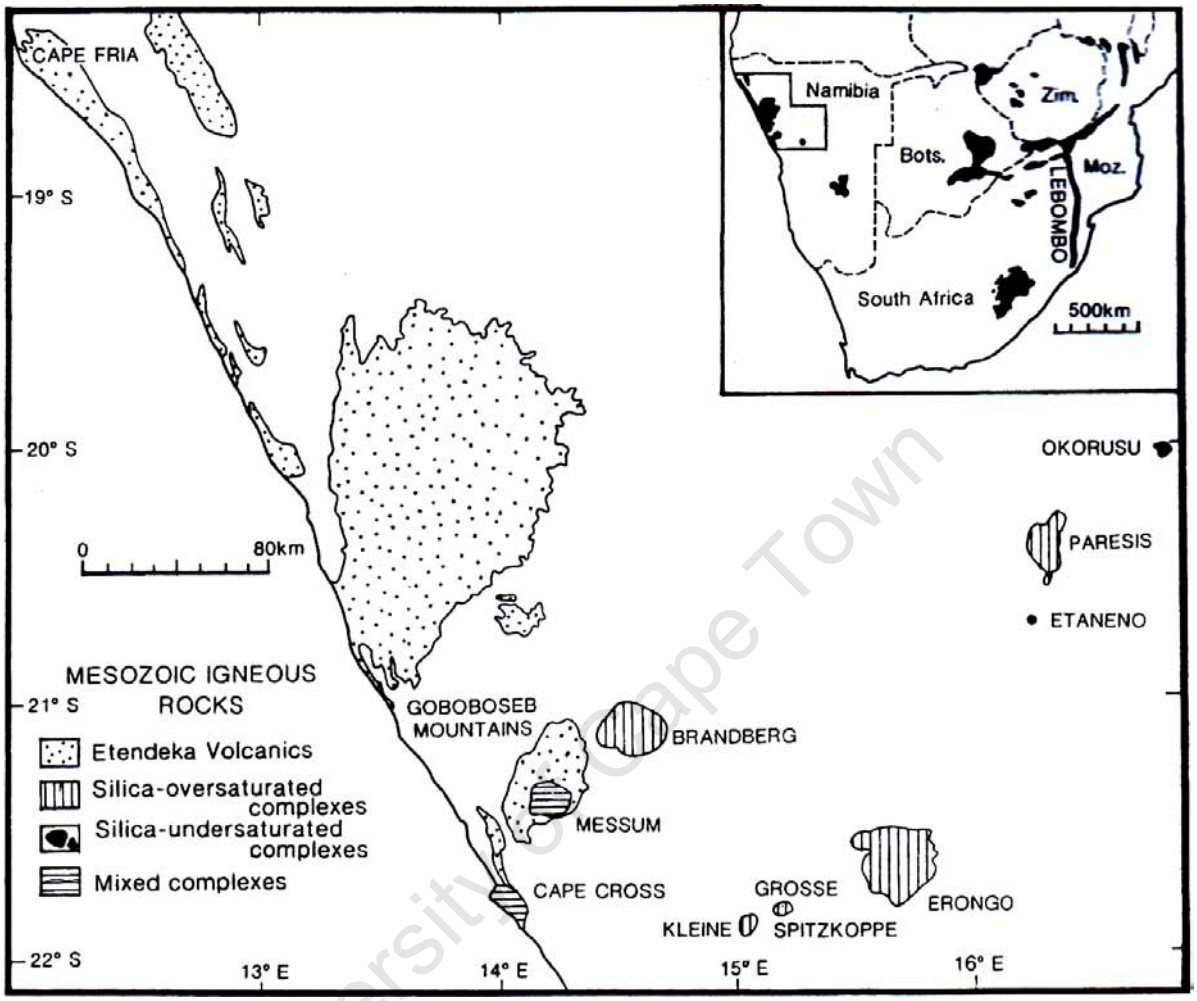

Figure 2.2: Present day location of the Damaraland ring complexes From Harris (1995).

The complexes consist of a wide range of different rock types ranging from alkaline and tholeiitic gabbro to carbonatite to granite and many complexes are comprised of two or more rock types. Martin *et al.* (1960) divided the plutons into three groups, those consisting of mostly granite, differentiated basic complexes and peralkaline and carbonatite complexes. Excluding the carbonatite complexes there are 7 major intrusive complexes; Brandberg, Cape Cross, Erongo, Messum, Okenyenya, Paresis and Spitzkoppe(le Roex *et al.*, 1996). These have been the subject of various geochemical and isotope studies by numerous authors (e.g. Martin *et al.*, 1960; Milner *et al.*, 1993; Watkins *et al.*, 1994; Harris, 1995; le Roex *et al.*, 1996). Most authors focus on the differentiated basic complexes, such as Okenyenya and Messum due to the large variety of rock types found at these centres. Brandberg has been studied due to the presence of hydrothermal mineral deposits at Brandberg West (Diehl, 1990; Macey and Harris,

2006). However, the alteration at Bandberg West occured during the Damaran Orogen, before the emplacement of the Brandberg Complex.

Harris (1995); Martinez *et al.* (1996); Trumbull *et al.* (2004) studied the oxygen isotopes of the Damaraland Complexes. None of the complexes show anomalously low oxygen isotope ratios except for Paresis (Harris, 1995). The silica oversaturated rocks in the differentiated basic complexes seem to have either evolved from undersaturated magmas through crustal contamination or formed by partial melting of the crust, (Harris, 1995). Trumbull *et al.* (2004) showed that all the major intrusive complexes have a negative correlation between oxygen isotope ratios and initial Nd isotope ratios. They proposed a mixing line for the silicic complexes with two end members, a mantle source similar in composition to the modern day Tristan Plume with minor amounts of depleted mantle and a crustal component. The crustal component for the majority of silicic complexes was in the lower crust and was similar to that of the Pan African anorogenic Damaran granites while Paresis had a crustal component from the Mesoproterozoic Angola Craton. Large amounts of crustal contamination can be seen at Okenyenya, where assimilation and crystal fractional played a major role in the petrogenesis of the older units, (Martinez *et al.*, 1996).

2.3 West Coast dyke swarms

Evidence of magmatism, in the form of dykes, stretches along the West Coast from the Etendeka in the north to the Cape Peninsula in the south. There are three major areas of intrusion, (Figure 2.3), the Henties Bay–Outjo Dyke swarm (HOD), the Mehlberg dykes and the False Bay dyke swarm, (Trumbull *et al.*, 2007). The majority of these dykes have a coast–parallel trend except the HOD which strikes NE–SW and extends inland for about 400km. Some dykes can be traced for tens of kilometres and range in size from less than a metre to over 20m, (Botha and Hodgson, 1976; de Beer *et al.*, 2002; Trumbull *et al.*, 2007).

The HOD and False Bay dykes are the most intensly studied of the dykes on the West Coast. Trumbull *et al.* (2007), identified, five different magma series in the HOD dykes, low Ti, olivine normative tholeiites, the Tafelberg series, nepheline normative basalts and the olivine normative Horingbaai type tholeiites. The nepheline normative basalts and the olivine normative Horingbaai type tholeiites are only found within the HOD dyke swarm. The False Bay dykes consist only of low Ti tholeiites and the dykes at Koegel Fontein tend to be tholeiitic and alkaline, (de Beer *et al.*, 2002; Trumbull *et al.*, 2007). The False Bay dykes contain less MgO (<8 wt%) than the HOD dykes (16 wt%) analysed, indicating higher melting tempera-

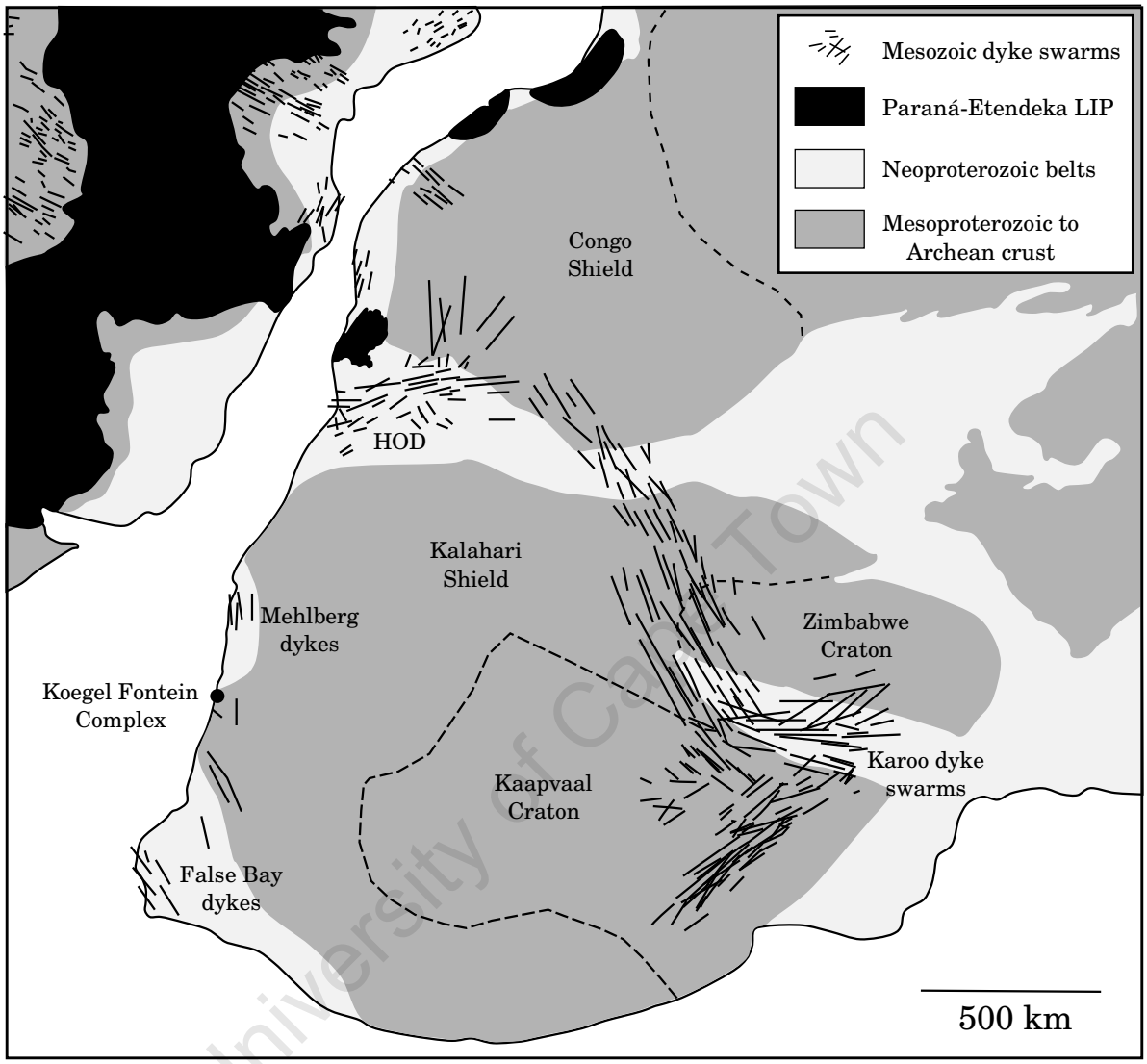

Figure 2.3: Location of West Coast dyke swarms. The Mesozoic (180 to 127Ma) dykes are associated with the break–up of Gondwana. Henties Bay–Outjo Dyke swarm (HOD) map after Trumbull *et al.* (2007). Karoo dyke swarm–180Ma. HOD, Mehlberg, and False Bay dyke swarms–138 to 127Ma

tures in the north, however, there is no direct evidence of plume melt within the HOD which is similar to the Etendeka low-Ti rocks (Trumbull *et al.*, 2004, 2007). The Tafelberg series has a source similar to that of the Etendeka volcanic rocks while the Horingbaai type dykes are more MORB–like (Erlank *et al.*, 1984). The nepheline normative rocks formed by mixing enriched and depleted mantle components.

The False Bay dykes are thought to represent one magma series. The dykes have incompatible trace element ratios and initial Sr– Nd– and Pb–isotope ratios indicative of a lithospheric

mantle or enriched lithospheric and asthenospheric mantle source (Trumbull *et al.*, 2007).

2.4 Geology of Koegel Fontein

The Koegel Fontein Complex has recently been re–mapped and described extensively by de Beer *et al.* (2002). Koegel Fontein is an anorogenic complex about 35km in diameter and consists of a variety of rock types (Figure 1.5). For the purposes of this thesis the Koegel Fontein rocks are divided into plutonic and hyperbyssal intrusions. The plutonic rocks include syenites, the Rooivleitjie granite, the Rietpoort granite and the Zout Rivier plug (diorite). The hyperbyssal rocks are bostonites, quartz porphyries and mafic dykes. The mafic dykes are further divided into a tholeiitic group and an alkaline group. The complex intruded at the intersection of two major faults one trending north–south and the other east–west and all of the igneous rocks in the area around Koegel Fontein, including the complex, have been emplaced along a north–south zone of crustal weakness (de Beer *et al.*, 2002). At the centre of the complex there is a small plug with an intermediate composition which was originally thought to be a 56Ma melilitite. The stratigraphy of the complex is shown in Figure 2.4 and described below.

Emplacement of the Koegel Fontein Complex began during Watkeys (2006) stage 3 of the break–up of Western Gondwana with the intrusion of the 144.4±2Ma syenites, associated Kerskloof bostonite dykes and the Rooivleitjie granite (de Beer *et al.*, 2002). This initial magmatism is older than that seen in the Paraná–Etendeka LIP (128–138Ma). Then a suite of WNW–striking dolerite dykes, the West Coast Dyke Swarm, was emplaced (de Beer *et al.*, 2002). A large regionally extensive dyke contains xenoliths of bostonite and is cut by the Zout Rivier Plug and a quartz porphyry dyke (de Beer personal communication).

After an apparent 10 million year hiatus felsic magmatic activity was renewed with the intrusion of a series of quartz porphyry dykes. The dykes were emplaced in conjunction with the Rietpoort Granite. The granite accounts for the greatest volume of material intruded at Koegel Fontein (de Beer *et al.*, 2002). de Beer and Armstrong (1998) found that the intrusion of the granite and quartz porphyry dykes occurred synchronously within error at 133.9±1.3Ma. The dykes are marginally older than the granite as they abut against the granite (de Beer *et al.*, 2002). Figure 2.5 is a cross section of the Koegel Fontein complex taken from the 1960 map drawn by Jansen. The cross section is of the centre of the complex and shows the relative ages of the Rietpoort granite and the quartz porphyry dykes.

Stratigraphy	Age (Ma)	
Biesjes Fontein Suite	56	
Rietpoort granite	133.9±1.3	Koegel Fontein Complex
Quartz prorphyry dyke	133.9±1.3	
Mafic dykes		
Rooivleijtie granite		
Bostonite dyke		
Syenite	144.4±2	
Regional dolerite dykes		
Jakkelshoek granite	1200-1000	Roof rocks

Figure 2.4: Stratigraphy of the field area. The stratigraphy of the Koegel Fontein complex is based on relative and absolute ages form de Beer *et al.* (2002).

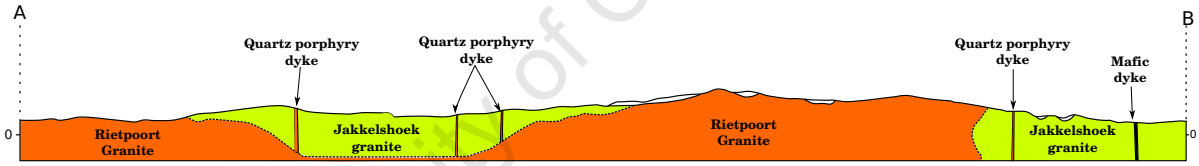

Figure 2.5: Cross section of the Koegel Fontein complex after Jansen (1960).

A second swarm of dolerite dykes intruded at about the same time as the quartz porphyry dykes. These can be divided into tholeiitic dolerite, plagioclase phyric basalt and alkaline mafic rocks and tend to be within a 25km radius of the Koegel Fontein Complex. Field relationships indicate that they intruded before the quartz porphyry dykes, (de Beer, personal communication). The alkali mafic rocks have been associated with the Koegel Fontein complex due to their alkaline nature (de Beer *et al.*, 2002).

The last phase of igneous activity in the area occurred post continental drift. The Biesjes Fontein suite, a series of small olivine melilitite and olivine nephelinite plugs, intruded at 56Ma (Moore and Verwoerd, 1985). There is a plug of intermediate composition in the centre of the complex which was identified as part of the Biesjes Fontein suite. Petrographic analysis shows that this is not the case (Chapter 3.2.3). The timing of the emplacement of this intermediate plug is unknown.

The Jakkelshoek granite forms the roof rocks of the Koegel Fontein complex. The granite

is an augan gneiss which is part of the little Namaqualand Suite (de Beer *et al.*, 2002). The gneiss shows varying degrees of contact metamorphism and fenitization. The fenitization is strongest along fractures in the centre of the complex (de Beer and Armstrong, 1998). In the field alteration of the gneiss was greatest near the intermediate plug in the centre of the complex. Outcrops of the granite are scarce, however, hand specimens and thin sections from the Council for Geoscience show that the gneiss has varying degrees of carbonate, chlorite and epidote alteration. There are some samples which have secondary aegerine. For a full description and mineralogy of the Jakkelshoek granite, refer to de Beer *et al.* (2002).

Descriptions of the different Koegel Fontein rock types are summarised below. These are taken from de Beer *et al.* (2002) and de Beer (personal communication).

2.4.1 Plutonic Rocks

Syenite

There are three outcrops of syenite at the Koegel Fontein complex, one large pluton (Figure 2.6A and B) and three small plutons in the southern, three small plutons in the centre and two in northern section of the complex. There are about 40km between the southern and northern outcrops and each appears to be a discrete pluton. The syenite is intruded by bostonite and apalite dykes.

The largest intrusion is a 10km^2 pluton, the Sandkop Syenite, and is found in the southern section of the complex. It is a quartz–hornblende to quartz–biotite syenite with minor amounts of monzonite in the centre. The syenite consists of orthoclase, oligoclase, microperthite, hornblende, biotite, apatite and zircon. The syenite bodies in the centre of the complex are 20m in diameter and are aegerine syenite and fenite. The northern most syenite is 30m across. The smaller outcrops are comprised of biotite syenite.

Rooivleitjie granite

The Rooivleitjie granite is a small plug about 2km to the east of the largest syenite. It weathers red and is <20m in diameter. The granite is thought to have intruded at the same time as the syenites as it is cut by a bostonite dyke. However, this has yet to be confirmed with radiogenic dating. It consists of orthoclase, microperthite, quartz and biotite (Figure 2.6C).

Rietpoort granite

The Rietpoort granite is a homogeneous medium grained pluton with little to no enclaves or

xenoliths. The granite is a relatively shallow intrusion as evidenced by miarolitic cavities. Jansen (1960) identified rare feldspar phenocrysts with Rapakivi texture. Mineralogically the granite consists of quartz, orthoclase, microperthite, albite–oligoclase, with minor amounts of biotite, hornblende, zircon and apatite (Figure 2.6D and E).

Zout Rivier plug

The Zout Rivier plug is 80m in diameter. The plug is a tholeiitic diorite and many of the tholeiitic mafic rocks are spatially associated with it. The diorite is older than the bostonite and quartz porphyry dykes as it is cut by both rock types. In the field the plug is characterised by an area of reddish sand with few outcrops in the centre (Figure 2.6F).

2.4.2 Hyperbyssal rocks

Kerskloof Bostonite suite

The Kerskloof bostonites are a suite of rocks which are characterised, in the field, by bostonitic texture: irregurally arranged, subparallel laths of feldspar (De Beer, In Press). The suite is hence forth grouped as bostonite. The bostonite occur as thin dykes on average 1m wide (<5m) and are khaki in colour (Figure 2.7). The dykes tend to strike E–ENE. They exhibit trachytic flow–banding parallel to the dyke walls which are almost vertical. The dykes are predominately alkali–feldspar microsyenites with some quartz, alkali–feldspar microsyenites which grade to a more granitic composition. The dykes are thought to bridge the gap between the syenites and the granites, although, they are more closely linked to the syenites. The bostonites consist of orthoclase, microperthite, plagioclase, micropegmatite, biotite and zircon. Rare dykes contain primary and secondary aegerine–augite with the latter occurring in veins.

Quartz porphyry

The quartz porphyry dykes strike W–NW and are mostly 3–10m wide with rare dykes reaching 20m in width. The dykes are light grey and resistant to weathering, although, they are a reddish orange when weathered (Figure 2.7A). There appears to be two quartz porphyry phases the older consists of dark coloured rocks and the younger is light grey. The former is found in the northwestern section of the complex and as xenoliths in the light grey dykes (Figure 2.7C). The light grey dykes are the most numerous of the two. The mineralogy of the quartz porphyries is quartz, orthoclase, albite–oligoclase, zircon and calcite. Jansen (1960) observed feldspar grains with quartz cores and altered quarts grains which grade into fine–grained mi-

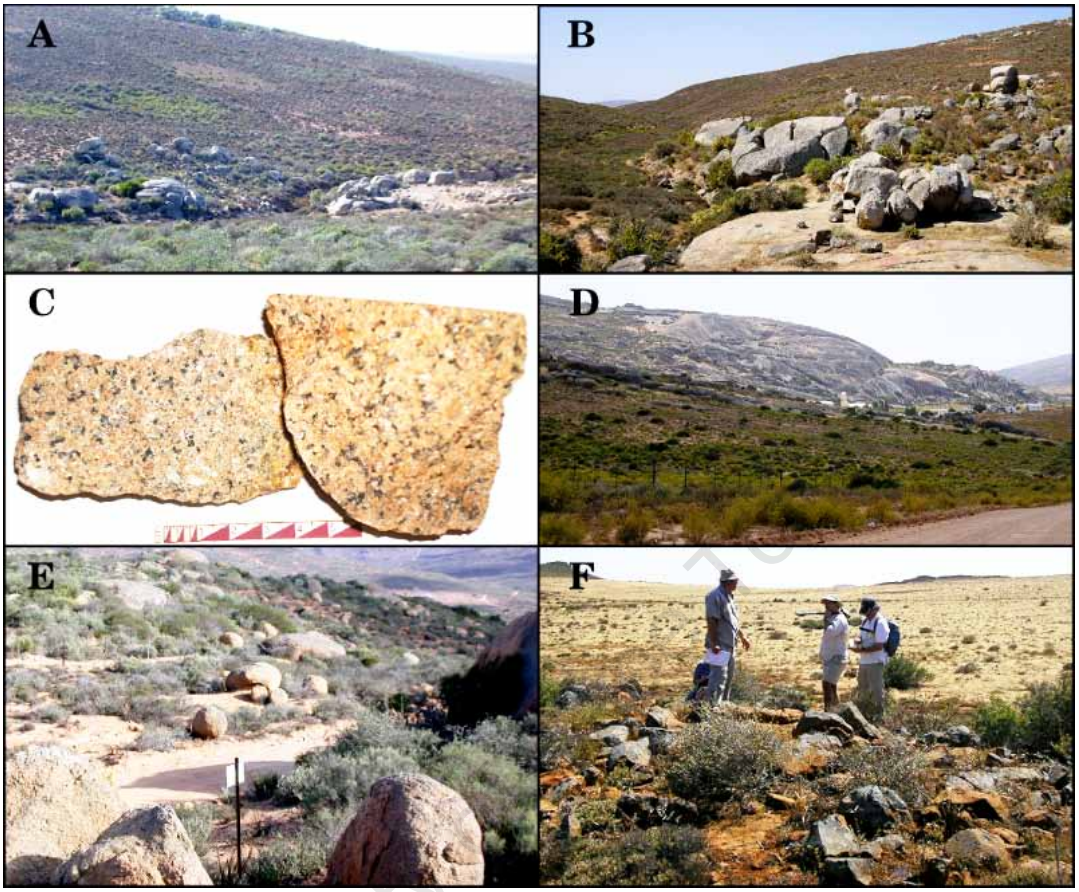

Figure 2.6: Outcrops of the Koegel Fontein plutonic rocks. A. Boulders of the Sandkop syenite, the largest syenite pluton at Koegel Fontein. B. Sandkop syenite core stones. C. Hand specimens of the Rooivleitjie granite. D. The Rietpoort type locality at the village of Rietpoort. E. Rietpoort granite core stones and the location of sample CCK19. F. Outcrop of the Zout Rivier plug characterised by red soil.

cropegmatite which can contain clinopyroxene.

Tholeiitic mafic rocks

The tholeiitic mafic dykes all fall within the tholeiitic field on a TAS diagram (Figure 5.1) and can be distinguished from the regional dolerite dykes by their small width (<2m) and their spatial association with the Koegel Fontein complex (Figure 2.7D and F).The majority of these dykes occur in the vicinity of the Zout Rivier plug. The larger dykes can show zonation while the thinner dykes tend to be altered often to epidote. The dykes tend to strike N–NW.

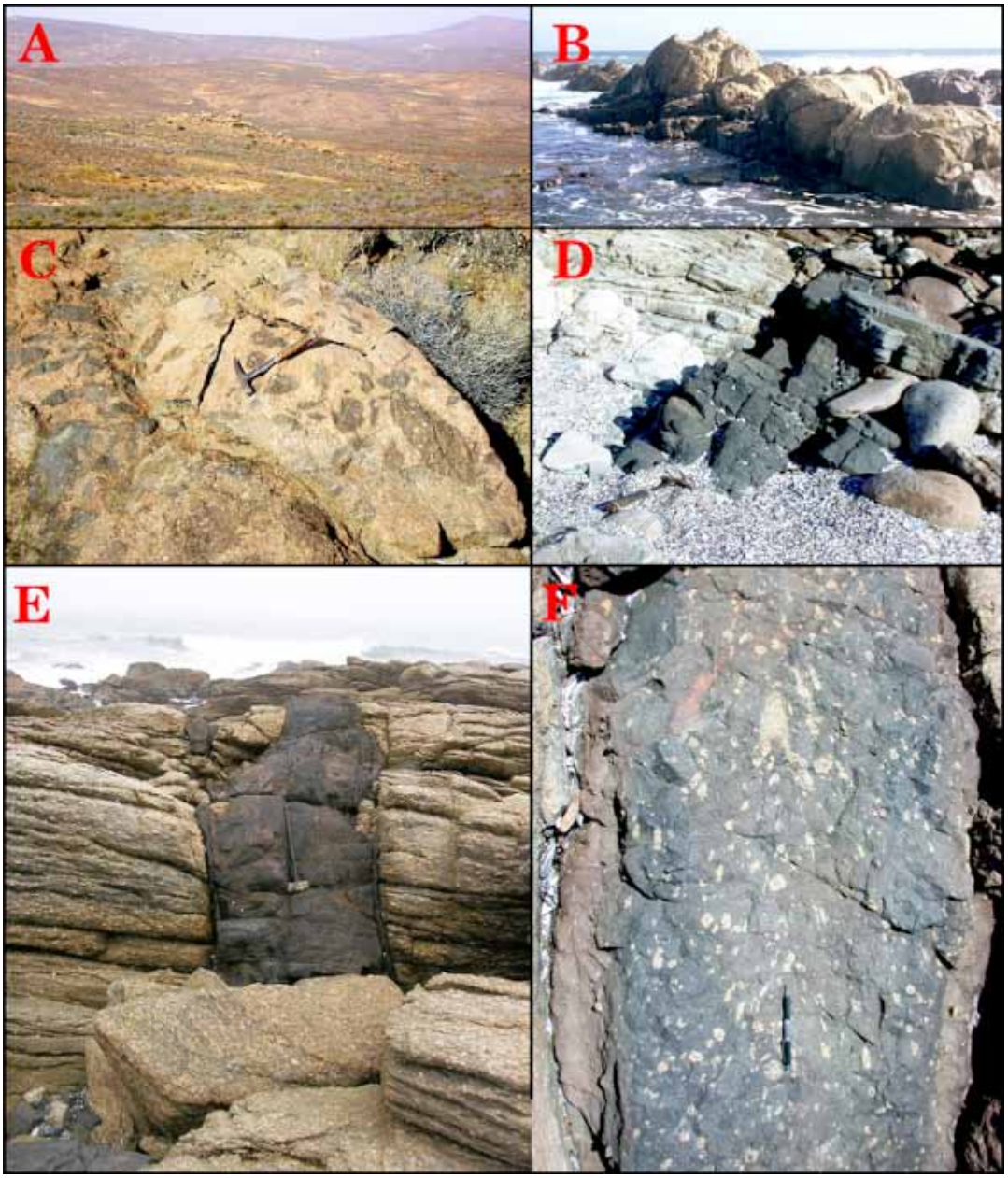

Figure 2.7: Outcrops of the hyperbyssal rocks from the Koegel Fontein complex. A. Weathering resistant quartz porphyry dyke. B. Large bostonite dyke and the sample locality of CCK26. C. Quartz porphyry dyke with xenoliths of the older dark quartz porphyry (samples CCK4 to 9). D. Tholeiitic mafic dyke E. Olivine–plagioclase alkali mafic dyke. F. Mafic dyke with entrained xenocrysts of quartz and feldspar (CCK36).

Alkali mafic rocks

Like the tholeiitic mafic rocks these rocks also tend to occur as thin 1m wide dykes. The alkali mafic rocks are also spatially associated with the Koegel Fontein complex and often

intrude along the same fractures as the bostonites. The dykes were emplaced along NE striking fractures and include rare lamprophyres (Figure 2.7E).

Intermediate plug

This is a small (<10m in diameter) plug consisting of very fine–grained material. It was originally assumed to be part of the Biesjes Fontein suite. Petrographic inspection showed the plug to be a breccia consisting of lithic fragments supported in a fine–grained matrix. Silica content for the plug is 56 wt.% (chapter 5.1) and the plug was renamed as intermediate.

Chapter 3

Petrography

The Koegel Fontein rock types can be divided into plutonic and hyperbyssal rocks with summaries of the main petrographic features presented below. The petrographic descriptions are subdivided into felsic and mafic rocks with the felsic rocks of each group being described first. Detailed petrographic descriptions of each thin section are in Appendix A.

3.1 Plutonic rocks

The plutonic rocks consist of three rock types, syenite, granite and gabbro. The rock types form at least four different plutons, syenite, the Rooivleitjie granite, the Zout Rivier plug and the Rietpoort granite. For a full description of each pluton and its mineral chemistry please refer to Chapter 2.4.1.

3.1.1 Felsic plutonic rocks

The syenites are medium– (1-5mm) to coarse– (>5mm) grained with anhedral to subhedral grains. The rocks consist of about 75% feldspar, 15% biotite and amphibole, <5% quartz and <5 apatite with trace amounts of clinopyroxene, zircon and opaque minerals (Figure 3.1A). The feldspar is often perthitic (Figure 3.1B) and granophyric intergrowths are present but rare (Figure 3.1B). Amphibole, possibly hornblende, grains are often poikilitic, subhedral and are either olive–green or brown (Figure 3.1A). The biotite has dark brown to light yellow pleochroism and tends to be interstitial.

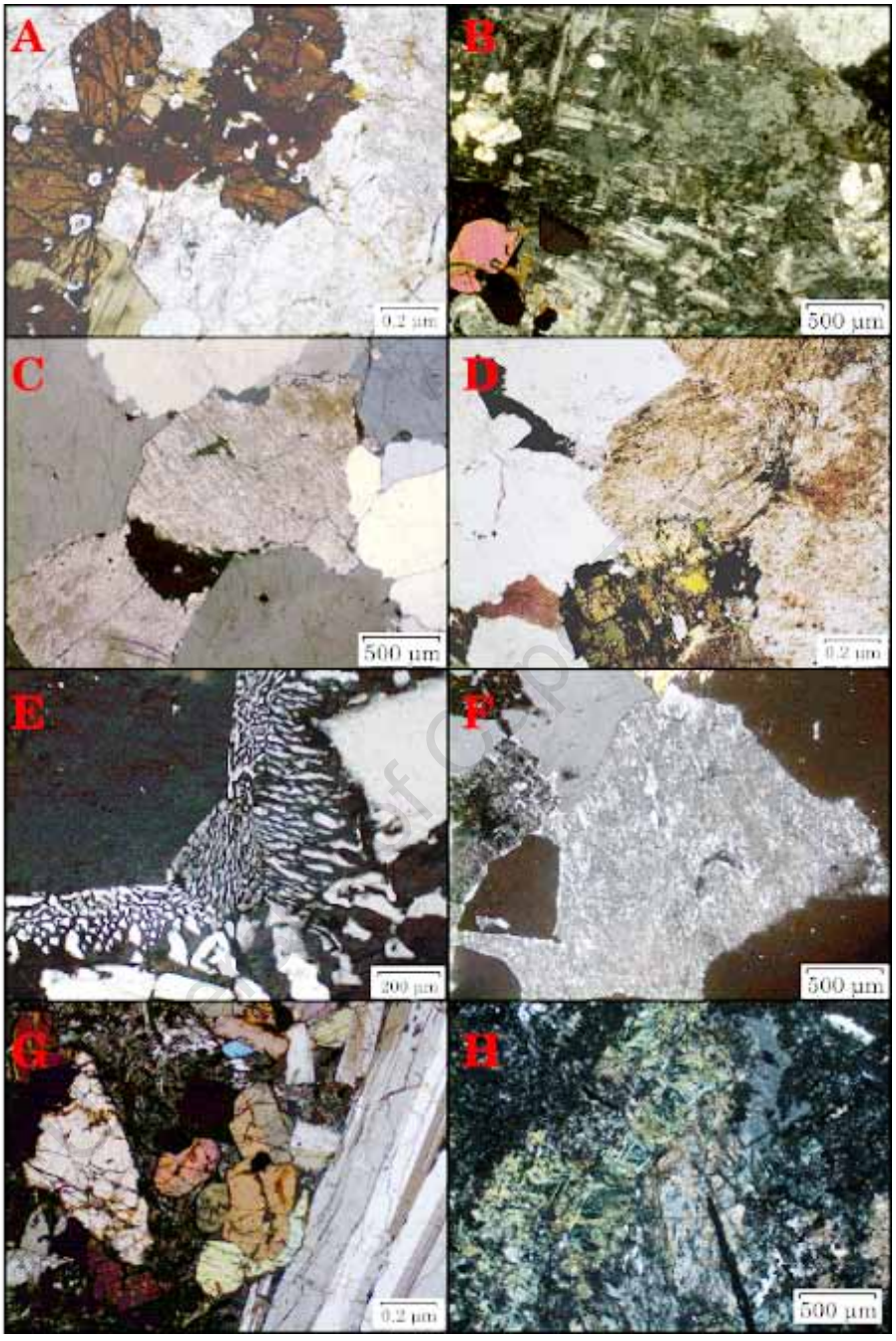

Figure 3.1: Petrographic features of the Koegel Fontein plutonic rocks. A. Mineralogy of the syenites (Plain polarised light; PPL). B. Coarse–patch perthite feldspar with clinopyroxene photomicrograph of a syenite (cross polarised light; XPL). C. Perthitic feldspar in the Rooivleitjie granite. Minerals have sutured grain boundaries (XPL). D. Amphibole showing green, green–brown, yellow–green pleochroism. Turbid feldspar also present. Photo micrograph of the Rooivleitjie granite (PPL). E. Granophyric texture in the Rietpoort granite (XPL). F. Perthitic texture in the Rietpoort granite (XPL). G. Zout Rivier plug phenocrysts showing glomeroporphyritic texture. Plagioclase and clinopyroxene both display twinning (XPL). H. Alteration in the Zout Rivier Plug is shown by a chloritized olivine phenocryst (PPL).

The Rooivleitjie granite is coarse–grained (>5mm) with sutured grain boundaries (Figure 3.1C and D).The granite is predominantly feldspar (70%) and quartz (20%) with a small amount of amphibole (<5%) and biotite (<5%) and traces of zircon and opaque minerals. Most grains are anhedral except for quartz which can be subhedral. Hornblende grains have green–brown to light green–yellow pleochroism (Figure 3.1D). The feldspar tends to be perthitic and turbid (Figure 3.1C), other signs of alteration are chloritized amphibole and biotite, secondary epidote and calcite.

The Rietpoort granite is coarse–grained (>5mm), inequigranular and comprises mostly alkali–feldspar (60%). There is about 35–40% quartz and traces of amphibole, biotite, zircon and opaque minerals present. Grains tend to be subhedral to anhedral and granophyric intergrowths are common, (Figure 3.1E). Feldspar grains are often perthitic and slightly turbid (Figure 3.1F). The amphibole is hornblende, and is pleochroic from pale to dark green and the biotite tends to have dark brown to straw brown pleochroism. The granite is homogeneous with almost no difference between thin sections.

3.1.2 Mafic plutonic rocks

The Zout Rivier plug is medium–grained (1–5mm) with coarse–grained (>5mm) phenocrysts. Phenocrysts make up about <40% of the rock and are plagioclase (60%), clinopyroxene (35%) and orthopyroxene (5%) and often have glomeroporphyritic texture. Both the plagioclase and clinopyroxene display twinning (Figure 3.1G). Some phenocrysts are altered to serpentine and chlorite (Figure 3.1H). The groundmass is about 50% plagioclase and 40% clinopyroxene and orthopyroxene with traces of opaque minerals. Alteration minerals in the groundmass are calcite, chlorite and epidote.

3.2 Hyperbyssal rocks

Hyperbyssal rocks include of bostonites, quartz porphyries, tholeiitic mafic rocks and alkali mafic rocks (Chapter 2.4.2 and 5.1). The bostonite dykes are the oldest, followed by the mafic dykes and the quartz porphyry dykes are the youngest. The relationship between the alkali and tholeiitic mafic rocks is unknown, however, both appear to be related to the Koegel Fontein Complex. For full descriptions of the occurrences of each rock type refer to Chapter 2.4.2.

3.2.1 Felsic hyperbyssal rocks

The bostonites are fine– (0.5–1mm) to medium– (1–5mm) grained holocrystalline rocks. These rocks are either almost equigranular and non–porphyritic (Figure 3.2A) or inequigranular feldspar–quartz porphyries (Figure 3.2B). The porphyritic rocks contain about 10% phenocrysts which are predominantly turbid feldspar and tend to be anhedral to subhedral. Granophyric texture is common in the more coarse–grained rocks and the groundmass in some of the fine–grained rocks has a quench texture. The groundmass is mostly feldspar (60–70%) and quartz (30–40%) with traces of opaque minerals. Carbonate and chlorite alteration is present to varying degrees in all the bostonite samples.

The amount of phenocrysts in the quartz porphyry dykes (5 to 30%) varies from dyke to dyke. Phenocrysts are predominately quartz (<55%) and feldspar (<45%) and minor biotite (<5%). Phenocrysts are subhedral to anhedral and glomeroporphyritic (Figure 3.2D). The quartz can show the "high quartz" form, and many of the phenocrysts have coronas, (Figure 3.2D). Feldspar grains can be poikilitic, have simple twinning and are often very altered with patches of carbonate minerals and sericite. The groundmass of the quartz porphyries ranges from phaneritic to aphanitic and all thin sections looked at were holocrystalline. Grains tend to be anhedral and sub–equigranular with varying degrees of alteration. The primary minerals present are quartz (<30%), feldspar (<60%), chloritized biotite (<15%), up to 2% zircon and traces of opaque minerals. One sample had a small amount of fluorite. The groundmass can have large amounts of carbonate minerals (<10%), chlorite, sericite and minor epidote. In some of the coarser samples granophyric intergrowths occur, (Figure 3.2C).

3.2.2 Mafic hyperbyssal rocks

The tholeiitic mafic rocks range from having a fine–grained (0.5–1mm), inequigranular phaneritic groundmass to a cryptocrystalline aphanitic groundmass. The rocks are comprised predominantly of plagioclase (70%) and clinopyroxene (<30%) with minor amounts of orthopyroxene and olivine. The pyroxene tends to be interstitial while the plagioclase is euhedral to subhedral. Some plagioclase grains have faint zoning (Figure 3.2E). The tholeiitic mafic rocks can have up to 5% phenocrysts which are mostly feldspar with some clinopyroxene and olivine (Figure 3.2F). Many of the tholeiitic samples are highly altered with varying amounts of chlorite, epidote and carbonate minerals.

The alkaline mafic rocks are fine– to medium–grained with porphyritic rocks containing up to 10% phenocrysts which are medium– to coarse–grained. The alkaline mafic rocks have similar

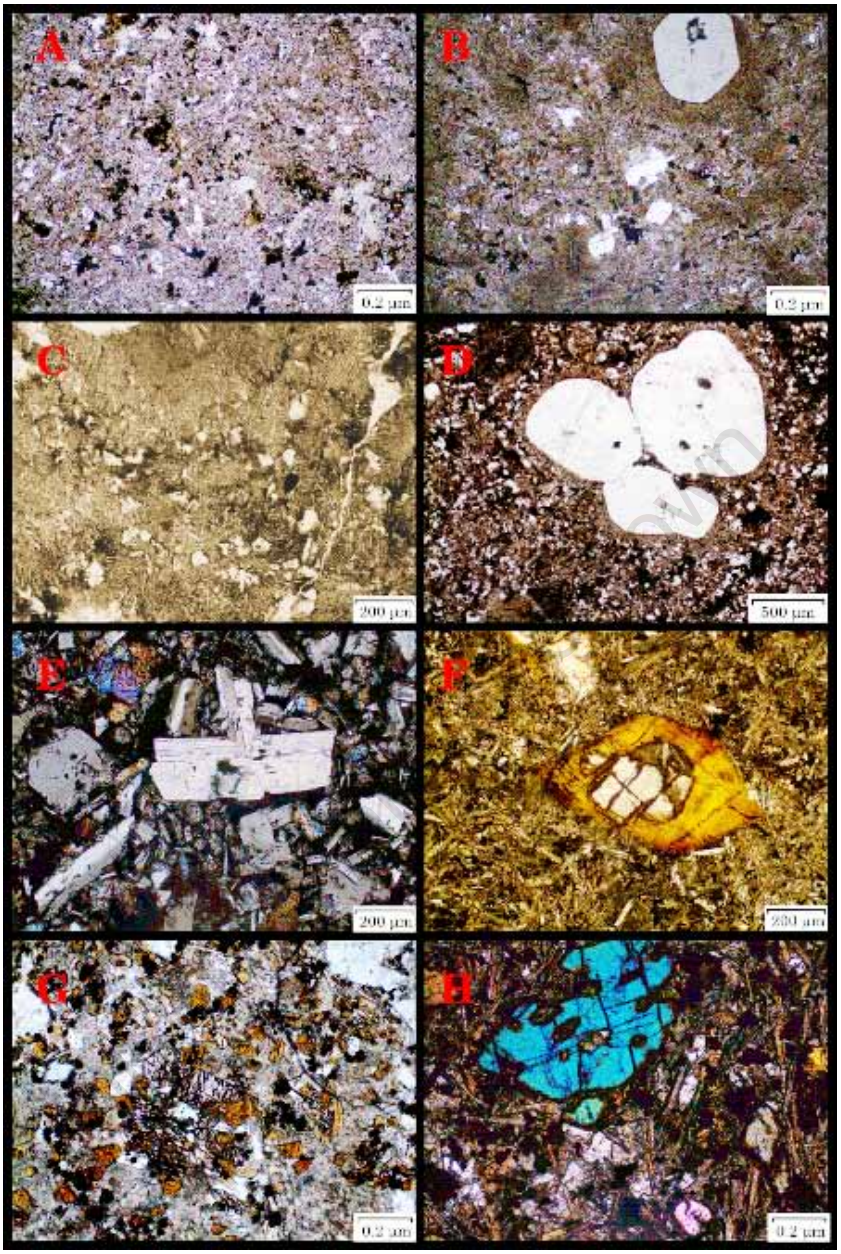

Figure 3.2: Petrographic features of the hyperbyssal rocks from the Koegel Fontein complex. A. Texture of the non–porphyritic bostonites (PPL). B. texture of the porphyritic bostonite dykes (XPL). C. Granophyric texture of the quartz porphyries (XPL). D. Glomeroporphyritic texture of the phenocrysts from the quartz porphyries. Coronas of fine–grained feldspar and quartz surround most phenocrysts. The texture of the groundmass is typical of the quartz porphyries (XPL). E. Texture of the tholeiiti mafic rocks, showing subhedral plagioclase and interstitial clinopyroxene (XPL). F. Porphyritic tholeiitic dyke with olivine phenocryst with a reaction rim of bowlingite. The groundmass is predominantly feldspar (PPL). G. Lamprophyre, alkali mafic rock, showing Ti–rich hornblende and clinopyroxene (PPL). H. Texture of the porphyritic alkali mafic rocks. A large clinopyroxene phenocryst in a groundmass of needle–like clinopyroxene and interstitial plagioclase (XPL).

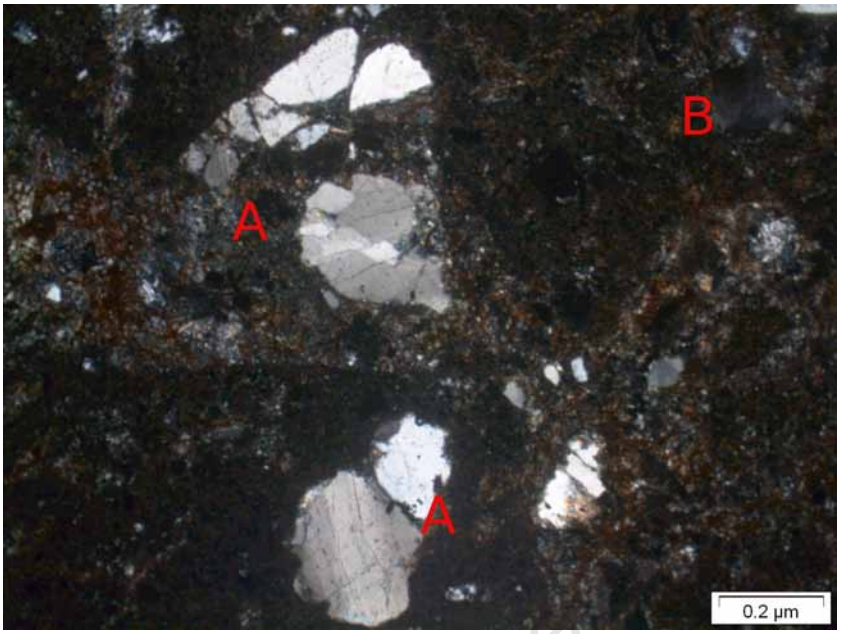

Figure 3.3: Petrographic features of the intermediate plug. The photomicrograph shows lithic fragments of Namaqua gneisses and fine–grained groundmass charater-istic of the plug.

mineralogy to the tholeiitic mafic rocks except the clinopyroxene can be slightly pink in plain polarised light and they contain a deep brown hornblende which indicate that these rocks are enriched in Ti relative to the tholeiitic rocks (Figure 3.2G). Some alkaline samples contain kaersutite. Phenocrysts tend to be plagioclase and clinopyroxene with the proportions of each varying from rock to rock. The groundmass is predominantly clinopyroxene (60%) which can form needle like laths (Figure 3.2H). The plagioclase in the groundmass is interstitial and can show sericite and carbonate alteration. There are some clinopyroxene grains with alteration rims of amphibole, chlorite and calcite. Some minerals which have been entirely serpentinized and chloritized with some chlorite showing the distinctive blue birefringence of prenite.

3.2.3 Intermediate hyperbyssal rocks

The intermediate plug has a very fine–grained (<0.5mm) groundmass. The groundmass forms about 40% of the rock with the remaining 60% consisting of xenoliths and xenocrysts (Figure 3.3). The xenoliths and xenocrysts are similar to the Jakkalshoek granite. All of the xenoliths and xenocrysts show evidence of deformation and are therefore, probably not from any of the early Koegel Fontein intrusive phases e.g. the syenites. The xenoliths and xenocrysts consist predominantly of quartz and highly altered feldspar. Alteration minerals are sericite

and carbonate and the feldspar is very turbid. The groundmass is too fine–grained to identify the mineralogy by optical microscopy.

3.2.4 Key points

It is important to note that none of the Koegel Fontein rocks show evidence of recrystallization or deformation. Quartz and feldspar phenocrysts appear to be in equilibrium with the groundmass. Feldspar in all rock types has been affected by alteration to varying degrees. Carbonate minerals, sericite, epidote, serpentine and chlorite are the alteration minerals indicating that the temperature of alteration was >150°C. Thin sections show that veins of secondary minerals are rare to non–existent in the plutonic rocks. Pyroxene grains in fresh samples are often cracked but appear unaltered. The intermediate plug contains a variety of different rock types the majority of which show evidence of deformation and are probably from the Jakkelshoek granite.

Chapter 4

Analytical methods

4.1 Sampling

There are three sets of samples used in this study, two from the Council for Geoscience (CGS), (CDB and CN), and one collected during this study, (CCK). The samples from the CGS were collected when Koegel Fontein was mapped between 1992 and 1998 and many of the samples have both a CDB and CN number. Where possible CDB numbers have been used. The CCK samples were collected from key sites at Koegel Fontein, identified by initial oxygen isotope results. All sample locations are recorded in Appendix B.

The samples from the CGS vary in size from about 10cm to over 30cm in diameter and many were collected using explosives. The CCK samples are on average about 10cm in diameter. Samples were split into three sections using a hydraulic splitter. One section was kept as a hand specimen, one was used for a thin section and the third crushed using a jaw crush with carbon steel ribbed jaws. Half of the crush was sieved and the size fraction 200μm to 600μm was used for mineral separation. The other half was ground using a Seibtechnik swing mill with an agate vessel and used for bulk rock geochemistry and whole–rock stable and radiogenic isotopes.

4.2 Whole rock geochemistry

Major element oxides and some trace element concentrations for all samples were analysed using standard XRF methods. 70 CDB and CN samples were analysed at the Helmholtz–Centre

Potsdam GFZ German Research Centre for Geoscienses (GFZ) and 47 CCK samples were analysed at the University of Cape Town, (UCT). The CDB and CN samples were analysed prior to the commencement of this project.

Major and trace elements of whole–rock powders of the CCK samples were analysed using a X–unique XRF wavelength spectrometer at UCT. Major elements were analysed using fusion disks where a LiT–LiM (57:43 respectively) flux and a LiBr releasing agent were used. The intensity data was processed using Philips X40 software. Trace elements were analysed using powder briquettes. Flux was used to bind 6g of whole–rock powder which was the supported in a boric acid base and prepared using a ten ton cold press. Data was refined using TRACE software.

Volatiles and loss on ignition (LOI) were calculated using a mass balance. Two grams of whole rock powder was weighed and heated for >12 hours at 450°C and then left to cool before being reweighed, with the mass difference being recorded as the volatile content. Samples where then reheated to 850°C and left for >12hrs, then allowed to cool and reweighed. The mass difference were recorded as LOI.

The dection limits for trace elements by XRF are between 1.1 and 4.7ppm. The error for the XRF is 5%.

The majority of the ICP–MS data was obtained prior to the start of this project, however, these were only for the mafic rocks. Rock type was used to select an additional 50 representative samples of the felsic rocks at Koegel Fontein. Included in the sample set were the two country rock samples analysed for radiogenic isotopes. Oxygen isotopes were used to distinguish the least altered samples by only selecting those with "normal" δ^{18}O values (δ^{18}O +6 to δ^{18}O +10‰). All ICP–MS analysis was done at the GFZ.

The ICP–MS equipment at the GFZ consist of inductively coupled plasma mass-spectrometer DRC-e (PerkinElmer/SCIEX) and the Geo- Las Pro M Laser Ablation System (Coherent) consisting of COMPexPro 102 excimer laser (optimized for ArF laser gas operation). The dection limits for these machines are between 0.005 and 0.1ppm

4.3 Stable isotopes

Stable isotope analysis was undertaken at UCT. Whole–rock powder, amphibole, biotite, feldspar (Figure 4.1A), quartz (Figure 4.1B) and groundmass were analysed for oxygen iso-

topes. Where necessary, quartz grains were cleaned in warm 10% HF for 15mins to remove any contaminants after which, the quartz was separated from any residual minerals. Whole–rock powder, amphibole and biotite were analysed for hydrogen. Oxygen and hydrogen isotope ratios were measured in the Stable Isotope Laboratory at the Department of Geological Sciences, UCT.

4.3.1 Mass spectrometry

All the isotope ratios from the gasses extracted were measured using the gas–source Finnegan Mat DeltaXP spectrometer in the Archaeology Department at UCT. Samples were analysed using the duel inlet mode with NBS19 reference gas and all the data was recorded in the standard δ-notation relative to SMOW where $\delta = (R_{sample}/R_{standard}\text{-}1) \times 1000$, R = $^{18}O/^{16}O$ and R = D/H for oxygen and hydrogen respectively.

4.3.2 Conventional oxygen isotopes

After powdering, samples were dried in an oven at 50°C for >12hrs. Normally ten samples weighing about 10mg each were run at a time, two of these were the quartz standard NBS–28. The samples were loaded into nickel tubes and degassed at 200°C and then reacted with ClF_3 at 550°C for three hours in order to liberate oxygen gas from the silicate samples. The O_2 gas was then passed over a hot carbon rod converting it to CO_2 gas, after which the pressure was measured using a Pirani Gauge. The carbon dioxide gas was then collected in "break seal" tubes.

The oxygen isotopes were measured off–line at the UCT Archaeology Dept. Raw $\delta^{18}O$ values were normalized to SMOW using a value of 9.64‰ for NBS–28 from Coplen *et al.* (1983). The average value for NBS–28 during the data acquisition period was 9.48‰, (σ = 0.14; n = 19) which is within error of the value recommended by Coplen *et al.* (1983) and indicates that the precision of the data is 0.14‰. The details for conventional oxygen extraction and the facilities at UCT are described by Harris and Ashwal (2002).

4.3.3 Oxygen isotopes by laser fluorination

Laser fluorination was used to analyse quartz phenocrysts from the quartz porphyries, quartz from the Rietpoort granite and vein quartz. Grains weighing between 1 and 3mg were anal-

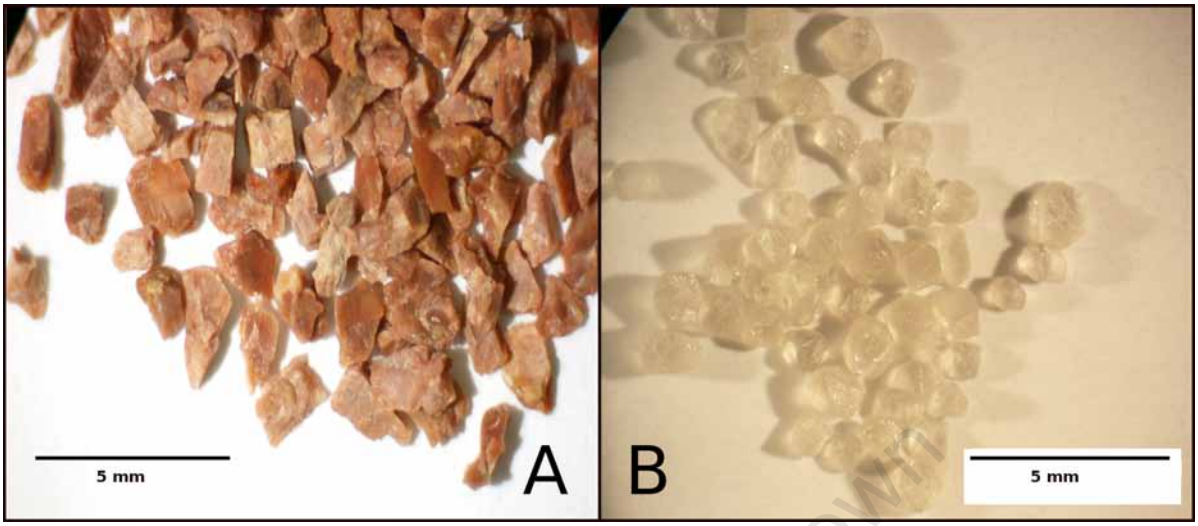

Figure 4.1: Mineral separates A. Feldspar B. Quartz showing the "high quartz" form which indicates that the mineral crystalized at temperatures above 600°C (Deer *et al.*, 1992).

ysed. Normally ten samples and two standards were loaded onto a highly polished nickel sample holder. In order to prevent absorbtion of moisture the sample holder was left for >2 hours in a 110°C oven and then placed directly into the reaction chamber. The chamber was degassed for one hour before being pre–fluorinated with about 10 kPa BrF_5 and then evacuated after 30 seconds to remove any remaining moisture. The chamber was then re–fluorinated with 10 kPa BrF_5 and left for >12hrs.

In order to check for contamination a blank sample was taken before oxygen extraction. The blank volume was measured on a Pirani gauge and was usually $<{}^{1}/_{200}$ of the sample volume. Individual samples were then reacted in the presence of about 10 kPa BrF_5 in a stepwise process, where the focus and intensity of the laser were increased in increments. Excess BrF_5 and the resaltant free Br were removed cryogenically. The remaining gas was passed through a KCl trap, heated to 200°C. Oxygen gas was then purified using a stainless steel double–U trap, immersed in liquid nitrogen and collected on grains of a 5 Å molecular sieve in glass sample vessels.

Oxygen–isotopes were measured off–line as O_2 gas in the Archeology department at UCT. The O_2 reference gas was calibrated by converting an aliquot of O_2 to CO_2 using the carbon convertor from the conventional extraction line. The measured isotope ratios were then used to calculated the raw δ values for each sample relative to SMOW (standard mean ocean water) scale.

The standards used for the silicate samples is the Monastery garnet (MON GT) a megacryst from the Monastery kimberlite pipe (Moore and Gurney, 1989; Harris *et al.*, 2000). The in–house standard (MON GT) was calibrated against UWG–2 from Valley *et al.* (1995) on the current UCT laser system. An average δ^{18}O value of 5.38‰, assuming δ^{18}O = 5.80‰ for UWG–2, was obtained for MON GT. All raw δ^{18}O data are, therefore, normalised to 5.38‰, the δ^{18}O value of the Monastery garnet. Precision for the laser data is about 0.10‰ for δ^{18}O as the average difference between δ^{17}O and δ^{18}O was 0.24 and 0.21‰, respectively.

The inlet pressure of the gas from each sample was measured at a constant volume. The correlation between pressure and amount of sample was 0.97 n = 34 for the data acquisition period. The line of best fit passes through the origin which suggests that the O_2 gas yields were close to 100%. Samples were discarded where pressure and sample weight did not correlate. It should also be noted that the correlation between δ^{17}O and δ^{18}O was excellent (0.97) throughout the data acquisition period. This shows that contamination by atmospheric oxygen did not occur.

4.3.4 Hydrogen isotopes

For hydrogen analysis 1–2mg of water per sample is needed. 50mg of amphibole or biotite and about 100mg of whole rock powder per sample was used. Hydrogen was extracted using the Zn–reduction method described byVennemann and O'Neil (1993). Samples, along with quartz chips and quartz wool were placed in quartz glass tubes and left to dry overnight at 110°C and degassed at room temperature on a vacuum line before the water was extracted by pryolysis at 1200°C and collected in a nitrogen trap. Low blank "Indiana zinc" was used to reduce the water to hydrogen gas by heating the "break seal" tubes to 450°C for 30 minutes shortly before being analysed on the mass spectrometer in the Archaeology Department.

Samples were normalized to SMOW using the internal water standard CTMP (δD = -7 ± 1 ‰, σ, n = 8). All data was normalized so that the Standard Light Antarctic Precipitation (SLAP) had a value of -428 ± on the SMOW scale. The voltage measured on collector two of the mass spectrometer was used to estimate the amount of water present in each sample. H-isotope values can be affected by the experimental blank when the water content of the sample is very low. This is detected when unusually low values of δD are measured as the blank tends to be very negative. These low δD values normally coincide with low water content and are ignored when interpreting the hydrogen–isotope results.

4.4 Radiogenic isotopes

All radiogenic isotopes were analysed at the Isotope Laboratories in the Department of Inorganic and Isotope Geochemistry at GFZ in Potsdam. Whole rock powder from 20 samples were used for radiogenic isotope analysis. Samples were chosen based on oxygen isotope ratios and whole–rock geochemistry. Oxygen–isotopes were used to determine whether samples had been hydrothermally altered. Of particular interest were samples with low–δ^{18}O quartz.

Samples were prepared by dissolving 100mg of powder in HF for three days at 160°C. They were then dried and placed in 6N HCl for a further three days. The same aliquot was used for Sr, Nd and Pb–isotopes. Pb, Sr and Nd were separated using ion chromatography. Details of radiogenic isotope extraction and the facilities at the GFZ are described by Romer *et al.* (2001); Romer and Xiao (2005).

4.4.1 Strontium and Neodymium isotopes

Strontium was separated using cation chromatography. Bio Rad AG50 W–X8 resin (3.8 ml volume) was used and the sample was dissolved in 2.5N HCL. Columns were cleaned using 2.5N HCL before elution. Rare earth elements (REE) were collected once Ba had been washed out using 2.5N HNO_3. Nd was then separated from the REE using HDEHP–coated Teflon, 2ml resin volume, (Romer *et al.*, 2001). The eluent used was 0.22N HCL.

Strontium was loaded on Ta–filaments and measured on a VG54–40 sector mass spectrometer using dynamic multi–collection. Nd was loaded onto double Re–filaments and $^{143}Nd/^{144}Nd$ was measured on a Finnigann MAT262 mass spectrometer using dynamic multi–collection. The standards used were NBS 987 and LaJolla for Sr and Nd respectively. Sr was normalized to $^{86}Sr/^{88}Sr = 0.1194$ and Nd was normalized to $^{146}Nd/^{144}Nd = 0.7219$ (Romer and Xiao, 2005).

Multiple analysis of NBS987 had an accuracy of 0.710249 ± 0.000004 to two standard deviations. Measured blanks are <50 pg Sr. Repeated measurements of La Jolla had an isotopic composition of 0.511850 ± 0.000004 at the two sigma level. Experimental blanks are <30 pg Nd.

4.4.2 Lead isotopes

Pb was separated using HCl–HBr ion chromatography. Teflon, 200μL ion–exchange columns with Bio Rad AGI–8X anion exchange resin were used. The resin was first cleaned using 6N HCL, water and 2.5 N HCL before the sample, dissolved in 2.5N HCL, was added (Romer *et al.*, 2001). Pb was then collected in a teflon container using 6N HCL and then purified by a second pass through the columns.

Lead, H_3PO_4 and silica gel were loaded onto single Re–filaments. Isotope ratios were measured on a Finnigann MAT262 mass spectrometer at 1200 to 1250°C. Isotopes were measured in a Faraday Collectors during static multi–collection. The standard used was NBS981 and samples were corrected for mass discrimination with 0.1% AMU. Analysis had an accuracy of 0.1% and at the two sigma level. Blanks were less than 15–30 pg Pb.

Chapter 5

Results

The main focus of this thesis is the reporting and interpretation of the stable isotope data. Therefore, the whole–rock geochemistry and radiogenic isotope data are only used to contextualize the stable isotope results. The whole–rock geochemical data presented below is an amalgamation of data gathered since 1998, when the Complex was first recognised as being Mesozoic. Isotope and additional whole–rock geochemical data were added as part of this project.

Oxygen isotope ratios indicate that the complex has been hydrothermally altered. The effects of this alteration on the whole–rock geochemistry and radiogenic isotopes will be discussed in Chapter 6. The aim of this chapter is to report all geochemical data objectively while the interpretation is done in Chapter 6. However, the ages obtained by de Beer and Armstrong (1998) have been used when reporting the radiogenic isotopes.

5.1 Whole–rock geochemistry

Major oxides, trace elements and CIPW normative mineralogy of the CCK samples analysed during this study are presented in Tables 5.1 and 5.2. The entire data set used for the project is reported in Appendix C. Chemical variability and lithological classification of the Koegel Fontein igneous assemblages are investigated using a series of graphs displayed in Figures 5.1 to 5.9.

Table 5.1: Major and trace elements for the Koegel Fontein CCK samples analysed. ND–Not detected and NM–Not measured

	CCK2	CCK3	CCK4	CCK6	CCK7	CCK8
Rock type	Gneiss	Bostonite	Quartz porphyry	Tholeiitic mafic rock	Quartz porphyry	Gneiss
XRF data						
SiO2	69	76	74	49	66	88
TiO2	0.52	0.24	0.26	1.7	0.76	0.19
Al2O3	14	13	12	15	14	5.63
Fe2O3	3.8	0.43	3.47	13	6.01	0.89
MnO	0.05	0.02	0.04	0.19	0.12	0.03
MgO	0.88	0.36	0.37	5.82	0.75	0.37
CaO	1.66	0.11	0.14	8.98	2.54	0.24
Na2O	2.58	3.27	2.68	2.73	2.82	1.17
K2O	6.19	5.4	5.5	0.35	5.32	2.96
P2O5	0.16	0.04	0.1	0.47	0.26	0.07
SO3	0.03	0.01	0.03	0.05	0.02	0.03
Cr2O3	0.01	0.01	0.01	0.02	0.01	0.01
NiO	0.01	0.01	0.01	0.02	0.01	0.01
H2O-	0.11	0.31	0.28	0.12	0.13	0.02
LOI	0.8	1.24	1.21	2.26	1.7	0.47
Total	99.62	100.35	100.4	100.09	100.26	99.96
Cr	ND	ND	ND	ND	ND	ND
Ga	ND	ND	ND	ND	ND	ND
Nb	17	120	193	14	89	3
Ni	ND	ND	ND	ND	ND	ND
Rb	332	344	367	7	192	101
Sr	111	7	69	391	226	76
V	ND	ND	ND	ND	ND	ND
Y	25	234	122	52	100	14
Zn	ND	ND	ND	ND	ND	ND
Zr	456	620	521	207	636	102
Mo	2	ND	2	1	ND	ND
Pb	45	15	44	6	25	19

continued . . .

	CCK2	CCK3	CCK4	CCK6	CCK7	CCK8
Rock type	Gneiss	Bostonite	Quartz porphyry	Tholeiitic mafic rock	Quartz porphyry	Gneiss
Sn	ND	14	ND	ND	ND	ND
Th	125	28	56	3	25	17
U	5	9	5	ND	2	ND
ICP–MS Data						
Y	36	NM	NM	NM	NM	NM
La	180	NM	NM	NM	NM	NM
Ce	405	NM	NM	NM	NM	NM
Pr	50	NM	NM	NM	NM	NM
Nd	181	NM	NM	NM	NM	NM
Sm	32	NM	NM	NM	NM	NM
Eu	1.5	NM	NM	NM	NM	NM
Gd	24	NM	NM	NM	NM	NM
Tb	2.5	NM	NM	NM	NM	NM
Dy	12	NM	NM	NM	NM	NM
Ho	1.6	NM	NM	NM	NM	NM
Er	3.2	NM	NM	NM	NM	NM
Tm	0.33	NM	NM	NM	NM	NM
Yb	2.1	NM	NM	NM	NM	NM
Lu	0.28	NM	NM	NM	NM	NM
Li	25	NM	NM	NM	NM	NM
Rb	317	NM	NM	NM	NM	NM
Sr	99	NM	NM	NM	NM	NM
Nb	20	NM	NM	NM	NM	NM
Mo	1.45	NM	NM	NM	NM	NM
Cd	0.04	NM	NM	NM	NM	NM
Sn	0.35	NM	NM	NM	NM	NM
Cs	0.83	NM	NM	NM	NM	NM
Hf	7.64	NM	NM	NM	NM	NM
Pb	35	NM	NM	NM	NM	NM
Bi	0	NM	NM	NM	NM	NM
Th	108	NM	NM	NM	NM	NM
U	5.81	NM	NM	NM	NM	NM
Sc	8.13	NM	NM	NM	NM	NM
Cr	6.4	NM	NM	NM	NM	NM

continued . . .

	CCK2	CCK3	CCK4	CCK6	CCK7	CCK8
Rock type	Gneiss	Bostonite	Quartz porphyry	Tholeiitic mafic rock	Quartz porphyry	Gneiss
Co	3.97	NM	NM	NM	NM	NM
Ni	2.74	NM	NM	NM	NM	NM
Cu	3.27	NM	NM	NM	NM	NM
Zn	92	NM	NM	NM	NM	NM
Ga	22	NM	NM	NM	NM	NM
Sb	0	NM	NM	NM	NM	NM
Tl	NM	NM	NM	NM	NM	NM

	CCK9	CCK10	CCK11	CCK12	CCK13	CCK14
Rock type	Gneiss	Quartz porphyry	Zout Rivier Plug	Quartz porphyry	Schist	Amphibolite
XRF data						
SiO2	71	71	50	73	91	57
TiO2	0.44	0.36	2.44	0.26	0.11	2.56
Al2O3	14	13	12	12	3.45	8.7
Fe2O3	2.79	4.35	15	3.61	2.33	19
MnO	0.06	0.12	0.24	0.07	0.02	0.32
MgO	0.8	0.35	1.84	0.31	0.35	3.39
CaO	1.79	0.14	6.59	0.57	0.05	1.45
Na2O	2.85	4.26	2.35	2.93	0.26	0.36
K2O	5.46	4.38	2.78	5.85	0.98	5.09
P2O5	0.1	0.18	1.06	0.03	0.03	1.09
SO3	0.02	0.05	0.1	0.02	0.04	0.03
Cr2O3	0.01	0.01	0.01	0.01	0.01	0.03
NiO	0.01	ND	ND	ND	ND	0.01
H2O-	0.06	0.19	0.07	0.15	0.1	0.15
LOI	1.12	1.62	4.98	0.99	1.08	0.79
Total	99.94	99.64	99.64	99.89	99.82	99.99
Cr	ND	ND	ND	ND	ND	ND
Ga	ND	ND	ND	ND	ND	ND
Nb	9	251	35	185	4	43
Ni	ND	ND	ND	ND	ND	ND

continued . . .

	CCK9	CCK10	CCK11	CCK12	CCK13	CCK14
Rock type	Gneiss	Quartz porphyry	Zout Rivier Plug	Quartz porphyry	Schist	Amphibolite
Rb	263	170	74	411	57	764
Sr	130	32	417	54	16	25
V	ND	ND	ND	ND	ND	ND
Y	18	128	116	146	ND	260
Zn	ND	ND	ND	ND	ND	ND
Zr	208	719	529	504	36	2313
Mo	ND	ND	3	ND	1	13
Pb	24	34	21	45	ND	6
Sn	ND	ND	ND	ND	ND	8
Th	15	66	9	55	3	58
U	ND	10	1	8	ND	16
ICP–MS Data						
Y	NM	81	NM	NM	NM	NM
La	NM	171	NM	NM	NM	NM
Ce	NM	277	NM	NM	NM	NM
Pr	NM	33	NM	NM	NM	NM
Nd	NM	109	NM	NM	NM	NM
Sm	NM	18	NM	NM	NM	NM
Eu	NM	1	NM	NM	NM	NM
Gd	NM	16	NM	NM	NM	NM
Tb	NM	2.5	NM	NM	NM	NM
Dy	NM	16	NM	NM	NM	NM
Ho	NM	3.3	NM	NM	NM	NM
Er	NM	10	NM	NM	NM	NM
Tm	NM	1.7	NM	NM	NM	NM
Yb	NM	11	NM	NM	NM	NM
Lu	NM	1.5	NM	NM	NM	NM
Li	NM	5.54	NM	NM	NM	NM
Rb	NM	157	NM	NM	NM	NM
Sr	NM	30	NM	NM	NM	NM
Nb	NM	208	NM	NM	NM	NM
Mo	NM	0.74	NM	NM	NM	NM
Cd	NM	0.02	NM	NM	NM	NM
Sn	NM	6.39	NM	NM	NM	NM

continued . . .

	CCK9	CCK10	CCK11	CCK12	CCK13	CCK14
Rock type	Gneiss	Quartz porphyry	Zout Rivier Plug	Quartz porphyry	Schist	Amphibolite
Cs	NM	0.11	NM	NM	NM	NM
Hf	NM	16	NM	NM	NM	NM
Pb	NM	29	NM	NM	NM	NM
Bi	NM	0.04	NM	NM	NM	NM
Th	NM	57	NM	NM	NM	NM
U	NM	11	NM	NM	NM	NM
Sc	NM	5.71	NM	NM	NM	NM
Cr	NM	0.79	NM	NM	NM	NM
Co	NM	1.2	NM	NM	NM	NM
Ni	NM	1.74	NM	NM	NM	NM
Cu	NM	2.21	NM	NM	NM	NM
Zn	NM	113	NM	NM	NM	NM
Ga	NM	27	NM	NM	NM	NM
Sb	NM	0.19	NM	NM	NM	NM
Tl	NM	NM	NM	NM	NM	NM

	CCK15	CCK17	CCK18	CCK19	CCK20	CCK21
Rock type	Bostonite	Rooivleitjie granite	Syenite Syenite	Rietpoort granite	Gneiss Gneiss	Intermediate plug
XRF data						
SiO2	75	70	61	75	70	56
TiO2	0.13	0.21	0.91	0.29	0.61	2.51
Al2O3	12	16	18	12	13	15
Fe2O3	2.07	1.64	4.92	2.37	4.29	11
MnO	0.05	0.03	0.17	0.06	0.08	0.17
MgO	0.29	0.28	1.25	0.31	1.59	3.54
CaO	0.07	0.11	2.02	0.77	1.9	4.87
Na2O	3.95	5.62	4.86	2.45	1.21	0.7
K2O	4.69	5.28	6.37	6.07	5.23	4.04
P2O5	0.01	0.07	0.41	0.03	0.21	0.26
SO3	0.01	0.03	ND	0.01	ND	0.01
Cr2O3	0.01	0.02	0.01	0.01	0.01	0.02
NiO	0.01	0.01	ND	ND	ND	0.02

continued . . .

	CCK15	CCK17	CCK18	CCK19	CCK20	CCK21
Rock type	Bostonite	Rooivleitjie granite	Syenite Syenite	Rietpoort granite	Gneiss Gneiss	Intermediate plug
H2O-	0.21	0.09	0.12	0.11	0.16	0.03
LOI	0.74	0.45	0.42	0.45	1.46	0.41
Total	99.39	99.6	99.74	99.54	99.6	99.39
Cr	ND	ND	ND	ND	ND	ND
Ga	ND	ND	ND	ND	ND	ND
Nb	555	601	115	39	19	62
Ni	ND	ND	ND	ND	ND	ND
Rb	334	709	145	284	181	247
Sr	32	24	552	54	200	283
V	ND	ND	ND	ND	ND	ND
Y	159	ND	58	91	66	39
Zn	ND	ND	ND	ND	ND	ND
Zr	1215	642	770	325	418	286
Mo	ND	ND	ND	2	5	ND
Pb	17	8	30	41	26	18
Sn	3	6	ND	ND	ND	ND
Th	57	42	12	24	49	11
U	7	11	ND	2	ND	3
ICP–MS Data						
Y	NM	20	36	76	NM	NM
La	NM	20	96	111	NM	NM
Ce	NM	28	188	215	NM	NM
Pr	NM	3.2	20	25	NM	NM
Nd	NM	8.9	76	93	NM	NM
Sm	NM	1.8	13	17	NM	NM
Eu	NM	0.04	3.2	1.1	NM	NM
Gd	NM	1.8	10	16	NM	NM
Tb	NM	0.32	1.2	2.5	NM	NM
Dy	NM	2.9	7.5	16	NM	NM
Ho	NM	0.8	1.5	3	NM	NM
Er	NM	3	4	9	NM	NM
Tm	NM	0.59	0.58	1.5	NM	NM
Yb	NM	5.4	3.6	9	NM	NM
Lu	NM	0.83	0.5	1.3	NM	NM

continued . . .

	CCK15	CCK17	CCK18	CCK19	CCK20	CCK21
Rock type	Bostonite	Rooivleitjie granite	Syenite Syenite	Rietpoort granite	Gneiss Gneiss	Intermediate plug
Li	NM	161	14	30	NM	NM
Rb	NM	661	132	264	NM	NM
Sr	NM	6.74	512	49	NM	NM
Nb	NM	622	107	43	NM	NM
Mo	NM	1.31	1.99	3.29	NM	NM
Cd	NM	0.13	0.45	0.12	NM	NM
Sn	NM	4.61	2.43	3.72	NM	NM
Cs	NM	2.89	0.89	1.55	NM	NM
Hf	NM	13	1.3	2.44	NM	NM
Pb	NM	7.86	25	37	NM	NM
Bi	NM	0.13	0.05	0.05	NM	NM
Th	NM	37	9.75	24	NM	NM
U	NM	11	1.56	3.35	NM	NM
Sc	NM	0.73	10	5.13	NM	NM
Cr	NM	0.6	2.58	1.5	NM	NM
Co	NM	0.32	2.7	0.95	NM	NM
Ni	NM	0.6	2.59	1.02	NM	NM
Cu	NM	2.24	2.09	2.95	NM	NM
Zn	NM	117	216	75	NM	NM
Ga	NM	53	24	20	NM	NM
Sb	NM	0.09	0.25	0.04	NM	NM
Tl	NM	NM	NM	NM	NM	NM

	CCK22	CCK23	CCK24	CCK25	CCK26	CCK27
Rock type	Gneiss	Quartz porphyry	Marble	Schist	Bostonite	Gneiss
XRF data						
SiO2	71	75	4.61	67	67	72
TiO2	0.62	0.16	0.04	0.72	0.18	0.31
Al2O3	13	12	0.32	11	16	14
Fe2O3	4.08	2.25	0.21	5.36	3.61	2.76
MnO	0.06	0.05	0.05	0.07	0.1	0.04
MgO	0.71	0.27	16	3.01	0.42	0.9

continued . . .

	CCK22	CCK23	CCK24	CCK25	CCK26	CCK27
Rock type	Gneiss	Quartz porphyry	Marble	Schist	Bostonite	Gneiss
CaO	0.96	0.9	36	2.95	0.69	0.61
Na2O	2.49	2.64	0.28	1.95	3.4	2.82
K2O	5.28	5.38	0.06	4.61	6.22	5.9
P2O5	0.2	0.01	0.01	0.54	0.02	0.07
SO3	0.01	0.03	ND	0.01	0.03	0.03
Cr2O3	0.01	0.01	0.01	0.03	0.01	0.01
NiO	ND	ND	ND	0.01	ND	ND
H2O-	0.08	0.07	0.05	0.09	0.5	0.11
LOI	0.72	0.62	42	1.92	1.29	0.52
Total	99.35	99.37	99.59	99.58	99.27	99.45
Cr	ND	ND	ND	ND	ND	ND
Ga	ND	ND	ND	ND	ND	ND
Nb	21	140	4	15	647	6
Ni	ND	ND	ND	ND	ND	ND
Rb	228	427	ND	142	547	407
Sr	218	24	83	112	46	85
V	ND	ND	ND	ND	ND	ND
Y	54	183	2	70	166	19
Zn	ND	ND	ND	ND	ND	ND
Zr	400	297	ND	531	1257	271
Mo	1	ND	ND	ND	ND	ND
Pb	38	47	1	27	30	43
Sn	ND	6	ND	13	ND	ND
Th	30	50	ND	42	59	9
U	1	13	ND	ND	8	3
ICP–MS Data						
Y	NM	176	NM	NM	NM	44
La	NM	128	NM	NM	NM	33
Ce	NM	244	NM	NM	NM	75
Pr	NM	32	NM	NM	NM	8.7
Nd	NM	113	NM	NM	NM	34
Sm	NM	24	NM	NM	NM	7.6
Eu	NM	0.46	NM	NM	NM	0.94
Gd	NM	26	NM	NM	NM	7.9

continued . . .

	CCK22	CCK23	CCK24	CCK25	CCK26	CCK27
Rock type	Gneiss	Quartz porphyry	Marble	Schist	Bostonite	Gneiss
Tb	NM	4.5	NM	NM	NM	1.3
Dy	NM	32	NM	NM	NM	8.2
Ho	NM	6.5	NM	NM	NM	1.7
Er	NM	21	NM	NM	NM	5.1
Tm	NM	3.3	NM	NM	NM	0.8
Yb	NM	21	NM	NM	NM	4.8
Lu	NM	2.6	NM	NM	NM	0.62
Li	NM	24	NM	NM	NM	26
Rb	NM	409	NM	NM	NM	375
Sr	NM	19	NM	NM	NM	69
Nb	NM	139	NM	NM	NM	12
Mo	NM	6.48	NM	NM	NM	0.08
Cd	NM	0	NM	NM	NM	ND
Sn	NM	9.58	NM	NM	NM	1.23
Cs	NM	0.77	NM	NM	NM	1.86
Hf	NM	6.56	NM	NM	NM	3.82
Pb	NM	38	NM	NM	NM	37
Bi	NM	0.1	NM	NM	NM	0.03
Th	NM	44	NM	NM	NM	8.35
U	NM	13	NM	NM	NM	3.49
Sc	NM	1.81	NM	NM	NM	6.36
Cr	NM	0.62	NM	NM	NM	2.14
Co	NM	0.35	NM	NM	NM	2.28
Ni	NM	0.67	NM	NM	NM	1.8
Cu	NM	3.42	NM	NM	NM	0.56
Zn	NM	82	NM	NM	NM	45
Ga	NM	27	NM	NM	NM	23
Sb	NM	0.29	NM	NM	NM	0.01
Tl	NM	NM	NM	NM	NM	NM

	CCK28	CCK30	CCK31	CCK32	CCK33	CCK34
Rock type	Schist	Gneiss	Bostonite	Quartz porphyry	Tholeiitic mafic rock	Amphibolite
XRF data						
SiO2	81	72	72	70	51	51
TiO2	0.17	0.55	0.22	0.45	2.98	2.69
Al2O3	8.92	14	17	12	13	17
Fe2O3	2.84	3.71	2.16	5.89	14.85	10
MnO	0.03	0.05	0.05	0.1	0.2	0.09
MgO	0.97	1.03	0.41	0.34	3.06	3.36
CaO	0.09	0.28	0.07	1.79	6.56	6.41
Na2O	0.51	0.48	0.44	1.71	2.42	4.63
K2O	3.57	6.25	4.04	5.8	2.21	2.22
P2O5	0.05	0.18	0.03	0.07	1.19	1.3
SO3	0.01	ND	0.01	0.05	0.25	0.05
Cr2O3	0.01	0.01	0.02	0.01	0.01	0.01
NiO	ND	ND	0.01	ND	ND	0.01
H2O-	0.32	0.24	0.51	0.29	0.23	0.21
LOI	1.55	1.92	2.96	2.02	2.09	0.77
Total	100.03	100.15	99.62	99.93	99.8	99.78
Cr	ND	ND	ND	ND	ND	ND
Ga	ND	ND	ND	ND	ND	ND
Nb	12	15	662	45	37	14
Ni	ND	ND	ND	ND	ND	ND
Rb	275	440	272	232	83	78
Sr	22	56	64	84	569	1586
V	ND	ND	ND	ND	ND	ND
Y	ND	42	189	175	103	95
Zn	ND	ND	ND	ND	ND	ND
Zr	138	392	1228	1007	564	1418
Mo	2	ND	ND	6	4	9
Pb	24	36	15	46	19	17
Sn	ND	10	ND	ND	ND	ND
Th	6	34	70	25	7	11

continued . . .

	CCK28	CCK30	CCK31	CCK32	CCK33	CCK34
Rock type	Schist	Gneiss	Bostonite	Quartz porphyry	Tholeiitic mafic rock	Amphibolite
U	2	2	3	2	ND	2
ICP–MS Data						
Y	NM	NM	NM	NM	NM	NM
La	NM	NM	NM	NM	NM	NM
Ce	NM	NM	NM	NM	NM	NM
Pr	NM	NM	NM	NM	NM	NM
Nd	NM	NM	NM	NM	NM	NM
Sm	NM	NM	NM	NM	NM	NM
Eu	NM	NM	NM	NM	NM	NM
Gd	NM	NM	NM	NM	NM	NM
Tb	NM	NM	NM	NM	NM	NM
Dy	NM	NM	NM	NM	NM	NM
Ho	NM	NM	NM	NM	NM	NM
Er	NM	NM	NM	NM	NM	NM
Tm	NM	NM	NM	NM	NM	NM
Yb	NM	NM	NM	NM	NM	NM
Lu	NM	NM	NM	NM	NM	NM
Li	NM	NM	NM	NM	NM	NM
Rb	NM	NM	NM	NM	NM	NM
Sr	NM	NM	NM	NM	NM	NM
Nb	NM	NM	NM	NM	NM	NM
Mo	NM	NM	NM	NM	NM	NM
Cd	NM	NM	NM	NM	NM	NM
Sn	NM	NM	NM	NM	NM	NM
Cs	NM	NM	NM	NM	NM	NM
Hf	NM	NM	NM	NM	NM	NM
Pb	NM	NM	NM	NM	NM	NM
Bi	NM	NM	NM	NM	NM	NM
Th	NM	NM	NM	NM	NM	NM
U	NM	NM	NM	NM	NM	NM
Sc	NM	NM	NM	NM	NM	NM
Cr	NM	NM	NM	NM	NM	NM
Co	NM	NM	NM	NM	NM	NM
Ni	NM	NM	NM	NM	NM	NM

continued . . .

	CCK28	CCK30	CCK31	CCK32	CCK33	CCK34
Rock type	Schist	Gneiss	Bostonite	Quartz porphyry	Tholeiitic mafic rock	Amphibolite
Cu	NM	NM	NM	NM	NM	NM
Zn	NM	NM	NM	NM	NM	NM
Ga	NM	NM	NM	NM	NM	NM
Sb	NM	NM	NM	NM	NM	NM
Tl	NM	NM	NM	NM	NM	NM

	CCK35	CCK36	CCK37	CCK38	CCK39	CCK41
Rock type	Tholeiitic mafic rock	Alkali mafic rock	Alkali mafic rock	Alkali mafic rock	Tholeiitic mafic rock	Quartz vein
SiO2	50	52	55	43	50	80
TiO2	1.38	1.27	1.94	2.81	1.44	0.28
Al2O3	14	15	13	14	13	9.42
Fe2O3	13	9.9	11	15	14	1.58
MnO	0.21	0.16	0.14	0.42	0.23	0.03
MgO	6.16	4.89	2.25	6.11	6.44	0.6
CaO	9.9	6.83	3.42	6.86	9.82	0.32
Na2O	2.22	1.99	2.03	0.66	2.13	1.41
K2O	0.84	4	4.66	4.33	0.73	5.18
P2O5	0.12	0.52	1.3	0.85	0.14	0.09
SO3	0.01	0.02	0.05	0.11	0.1	0.01
Cr2O3	0.02	0.02	0.01	0.04	0.02	0.01
NiO	ND	0.01	ND	0.01	ND	ND
H2O-	0.23	0.25	0.82	0.59	0.3	0.11
LOI	1.45	3.04	4.26	4.57	1.59	0.83
Total	99.72	99.32	100.16	99.37	99.6	99.86
Cr	ND	ND	ND	ND	ND	ND
Ga	ND	ND	ND	ND	ND	ND
Nb	6	20	53	91	7	4
Ni	ND	ND	ND	ND	ND	ND
Rb	66	355	231	237	46	351
Sr	112	300	409	631	126	62
V	ND	ND	ND	ND	ND	ND

continued . . .

	CCK35	CCK36	CCK37	CCK38	CCK39	CCK41
Rock type	Tholeiitic mafic rock	Alkali mafic rock	Alkali mafic rock	Alkali mafic rock	Tholeiitic mafic rock	Quartz vein
Y	27	12	97	21	33	16
Zn	ND	ND	ND	ND	ND	ND
Zr	95	231	674	361	106	228
Mo	ND	ND	2	3	ND	1
Pb	1	18	18	7	1	42
Sn	ND	ND	ND	ND	ND	ND
Th	4	9	10	7	3	61
U	ND	ND	1	1	ND	20
ICP–MS Data						
Y	NM	NM	NM	44	NM	NM
La	NM	NM	NM	33	NM	NM
Ce	NM	NM	NM	75	NM	NM
Pr	NM	NM	NM	8.7	NM	NM
Nd	NM	NM	NM	34	NM	NM
Sm	NM	NM	NM	7.6	NM	NM
Eu	NM	NM	NM	0.94	NM	NM
Gd	NM	NM	NM	7.9	NM	NM
Tb	NM	NM	NM	1.3	NM	NM
Dy	NM	NM	NM	8.2	NM	NM
Ho	NM	NM	NM	1.7	NM	NM
Er	NM	NM	NM	5.1	NM	NM
Tm	NM	NM	NM	0.8	NM	NM
Yb	NM	NM	NM	4.8	NM	NM
Lu	NM	NM	NM	0.62	NM	NM
Li	NM	NM	NM	26	NM	NM
Rb	NM	NM	NM	375	NM	NM
Sr	NM	NM	NM	69	NM	NM
Nb	NM	NM	NM	12	NM	NM
Mo	NM	NM	NM	0.08	NM	NM
Cd	NM	NM	NM	ND	NM	NM
Sn	NM	NM	NM	1.23	NM	NM
Cs	NM	NM	NM	1.86	NM	NM
Hf	NM	NM	NM	3.82	NM	NM
Pb	NM	NM	NM	37	NM	NM

continued . . .

	CCK35	CCK36	CCK37	CCK38	CCK39	CCK41
Rock type	Tholeiitic mafic rock	Alkali mafic rock	Alkali mafic rock	Alkali mafic rock	Tholeiitic mafic rock	Quartz vein
Bi	NM	NM	NM	0.03	NM	NM
Th	NM	NM	NM	8.35	NM	NM
U	NM	NM	NM	3.49	NM	NM
Sc	NM	NM	NM	6.36	NM	NM
Cr	NM	NM	NM	2.14	NM	NM
Co	NM	NM	NM	2.28	NM	NM
Ni	NM	NM	NM	1.8	NM	NM
Cu	NM	NM	NM	0.56	NM	NM
Zn	NM	NM	NM	45	NM	NM
Ga	NM	NM	NM	23	NM	NM
Sb	NM	NM	NM	0.01	NM	NM
Tl	NM	NM	NM	NM	NM	NM

	CCK42	CCK43	CCK44	CCK45	CCK46	CCK47
Rock type	Quartz vein	Quartz vein	Quartz vein	Gneiss	Gneiss	Tholeiitic mafic rock
SiO2	83	89	83	75	71	52
TiO2	0.2	0.12	0.14	0.27	0.18	1.56
Al2O3	7.77	4.98	8.02	13	14	13
Fe2O3	1.31	0.87	0.91	1.91	2.05	14
MnO	0.03	0.03	0.03	0.04	0.04	0.22
MgO	0.54	0.44	0.51	0.5	0.46	4.44
CaO	0.38	0.66	0.23	0.53	0.81	9.42
Na2O	0.43	0.36	0.47	1.66	1.85	1.51
K2O	5.41	3.35	5.93	5.62	7.39	0.93
P2O5	0.08	0.04	0.05	0.08	0.09	0.14
SO3	0.06	0.17	0.09	0.02	0.01	0.03
Cr2O3	0.01	0.01	0.01	0.01	0.01	0.02
NiO	ND	ND	ND	0.01	ND	0.01
H2O-	0.15	0.16	0.15	0.29	0.28	0.37
LOI	0.79	0.33	0.76	0.72	0.68	1.36
Total	99.84	100.26	100.05	99.64	99.44	99.56
Cr	ND	ND	ND	ND	ND	ND

continued . . .

	CCK42	CCK43	CCK44	CCK45	CCK46	CCK47
Rock type	Quartz vein	Quartz vein	Quartz vein	Gneiss	Gneiss	Tholeiitic mafic rock
Ga	ND	ND	ND	ND	ND	ND
Nb	4	3	3	8	ND	8
Ni	ND	ND	ND	ND	ND	ND
Rb	336	181	304	283	329	56
Sr	65	49	50	77	112	110
V	ND	ND	ND	ND	ND	ND
Y	ND	ND	ND	2	7	32
Zn	ND	ND	ND	ND	ND	ND
Zr	186	91	118	223	224	111
Mo	ND	8	2	ND	ND	ND
Pb	99	29	34	52	51	3
Sn	ND	ND	ND	ND	ND	ND
Th	62	28	45	50	42	4
U	6	3	2	6	3	ND
ICP–MS Data						
Y	NM	NM	NM	NM	NM	NM
La	NM	NM	NM	NM	NM	NM
Ce	NM	NM	NM	NM	NM	NM
Pr	NM	NM	NM	NM	NM	NM
Nd	NM	NM	NM	NM	NM	NM
Sm	NM	NM	NM	NM	NM	NM
Eu	NM	NM	NM	NM	NM	NM
Gd	NM	NM	NM	NM	NM	NM
Tb	NM	NM	NM	NM	NM	NM
Dy	NM	NM	NM	NM	NM	NM
Ho	NM	NM	NM	NM	NM	NM
Er	NM	NM	NM	NM	NM	NM
Tm	NM	NM	NM	NM	NM	NM
Yb	NM	NM	NM	NM	NM	NM
Lu	NM	NM	NM	NM	NM	NM
Li	NM	NM	NM	NM	NM	NM
Rb	NM	NM	NM	NM	NM	NM
Sr	NM	NM	NM	NM	NM	NM
Nb	NM	NM	NM	NM	NM	NM

continued . . .

	CCK42	CCK43	CCK44	CCK45	CCK46	CCK47
Rock type	Quartz vein	Quartz vein	Quartz vein	Gneiss	Gneiss	Tholeiitic mafic rock
Mo	NM	NM	NM	NM	NM	NM
Cd	NM	NM	NM	NM	NM	NM
Sn	NM	NM	NM	NM	NM	NM
Cs	NM	NM	NM	NM	NM	NM
Hf	NM	NM	NM	NM	NM	NM
Pb	NM	NM	NM	NM	NM	NM
Bi	NM	NM	NM	NM	NM	NM
Th	NM	NM	NM	NM	NM	NM
U	NM	NM	NM	NM	NM	NM
Sc	NM	NM	NM	NM	NM	NM
Cr	NM	NM	NM	NM	NM	NM
Co	NM	NM	NM	NM	NM	NM
Ni	NM	NM	NM	NM	NM	NM
Cu	NM	NM	NM	NM	NM	NM
Zn	NM	NM	NM	NM	NM	NM
Ga	NM	NM	NM	NM	NM	NM
Sb	NM	NM	NM	NM	NM	NM
Tl	NM	NM	NM	NM	NM	NM

	CCK48	CCK51	CCK52	CCK53	CCK54	CCK55
Rock type	Quartz vein	Rietpoort granite	Rietpoort granite	Rietpoort granite	Gneiss	Rietpoort granite
SiO2	89	75	77	75	63	78
TiO2	0.21	0.33	0.25	0.35	0.3	0.21
Al2O3	3.42	12	12	12	9.95	11
Fe2O3	2.1	2.79	1.98	2.75	2.24	1.91
MnO	0.05	0.05	0.05	0.04	0.04	0.05
MgO	0.59	0.29	0.25	0.31	0.27	0.25
CaO	2.66	0.54	0.63	0.82	0.67	0.75
Na2O	0.36	1.63	1.59	1.61	1.39	1.58
K2O	0.1	5.9	6.14	5.61	4.92	5.8
P2O5	0.02	0.06	0.02	0.04	0.04	0.02
SO3	0.07	0.03	0.01	0.03	0.02	0.01

continued . . .

	CCK48	CCK51	CCK52	CCK53	CCK54	CCK55
Rock type	Quartz vein	Rietpoort granite	Rietpoort granite	Rietpoort granite	Gneiss	Rietpoort granite
Cr2O3	0.01	0.01	0.01	0.01	ND	0.01
NiO	ND	ND	ND	ND	ND	ND
H2O-	0.32	0.31	0.19	0.09	0.13	0.14
LOI	0.55	0.48	0.29	0.59	16.28	0.28
Total	99.74	99.72	99.56	99.19	99.67	99.96
Cr	ND	ND	ND	ND	ND	ND
Ga	ND	ND	ND	ND	ND	ND
Nb	18	46	39	47	10	34
Ni	ND	ND	ND	ND	ND	ND
Rb	6	281	299	276	310	306
Sr	48	58	45	67	122	42
V	ND	ND	ND	ND	ND	ND
Y	5	69	69	77	67	70
Zn	ND	ND	ND	ND	ND	ND
Zr	5	389	241	394	414	240
Mo	ND	3	2	3	2	1
Pb	4	40	56	47	48	390
Sn	ND	ND	ND	ND	ND	ND
Th	1	27	27	23	107	29
U	ND	2	2	1	10	6
ICP–MS Data						
Y	NM	62	68	70	NM	74
La	NM	87	104	94	NM	104
Ce	NM	220	201	189	NM	206
Pr	NM	22	24	21	NM	24
Nd	NM	80	86	79	NM	87
Sm	NM	15	15	15	NM	16
Eu	NM	1.2	0.97	1.2	NM	0.84
Gd	NM	14	14	13	NM	15
Tb	NM	2.2	2.1	2	NM	2.3
Dy	NM	14	13	14	NM	15
Ho	NM	2.5	2.6	2.6	NM	2.7
Er	NM	7.9	8	8.5	NM	8.7
Tm	NM	1.3	1.4	1.4	NM	1.5

continued . . .

	CCK48	CCK51	CCK52	CCK53	CCK54	CCK55
Rock type	Quartz vein	Rietpoort granite	Rietpoort granite	Rietpoort granite	Gneiss	Rietpoort granite
Yb	NM	8	8	8.8	NM	9
Lu	NM	1.1	1.1	1.3	NM	1.3
Li	NM	26	20	24	NM	30
Rb	NM	259	279	262	NM	289
Sr	NM	50	39	61	NM	34
Nb	NM	46	41	48	NM	38
Mo	NM	4.05	5.83	3.71	NM	5.34
Cd	NM	0.02	0.23	0.07	NM	0.17
Sn	NM	5.24	4.58	5.66	NM	3.28
Cs	NM	1.52	2	1.89	NM	1.9
Hf	NM	3.29	3.7	2.11	NM	1.94
Pb	NM	35	46	41	NM	331
Bi	NM	0.31	0.08	0.07	NM	0.09
Th	NM	26	24	22	NM	25
U	NM	4.42	2.92	3.14	NM	5.28
Sc	NM	5.37	4.88	6.7	NM	4.15
Cr	NM	3.28	1.13	1.51	NM	5.62
Co	NM	0.9	0.61	1.27	NM	0.6
Ni	NM	2.29	1.41	1.27	NM	3.71
Cu	NM	2.96	5.71	4.66	NM	3.67
Zn	NM	63	87	99	NM	62
Ga	NM	21	20	21	NM	20
Sb	NM	0.04	0.08	0.07	NM	0.04
Tl	NM	NM	NM	NM	NM	NM

Table 5.2: Normative mineralogy for all the Koegel Fontein samples analysed. When calculating CIPW norms FeO total was calculated using Fe_2O_3 = 1.5 + TiO_2 after Irvine and Baragar (1971).

	CCK3	CCK4	CCK6	CCK10	CCK11	CCK12
Rock type	Bostonite	Quartz porphyry	Tholeiitic mafic rock	Quartz porphyry	Zout Rivier Plug	Quartz porphyry
Q	35.74	37.23	3.11	28.59	8.47	31.74
Or	32.32	32.97	2.19	26.59	17.67	35.16
Ab	28.01	23.02	24.03	36.98	21.41	25.13
An	0.28	0.04	29.82	-	15.28	2.68
Ne	-	-	-	-	-	-
C	1.99	1.62	-	1.36	-	0.16
Di	-	-	10.88	-	10.59	-
Hy	0.92	1.99	21.13	3.26	13	2.16
Ol	-	-	-	-	-	-
Mt	-	2.57	4.73	2.71	5.97	2.57
Il	0.04	0.51	3.34	0.7	4.98	0.51
Hem	0.43	-	-	-	-	-
Ap	0.09	0.23	1.14	0.42	2.64	0.07
Ru	0.29	-	-	-	-	-
Tot	100.12	100.18	100.36	100.27	100.01	100.18

	CCK15	CCK17	CCK18	CCK19	CCK23	CCK26
Rock type	Bostonite	Rooivleitjie granite	Syenite	Rietpoort granite	Quartz porphyry	Bostonite
Q	33.99	16.76	2.61	36.24	37.64	21.39
Or	28.25	31.56	38.18	36.28	32.27	37.88
Ab	34.02	48.15	41.63	20.99	22.76	29.7
An	0.33	0.09	7.41	2.71	4.27	3.39
Ne	-	-	-	-	-	-
C	0.57	0.86	-	-	-	2.05
Di	-	-	0.02	0.75	0.18	-
Hy	0.75	0.7	4.18	0.45	0.59	2.91
Ol	-	-	-	-	-	-
Mt	1.17	-	3.51	1.13	1.54	2.45
Il	0.25	0.06	1.75	0.55	0.3	0.36

continued . . .

	CCK15	CCK17	CCK18	CCK19	CCK23	CCK26
Rock type	Bostonite	Rooivleitjie granite	Syenite	Rietpoort granite	Quartz porphyry	Bostonite
Hem	0.82	1.66	-	1.01	0.6	-
Ap	0.02	0.16	0.97	0.07	0.02	0.05
Ru	-	0.22	-	-	-	-
Tot	100.17	100.22	100.24	100.18	100.17	100.18

	CCK31	CCK32	CCK33	CCK35	CCK36	CCK37
Rock type	Bostonite	Quartz porphyry	Alkali mafic rock	Tholeiitic mafic rock	Alkali mafic rock	Alkali mafic rock
Q	55.79	32.51	11.02	3.93	2.64	16.59
Or	24.88	35.34	13.65	5.14	24.88	29.31
Ab	3.81	14.98	21.41	19.46	17.68	18.28
An	0.09	7.57	17.29	25.31	21.84	9.03
Ne	-	-	-	-	-	-
C	11.97	-	-	-	-	1.4
Di	-	0.94	7.15	19.32	8.35	-
Hy	1.07	4.94	13.92	19.22	17.03	13.44
Ol	-	-	-	-	-	-
Mt	1.01	2.86	6.68	4.23	4.12	5.18
Il	0.44	0.89	5.91	2.7	2.54	3.93
Hem	1.03	-	-	-	-	-
Ap	0.09	0.19	2.87	0.28	1.27	3.22
Ru	-	-	-	-	-	-
Tot	100.18	100.21	99.9	99.59	100.36	100.37

	CCK38	CCK39	CCK47	CCK51	CCK52	CCK53	CCK55
Rock type	Alkali mafic rock	Tholeiitic mafic rock	Tholeiitic mafic rock	Rietpoort granite	Rietpoort granite	Rietpoort granite	Rietpoort granite
Q	-	4.11	11.58	42.52	42.69	43.01	44.51
Or	27.66	4.49	5.73	35.34	36.7	33.74	34.51
Ab	6.09	18.79	13.28	14.05	13.54	13.88	13.45
An	23.88	23.26	28.29	2.34	2.99	3.86	3.64
Ne	-	-	-	-	-	-	-
C	-	-	-	1.97	1.29	1.72	1.23
Di	5.63	20.94	16.08	-	-	-	-

continued . . .

	CCK38	CCK39	CCK47	CCK51	CCK52	CCK53	CCK55
Rock type	Alkali mafic rock	Tholeiitic mafic rock	Tholeiitic mafic rock	Rietpoort granite	Rietpoort granite	Rietpoort granite	Rietpoort granite
Hy	13.68	20.74	17.33	0.72	0.62	0.77	0.62
Ol	8.88	-	-	-	-	-	-
Mt	6.57	4.35	4.52	2.01	0.18	1.86	0.17
Il	5.75	2.85	3.08	0.65	0.47	0.68	0.4
Hem	-	-	-	0.45	1.63	0.58	1.59
Ap	2.13	0.32	0.32	0.14	0.05	0.09	0.05
Ru	-	-	-	-	-	-	-
Tot	100.27	99.85	100.22	100.18	100.16	100.19	100.17

The data recorded in Table 5.1 is the raw (unaltered) XRF and ICP–MS data. Total Fe is analysed in its oxidized state and is therefore, recorded as Fe_2O_3. The ratio for Fe^{3+}/Fe^{2+} had to be recalculated. This was done using the standard molecular ratio: $Fe_2O_3/FeO = 0.15$. The Bulk of the CIPW normative calculations were done with Igpet for Windows which uses the method of Irvine and Baragar (1971) where $Fe_2O_3 = 1.5 + TiO_2$ if only Fe_2O_3 or FeO is analysed. A sample of norms were calculated using Fe_2O_3 and FeO calculated from the molecular ratio and then recalculated using only Fe_2O_3. The results were the same and all CIPW norms in Table 5.2 were calculated using Igpet's internal method following Irvine and Baragar (1971).

5.1.1 Major elements

The plutonic samples which plot within the syenite field on a total alkalis–silica (TAS) diagram (Figure 5.1) are metaluminous (Figure 5.2). The syenites are silica oversaturated with <4 wt. % normative quartz. They display a limited range in silica content (61 wt. % to 62 wt. %) and little variation for other major oxides (Figure 5.3). MgO and K_2O correlate negatively with SiO_2 whereas FeO* and Na_2O increase with increasing silica. There is no correlation between CaO, MnO, TiO_2 or P_2O_5 with SiO_2.

The Rooivleitjie granite plots in the syenite and granite fields on the TAS diagram (Figure 5.1). Figure 5.2 shows that the granite is peraluminous which is confirmed by the presence of normative corundum. Silica ranges from 71 to 76 wt. % (Figure 5.3) and all major oxides with the exception of MnO and FeO* decrease with increasing SiO_2. FeO* and MnO both increase

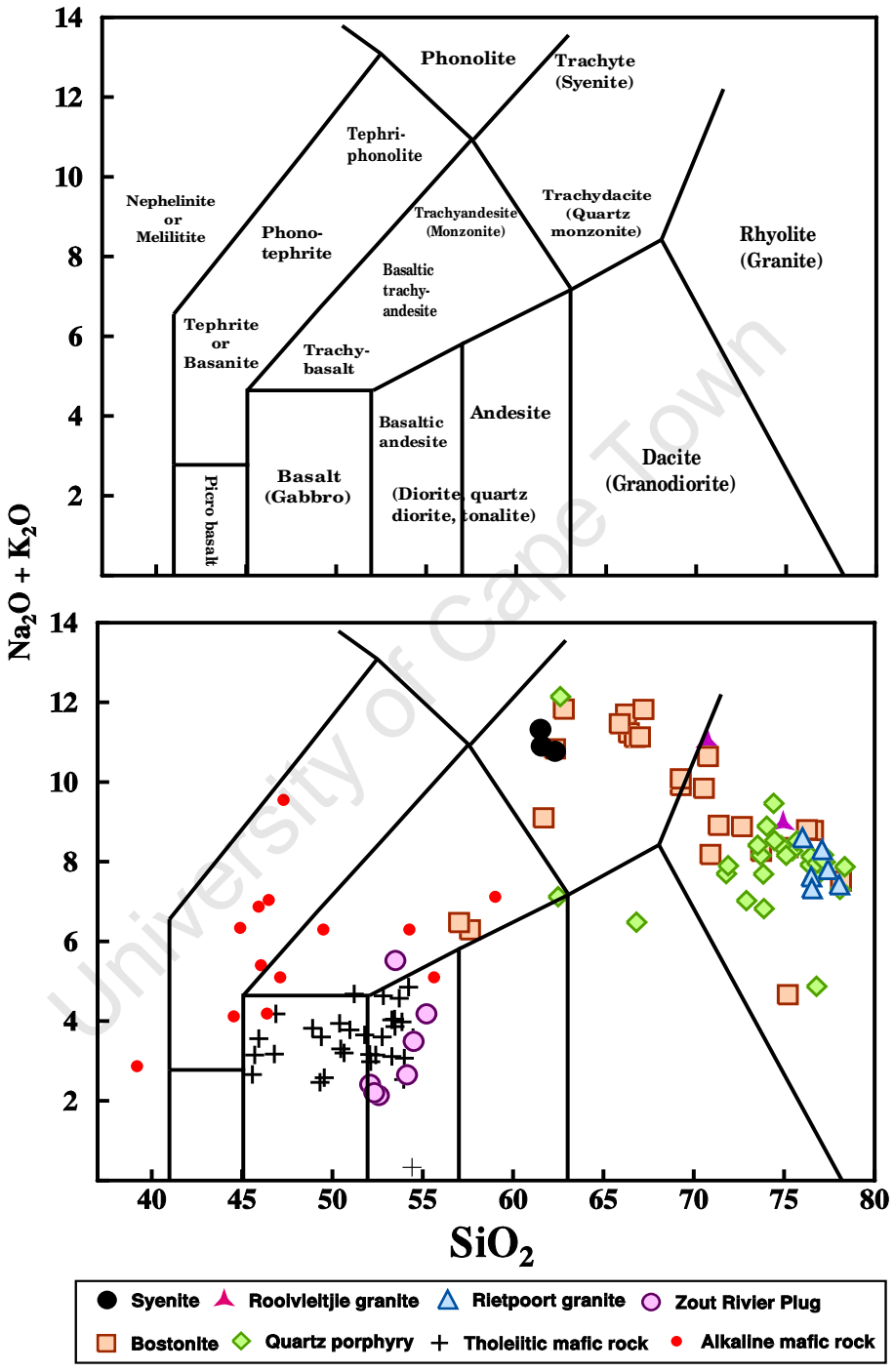

Figure 5.1: Total alkalies–silica diagram with fields taken from LaBas *et al.* (1986) and Best and Christiansen (2001).

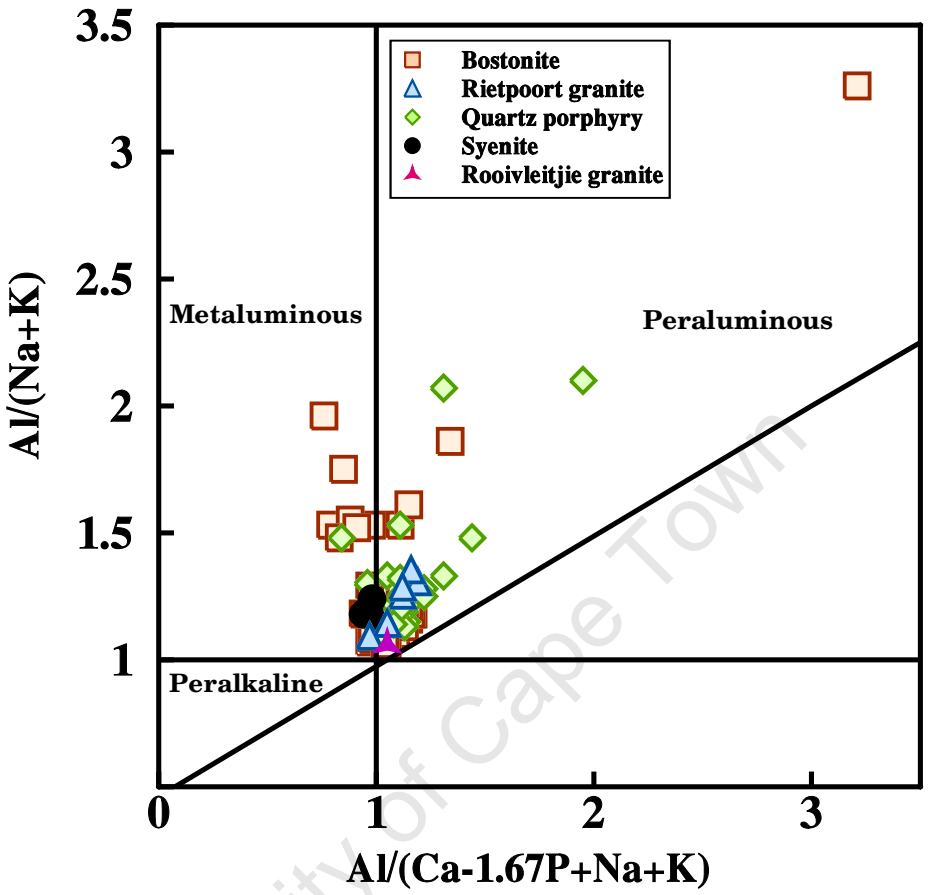

Figure 5.2: Aluminium saturation index (ASI) for all of the Koegel Fontein felsic rocks. The term CaO–1.67P accounts for the presence of apatite and is taken from Frost *et al.* (2001). Fields taken from Shand (1943).

as silica increases.

On the TAS classification the bostonite ranges from basaltic trachy–andesite to trachyte and rhyolite (Figure 5.1). All bostonite samples analysed are silica oversaturated with modal quartz. They range from peraluminous to metaluminous (Figure 5.2) with the majority of samples being peraluminous and corundum normative. The bostonites range from 57 wt. % to 78 wt. % SiO_2 (Figure 5.3). CaO, FeO*, MgO, MnO, P_2O_5 and TiO_2 decrease with increasing SiO_2. Silica has no correlation with Al_2O_3, Na_2O or K_2O.

The quartz porphyries are mostly rhyolitic in composition (Figure 5.1). Three samples plot outside of this field, one in the dacite field, one in the trachyte field and one on the trachy–andesite and andesite boundary. They are peraluminous to metaluminous with the majority of samples being weakly peraluminous (Figure 5.2). This is reflected in the normative mineral-

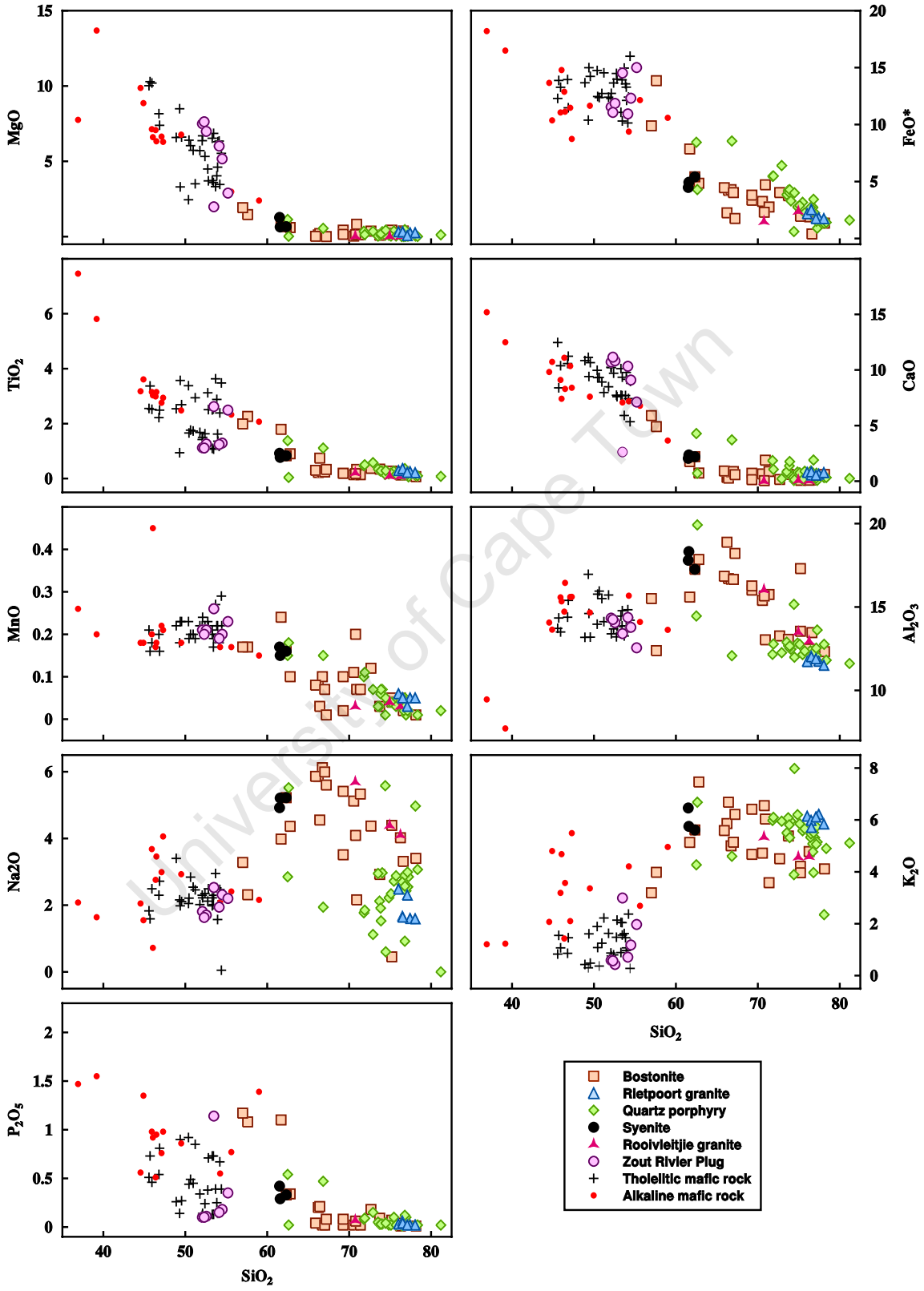

Figure 5.3: Harker diagram for selected major element oxides, of all analysed Koegel Fontein rock types.

ogy with those samples being metaluminous also containing modal diopside. Silica content ranges from 62 to 81 wt. % (Figure 5.3). All major elements except for K_2O and Na_2O have a poor negative correlation with silica. The alkalies have no correlation with SiO_2.

All samples of the Rietpoort granite analysed plot in the granite field on the TAS diagram (Figure 5.1). The granite tends to be relatively homogeneous with a limited range for all major oxide concentrations (Figure 5.3). SiO_2 ranges from 76 to 78 wt. % and has a slight negative correlation with Al_2O_3, MgO, MnO, Na_2O and P_2O_5. There is no correlation for either CaO or K_2O versus SiO_2. TiO_2 and FeO* decrease with increasing silica. The Rietpoort granite has <2% corundum in the norm which agrees with the peraluminous nature of the granite shown in Figure 5.2. However, there is evidence that many rocks from the Koegel Fontein complex have been hydrothermally altered which may have affected the alkali concentrations of these rocks.

The Zout Rivier plug samples are intermediate in composition and range from gabbro to diorite (Figure 5.1). SiO_2 ranges from 52.1 to 55.2 wt. % (Figure 5.3). Silica correlates negatively with Al_2O_3, CaO and MgO whereas FeO*, K_2O, Na_2O and TiO_2 have a slight positive correlation with SiO_2. There is no correlation for MnO or P_2O_5 versus silica. All Zout Rivier plug samples have modal quartz, diopside and hypersthene.

The Koegel Fontein mafic dykes have been divided into two groups tholeiitic and alkaline based on their silica and total alkalis content, normative mineralogy and classification by de Beer (personal comm.). The tholeiitic rocks plot in the basalt to basaltic–andesite fields on the TAS diagram (Figure 5.1). Silica content ranges from 46 to 56 wt. % (Figure 5.3). MgO and CaO have a negative correlation with silica. There is no correlation between any of the other major elements and silica. All tholeiitic samples have modal hypersthene and most samples are silica oversaturated with quartz and diopside in the norm.

The alkaline mafic rocks are predominantly silica undersaturated SiO_2 with concentrations ranging from 37 to 59 wt. % (Figure 5.3). Classification on the TAS diagram ranges from melilitite to phonotephrite and trachyandesite with on sample plotting in the basaltic field and one in the basaltic andesite field (Figure 5.1). The alkaline rocks MgO content ranges from 1.98 to 13.68 wt. % with an average of $6.48 pm 2.98$ wt. %. The MgO content of the tholeiitic rocks ranges from 2.45 to 10.02 wt. % with an average of $5.72 pm 2.06$ wt. %. CaO, MgO and TiO_2 have good negative correlations with silica, with R^2 values of 0.84, 0.71 and 0.68 respectively. FeO* decreases slightly with increasing SiO_2 whereas Al_2O_3 and K_2O increase slightly with increasing silica. There is no correlation for MnO, Na_2O or P_2O_5 versus SiO_2. The majority of samples have normative olivine and nepheline.

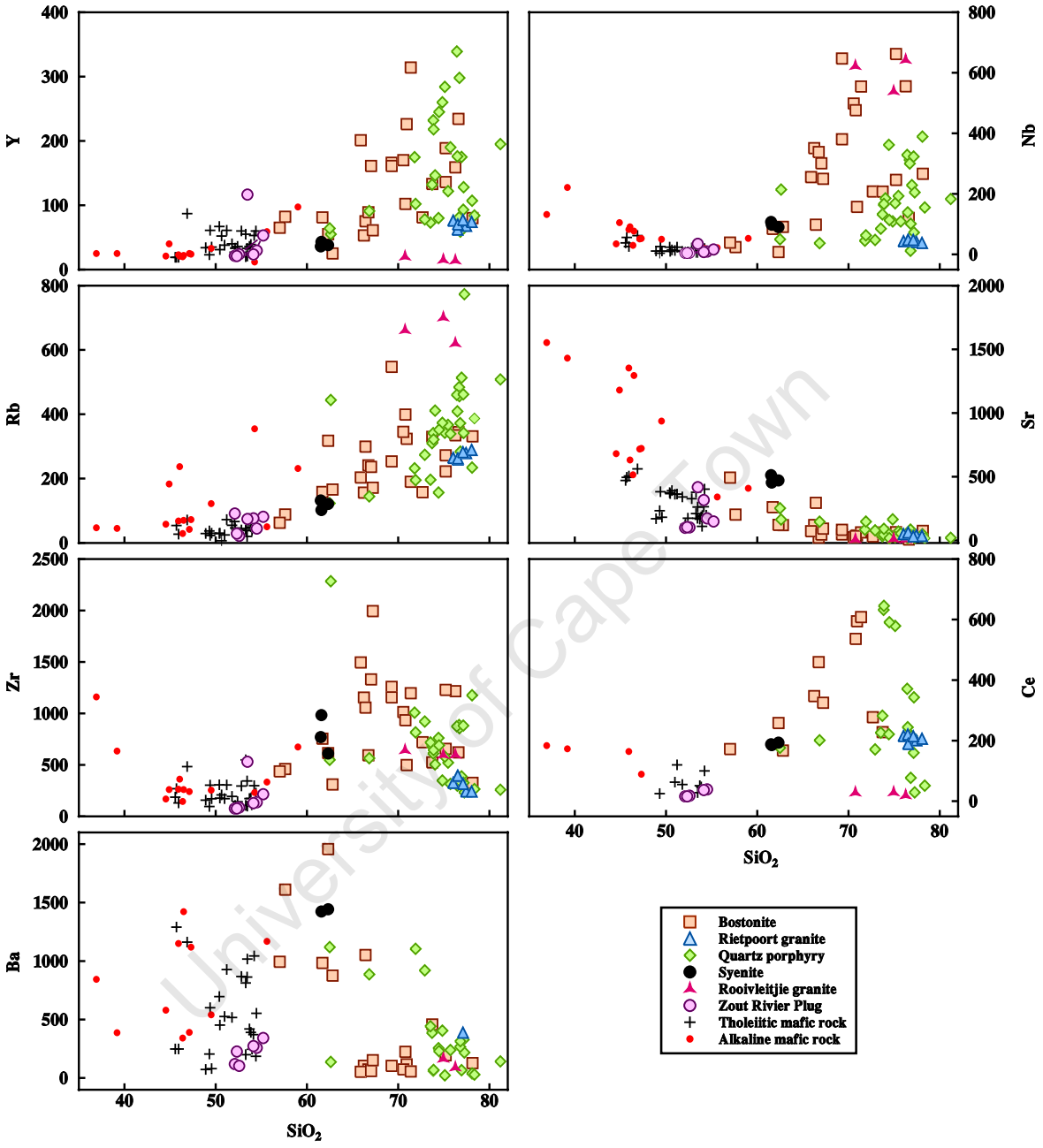

Figure 5.4: Selected trace elements verses silica for all analysed Koegel Fontein rock types. Y, Nb, Rb and Sr were analysed using XRF and ICP–MS. Ce was analysed using only ICP–MS and Zr and Ba were analysed by XRF.

5.1.2 Trace elements

Selected trace elements are plotted against SiO_2 and Zr in Figures 5.4 and 5.5, respectively. The Rietpoort granite and syenite samples show very little variation in trace element concen-

trations.

The high field strength element (HFSE) Nb increases slightly with increasing silica whereas Zr has a negative correlation with SIO_2 for the quartz porphyry samples (Figure 5.4). Niobium has a positive correlation with Zr for these rocks (Figure 5.5). Zirconium in the bostonite samples increases with increasing silica between 57 and 68 wt. % SiO_2 after which it begins to decrease (Figure 5.4). Niobium has a positive correlation with both silica and Zr for the bostonites (Figure 5.5). Both HFSE decrease with increasing SiO_2 in the Rietpoort granite (Figure 5.4). Zirconium and Nb have a good positive correlation with an $R^2 = 0.7$ for the Rietpoort granite (Figure 5.5). The Rooivleitjie granite has a positive correlation for Zr with both silica and Nb. Niobium has no correlation with silica (Figures 5.4 and 5.5). Syenite samples show a negative correlation between Zr and silica (Figure 5.4). Only two syenite samples have Nb data, however, Nb has an apparent negative correlation with Zr and no correlation with silica (Figures 5.4 and 5.5). Samples of the Zout Rivier plug show a slight increase in Nd ($R^2 = 0.13$) and Zr ($R^2 = 0.08$) with increasing silica (Figure 5.4). Niobium has an excellent positive correlation with Zr with an R^2 of 0.99 (Figure 5.5). Niobium has a negative correlation with SiO_2 and a positive correlation with Zr for both the tholeiitic and alkaline mafic rocks (Figures 5.4 and 5.5). Zirconium has no relationship with silica for these samples.

There is a slight increase in Ce and Y with increasing SiO_2 for the bostonites (Figure 5.4). Neither Ce or Y correlate with Zr (Figure 5.5). Ce and Y have no correlation with Zr or silica for the quartz porphyries (Figures 5.4 and 5.5). The Rietpoort granite samples show no correlation between either Y or Ce with SiO_2 (Figure 5.4). Y has a slight positive correlation with Zr whereas Ce and Zr have no relationship for the granite (Figure 5.5). Ce and Y have no correlation with silica for the syenites (Figure 5.4). Yttrium increases and Ce decreases with increasing Zr for these rocks (Figure 5.5). Both Ce and Y have a negative correlation with silica for the Rooivleitjie granite (Figure 5.4). Ce increases slightly with increasing Zr ($R^2 = 0.15$) while Y has a good possitive correlation with Zr ($R^2 = 0.96$) for the granite (Figure 5.5). The Zout Rivier plug samples show no relationship between Y and SiO_2 and a positive correlation for Y and Zr (Figures 5.4 and 5.5). Ce has an excellent positive correlation with both SiO_2 and Zr with R^2 values of 0.99 and 1 respectively (Figures 5.4 and 5.5). Samples of the tholeiitic mafic dykes show no correlation between either Y or Ce with SiO_2 (Figure 5.4). Both elements have a positive correlation with Zr (Figure 5.5). Ce versus Zr for the tholeiitic rocks has an R^2 of 0.99. Y has a positive correlation with both silica and Zr for the alkali mafic rocks (Figures 5.4 and 5.5). Ce decreases with increasing SiO_2 and increases with Zr (Figures 5.4 and 5.5).

Ba and Sr have a negative correlation and Rb has a positive correlation with SiO_2 for the

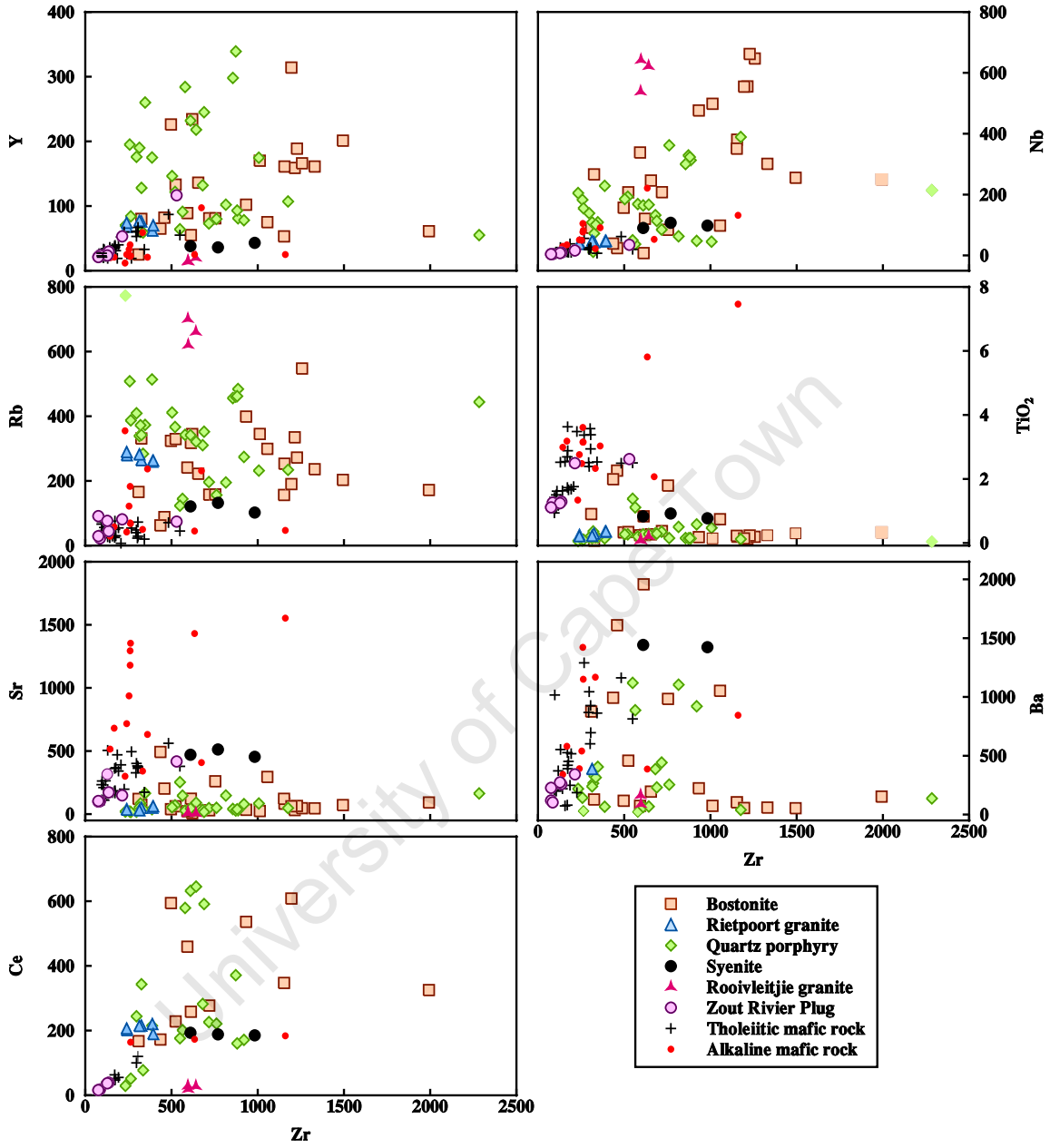

Figure 5.5: Selected trace elements plotted against Zr for all Koegel Fontein rock types.

bostonites (Figure 5.4). Neither Rb or Sr correlate with Zr whereas Ba decreases with increasing Zr (Figure 5.5). The quartz porphyries show negative correlations for Ba and Sr versus silica and a positive correlation between Rb and SiO_2 (Figure 5.4). None of the large ion lithophile elements (LILE) correlate with Zr (Figure 5.5). Rb has a positive correlation with silica and a negative correlation with Zr in the Rietpoort granite whereas the inverse is true for

Sr (Figures 5.4 and 5.5). Only one Rietpoort sample has data for Ba. There is no correlation between Rb and SiO_2 for the syenites (Figure 5.4). Sr decreases with increasing silica in these rocks. Both Rb and Sr decrease with increasing Zr (Figure 5.5). There is insufficient data (two points) to determine a correlation for Ba with silica or Zr. Ba was not analysed by XRF at UCT where one syenite sample, CCK18, was analysed. The Rooivleitjie granite shows on relationship for Rb versus SiO_2 (Figures 5.4 and 5.5). Sr has a positive correlation with silica and a negative correlation with Zr (Figures 5.4 and 5.5). Samples from the Zout Rivier plug show a positive correlation between both Sr and Ba versus silica whereas Rb has no relationship with SiO_2 (Figure 5.4). All three LILE correlate positively with Zr (Figure 5.5). Ba and Rb have no relationship with silica for the tholeiitic mafic rocks (Figure 5.4). Sr decreases with increasing SiO_2. Sr and Ba have a positive correlation with Zr and Rb has no correlation with Zr (Figure 5.5). The alkali mafic rocks have a negative correlation between Sr and SiO_2 and a slight positive correlation between Rb and silica, $R^2 = 0.12$ (Figure 5.4). Ba has no correlation with silica. Neither Ba, Rb or Sr correlate with Zr (Figure 5.5).

Figure 5.6 shows the relationships between Ba, Rb and Sr. There is insufficient Ba data for the Rietpoort granite, syenites and the Rooivleitjie granite to determine correlation coefficients. Rubidium and Sr have a negative correlation for the Rietpoort granite, quartz porphyries, bostonites and alkali mafic rocks (Figure 5.6A). There is a positive correlation between the two LILE for the syenites, Rooivleitjie granite and Zout Rivier plug and no correlation between Rb and Sr for the tholeiitic mafic rocks (Figure 5.6A). Barium increases with increasing Sr for the quartz porphyries, bostonites, Zout Rivier plug and tholeiitic mafic rocks whereas there is no correlation between the two elements for the alkali mafic rocks (Figure 5.6B). There is no relationship between Ba and Rb for the bostonites, Zout Rivier plug, tholeiitic mafic rocks and alkali mafic rocks (Figure 5.6C). Barium and Rb have a slight negative correlation with a R^2 value of 0.27 for the quartz porphyries.

Rare earth elements (REE) have been normalized using the values for Chondrite Meteorites (Sun and McDonough, 1989). All REE values and ratios referred to henceforth are Chondrite normalized. The syenites and three bostonites have similar REE patterns with no Eu anomaly (Figure 5.7A). Most of the bostonite samples have a negative Eu anomaly and higher REE concentrations than the syenites and syenite–like bostonites (Figure 5.7A). All the bostonites and syenites are enriched in light rare earth elements (LREE) compared to heavy rare earth elements (HREE). The Rooivleitjie granite has a "gull wing" type REE pattern where the middle rare earth elements (MREE) are depleted relative to the LREE and HREE (Figure 5.7A). The Rooivleitjie granite also has a pronounced negative Eu anomaly.

There is almost no variation in REE concentrations and REE patterns for the Rietpoort granite

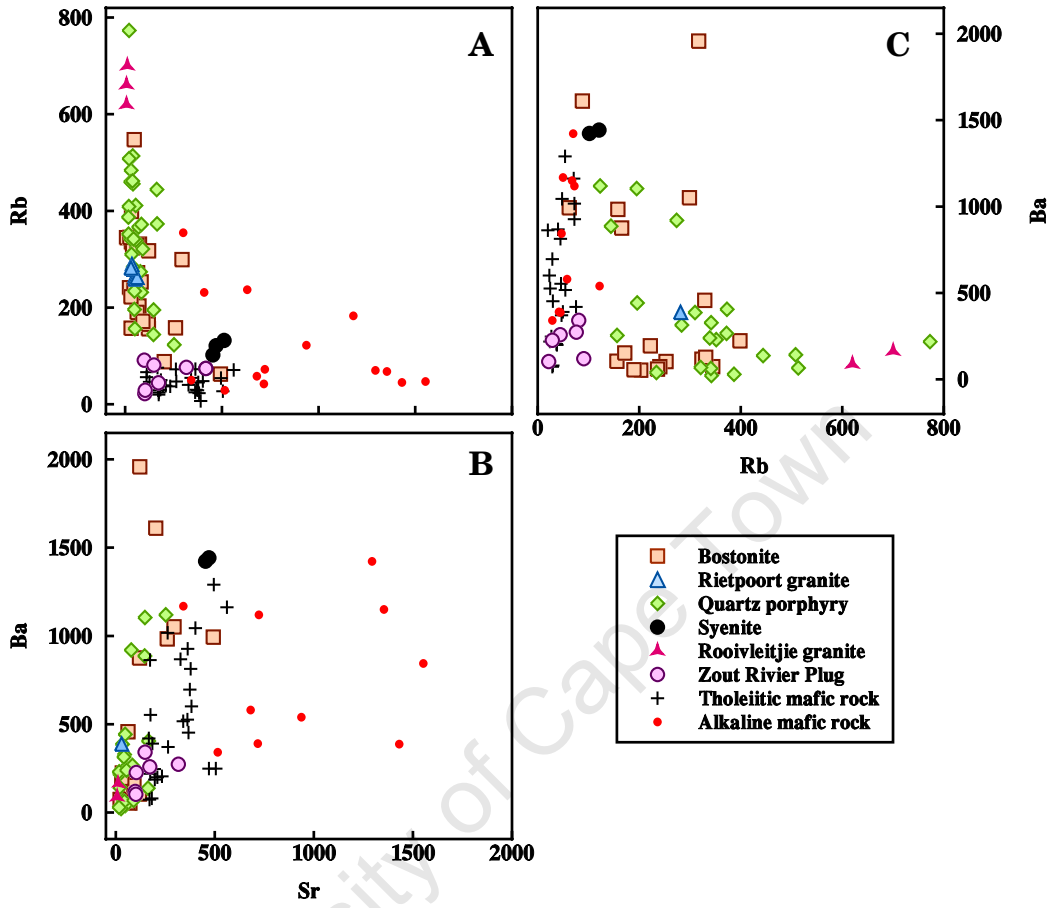

Figure 5.6: Relationships between the large ion lithophile elements Ba, Rb and Sr for all of the Koegel Fontein rock types analysed. Ba was analysed by XRF at the GFZ while Sr and Rb were analysed by XRF at the GFZ and UCT and by ICP–MS at the GFZ.

(Figure 5.7B). All of the granite samples have a moderate negative Eu anomaly and are enriched in LREE relative to HREE. Most of the quartz porphyry samples have the same REE pattern as the Rietpoort granite only with higher REE concentrations and in some cases a larger negative Eu anomaly (Figure 5.7B). There are three quartz porphyry samples which have the "gull wing" REE pattern (Figure 5.7B).

Samples from the Zout Rivier plug have a large variation in LREE concentrations whereas the HREE are relatively homogeneous (Figure 5.7C). Samples with higher LREE concentrations have a slight negative Eu anomaly and these samples overlap with the tholeiitic mafic rocks. The tholeiitic mafic rocks have relatively flat REE patterns (La/Yb = 2 to 15) and a wide range in REE concentrations (Figure 5.7C). Samples with the highest REE concentrations have small

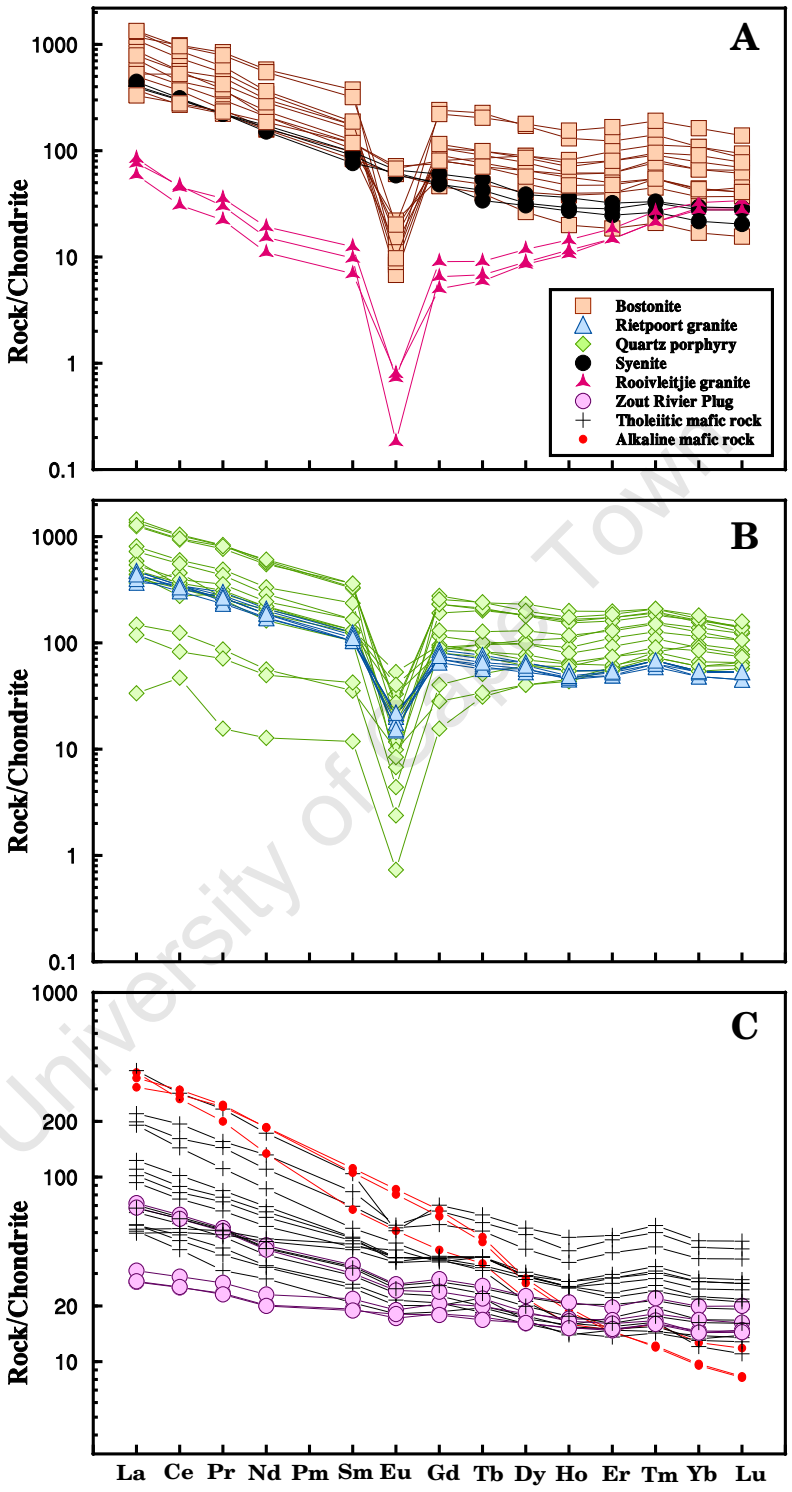

Figure 5.7: Chondrite normalised REE patterns. A. Syenites, bostonites and Rooivleitjie granite REE patterns. B. Rietpoort granite and quartz porphyries REE patterns. C. REE patterns of the tholeiitic and alkali mafic rocks. Chondrite values are taken from Sun and McDonough (1989).

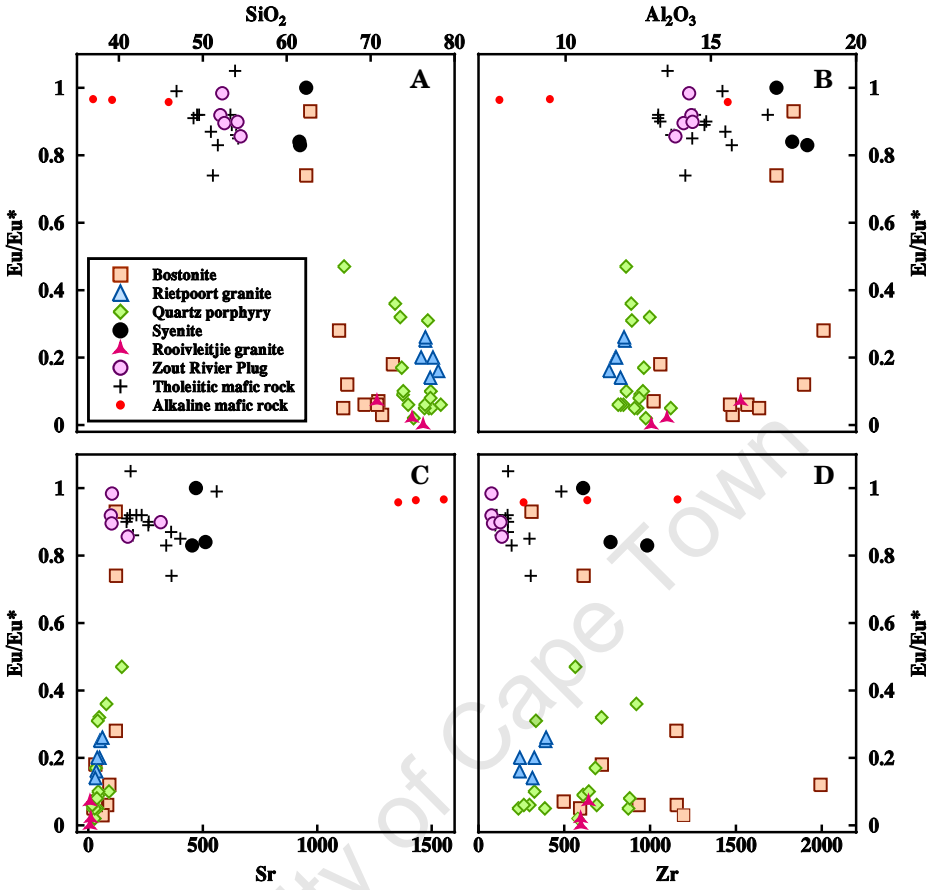

Figure 5.8: Eu/Eu* plotted with other elements and oxides which are common in feldspars. All values are whole–rock data. Eu/Eu* = Eu/(Sm+Gd). The ratio was calculated using Chondrite normalized data.

negative Eu anomalies. The alkali mafic rocks have steep REE patterns (La/Yb = 29 to 35) and are HREE depleted (Figure 5.7C).

The negative Eu anomaly of the Koegel Fontein rock types show a bimodal distribution (Figure 5.8). The mafic rocks, syenites and two bostonite samples (CDB683 and CDB702) have little or no Eu anomaly and a relatively high Eu/Eu* ratio (0.93 and 0.74, respectively). Whereas the remaining bostonites, quartz porphyries and granites have a pronounced negative Eu anomaly and corresponding lower Eu/Eu* ratio (0.01 to 0.47). All graphs plotted in Figure 5.8 have a bostonite outlier (CDB719) which has a Eu/Eu* value of 5.7 and is not shown. The Rietpoort and Rooivleitjie granites, bostonites, Zout Rivier plug and alkali mafic rocks have a negative correlation between SiO_2 and Eu/Eu* (Figure 5.8A). Silica and Eu/Eu* have a positive correlation for the syenites whereas the quartz porphyries and tholeiitic mafic rocks have no relationship between the two parameters (Figure 5.8A). Eu/Eu* increases with increasing

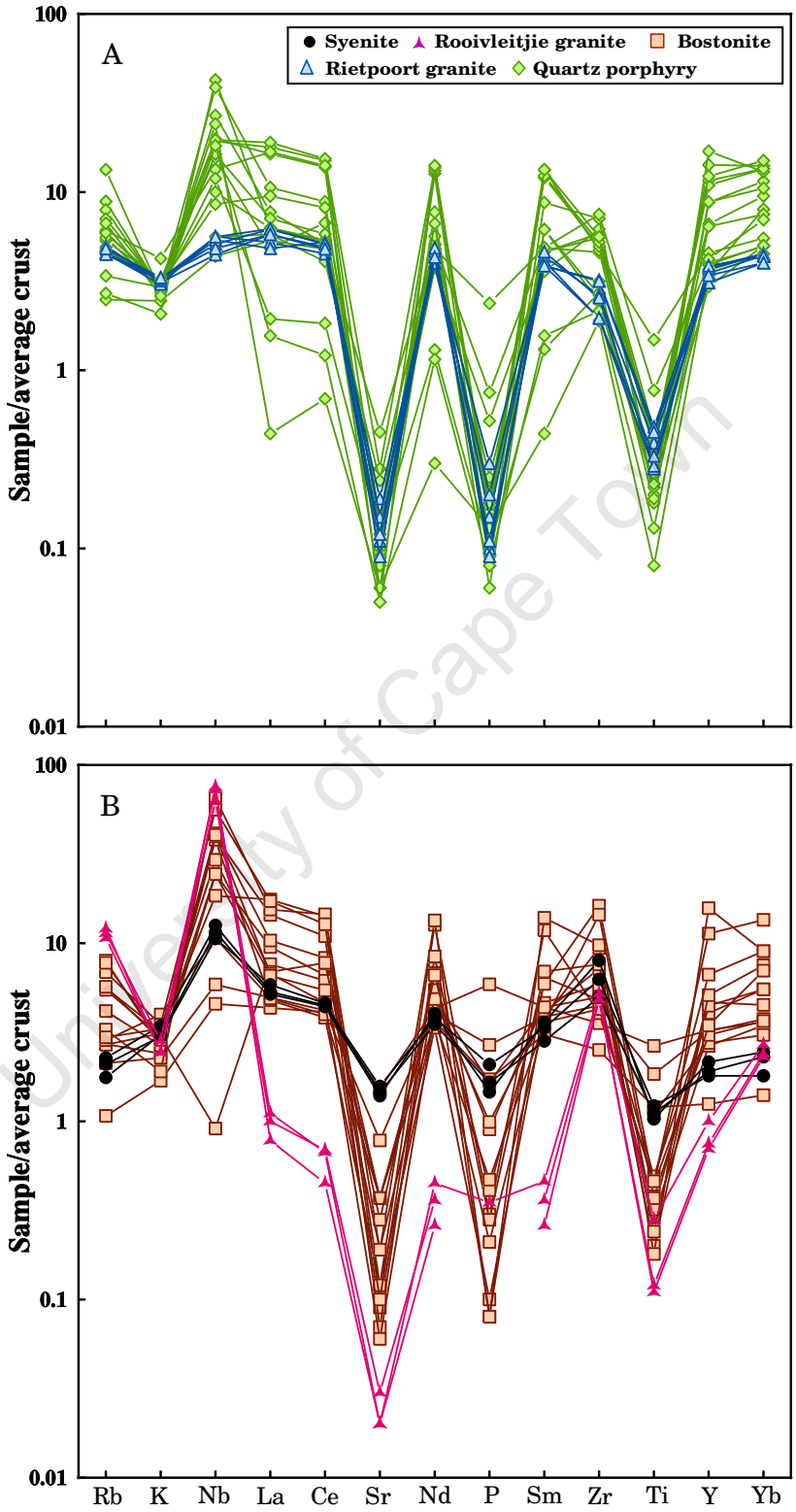

Figure 5.9: Trace element spider diagrams for all analysed Koegel Fontein felsic rocks.

Al_2O_3 for both granites, the quartz porphyries, bostonites and the Zout Rivier plug (Figure 5.8B). The syenites and alkali mafic rocks have a negative correlation between Eu/Eu* and Al_2O_3 (Figure 5.8B). There is no correlation between Eu/Eu* and Al_2O_3 for the tholeiitic mafic rocks (Figure 5.8B). Strontium and Eu/Eu* have a positive correlation for the Rietpoort granite, bostonites and alkali mafic rocks whereas the tholeiitic mafic rocks and Zout Rivier plug have a negative correlation between the Sr and Eu/Eu* (Figure 5.8C). The quartz porphyries, syenites and Rooivleitjie granite show no correlation between Sr and Eu/Eu* (Figure 5.8C). Eu/Eu* increases with increasing Zr for the Rietpoort and Rooivleitjie granites and the alkali mafic rocks (Figure 5.8D). The syenites, quartz porphyries, bostonites, Zout Rivier plug and tholeiitic mafic rocks have a negative correlation between Eu/Eu* and Zr (Figure 5.8D).

Figure 5.9 shows trace element patterns for the felsic units from Koegel Fontein. The Rietpoort granite has little variation in element concentrations between samples (Figure 5.9A). It has pronounced negative Sr, P and Ti anomalies and a slightly negative K anomaly. The Quartz porphyries have wide range in element concentrations and a very similar pattern to the granite with negative Sr, P, Ti and K anomalies (Figure 5.9A). Unlike the granite the quartz porphyries have a positive Nb anomaly. There are three samples which have lower REE concentrations but they follow the same pattern as the quartz porphyry samples with high concentrations.

The syenites have almost no variation in element concentrations between samples (Figure 5.9B). They have slight negative Rb, Sr, P and Ti anomalies whereas Nb and Zr have positive anomalies. There is a wide range in element concentrations for the bostonites (Figure 5.9B). The majority of bostonite samples have pronounced negative Sr, P and Ti and positive Nb anomalies. There are two samples with similar patterns to the syenites and one sample with a low Nb content. The Rooivleitjie granite has lower REE. concentrations than the syenites and bostonites, although, they still follow the same trace element pattern as the other rock types (Figure 5.9B). The granite has positive Rb and Nb and negative Sr and Ti anomalies. The P content is very low with the majority of samples being below the detectable limit of the XRF.

Table 5.3: Stable isotopes. All data is recorded in ‰ and has been calculated relative to SMOW.

		δ^{18} O						δ D			
Sample	Rock type	Whole rock	Groundmass	Quartz	Quartz phenocrysts	Feldspar	Amphibole	Whole rock	Amphibole	Biotite	Water (wt%)
CCK1	Pan African vein	10.7									
CCK2	Banded gneiss	8.8						-75			0.6
CCK3	Bostonite	3.3						-65			0.7
CCK4	Quartz porphyry	5.2						-101			0.7
CCK5	Pan African vein	10.2									
CCK6	Tholeiitic mafic rock	2.6						-101			2.5
CCK7	Quartz porphyry	3.5				5.7		-102			0.1
CCK8	Banded gneiss	9.6						-173			
CCK9	Augen gneiss	5.6						-101			0.6
CCK10	Quartz porphyry	6.8						-111			0.8
CCK11	Tholeiitic mafic rock	1.3						-97			2.6
CCK12	Quartz porphyry	6.6			8	3.2		-184			0.1
CCK13	Pan African shear zone	10.1						-97			0.7
CCK14	Amphibolite	4.6						-122			1.4

continued . . .

		δ^{18} O						δ D			
Sample	Rock type	Whole rock	Groundmass	Quartz	Quartz phenocrysts	Feldspar	Amphibole	Whole rock	Amphibole	Biotite	Water (wt%)
CCK15	Bostonite	6.3						-97			0.4
CCK16	Pan African vein	9.9									
CCK17	Rooivleitjie granite	4.1		7.9		1.8		-95			0.2
CCK18	Syenite	6.5						-113			0.4
CCK19	Rietpoort granite	8.8		8.9	8.2	8.2		-108			0.2
CCK20	Augen gneiss	-2.8						-112			
CCK21	Melilitite	-4.1						-112			
CCK22	Augen gneiss	0.2						-105			
CCK23	Quartz porphyry	1			1.2	0.4		-110			0.5
CCK25	Schist	17.4						-84			0.8
CCK26	Bostonite	2.2						-110			1
CCK27	Augen gneiss	8.2						-111			0.5
CCK28	Schist	8.1						-93			1.4
CCK29	Pan African vein	10.1									
CCK30	Augen gneiss	3.6						-89			2.1
CCK31	Bostonite	4.2						-94			2.3
CCK32	Quartz porphyry	2.6						-95			0.9
CCK33	Tholeiitic mafic rock	3.9						-103			1.7
CCK34	Amphibolite	-3						-120			1

continued . . .

		δ^{18} O						δ D			
Sample	Rock type	Whole rock	Groundmass	Quartz	Quartz phenocrysts	Feldspar	Amphibole	Whole rock	Amphibole	Biotite	Water (wt%)
CCK35	Tholeiitic mafic rock	-1.7						-97			2.1
CCK36	Tholeiitic mafic rock	-3.1		8		-1.5		-94			2.5
CCK37	Bostonite	-2.2						-103			2.1
CCK38	Tholeiitic mafic rock	-2.9						-106			4.6
CCK39	Tholeiitic mafic rock	-1.2						-111			2.1
CCK40	Pan African vein	9.6									
CCK41	Cretaceous quartz vein	-1.5						-107			0.5
CCK42	Cretaceous quartz vein	2.2						-118			0.5
CCK43	Cretaceous quartz vein	-1.4						-111			0.3
CCK44	Cretaceous quartz vein	-1.7						-85			0.7
CCK45	Augen gneiss	3.2						-110			0.6
CCK46	Augen gneiss	1.1						-106			0.5
CCK47	Tholeiitic mafic rock	-2.2						-94			2
CCK48	Cretaceous quartz vein	-0.9						-101			0.3
CCK49	Pan African vein	9.2									
CCK50	Pan African vein	5.6									
CCK51	Rietpoort granite	7.9		7.7	8.4	8.0		-117			0.3
CCK52	Rietpoort granite	5.7		7.7	7.4	5.8		-134			0.2
CCK53	Rietpoort granite	7.4				6.8		-104			0.3

continued . . .

		δ^{18} O						δ D			
Sample	Rock type	Whole rock	Groundmass	Quartz	Quartz phenocrysts	Feldspar	Amphibole	Whole rock	Amphibole	Biotite	Water (wt%)
CCK54	Augen gneiss	2.6						-95			0.3
CCK55	Rietpoort granite	7.2		8.7	8.5	7.9		-115			0.2
CDB336	Quartz porphyry	6.4	6.4	9.4				-91			0.9
CDB383	Quartz porphyry	7.1		8.8	9.1	4.3		-80			0.8
CDB388	Quartz porphyry	6.1						-67			0.7
CDB541	Quartz porphyry	5.1						-83			0.5
CDB564	Quartz porphyry	4.2			8.8	1.5		-91			0.6
CDB572	Quartz porphyry	0.3		0.5	1.8	-0.7		-123			0.1
CDB580	Quartz porphyry	3.1			4.5	2.1		-105			0.2
CDB588	Quartz porphyry	-1			1.6	-1.5		-104			0.3
CDB594	Quartz porphyry	-0.3	-1.1	3.2	1.7	-2.6		-124			0.2
CDB601	Quartz porphyry	1.2						-111			0.2
CDB604	Quartz porphyry	-1	-0.2					-81			0.4
CDB639	Quartz porphyry	-0.3						-91			0.5
CDB650	Quartz porphyry	1.4	1.2	8.5	8.3	0.6		-107			1.6
CDB678	Bostonite	4.1						-68			0.3
CDB681	Bostonite	-2.9						-90			2
CDB683	Bostonite	2.5						-100			0.6
CDB687	Rooivleitjie granite	5.8			7.8	3.7		-86			0.2

continued . . .

		δ^{18} O						δ D			
Sample	Rock type	Whole rock	Groundmass	Quartz	Quartz phenocrysts	Feldspar	Amphibole	Whole rock	Amphibole	Biotite	Water (wt%)
CDB703	Syenite	8.5			8	7.1	5.6	-107		-114	0.5
CDB753	Syenite	7.6		8.5		7.5	6.3	-81	-90	-94	0.4
CDB825	Rietpoort granite	15.3			8.7	8.3		-95			0.3
CDB1491	Tholeiitic mafic rock	5.9						-82			1.2
CN495	Bostonite	4.7	4.7	8.5	8.8	3.3		-96			0.6

5.2 Stable isotopes

Oxygen and hydrogen isotope ratios for whole–rock, groundmass and mineral separates are presented in Table 3. The mineral separates include quartz, feldspar, biotite and amphibole. Quartz separates were divided into two groups one showing the "high quartz" double pyramid crystal form and assumed to be quartz phenocrysts or magmatic quartz in plutonic rocks. The "high quartz" form is typical of quartz which has crystallized at high temperature (¿600°C). The second group was characterised by anhedral grains and interpreted to be broken or corroded phenocrysts, xenocrysts or veins. Feldspar separates probably consist of a mixture of plagioclase and alkali feldspar. Fresh amphibole and biotite were only analysed from the syenite. There was not enough fresh material in the granites, quartz porphyry or bostonite samples for analysis. Fine–grained material, groundmass, was separated from phenocryst phases for the fine grained rock types.

The δ^{18}O values of whole rock–samples range from, -4.1‰ to +17.4‰, (mean: 4.0 ± 1.0‰, n = 76, all errors are calculated using the 95% confidence limit). The majority of samples have δ^{18}O values <6‰ (Figure 5.10A and 5.11A). The lowest oxygen ratio (-4.1‰) was from a diatreme with an intermediate composition from the centre of the complex (CCK21). Gariep schist (CCK25) had the highest oxygen ratio.

Whole–rock powders from the Rietpoort granite range from +5.7 to +15.3‰ and syenites range from +6.5 to +8.5 ‰ (Figure 5.11B). Samples analysed from the Rooivleitjie granite have δ^{18}O values of +4.1 and +5.8‰ (Figure 5.11B). Oxygen isotope ratios for the bostonites and quartz porphyries range from -2.9 to +7.1‰ (Figure 5.11B).

Whole–rock powders of the tholeiitic mafic rocks where analysed. The oxygen isotope ratios range from -3.1 to +5.9‰ (Figure 5.11B). All of the samples analysed have δ^{18}O values less than the mantle (<5.7‰).

low δ^{18}O values ranging from -1.73 to -0.88‰. Those veins presumed to be older than the Koegel Fontein complex have δ^{18}O ranging from 5.6 to 10.7‰. The relative ages of the quartz veins are based on field relationships.

The wide range in δ^{18}O values seen for the whole–rocks is also present in the mineral separates (Figure 5.11A). Oxygen–isotope ratios for non–phenocryst quartz ranges between +0.5‰ and +9.4‰, although, quartz phenocrysts show a slightly narrower range of +1.2 to +9.0‰. Feldspar δ^{18}O values range from -2.6‰ to +8.3‰ (Figure 5.11A). There is very little difference in δ^{18}O between the amphibole separates (6.3‰ and 5.6‰) as both were taken from

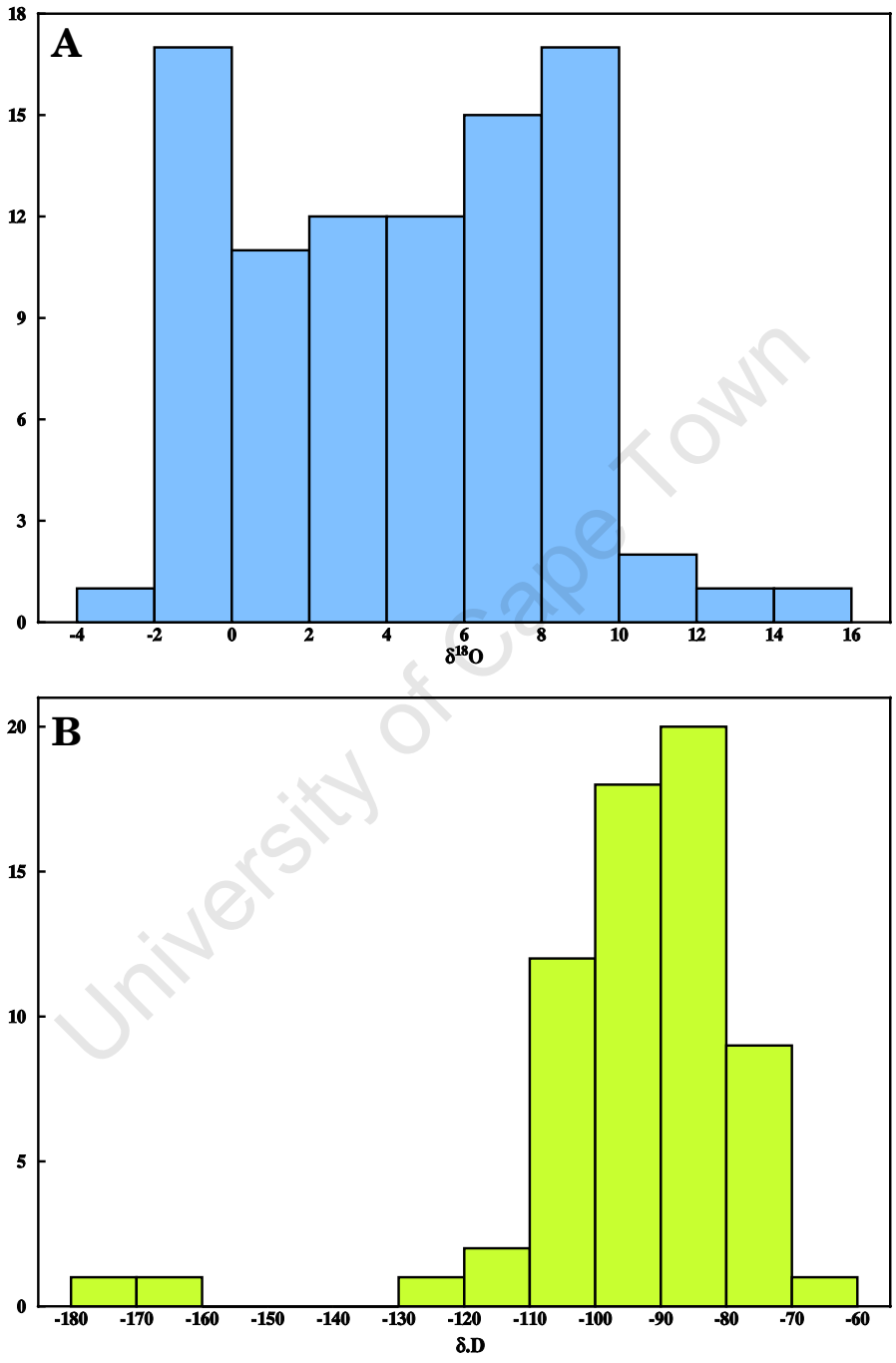

Figure 5.10: Stable isotope histograms for all samples analysed and includes both whole rock and mineral separate data. All data normalised to SMOW. A. Oxygen B. Hydrogen.

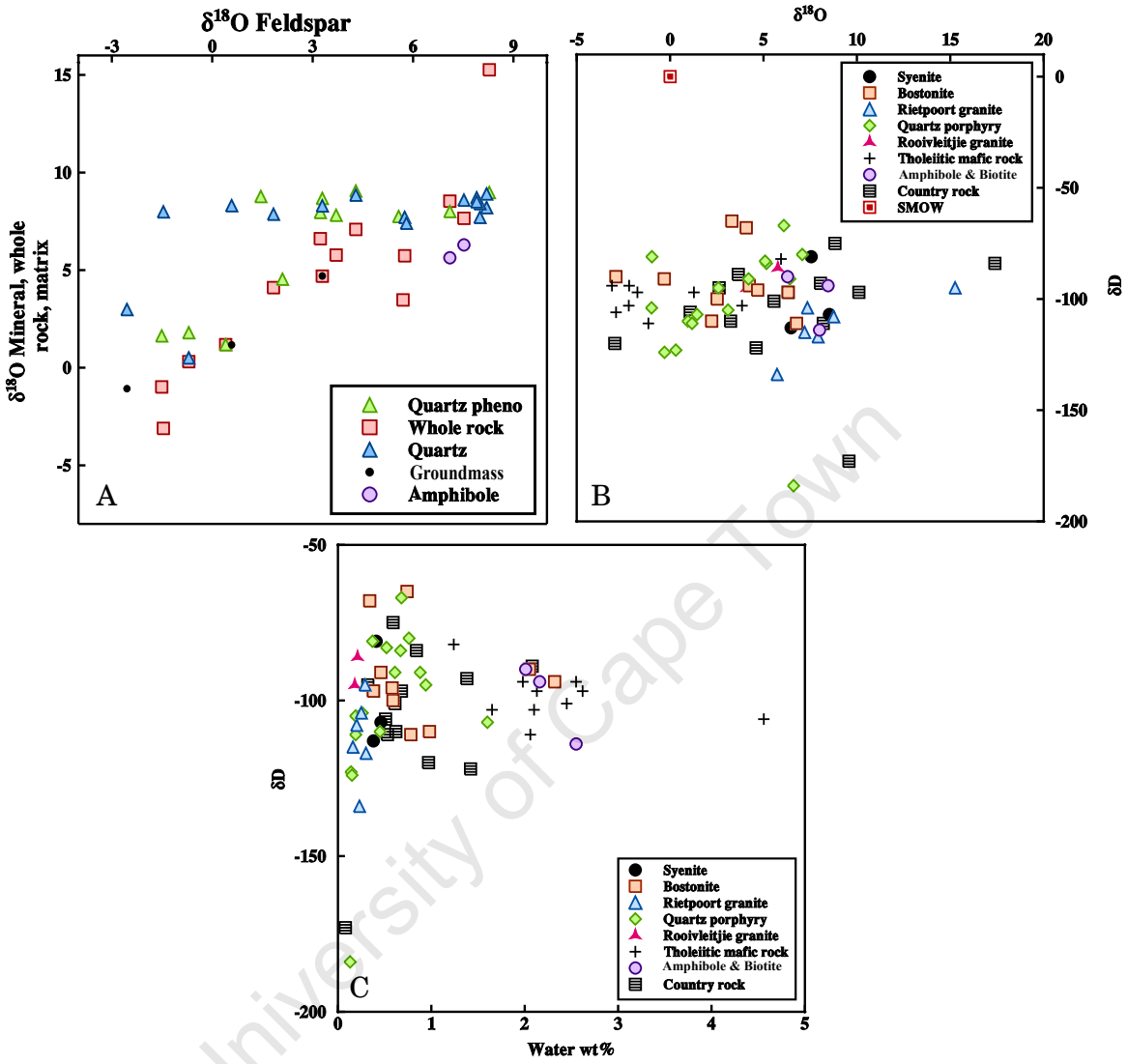

Figure 5.11: Stable isotope results. A. Oxygen isotope data for whole rock and mineral separates from the Koegel Fontein felsic rocks. B. δD and δ^{18} values for whole rock and minerals separates plotted with SMOW. C. Whole rock δD and water content for all Koegel Fontein rock types.

syenite which also has relatively uniform δ^{18}O quartz and feldspar values (δ^{18}O of the quartz = +8.0 and +8.5‰; δ^{18}O of the feldspar = +7.5 and +7.1‰: Figure 5.11A). There is an apparent positive correlation between the δ^{18}O of the feldspar and the δ^{18}O of the whole rocks which is expected as the majority of the Koegel Fontein rock types are comprised mostly of feldspar.

Where measured the δ^{18}O values of the groundmass (+6.37 to -1.07‰) were similar to those of the associated phenocryst phases (Figure 5.11A). There is a finite difference between the phenocryst and groundmass δ^{18}O values caused by fractionation between the magma and the

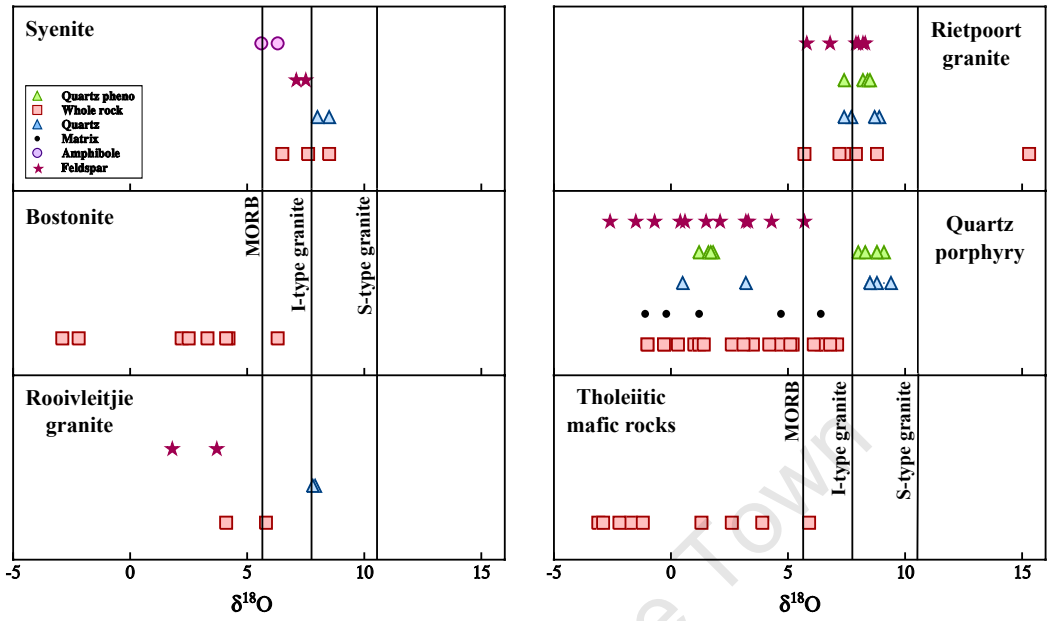

Figure 5.12: A comparison between mineral separates, whole–rock and matrix oxygen isotope data. Samples are plotted with the average values for I– and S–type granites (Harris *et al.*, 1997) and the $\delta^{18}O$ value of the mantle

crystals. Small differences between the δ^{18}O of the magma (groundmass) and the δ^{18}O of the phenocrysts would indicate that the phenocrysts were in equilibrium with the magma and not inherited.

A comparison between the different oxygen isotope data, whole–rock and mineral separates, is shown in Figure 5.12. The whole–rock, groundmass and feldspar data tend to be very similar. This is expected, as most Koegel Fontein rock types are comprised predominantly of feldspar. The quartz and quartz phenocryst δ^{18}O values are very similar. The quartz porphyry, mineral separate δ^{18}O values show tow distinct groups for the quartz and quartz phenocryst data. There is one group with δ^{18}O values lower than that of the mantle (<5.7‰) and the second has δ^{18}O values similar to the average value of I-type granites. The unusual nature of the low δ^{18}O mineral separates will be discussed in detail in Chapter 6.2.

Whole–rock δD ranges from -65‰ to -184‰ with an average of -102 ± 4‰ (n = 69: Figure 5.10B). A quartz porphyry sample had the lowest δD value measured. The whole–rock δD values for all the Koegel Fontein rock types have a wide variation (Figure 5.11B). Biotite and amphibole separates had similar δD values (δD biotite = -114 and -94‰ and δD amphibole = -90‰). Although, there was variation between the biotite samples. Whole–rock and mineral δD and δ^{18}O values are plotted in Figure 5.11B. The majority of samples fall between δD =

-134 and -65‰ and $\delta^{18}O$ = -4.1 and +10‰. There is no correlation between δD and $\delta^{18}O$.

There is a wide range in water content (0.1 to 4.6wt%) for all samples analysed (Figure 5.11C). The two samples with the lowest δD values (-173 and -184‰) also have very low water content (Figure 5.11C). This is expected when samples have been contaminated by the blank which has a very low δD. These samples are ignored when interpreting the hydrogen–isotope data.

5.3 Radiogenic isotopes

The 20 samples chosen for radiogenic isotope analysis encompass the wide range of oxygen isotope values and are representative of the Koegel Fontein felsic rocks. The syenite, Rooivleitjie granite and bostonite dykes are the oldest rocks in the complex while the Rietpoort granite and quartz porphyry dykes are the youngest. The two basement samples were chosen to give an indication as to how the country rock around Koegel Fontein compares to other rocks of Namaqua age. The element concentration data, measured ratios, calculated initial ratios and epsilon values for Sr, Nd and Pb are shown in Table 4. The regression, MSWD (best fit), $^{87}Rb/^{86}Sr$, initial Sr and Pb ratios and ϵNd values were calculated using GEODATE version 1.3 (Eglington and Harmer, 1999). The regression techniques used by GEODATE are based on those of York (1969), William (1968) and Titterington and Halliday (1979). The aim of the radiogenic isotope study was to look at whether the isotope systems have undergone open system behaviour and to help interpret the stable isotope results. Radiogenic isotopes were not analysed as a geochronological exercise.

The measured Sr–isotope data are displayed in Figure 5.13. $^{87}Rb/^{86}Sr$ was calculated using ICP–MS data. Blanket errors for $^{87}Rb/^{86}Sr$ (1%) and $^{87}Sr/^{86}Sr$ (0.006%) were used. The MSWD for all the regressions was larger than the critical F value and any date obtained is subject to high uncertainty. The Rietpoort granite and quartz porphyry samples all plot close to or on the regression line (Figure 5.13A.). These samples have a wide range of $^{87}Rb/^{86}Sr$ and the measured $^{87}Sr/^{86}Sr$ values and very little scatter in for the initial $^{87}Sr/^{86}Sr$ ratios (Figure 5.13A and 5.14). The regression line for the syenite, bostonite and Rooivleitjie granite was calculated excluding sample CDB552 as this decreased the MSWD by ten fold, from 3760 to 351 (Figure 5.13B). The remaining bostonite and syenite data correlate fairly well. However, the Rooivleitjie granite does not. There is very little variation for the $^{87}Rb/^{86}Sr$ and $^{87}Sr/^{86}Sr$ values (initial and measured) for the syenite, and the two bostonite samples analysed (Figure 5.13B and 5.14). The Rooivleitjie has similar initial Sr–isotope values to the syenite but a very high $^{87}Rb/^{86}Sr$ ratio.

Table 5.4: Radiogenic isotopes. The element ratios are calculated using ICP–MS data.

Sample	Rock type	Rb	Sr	$^{87}Rb/^{86}Sr$	$^{87}Sr/^{86}Sr$	$^{87}Sr/^{86}Sr_i$	Sm	Nd	$^{147}Sm/^{144}Nd$	$^{143}Nd/^{144}Nd$	ϵ Nd
CCK2	Grey gneiss	317	99	9	0.744142±5	0.726315	32	181	0.107	0.512046±6	-9.9
CCK10	Quartz porphyry	157	30	15	0.744642±7	0.715504	18	109	0.1	0.512261±6	-5.58
CCK17	Rooivleitjie granite	661	7	287	1.25398±9	0.702348	1.8	8.9	0.122	0.512504±6	-1.23
CCK18	Syenite	132	512	1	0.707447±4	0.706017	13	76	0.103	0.512526±5	-0.47
CCK23	Quartz porphyry	409	19	63	0.830019±17	0.709175	24	113	0.128	0.512319±4	-4.94
CCK27	Augen gneiss	375	69	16	0.940702±4	0.909869	7.6	34	0.135	0.512164±5	-8.08
CCK52	Rietpoort granite	279	39	21	0.767108±15	0.72719	15	86	0.105	0.512232±4	-6.24
CCK53	Rietpoort granite	262	61	12	0.749619±4	0.725696	15	79	0.115	0.512235±4	-6.35
CCK55	Rietpoort granite	289	34	25	0.772047±6	0.724595	16	87	0.111	0.512247±5	-6.05
CDB336	Quartz porphyry	144	146	3	0.725819±9	0.720337	19	96	0.12	0.512247±5	-6.2
CDB388	Quartz porphyry	773	20	114	0.951374±17	0.731879	1.7	5.9	0.174	0.512335±5	-5.42
CDB552	Bostonite	156	120	4	0.743972±3	0.736734	15	97	0.093	0.512492±6	-0.96
CDB580	Quartz porphyry	342	43	23	0.75712±9	0.712783	24	133	0.109	0.5123±5	-4.98
CDB588	Quartz porphyry	284	41	20	0.754404±4	0.7158	5.1	26	0.119	0.512294±5	-5.26
CDB594	Quartz porphyry	387	17	67	0.84403±15	0.716063	6.1	23	0.16	0.512329±5	-5.3
CDB650	Quartz porphyry	274	78	10	0.744771±6	0.725212	19	102	0.113	0.512205±5	-6.9

continued . . .

Sample	Rock type	Rb	Sr	$^{87}Rb/^{86}Sr$	$^{87}Sr/^{86}Sr$	$^{87}Sr/^{86}Sr_i$	Sm	Nd	$^{147}Sm/^{144}Nd$	$^{143}Nd/^{144}Nd$	ϵ Nd
CDB703	Syenite	102	453	1	0.705924±6	0.704785	14	80	0.106	0.5125±6	-1.82
CDB704	Bostonite	171	91	5	0.71848±7	0.708044	19	132	0.087	0.512518±5	-0.35
CDB753	Syenite	NM	NM	1	0.706034±10	-	NM	NM	-	0.512459±7	-
CN495	Quartz porphyry	329	61	16	0.752718±3	0.722665	14	74	0.114	0.512316±5	-4.76

Sample	Rock type	Th	U	Pb	$^{238}U/^{204}Pb$	$^{206}Pb/^{204}Pb_a$	$^{235}U/^{204}Pb$	$^{207}Pb/^{204}Pb_a$	$^{232}Th/^{204}Pb$	$^{208}Pb/^{204}Pb_a$
CCK2	Grey gneiss	108	5.81	35	9	18.995	0.06	15.731	145	47.416
CCK10	Quartz porphyry	57	11	29	15	18.375	0.11	15.647	73	38.817
CCK17	Rooivleitjie granite	37	11	7.86	231	20.288	1.68	15.742	184	39.522
CCK18	Syenite	9.75	1.56	25	3	18.516	0.02	15.661	15	38.94
CCK23	Quartz porphyry	44	13	38	11	18.298	0.08	15.626	43	38.499
CCK27	Augen gneiss	8.35	3.49	37	3	18.689	0.02	16.693	8	37.736
CCK52	Rietpoort granite	24	2.92	46	1.71	17.945	0.01	15.644	19	38.423
CCK53	Rietpoort granite	22	3.14	41	2	17.959	0.02	15.635	21	38.422
CCK55	Rietpoort granite	25	5.28	331	0.06	18.652	0	15.722	3	38.406
CDB336	Quartz porphyry	14	2.57	25	5	17.916	0.03	15.608	20	38.122
CDB388	Quartz porphyry	60	9.47	25	19	18.348	0.14	15.629	91	38.676
CDB552	Bostonite	33	7.78	29	12	19.274	0.09	15.69	45	39.947

continued . . .

Sample	Rock type	Th	U	Pb	$^{238}U/^{204}Pb$	$^{206}Pb/^{204}Pb_a$	$^{235}U/^{204}Pb$	$^{207}Pb/^{204}Pb_a$	$^{232}Th/^{204}Pb$	$^{208}Pb/^{204}Pb_a$
CDB580	Quartz porphyry	38	8.23	34	9	18.312	0.07	15.642	44	39.237
CDB588	Quartz porphyry	36	8.36	38	7	18.187	0.05	15.636	35	38.341
CDB594	Quartz porphyry	52	16	31	21	18.458	0.15	15.63	63	38.58
CDB650	Quartz porphyry	20	3.47	36	3	17.869	0.02	15.617	22	38.188
CDB703	Syenite	16	2.63	17	11	18.422	0.08	15.626	34	38.462
CDB704	Bostonite	33	3.36	15	17	18.459	0.13	15.649	82	38.787
CDB753	Syenite	NM	NM	NM		18.545		15.635		38.64
CN495	Quartz porphyry	48	7.78	25.33	15	18.341	0.11	15.646	72	38.817

The remaining bostonite sample has a similar $^{87}Rb/^{86}Sr$ but different initial $^{87}Sr/^{86}Sr$ to the syenite. The initial isotope ratios are similar to those of the bulk silicate earth. All the Koegel Fontein samples analysed have similar initial Sr–isotope ratios. Sample CCK2, a Namaqua gneiss, has a relatively unradiogenic $^{87}Sr/^{86}Sr$ measured ratio and a low $^{87}Rb/^{86}Sr$. The Namaqua augan gneiss, CCK27, has a relatively high $^{87}Rb/^{86}Sr$ value, although, not as high as the Rooivleitjie granite. The country rock samples have very different $^{87}Rb/^{86}Sr$ and $^{87}Sr/^{86}Sr$ values.

The ϵNd values where calculated using GEODATE and are plotted in Figure 5.14. The syenite shows very little scatter in the $^{147}Sm/^{144}Nd$, and ϵNd values. The values for the syenite, Rooivleitjie granite and the bostonite samples are very similar and plot close to the bulk silicate earth values. The Rietpoort granite and quartz porphyry samples range from ϵNd = -5.06 to -7.04 (Rietpoort granite; ϵNd = -6.19 to -6.49). The granite shows very little variation in its $^{147}Sm/^{144}Nd$, and ϵNd values while the quartz porphyry shows great variation in both parameters. The Namaqua country rock samples show a large amount of scatter in their the $^{147}Sm/^{144}Nd$ and ϵNd values.

Figure 5.15 shows the isotope plots for the U–Th–Pb system. The dashed lines on each diagram are reference isochrons for 144.4 Ma and 133.9 Ma, black and red respectively. The initial Pb–isotope ratios are taken from the Pb-Pb diagram shown in Figure 5.16 and are estimated using Pb-Pb isochrons. The initial isotope values used for the reference isochrons are $^{206}Pb/^{204}Pb$ = 17.65, $^{207}Pb/^{204}Pb$ = 15.58 and $^{208}Pb/^{204}Pb$ = 39.

There is no correlation between $^{238}U/^{204}Pb$ and $^{206}Pb/^{204}Pb$ for any of the Koegel Fontein rock types (Figure 5.15A). The best fit lines, calculated by GEODATE, for the syenites, bostonites and the Rooivleitjie granite (solid black line) and the Rietpoort granite and quartz porphyries (solid red line) have high MSWD values, 205 and 38221, respectively. The initial isotope ratios and calculated ages are, therefore, subject to large errors. This is also seen in the $^{235}U/^{204}Pb$–$^{207}Pb/^{204}Pb$ plot (Figure 5.15B). The regression line calculated for the syenites, bostonites and Rooivleitjie granite is subject to greater uncertainty with an MSWD of 568. The Rietpoort granite and quartz porphyries best fit line is much better constrained with an MSWD of 86. However, this is still outside of the analytical uncertainty as these rocks still have a large error associated with the calculated age and initial isotope ratio. For both U–Pb isotope systems the amount of U present is too low to account for the amount of radiogenic lead present indicating that U has been lost from the system. However, in order to account for the high Pb–isotopes the amount of U loss needed for some samples is in excess of 50% or a heterogeneous source.

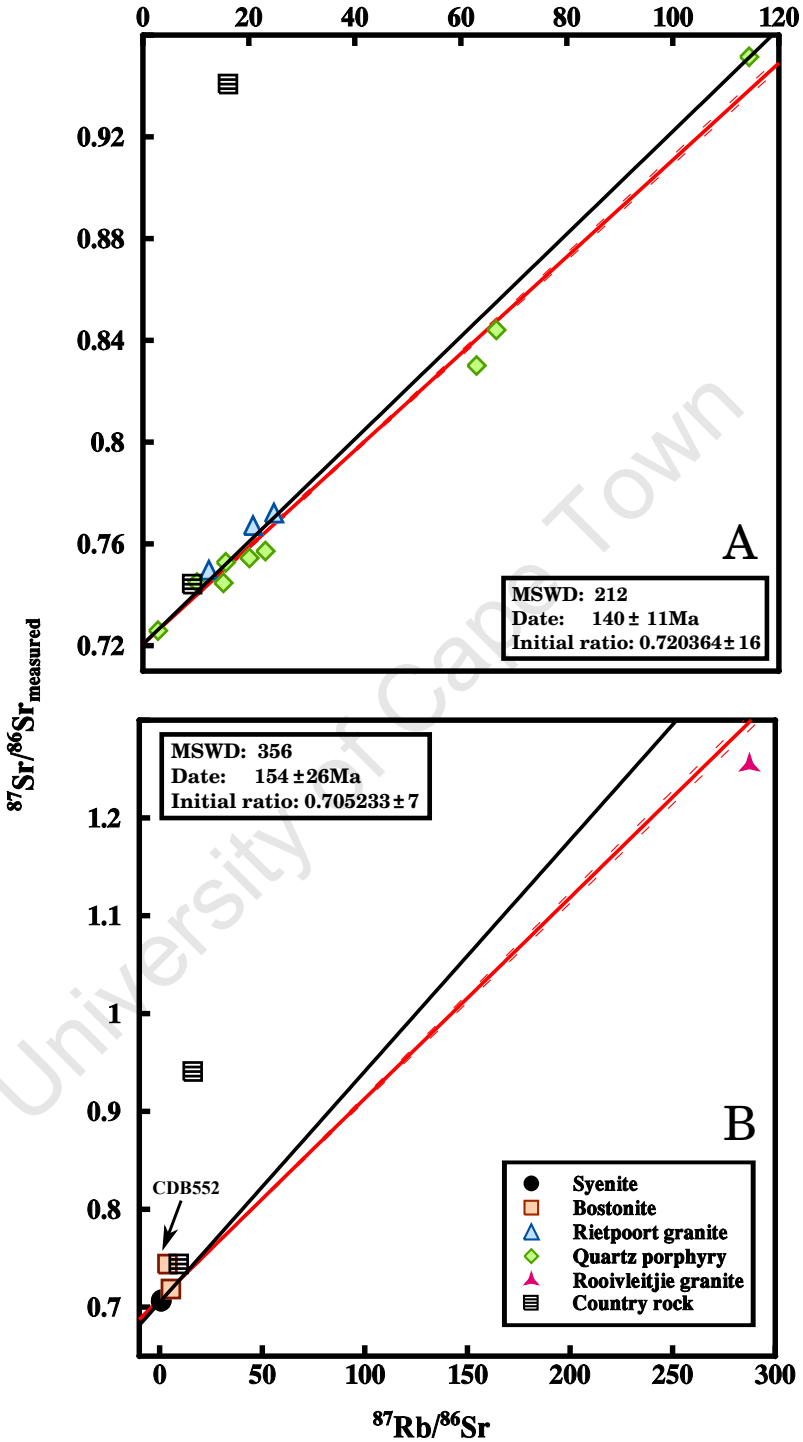

Figure 5.13: Whole rock Sr–isotope data A. The Rietpoort granite and quartz porphryies. The red line is a 133.9 Ma reference isochron B. Syenites, bostonites and the Rooivleitjie granite. The red line is the 144.4 Ma reference isochron. The black line in both graphs is the regression line calculated in GEODATE.

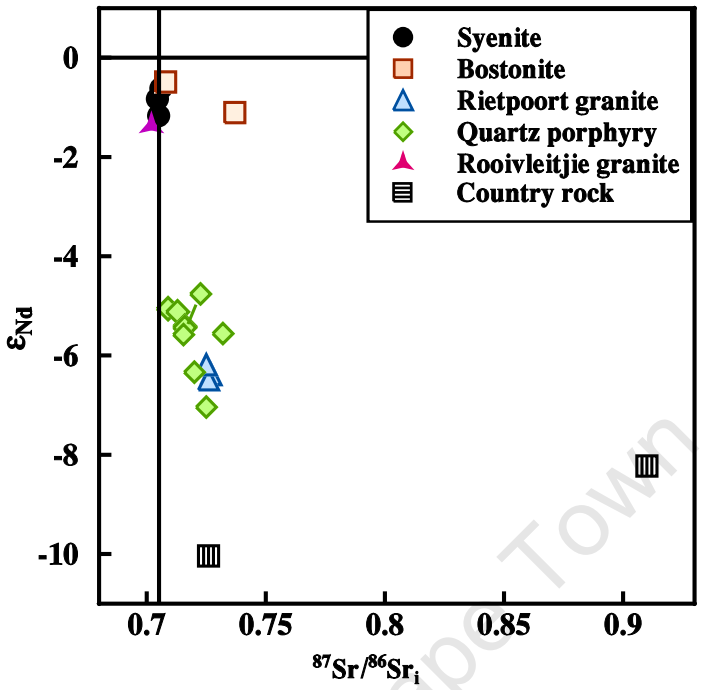

Figure 5.14: ϵ_{Nd} and initial Sr–isotope values for all samples analysed from the Koegel Fontein complex. The lies represent the values for bulk silicate earth. The initial ratios and ϵ_{Nd} values were calculated assuming an age of 135 Ma.

Thorium shows no correlation with its daughter isotope (Figure 5.15C). All regression lines have high MSWD values (6046 for the syenites, bostonites and Rooivleitjie granite and 3865 for the Rietpoort granite and quartz porphyries) and give ages ranging from 291 ± 154 Ma to 1565 ± 4196 Ma for the syenite–bostonite–Rooivleitjie granite and the Rietpoort granite–quartz porphyry respectively. Sample CCK2 was taken from a Namaqua grey gneiss and has low $^{206}Pb/^{204}Pb$ and $^{207}Pb/^{204}Pb$ relative to $^{208}Pb/^{204}Pb$.

In Figure 5.16 all but four samples lie between the 4.55Ga Geochron and the Northern Hemisphere reference line. There are two Rietpoort granite and two quartz porphyry samples which lie to the left of the Geochron. The syenites, one bostonite and the majority of the quartz porphyries are clustered between $^{206}Pb/^{204}Pb$ ratios of 18 and 18.55 and $^{207}Pb/^{204}Pb$ of 15.6 and 15.65. There are no correlations between the different Pb–isotopes. The Stacey and Kramer two stage model (not shown) does not fit the Pb data for the Koegel Fontein complex. The Koegel Fontein rocks do not follow a single stage growth curve (not shown).

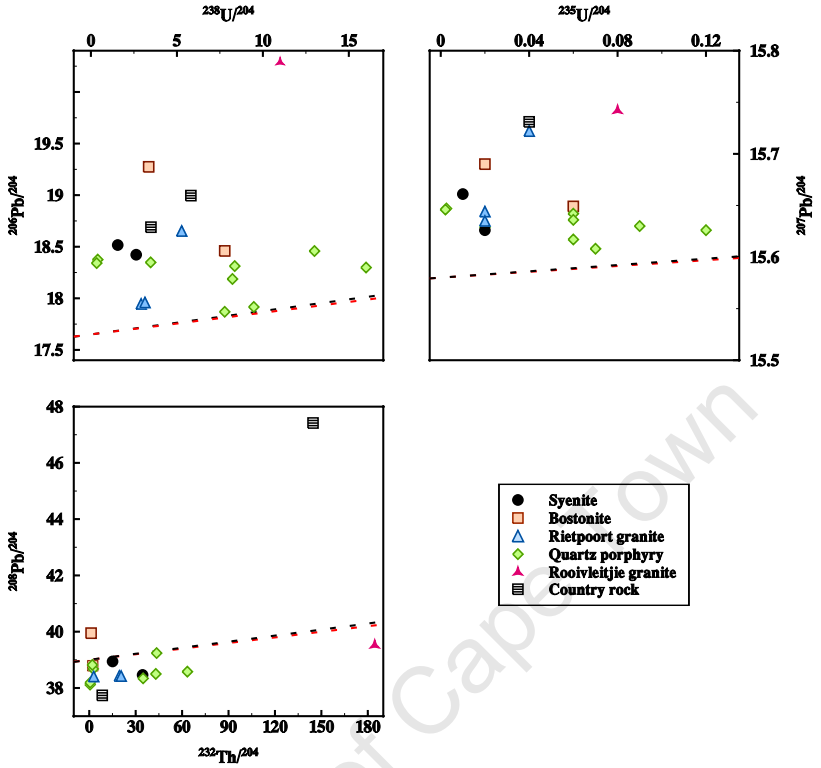

Figure 5.15: U–Pb and Th–Pb plots. The red dashed line is the 133.9 Ma reference isochron. The black dashed line is the 144.4 Ma reference isochron. A. The ^{238}U–^{206}Pb system. B. the ^{235}U–^{207}Pb system. C. The ^{232}Th–^{208}Pb system.

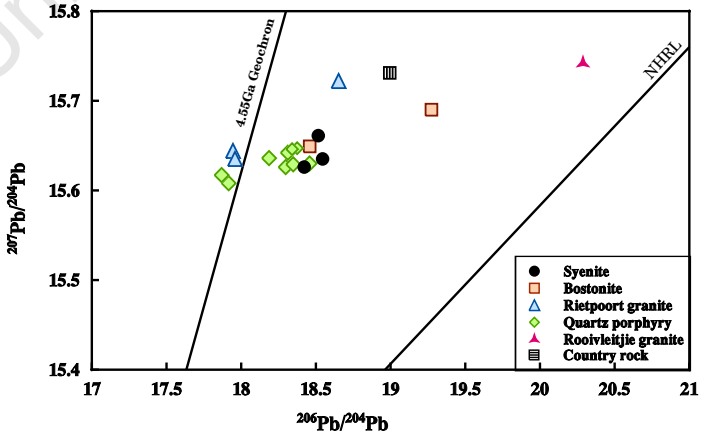

Figure 5.16: ^{207}Pb/^{204}Pb versus ^{206}Pb/^{204}Pb plot for all Koegel Fontein samples analysed plotted with the 4.55Ga Geochron and the Northern Hemisphere reference line (NHRL) (Hart, 1984).

Chapter 6

Discussion

The Koegel Fontein Complex is unique among the southwestern African Cretaceous ring complexes as there is no published geochemical or petrogenetic model for the complex. What follows below is a brief discussion about the genesis of the complex. This is done in order to contextualise the stable isotope data which form the main focus of this thesis.

6.1 Whole–rock geochemical relationships between Koegel Fontein magmas

6.1.1 Major elements

Verwoerd and de Beer (2006) postulated that the syenites, bostonites and Rooivleitjie granite belong to a petrogenetically related suite of rocks. The major element concentrations of the bostonites overlap with those of both the syenite and the Rooivleitjie granite. The less evolved bostonites have similar element concentrations to the syenites and the more evolved samples have similar element concentrations to the granite (Figure 5.3). Negative correlations between MgO, FeO*, TiO_2, CaO and P_2O_5 suggest that the low silica bostonites (<60wt% SiO_2) are petrogenetically linked by fractional crystallization with the high silica (>75wt% SiO_2) samples. Crystallization of feldspar along with ferromagnesan minerals, iron oxides and apatite can explain these trends.

The major element concentrations of the Rietpoort granite and quartz porphyries are almost indistinguishable. There are either very poor or no correlations between the major elements

and silica for these rocks.

6.1.2 Trace elements

The correlations for Nb, Rb, Sr, Ba and Zr versus silica could be explained by fractional crystallization where the bostonites appear to link the syenites and the Rooivleitjie granite (Figure 5.4). The decrease in Zr concentrations after 68 wt. % silica in the bostonites samples can be explained by zircon crystallization. Low Y (14–20ppm) and Ce (19–29ppm) content of the Rooivleitjie granite compared to the bostonites (Y = 25 to 314ppm and Ce = 167 to 608ppm) and syenites (Y = 36 to 43ppm and Ce = 185 to 193ppm) might be the result of apatite or allanite crystallization. The relationship between the Rooivleitjie granite and the bostonites is less clear when trace elements are plotted against Zr (Figure 5.5). However, this ambiguity might be the result of the changes in Zr concentrations caused by zircon crystallization.

The bostonites can be divided into two groups on the Ba and Rb vs Sr and Ba vs Rb plots. The first group includes the syenite and has a sub–horizontal correlations between Sr and Rb and a sub–vertical correlations between Rb and Ba (Figure 5.6). The second group includes the Rooivleitjie granite and has a sub–vertical correlations between Sr and Rb and a sub–horizontal correlations between Rb and Ba (Figure 5.6). The change in element concentrations in the first group may be the result of fractional crystallization of feldspar. Compatible elements, Sr and Ba, both vary in concentration while the incompatible element Rb remains relatively constant. This element behaviour is expected during fractional crystallization (Robb, 1983). Group two shows great variation in Rb concentrations while Ba and Sr content remains almost unchanged. This behaviour can be explained by different degrees of partial melting (Robb, 1983). However, this interpretation must be used with caution as the Koegel Fontein rocks have been altered by hydrothermal fluids, which may have resulted in element mobility.

Figure 6.1 shows the REE patterns of the Koegel Fontein felsic rocks with the average composition of the upper, middle and lower crust. The syenites and three syenite–like bostonites have the most primitave REE patterns for the older group of felsic rocks (Figure 6.1A). The majority of the bostonite samples have an Eu anomaly which appears to be linked with increasing silica. Eu/Eu* decreases from 0.93 to 0.03 as SiO_2 increases from 62 to 71 wt. % (Figure 5.8). This relationship could be explained by the crystallization of feldspar. Rare earth element patterns for the Rooivleitjie granite are unusual for Koegel Fontein as the granite samples have the “gull wing” REE pattern (Figure 6.1A). The light rare earth element (LREE) and

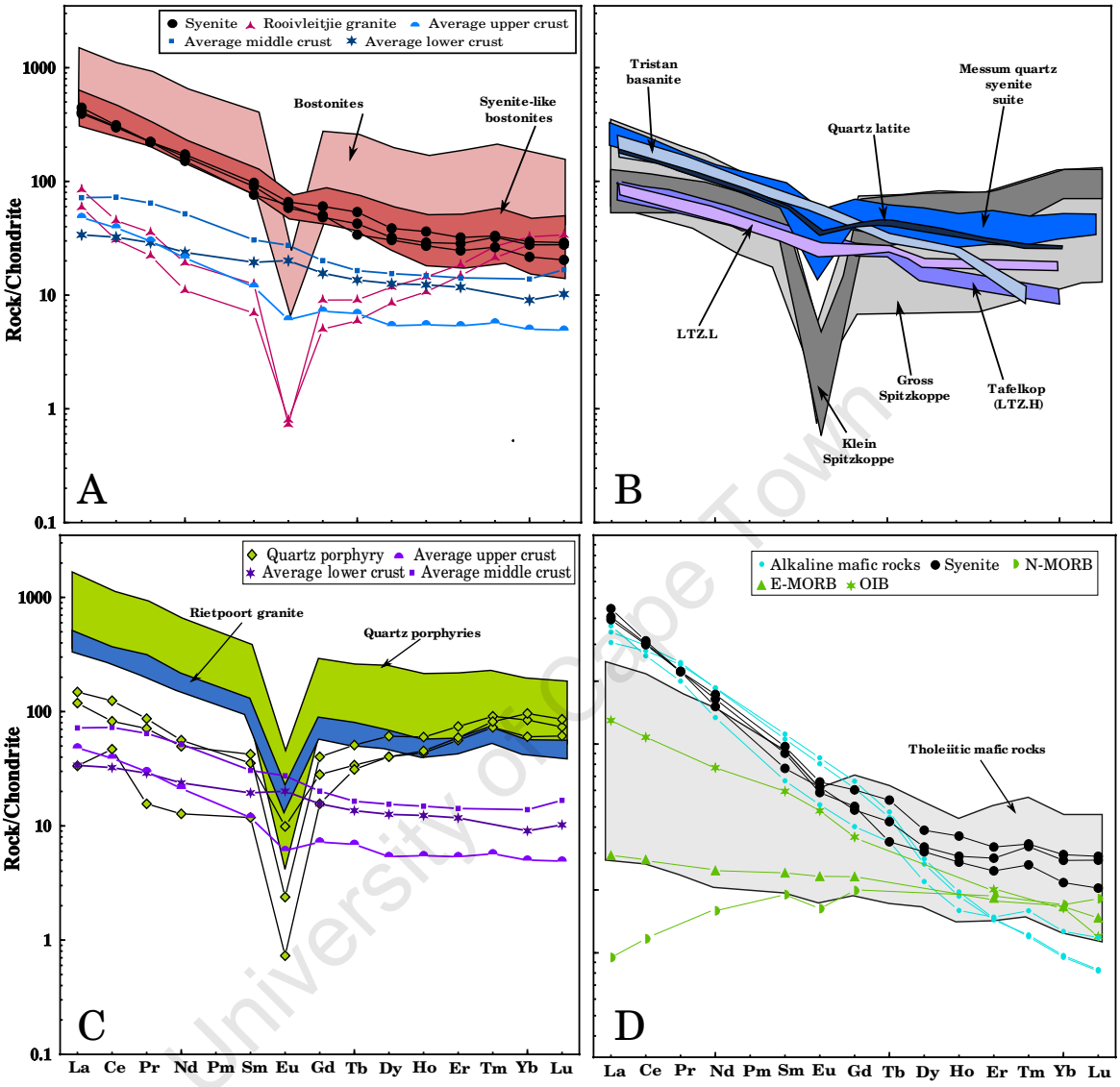

Figure 6.1: REE plots for all of the Koegel Fontein rock types. The felsic rocks are plotted with the average values for the upper, middle and lower crust. The mafic rocks are plotted with the values for the Normal and Enriched Mid Ocean Ridge Basalt (N–MORB and E–MORB respectively) and the Ocean Island Basalts (OIB). A. Syenite–bostonite–Rooivleitjie granite series. B. REE patterns for The Etendeka low–Ti–Zr.high and low–Ti–Zr.low; LTZ.H and LTZ.L respectively, the Etendeka quartz latite, the Tristan basanite and the Damaraland complexes, Messum and Gross and Klein Spitzkoppe. C. Rietpoort granite–quartz porphyry series. D. Tholeiitic and alkaline mafic rocks. The average crustal values are from Wedepohl (1995). The Gross and Klein Spitzkoppe REE patterns were taken from Haapala *et al.* (2007) and the REE pattern for the Etendeka rocks and the Messum complex are from Harris *et al.* (1999). The values for E-MORB, N-MORB and OIB are from Sun and McDonough (1989).

middle rare earth element (MREE) concentrations of the Rooivleitjie granite are much lower than those of the syenites and bostonites. Light REE can behave as compatible elements in felsic magmas with the crystallization of small amounts of allanite or monzonite (Miller and Mittlefehldt, 1982). This added to apatite crystallization could result in the unusual REE pattern seen in the Rooivleitjie granite. The crystallization of titanite can also account for the "gull wing" pattern (Fengming and Xiang, 1994). However, none of these minerals seem to be present in the bostonites or syenites which are thought to be the precursors to the granite (de Beer and Armstrong, 1998). There are three quartz porphyry samples with "gull wing" REE profiles which are not spatially associated with the Rooivleitjie granite. The strange REE patterns may therefore indicate heterogeneities in the Koegel Fontein source region.

For the Rietpoort granite and quartz porphyry dykes Sr, Zr and Ba show trends with silica which are consistent with crystallization of feldspar and zircon whereas Rb and Nb are concentrated in the more evolved rocks which is consistent with magma differentiation. The relationship between Sr and Rb and Rb and Ba suggest that the variation may in part be caused by partial melting or crustal contamination as the compatible elements show little variation while Rb has a great range in concentration.

The REE patterns for the Rietpoort granite and the quartz porphyries are similar (Figure 6.1C). Although, the granite is more homogeneous which may be due to its size (>30km diameter) and there is little to no macroscopic evidence for magma mixing (Chapter 2.4.1). There are three samples of quartz porphyry which have a "gull wing" REE pattern. This may be result of the crystallization of allanite and monzonite as discussed for the Rooivleitjie granite. However, no allanite, monzonite or sphene have been found in any quartz porphyry or Rietpoort granite samples. It should also be noted that two of the samples with the "gull wing" REE pattern also have quartz phenocrysts with low–δ^{18}O values. There is a large variation in REE values in the quartz porphyry samples which may be a result of magma differentiation as the Eu/Eu* and SiO_2 values have a negative correlation indicating that the Eu anomaly could be linked to differentiation.

de Beer *et al.* (2002) grouped the Zout Rivier plug associated tholeiitic mafic dykes and alkali mafic dykes with the Koegel Fontein complex because of similar mafic and felsic associations described in the Damaraland complexes in northern Namibia. McIver (1981) ruled out a petrogenetic link between the alkali mafic rocks and the syenites and without radiogenic isotope data, the relationship of these rocks with the Koegel Fontein complex remains ambiguous. However, it should be noted that the syenites and alkali mafic rocks have similar REE patterns which may indicate that they share a component from a similar source such as the asthenosphere. The petrogenetic links between the tholeiitic and alkali mafic rocks and the

Zout Rivier plug are beyond the scope of this project.

6.1.3 Radiogenic isotopes

Syenite samples, one bostonite sample and the Rooivleitjie granite have very similar ϵ_{Nd} values and initial Sr–isotope ratios (Figure 6.2), which may be an indication that these rocks are derived from the same source. However, more samples from each rock type need to be analysed to confirm this. There is one bostonite sample (CDB552) which has a higher initial Sr–isotope ratio than the syenites, the other bostonite and the Rooivleitjie granite. The ϵ_{Nd} values of all the syenite, bostonite and Rooivleitjie granite samples are the same within error. This might be the result of a heterogeneous source region, contamination by the Namaqua upper crust and/or element mobility caused by hydrothermal alteration. The Koegel Fontein Complex has been subjected to intense alteration (Chapter 6.2.2), which may have caused ^{87}Sr to move into the system. However, more analysis needs to be done to confirm the cause of the high initial $^{87}Sr/^{86}Sr$.

Figure 6.3 is a $^{207}Pb/^{204}Pb$ versus $^{206}Pb/^{204}Pb$ plot. The Pb–isotopes of the syenites and the bostonites shows a similar pattern to the ϵ_{Nd} and initial Sr–isotope ratios whereby the syenites and one bostonite sample are clustered (Figure 6.3), whereas the other bostonite sample has high Pb–isotope ratios. However, the Rooivleitjie granite sample has a very different Pb–isotope ratio compared to the syenite. This indicates that these rocks either have a heterogeneous source or have been contaminated by the Namaqua upper crust (Chapter 5.3). Lead–isotopes for the country rock samples suggest that the Namaqua rocks have heterogeneous isotope ratios. The grey gneiss (CCK2) shows evidence of high grade metamorphism, where U–loss has occurred and Th has remained immobile, lower than expected $^{206}Pb/^{204}Pb$ and $^{207}Pb/^{204}Pb$ compared to $^{208}Pb/^{204}Pb$ (Peucat *et al.*, 1989). The less deformed augen gneiss (CCK27) does not have this feature. The Pb–isotopes for all Koegel Fontein samples are such that, a larger time integrated, heterogeneous source is required to explain the variation in isotope ratios (Figure 5.15).

The Rietpoort granite and quartz porphyries have similar ϵ_{Nd} values (Figure 6.2). There is little variation in Sr– and Nd–isotope values between the Rietpoort granite samples. Strontium–isotopes between the quartz porphyry samples have a wide variation. The $^{87}Sr/^{86}Sr$ initial ratios indicate that the 133Ma felsic rocks have either undergone different degrees of, alteration, crustal contamination or originated from a heterogeneous source. Except for one quartz porphyry sample, the Rietpoort granite has the highest initial Sr–isotopes of the 133Ma Koegel

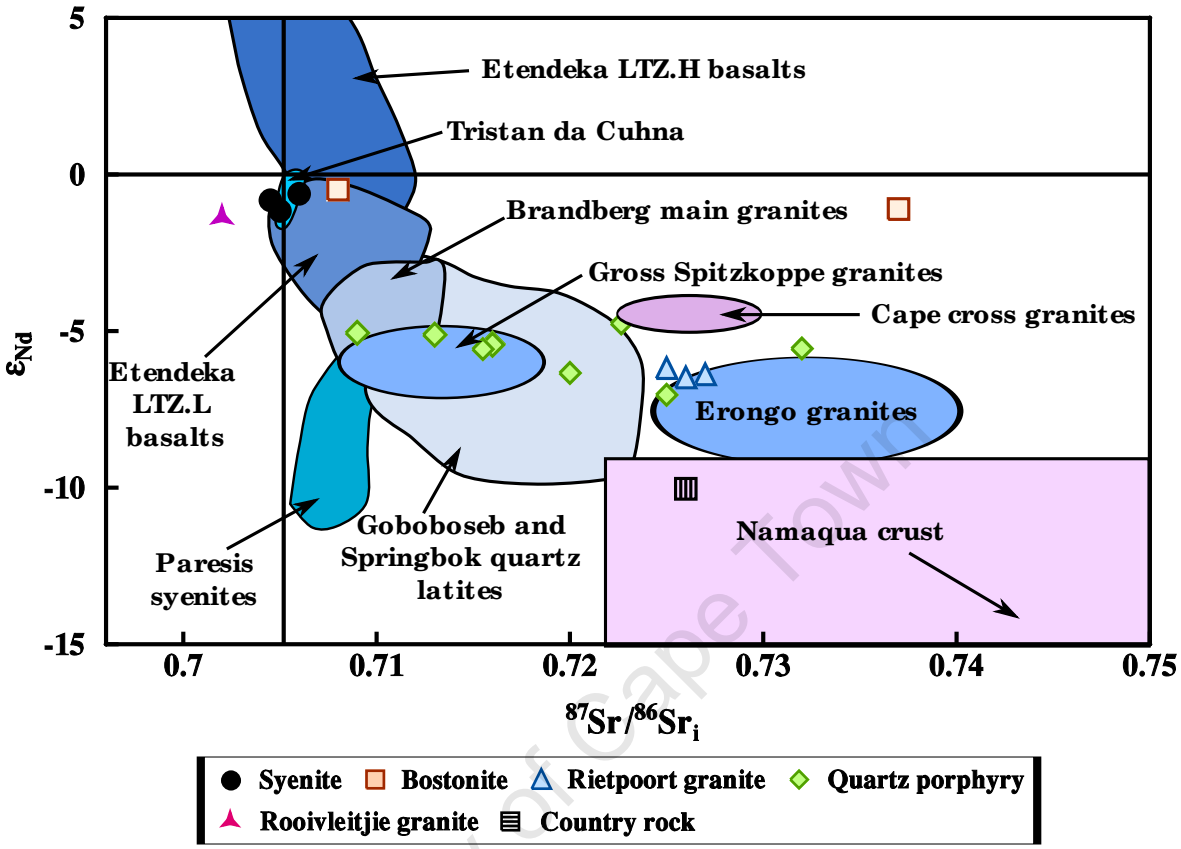

Figure 6.2: Initial Sr and ϵ_{Nd} composition of the Koegel Fontein complex plotted with values for the Damaraland complexes, Etendeka flood basalts, Tristan da Cuhna and Namaqua country rock. The Koegel Fontein and Namaqua initial Sr ratios and ϵ_{Nd} values were calculated at 135Ma using GEODATE. The measured data for the Namaqua country rock is from Reid (1979, 1999). The fields for the Brandberg, Gross Spitzkoppe and Erongo complexes as well as the data for the Goboboseb and Springbok quartz latites, LTZ.L and LTZ.H are taken from Frindt *et al.* (2004). The field for Paresis is from Mingram *et al.* (2000) and the fields for Tristan da Cuhna and the Cape Cross complex are from Haapala *et al.* (2007).

Fontein felsic rocks. This suggests that the granite is the most contaminated of the two rock types. However, there is no macroscopic (Chapter 2.4.1) or microscopic (Chapter 3.1.1) evidence for contamination.

Lead–isotopes indicate a heterogeneous source for the Rietpoort granite and quartz porphyry dykes (Figure 6.3). Only the Pb–isotopes show evidence of heterogeneity in the Rietpoort granite. The quartz porphyries which are thought to be precursor intrusions for the granite (de Beer *et al.*, 2002) are very heterogeneous in both trace element concentrations and radiogenic isotopes. It is possible that the quartz porphyries represent small scale melts from a

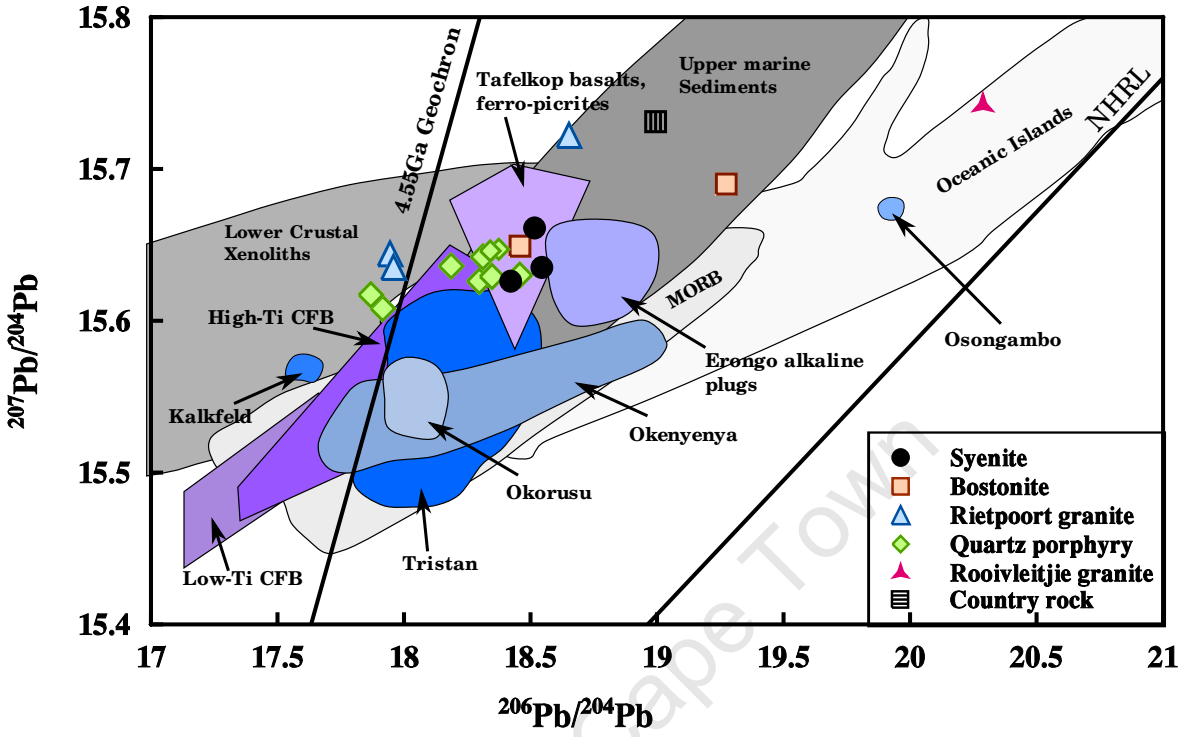

Figure 6.3: Pb–Pb plot of all the Koegel Fontein and country rock samples analysed. The fields for the major terrestrial reservoirs, the Northern Hemisphere Reference Line (NHRL) and the data for the Etendeka flood basalts, Tristan plume and the Damaraland complexes are plotted for comparison. The ocean island field represents the deep mantle and the MORB field represents the upper mantle. The Fields for the terrestrial reservoirs are taken from White (2007) and the fields for the Tristan plume and all the Damaraland Complexes, except Erongo, are taken from le Roex and Lanyon (1998). The values for the Etendeka flood basalts and the Erongo complex are from Trumbull *et al.* (2003).

source with localized heterogeneities. This heterogeneous source was subsequently homogenized by the emplacement of the larger Rietpoort granite.

6.1.4 Whole–rock geochemical comparison between Koegel Fontein and the similar aged rocks in Damaraland

The REE values for the Koegel Fontein complex tend to be higher than those for the Damaraland complexes, Tristan da Cuhna and the Etendeka volcanic rocks (Figure 6.1B). The Koegel Fontein rocks tend to be more evolved than the northern Namibian rocks (Chapter 2.3, Table 5.4). However, the LTZ.L (low-Ti-Zr.low) quartz latites and the Koegel Fontein syenites are

similar and the LTZ.L REE values overlap with the tholeiitic mafic rocks. The similarities between the Koegel Fontein and Damaraland rocks may indicate a similar source component for these rocks. However, Mg–numbers suggest that melting temperatures for the Koegel Fontein Complex were lower than those in Damaraland (e.g. the West Coast Dyke Swarm, Trumbull *et al.*, 2007). The Sr– and Nd–isotopes for Koegel Fontein and northern Namibia show that the Rietpoort, Spitzkoppe and Erongo granites have similar Sr– and Nd–isotope compositions. The Spitzkoppe and Erongo granites are interpreted to be crustal melts (Harris, 1995). A similar model might also apply to the Rietpoort granite based on the similarity in its Sr and Nd isotopes with Spitzkoppe and Erongo.

6.1.5 Summary of the whole–rock geochemical relationships between the Koegel Fontein magmas

The major and trace elements, REE element patterns, initial Sr–isotope ratios and ϵ_{Nd} values show that it is plausible for the syenites, bostonites and Rooivleitjie granite to be petrogenetically linked. However, a caveat is that no allanite, monzonite or sphene was observed in thin section. These minerals are needed to explain the REE patterns of the Rooivleitjie granite. If the syenites, bostonites and Rooivleitjie granite are linked by fractional crystallization then feldspar would appear to be the main fractionating phase.

It is possible that the quartz porphyries are precursor intrusions to the Rietpoort granite as these rocks appear to have a very similar source. There is almost no difference in major element concentrations for these rocks and variations in the trace element data can be easily explained by different degrees of partial melting. However, the radiogenic isotopes indicate that there is some heterogeneity in the source region.

6.2 ^{18}O depletion in the Koegel Fontein rocks

The most notable geochemical feature of the Koegel Fontein Complex is the anomalously low stable isotope ratios. The δ^{18}O and δD values of normal igneous rocks range from +6 to +10‰ and -85 to -50‰ respectively (Taylor, 1977, 1978; Taylor and Sheppard, 1986). Igneous rocks with delta values below +6‰ are termed low δ^{18}O rocks and are usually the result of subsolidus interaction with a high–temperature fluid (Taylor, 1977, 1978). The majority of the rocks analysed from Koegel Fontein have whole rock and mineral δ^{18}O and δD values below +6‰ and -85‰, respectively (Figure 5.10).

6.2.1 Determining magmatic $\delta^{18}O$

Quartz is a relatively inert mineral which is resistant to alteration (e.g. O'Neil and Tayler, 1967; Taylor, 1974; Giletti and Yund, 1984; Giletti, 1986; Larson and Taylor, 1986; Gregory *et al.*, 1989). Igneous rocks with low $\delta^{18}O$ quartz crystallized from low–$\delta^{18}O$ magmas. Low $\delta^{18}O$ magmas make up a small fraction of igneous rocks world wide (e.g. Taylor and Sheppard, 1986; Balsley and Gregory, 1998). Although, recently Boroughs *et al.* (2005) and Bindeman (2008) suggested that low–$\delta^{18}O$ magmas might be more widespread based on the discovery of low–$\delta^{18}O$ rhyolites in the Snake River Plain.

The $\delta^{18}O$ value of the magma can be estimated using $\delta^{18}O$ values and modal proportions of the different minerals of a fresh rock (e.g. Gregory and Criss, 1986; Harris *et al.*, 1997). The rocks from Koegel Fontein are comprised mainly of feldspar which has been altered and presumably, has not retained its original $\delta^{18}O$ value. Quartz is resistant to alteration and should retain its original $\delta^{18}O$ values and can be used to estimate the $\delta^{18}O$ of the magma (Giletti, 1986; Harris *et al.*, 1997). However, the difference between the δ value of the mineral and the δ value of the magma is controlled by the $\Delta_{mineral-melt}$, grain size, rate of cooling and closure–temperature for O diffusion of the minerals in the rock (Giletti, 1986; Taylor and Sheppard, 1986). The $\delta^{18}O$ values for the Koegel Fontein magmas were estimated using the $\delta^{18}O$ values of quartz phenocrysts and quartz separates and assuming $\Delta_{quartz-magma}$ is 2‰ for the coarse–grained rocks and 1‰ for the quartz porphyry (Taylor and Sheppard, 1986; Harris *et al.*, 1997). The estimated $\delta^{18}O$ values of the magma are given in Table 6.1.

Samples from Koegel Fontein can be divided into two groups on the basis of their estimated, magmatic $\delta^{18}O$ values. The first has normal $\delta^{18}O$ values and includes the syenite, the Rooivleitjie granite, the Rietpoort granite and the majority of the quartz porphyry samples. The second group has anomalously low $\delta^{18}O$ values and are forthwith referred to as the low $\delta^{18}O$ quartz porphyries. They are unusual amongst the Cretaceous igneous complexes along the west coast of Africa as they are the only known rocks to have crystallized from a low $\delta^{18}O$ magma (Figure 6.4). All but two bostonite samples have whole–rock $\delta^{18}O$ values below that of normal igneous rocks (6.0‰). They are low $\delta^{18}O$ rocks but it is not certain if they crystallized from a low $\delta^{18}O$ magma as no phenocryst data exist. A small plug of intermediate composition (SiO_2 = 55 wt. %), from the centre of the complex, has the lowest $\delta^{18}O$ value (-4.1‰) measured at Koegel Fontein.

The tholeiitic mafic rocks and alkali mafic rocks all have low $\delta^{18}O$ whole–rock values. No pyroxenes were separated as a detailed study of the mafic rocks was not one of the aims of

Table 6.1: Calculated δ^{18}O values for the Koegel Fontein felsic magmas using the δ^{18}O values for the quartz (Qtz) and quartz phenocrysts (Qtz pheno).

Sample	Rock type	$\delta^{18}O_{magma}$ (Qtz; ‰)	$\delta^{18}O_{magma}$ (Qtz pheno; ‰)
CCK12	Quartz porphyry	-	7.0
CCK23	Quartz porphyry	-	0.2
CDB336	Quartz porphyry	8.4	-
CDB383	Quartz porphyry	7.8	8.1
CDB564	Quartz porphyry	-	7.8
CDB572	Quartz porphyry	-0.5	0.8
CDB580	Quartz porphyry	-	3.5
CDB588	Quartz porphyry	-	0.6
GDB594	Quartz porphyry	2.2	0.7
GDB650	Quartz porphyry	7.5	7.3
CN495	Quartz porphyry	7.5	7.8
CCK19	Rietpoort granite	6.9	6.2
CCK51	Rietpoort granite	5.7	6.4
CCK52	Rietpoort granite	5.7	5.4
CCK55	Rietpoort granite	6.7	8.5
CDB825	Rietpoort granite	-	6.7
CCK17	Rooivleitjie granite	5.9	-
CDB687	Rooivleitjie granite	-	5.8
CDB703	Syenite	-	6.0
CDB753	Syenite	6.5	-

this project. Although, it should be noted that some mafic dykes and the Zout Rivier plug have low–δ^{18}O values whereas the surrounding country rock has normal δ^{18}O values (> +6‰). This suggests that hydrothermal alteration synchronous with the emplacement of the complex is not solely responsible for the low–δ^{18}O values measured at Koegel Fontein.

6.2.2 Post - crystallization alteration

Petrographic evidence for alteration includes cloudy or turbid feldspar, minor chloritization and sericitation and in some samples veins of chlorite, epidote and calcite. Phenocrysts often

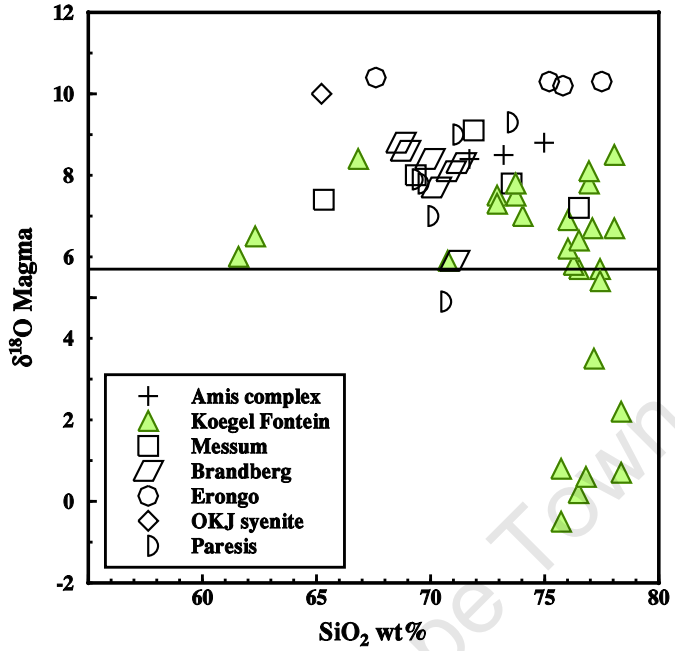

Figure 6.4: Comparison between the magmatic δ^{18}O of the Koegel Fontein Complex and the Damaraland Complexes from northern Namibia. The low δ^{18}O quartz porphyry from Koegel Fontein is the only rock type, with the exception of one sample from Paresis from the south west Atlantic coast, to have crystallized from low δ^{18}O magmas. All are anorogenic complexes of similar ages and are thought to be related to the break–up of western Gondwana. The oxygen data are from Trumbull *et al.* (2004) and all the references therein.

have coronas of fine–grained feldspar, carbonate minerals and sericite. Some feldspar phenocrysts in the quartz porphyries are partially altered to calcite. In the tholeiitic and alkali mafic samples there are minor amounts prenite and bowligite. In the core of the complex the roof rocks have been fenitized (Chapter 2.4). The presence of minerals such as epidote indicate that the temperature of the hydrothermal fluid was between 300 and 400°C (Deer *et al.*, 1992).

Figure 6.5 is a δ–δ plot which shows the relationship between the δ^{18}O values of the feldspar, quartz, amphibole, whole–rock and groundmass oxygen–isotope ratios. The equilibrium $\Delta_{quartz-feldspar}$ value at magmatic temperatures is in between 1 to 2.5‰ depending on the calcium content of the feldspar, with $\Delta_{quartz-anorthite}$ = 2.5‰. If $\Delta_{quartz-feldspar}$ is outside of this range, post–crystallization alteration has occurred (Taylor, 1977). The felsic rocks from Koegel Fontein contain very little plagioclase and the $\Delta_{quartz-feldspar}$ at magmatic equilibrium is more likely to be 1 to 2‰. If $\Delta_{quartz-feldspar}$ >2‰ then the minerals are not in equilibrium at high–

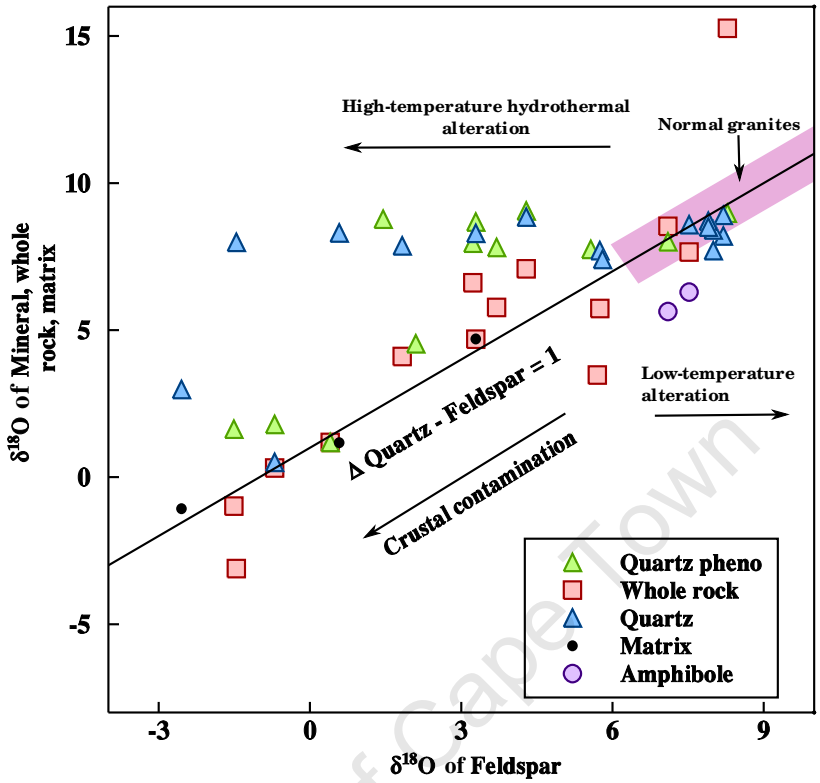

Figure 6.5: Oxygen isotope data. $\Delta_{quartz-feldspar}$=1‰ represents equilibrium at magmatic temperatures. $\Delta_{quartz-feldspar}$>2‰ indicates intreaction with a high–timperature fluid. The effect of crustal contamination lowering δ^{18}O values is discussed in Section 6.2.7

temperature. This is most likely caused by interaction with a high–temperature fluid, i.e. the δ^{18}O value of the feldspar decreases. If $\Delta_{quartz-feldspar}$ <1‰ then alteration was caused by a low–temperature fluid, the δ^{18}O value of the feldspar has increased. This is due to oxygen isotope fractionation being temperature dependent and at 400°C $\Delta_{feldspar-water}$ is about 6‰ (Criss and Taylor Jr., 1986). Isotope exchange between a mineral and a hydrothermal fluid is partially controlled by diffusion while the hydrothermal fluid facilitates the dissolution and recrystallization of feldspar. The rate of diffusion is controlled by temperature (Giletti and Yund, 1984). Diffusion rates for quartz and feldspar are similar at high temperatures (>800°C). Diffusion and reaction rates diverge as temperature decreases with diffusion in quartz becoming much slower than diffusion in feldspar. When the temperature of a hydrothermal fluid drops below 500°C, diffusion in quartz will be negligible, while feldspar will still be highly affected by isotope exchange (Giletti and Yund, 1984).

The syenites and one sample of Rietpoort granite and one of the low–δ^{18}O quartz porphyries

have $\Delta_{quartz-feldspar}$ that suggest equilibrium at magmatic temperatures, ($\Delta_{quartz-feldspar} \simeq 1$). The Rooivleitjie granite, quartz porphyries and the majority of the low–δ^{18}O quartz porphyry samples have $\Delta_{quartz-feldspar} > 2‰$ which indicates that the δ^{18}O of the feldspar has been lowered by hydrothermal alteration. Sample CDB825 (Rietpoort granite) has $\Delta_{quartz-feldspar} = 0.4$ which is indicative of low–temperature alteration. The increase in the δ^{18}O of the feldspar in this sample is probably the result of more recent weathering.

Figure 6.6 is a histogram of whole–rock δ^{18}O values of all the Koegel Fontein rocks analysed, grouped by age. There is no correlation between age and δ^{18}O value. Whole–rock δ^{18}O contours indicate that there might have been more than one hydrothermal system related to the Koegel Fontein complex (Figure 6.7). There appears to be a hydrothermal system centred around the Sandkop syenite, the largest syenite intrusion at the complex, and another around the Rietpoort granite. The Rietpoort granite and Sandkop syenite both have normal δ^{18}O values and are surrounded by hydrothermally altered rocks. These two plutons are the largest intrusive bodies found at the Koegel Fontein Complex, with the Rietpoort granite being the main intrusive phase. The extent of the syenite is unknown. Outcrops of syenite occur in the centre of the complex and to the north of the Rietpoort granite, although, these appear to be discrete intrusions. Only the southern most syenite outcrop, the Sandkop Syenite, was analysed. The normal δ^{18}O values and lack of hydrothermal alteration phases suggests that the Sandkop syenite and Rietpoort granite were at the centre of two distinct hydrothermal systems (Figure 6.7). However, distinct hydrothermal systems can not be distinguished by age alone, as the older Sandkop syenite system is affected by the subsequent Rietpoort granite hydrothermal system. The contours plotted in Figure 6.7 are based on the GPS locations of all the samples analysed at Koegel Fontein. Therefore, the map shows the known extent of the hydrothermal system. It is possible that low δ^{18}O rocks can be found south of the Sandkop syenite, however, no samples were analysed south of this point. It appears as if the size of the intrusion is linked to the δ^{18}O value as only small plugs (e.g. the Rooivleitjie granite), and dykes are heavily affected by the hydrothermal alteration. The most negative δ^{18}o values are also spatially related to large shear zones in the area.

6.2.3 Effect of degassing on δD

The majority of samples from the Koegel Fontein Complex have δD values below -85‰ (average = -102±4). Amphibole and biotite separated from the syenite also have low δD values. Low δD values can be achieved through degassing. If water exolves from a magma as a vapour phase, deuterium will partition preferentially into the vapour phase. If this phase is removed

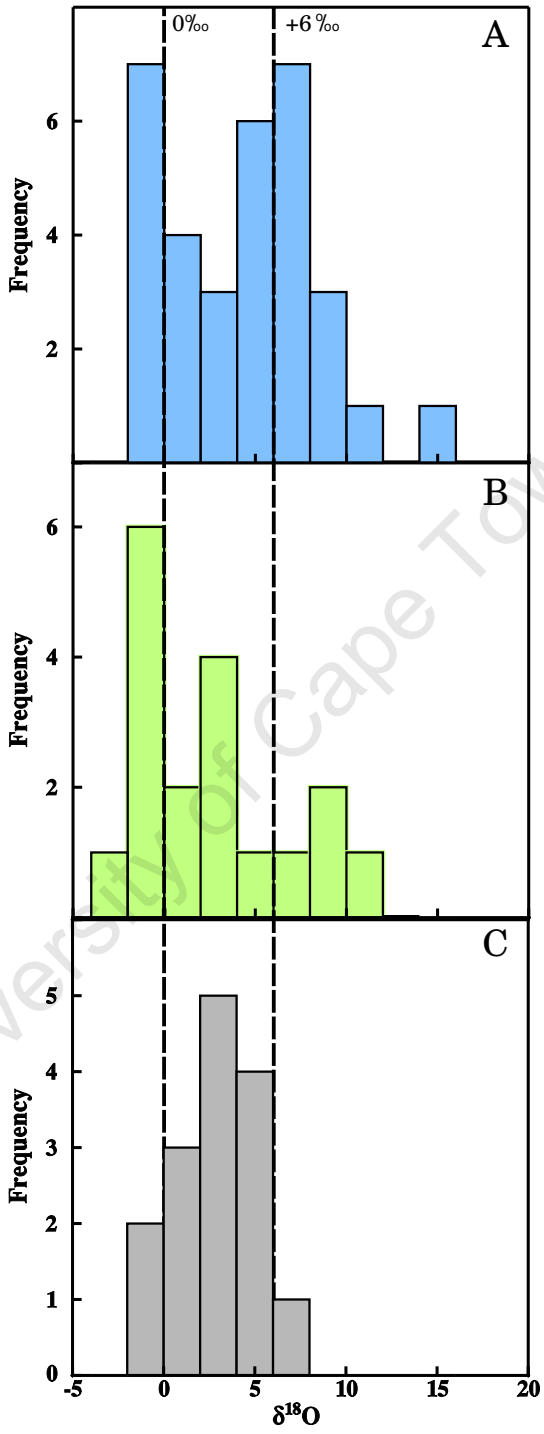

Figure 6.6: Whole–rock oxygen isotope ratios grouped by age. A. The Rietpoort granite–quartz porphyryies suite, 133.9Ma. B. The alkali and tholeiitic mafic rocks. Relative ages put these rocks between the syenites and the Rietpoort granites. C. Syenites–bostonites–Rooivleitjie granite suite, 144.4Ma The dashed lines are the contours in Figure 6.7 and 6‰ was chosen as it is the lower limit for normal δ^{18}O magmas and rocks with δ^{18}O values < 0‰ have been altered by meteoric–hydrothermal fluids.

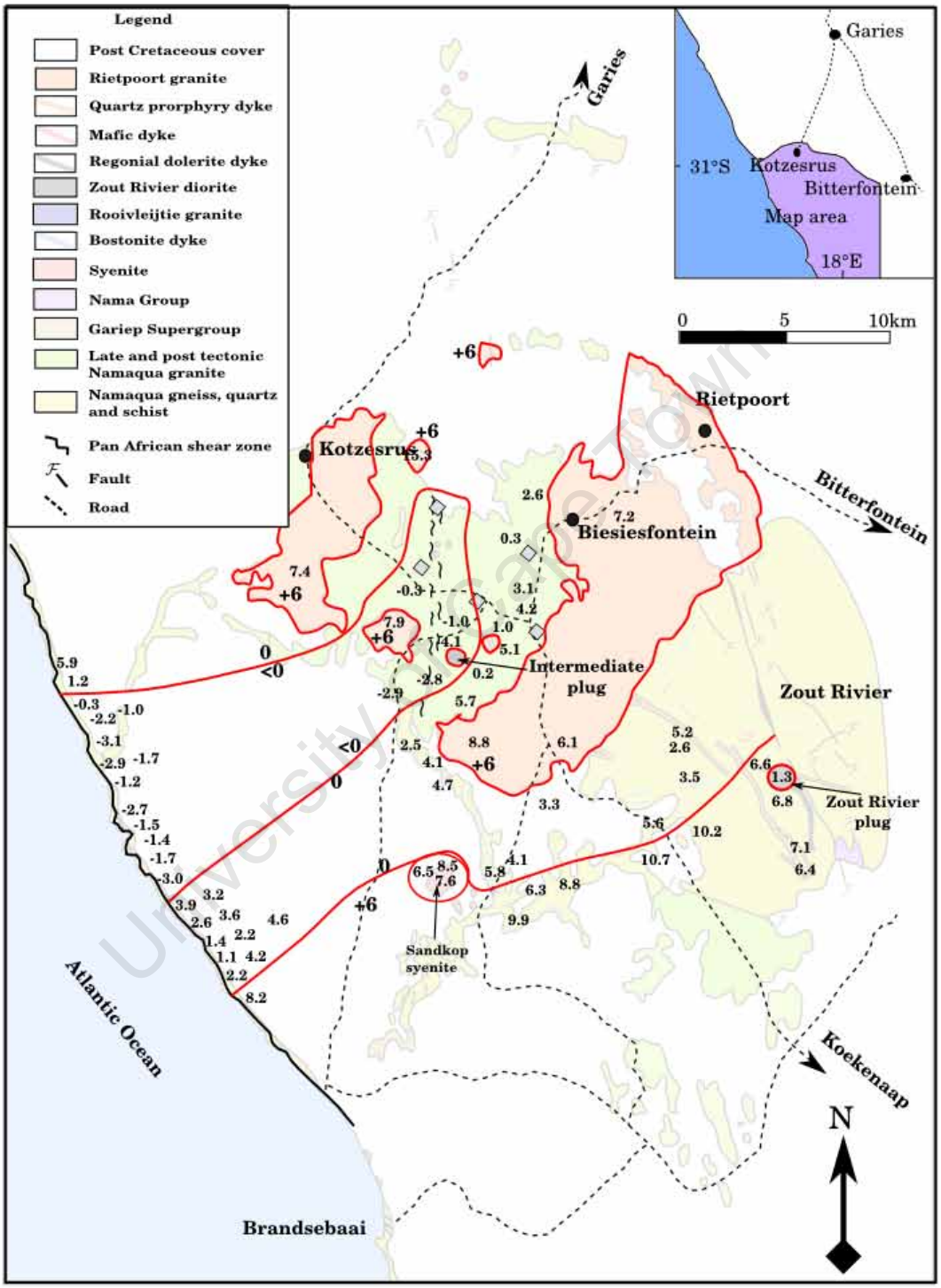

Figure 6.7: Whole–rock oxygen isotope ratio contours. The intermediate plug has the lowest isotope ratio measured at the Koegel Fontein complex, 4.1‰. The grey diamonds represent the low–δ^{18}O magmas. All contours are in ‰.

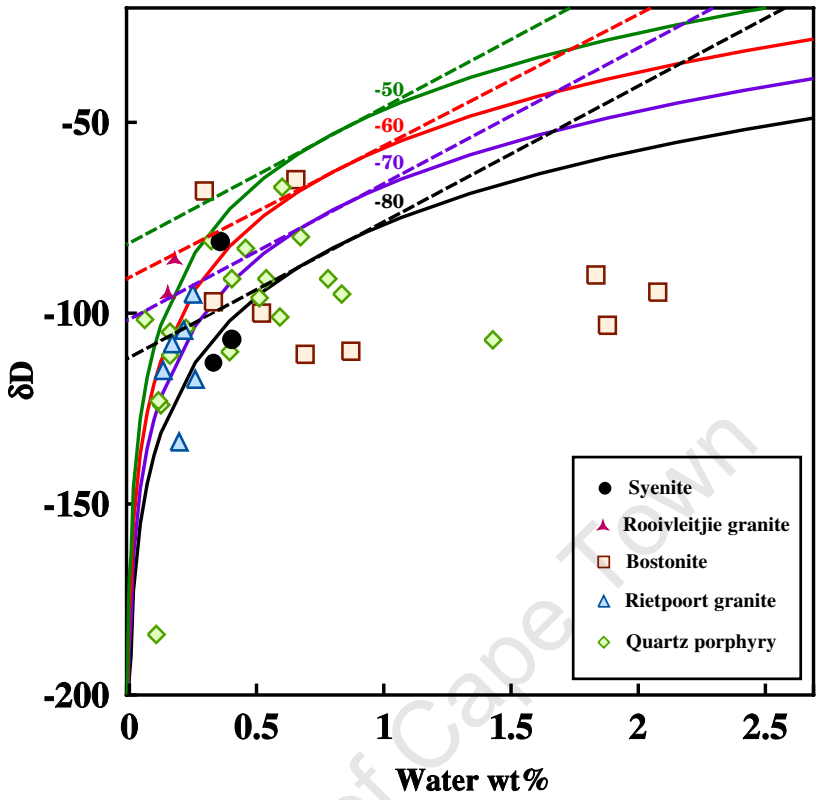

Figure 6.8: The δD and water content for the felsic samples from Koegel Fontein plotted with the Rayleigh (solid line) and batch (dashed line) degassing curves. The assumed initial δD used is written next to each curve.

by open system behaviour, such as degassing, the δD of the remaining water will be lowered, sometimes to values as low as -130‰ (Taylor *et al.*, 1983). Figure 6.8 shows the δD and water content of Koegel Fontein samples plotted with Rayleigh and batch degassing curves. The curves were calculated assuming an initial water content of 3 wt. % which is the estimated value for anorogenic granites (e.g. Patino Dounce, 1997; Wei *et al.*, 2000). The assumed $\Delta_{H_2O-magma}$ used was -32‰ for fractionation at 900°C (Wei *et al.*, 2000) and initial δD values of the magma used, were -50, -60, -70 and -80‰. The Koegel Fontein samples do not follow a degassing curve. It is, therefore, unlikely that the low δD values are the result of degassing. The extremely δD low values of two samples (<-150‰) may be the result of the"blank" effect as the water content in these samples is very low. They are not considered when interpreting the H–isotope data. However, samples with >1 wt. % water have low δD values, therefore, the majority of the low δD values measured are probably a true feature of the complex.

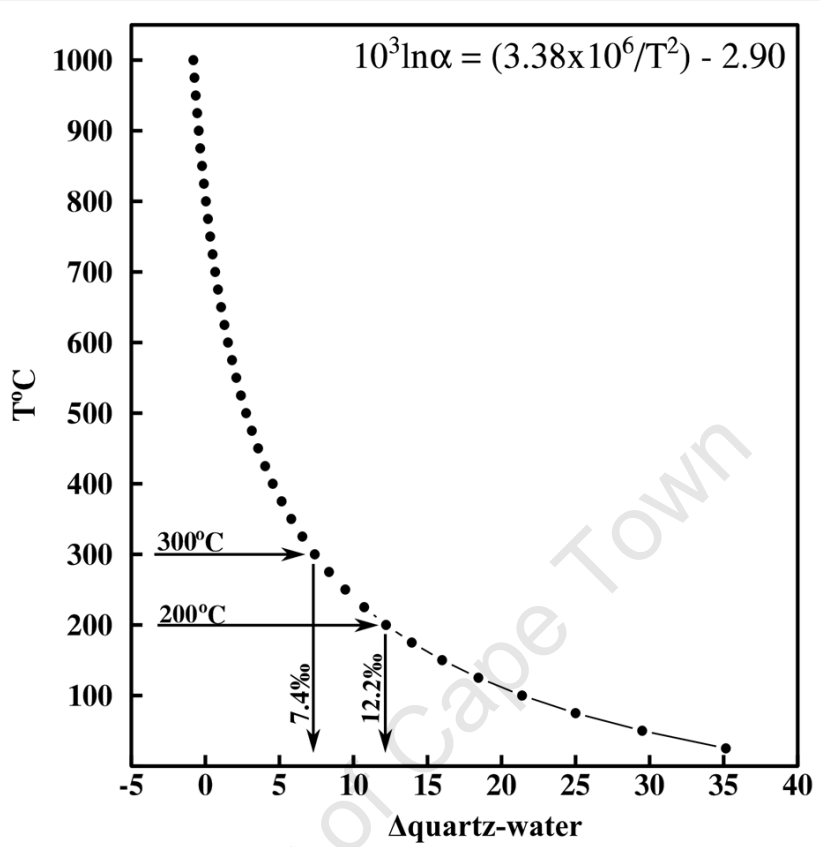

Figure 6.9: The effect of temperature on $\Delta_{quartz-water}$. Values on the graph show likely temperatures of quartz vein formation, the corresponding $\Delta_{quartz-water}$ and the estimated δ^{18}O of the hydrothermal fluid.

6.2.4 Low δ^{18}O quartz veins

Quartz veins associated with the Koegel Fontein Complex have anomalously low stable isotope ratios (whole–rock δ^{18}O = -0.88 to -1.73‰ and whole–rock δD = -85 to -118‰). Oxygen–isotope fractionation between quartz and water is such that a fluid dominated by sea water, which has a δ^{18}O close to zero, could not result in quartz veins with negative δ^{18}O values even if the $\Delta_{quartz-water}$ is almost zero. Assuming that the veins were formed at 300°C the $\Delta_{quartz-water}$ would be 7.4‰ which equates to a minimum δ^{18}O value for the hydrothermal fluid of -9.1‰ (Figure 6.9). The fluid responsible for the quartz veins at Koegel Fontein was dominated by meteoric water.

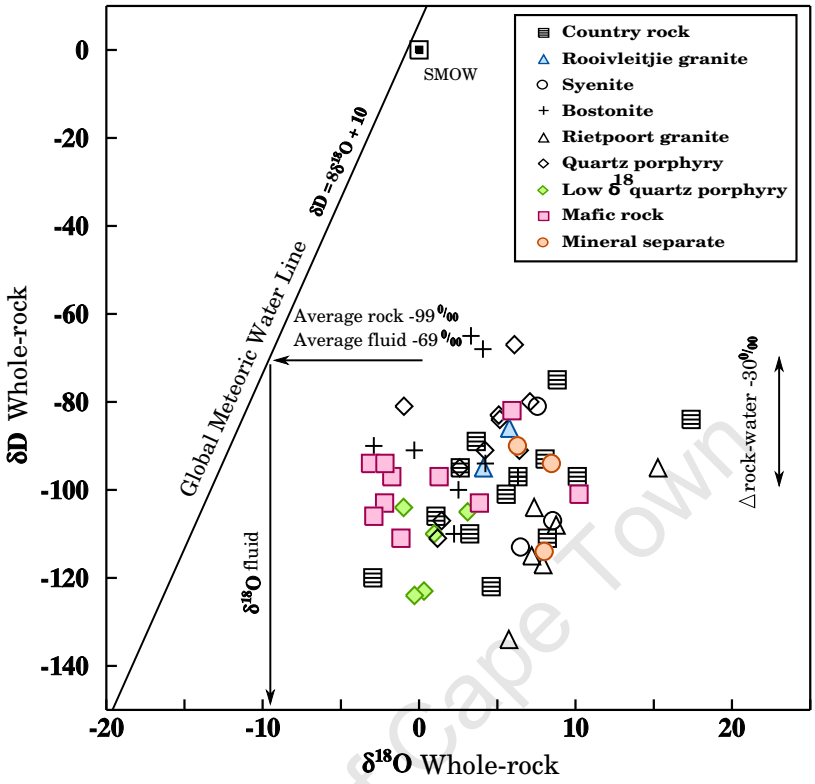

Figure 6.10: Whole–rock and mineral δ^{18}O and δD values for all samples analysed from the Koegel Fontein complex.

6.2.5 The isotopic composition of the hydrothermal fluid

Koegel Fontein has whole rock δ^{18}O values as low as -4.1‰ and associated quartz veins with extremely low δ^{18}O values (Chapter 6.2.4).

Hydrogen isotopes in rocks are more sensitive to alteration than oxygen isotopes as hydrogen is less abundant in igneous rocks. An average igneous rock has about 50 wt. % oxygen and 0.18 wt. % hydrogen per weight percent water (Taylor and Sheppard, 1986; Sheppard, 1986). In modern meteoric–hydrothermal systems the final δD of the meteoric–hydrothermal fluid is normally very close to that of the ambient rain water whereas the δ^{18}O is higher after water–rock interaction. The δD of the rock equilibrates with the water after a small amount of exchange with the meteoric–hydrothermal fluid. A much larger amount of exchange is needed for the δ^{18}O of the rock to be affected (Taylor, 1978; Criss and Taylor Jr., 1986). The δD of the rock can be used as a proxy for the δD of the surface water with which it interacted (Taylor, 1978; Criss and Taylor Jr., 1986). Meteoric waters from around the globe have been characterised (e.g. Craig, 1961; Dansgaard, 1964) and the δD and δ^{18}O form a linear

correlation called the global meteoric water line (GMWL; Craig, 1961). The δD of the rock can, therefore, be used to estimate the isotopic δD of the fluid and hence composition of the meteoric–hydrothermal fluid with reference to the equation for the GMWL.

The average δD value for the Koegel Fontein complex is -99‰ (n = 66, excluding samples with very low water content and anomalously low δD values). Assuming that $\Delta_{rock-water}$ = -30‰, at temperatures between 200 and 300°C, the estimated average δD of the hydrothermal fluid would be -69‰ and the calculated δ^{18}O of the meteoric–hydrothermal fluid is -9.9‰ (Figure 6.10). The average δ^{18}O of the alteration fluid calculated from the associated quartz veins is -9.1‰ (n = 5). The δ^{18}O values of the meteoric water, in the recharge region of the hydrothermal system, are extremely low for the Southern Africa. Such low values are usually only found at high latitudes, high altitudes or far inland (Dansgaard, 1964; Taylor, 1977; Criss and Taylor Jr., 1986) (Chapter 6.2.7). Koegel Fontein was about 40°S at the time of emplacement (Scotese, 1997) which suggests that the ambient meteoric water should not have been as low as -9‰.

6.2.6 Water/rock ratios

The stable isotope composition of the hydrothermal fluid can be used to estimate the amount of water that exchanged with the Koegel Fontein rocks. Water–rock interactions can be divided into four categories: 1) a true–closed system where no fluid interacts with the rocks, 2) a "closed" system where limited amounts of fluid–rock interaction occurs and the mineral phases and coexisting fluid remain in constant relative proportions, 3) an open system where isotopic interaction between mineral and an externally–derived fluid phase with the fluid/rock ratio increasing over time, 4) a "buffered" open system which is controlled by reservoir and the fluid flux is much larger than the isotopic exchange rates between the fluid and mineral phases (Gregory and Criss, 1986). Water–rock interaction is usually a combination between the "closed" and "buffered" open systems and equilibrium between phases is usually assumed (Gregory and Criss, 1986). The "actual" and "effectual" or "isotopic" Water/Rock (W/R) ratios can be calculated using mass balance. When assuming that equilibrium has occurred between the fluid and mineral phases the "effectual" W/R ratios tend to be lower than "actual" W/R ratios.

Below is the equation for calculating the "effective" W/R ratios from Taylor (1977). The equation for the "closed" system water–rock interaction is:

$$W/R_{closed} = \frac{\delta rock_f - \delta rock_i}{\delta_{H_2O} - (\delta rock_f - \Delta)} \tag{6.1}$$

Where W/R is in atom–atom units. δrock$_i$ and δrock$_f$ are the initial and final δ^{18}O values of the rock while δ_{H_2O} is the δ^{18}O of the hydrothermal fluid and Δ is the rock–water fractionation factor.

The equation for open system water–rock interaction from Taylor (1977) is:

$$W/R_{open} = ln(W/R_{closed} + 1) \tag{6.2}$$

Feldspar is the dominant mineral in the Koegel Fontein rocks. W/R ratios for Koegel Fontein were calculated assuming that $\Delta_{rock-water} = \Delta_{feldspar-water}$. The δ^{18}O values of the feldspar separates were used as the final δ^{18}O values of the rock, whereas the initial δ^{18}O values of the rock were estimated using $\Delta_{quartz-feldspar} = 2$. Using a $\Delta_{feldspar-water}$ of 2‰ at 400°C, the calculated δ^{18}O value of the meteoric–hydrothermal fluid (-9.9‰) the range of W/R ratios required to lower the rock δ^{18}O were calculated and are presented in Table 6.2.

The largest W/R for the Koegel Fontein complex was calculated using the highest initial and lowest final feldspar δ^{18}O vales measured for the complex (+7.5 and -1.5‰). There is a large range of calculated W/R values for Koegel Fontein, (0.02 to 1.39). This suggests that either the W/R or the temperature of the hydrothermal fluid and therefore, the fractionation factors have varied for different parts of the complex. The W/R ratios for most samples in Table 6.2 are relatively high which is expected as extensive exchange is needed in order to change the δ^{18}O of the rocks.

6.2.7 Origin of the low δ^{18}O fluid

The isotopic composition of meteoric water is dependent on altitude, latitude, temperature, distance inland and the mean annual rainfall (Sheppard, 1986). The latitude of Southern Africa

Table 6.2: Water–rock ratios for all samples where feldspar was separated. The δRock_f for sample CDB336 was calculated using the relationship of $\Delta_{quartz-feldspar} = 1$ for quartz and feldspar in magmatic equilibrium

Sample	Rock type	δRock_i (‰)	δRock_f (‰)	W/R_{closed}	W/R_{open}
CN495	Quartz porphyry	6.5	3.3	0.29	0.25
CCK7	Quartz porphyry	6	5.7	0.02	0.02
CCK12	Quartz porphyry	6	3.2	0.25	0.22
CDB336	Quartz porphyry	7.4	7.4	0	0
CDB383	Quartz porphyry	6.8	4.3	0.20	0.19
CDB564	Quartz porphyry	6.8	1.5	0.56	0.45
CDB580	Quartz porphyry	2.5	2.1	0.04	0.04
CDB650	Quartz porphyry	6.5	0.6	0.69	0.53
CCK17	Rooivleitjie granite	5.9	1.8	0.42	0.35
CDB687	Rooivleitjie granite	5.8	3.7	0.18	0.17
CCK36	Xenocrysts	6.0	-1.5	1.17	0.78
δ^{18}O hydrothermal fluid		-9.9			
Largest W/R ratio		7.4	-1.5	1.39	0.87

has remained virtually constant (30 to 40°S) over the last 130 million years (e.g. Scotese, 1997). Therefore, latitude is not responsible for the low δ^{18}O vales calculated. Koegel Fontein was relatively close to the nearest ocean (<1000km), at the time of its intrusion (Figure 1.3). Most of Gondwana is thought to have been covered in deserts and very low δ^{18}O values have been found in very dry places. However, the complex is close to paleorivers and there are Cretaceous lacustrine deposits off–shore suggesting that the area was not as dry as the Paraná–Etendeka basin further north where no low low δ^{18}O values have been found (Broad *et al.*, 2006; Kounov *et al.*, 2008).

The altitude of Namaqualand at the time of intrusion is unknown. Regional fission track studies have indicated that a maximum of three kilometres of erosion has occurred along the West Coast of South Africa (Gallagher and Brown, 1999; Kounov *et al.*, 2008), however, the paleoelevation in the Koegel Fontein area remains unknown. It has been suggested that offshore felsic–volcanic material is related to the Koegel Fontein Complex (Verwoerd and de Beer, 2006). If this is the case the structure and height of the Koegel Fontein edifice is unknown. However, if Koegel Fontein reached a similar height as Mt. Kenya (4200–5200m) then alpine type glaciers could explain the low δ^{18}O value calculated for the meteoric–hydrothermal fluid.

The δ^{18}O of the waters (e.g. glacial melt–water and frost) at Mt. Kenya ranges from -6.6 to 1.9‰ (Rietti-Shati *et al.*, 2000). None of the values measured by Rietti-Shati *et al.* (2000) are as low as -9.9‰. Mt. Kenya is closer to the equator than the Koegel Fontein complex which might account for this discrepancy. The conditions required for the low–δ^{18}O meteoric water do not seem to have been met at the time of intrusion. This suggests that the mechanism responsible for generating the low δ^{18}O values occurred prior to the emplacement of the Koegel Fontein Complex.

An alternative explanation for the unusually low δ^{18}O values recorded at the Koegel Fontein complex is the "Fluke–hypothesis", such as that proposed by (Boroughs *et al.*, 2005) for Yellowstone. The "Fluke–hypothesis" suggests that magmas with low–δ^{18}O values intruded an area with pre-existing low–δ^{18}O crust and assimilated the low–δ^{18}O crust or resulted from melting of low–δ^{18}O crust. Figure 2.5 is a cross section of the Koegel Fontein Complex. Magmatic oxygen–isotope values are lowest in the centre of the complex and become progressively more "normal" towards the edge of the complex. This increase in the δ^{18}O values seems to correlate with increased distance from large scale shear zones in the area. The above suggests that it is highly likely that the Koegel Fontein magmas intruded, or resulted from the melting of pre-existing low–δ^{18}O crust. The alteration of the country rocks may have occurred during the Pan–African as the region was extensively deformed during this period (de Beer *et al.*, 2002).

6.2.8 Summary of the ^{18}O depletion in the Koegel Fontein rocks

At Koegel Fontein there are rocks with low–δ^{18}O values achieved by sub–solidus exchange with fluids and crystallization form low–δ^{18}O magmas. The level of intrusion for the complex is estimated to be as high as 3.5 to 2km due to the presence of miarolitic cavities (Candela, 1997; Stevenson *et al.*, 2007, e.g.). Deep circulation of surface waters responsible for the hydrothermal alteration seems to have been facilitated by large scale shear zones reactivated during the rifting of Africa from South America. The lowest δ^{18}O values (> -4.1‰) measured are found near the largest of these structures in the centre of the complex. Calculated W/R ratios for Koegel Fontein are high (<1.39) which is expected as high fluid flow is required to decrease the δ^{18}O of a rock.

Hydrogen–isotope ratios for the complex are also consistently low, have no correlation with water content and do not follow degassing curves. These low δD values are therefore more likely the result of water–rock exchange than magmatic processes. The δD and the δ^{18}O of

the hydrothermal fluid were calculated to be -69 and -9.9‰, respectively. This along with the presence of low–δ^{18}O quartz veins is consistent with a meteoric origin for the alteration fluid. However, these are inconsistent with the stable isotope values expected for the region in the Cretaceous as conditions for generating such low δ^{18}O values were not met.

The complex intruded a region which is at least 1000Ma in age and has experienced a minimum of two Wilson cycles it is possible that the Namaqua crust was altered prior to the intrusion of the Koegel Fontein complex. The association of the low–δ^{18}O magmas with the regional structures, the limited distribution of the low–δ^{18}O magmas and the presence of mafic dykes with low–δ^{18}O whole–rock values which intrude rocks with normal (6-10‰) oxygen–isotope ratios suggests that the low–δ^{18}O magmas may reflect heterogeneities in the source. Unpublished oxygen–isotope data for the Namaqua Metamorphic Province show that there are low–δ^{18}O rocks present in the region (Reid, personal comm.). Although, values low enough to produce the ^{18}O depletion at Koegel Fontein have not been observed.

The complex has the only known low–δ^{18}O rocks associated with the break–up of West Gondwana on the South West African coast. There are limited occurrences of low–δ^{18}O magmas world wide. A possible model for the formation of the Koegel Fontein complex would be similar to the model proposed for the generation of the Snake River Plain Rhyolites by Boroughs *et al.* (2005), where the Koegel Fontein magmas intruded an area previously altered by high–temperature fluids.

6.3 Origin of low δ^{18}O magma

The most well known example of low–δ^{18}O magmas are the inter–caldera lavas found at Yellowstone. These formed as a result of re–melting of earlier erupted phases which had been hydrothermally altered. (Boroughs *et al.*, 2005; Bindeman and Valley, 2001, 2000).

The Koegel Fontein Complex was emplaced where two Pan African shear zones, one trending north–south and the other east–west, intersect. Rocks most affected by the hydrothermal alteration are found along or close to these shear zones. The known low–δ^{18}O magmas are near the north–south trending shear zone which is the largest structure in the Koegel Fontein area (Figure 6.7). This suggests that ^{18}O depletion responsible for the low–δ^{18}O magmas predates the complex. de Beer *et al.* (2002) show that the quartz porphyry dykes are likely to be precursor intrusions for the Rietpoort granite. The Koegel Fontein quartz porphyry dykes that are not close to the large scale shear zones have an average magmatic δ^{18}O = 7.7±0.6‰ and

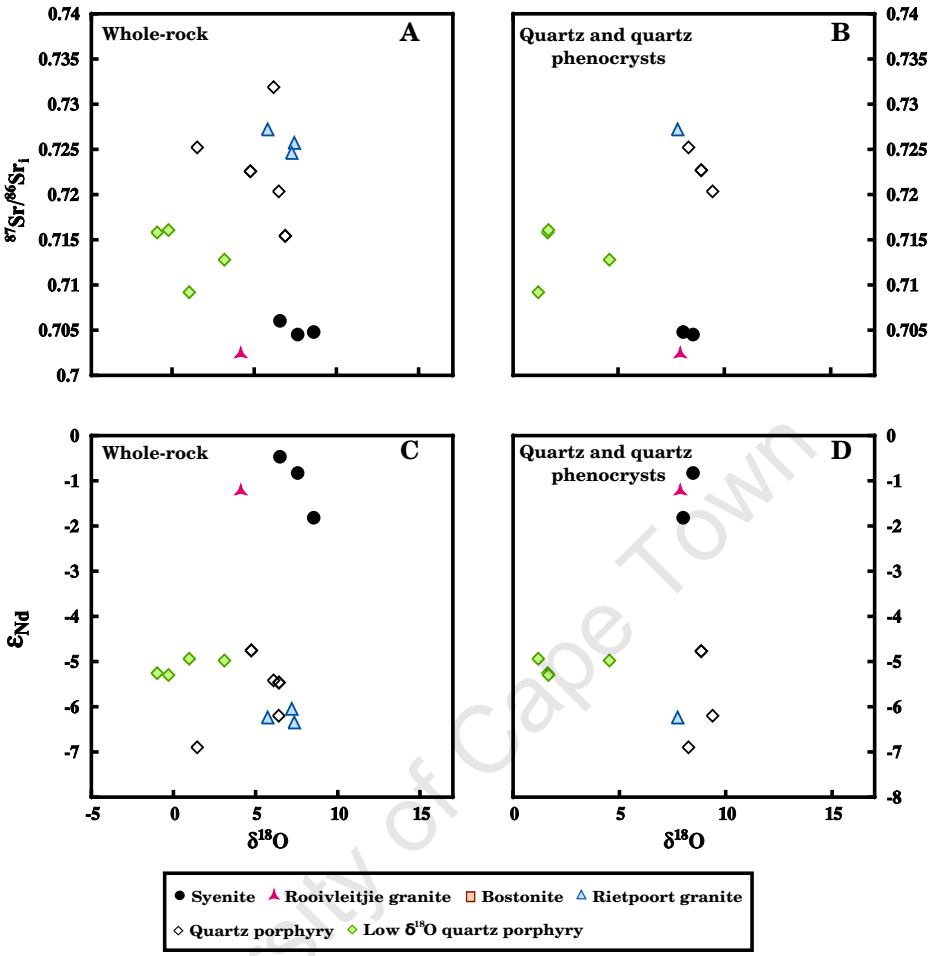

Figure 6.11: Radiogenic isotope versus oxygen–isotope compositions of the Koegel Fontein complex. A. Whole–rock O– and Sr–isotope data. B. Quartz phenocryst O–isotope data and whole–rock Sr–isotope data. C. Whole–rock Nd– and O–isotope data. D. Quartz phenocryst O–isotope data and whole–rock Nd–isotope data.

the Rietpoort granite has a magmatic $\delta^{18}O = 6.3 \pm 0.5‰$ indicating that the Rietpoort $\delta^{18}O$ has been lowered.

6.3.1 Mechanisms for generating low $\delta^{18}O$ magmas

There are three possible explanations for the formation of low $\delta^{18}O$ magmas (Taylor, 1977, 1978). Firstly, the $\delta^{18}O$ values could be the result of partial melting or assimilation of material whose $\delta^{18}O$ value was lowered by high–temperature fluid–rock interaction prior to the emplacement of the Koegel Fontein complex (e.g Seychelles; Harris and Ashwal, 2002). Secondly, a hydrothermal system could have developed during an early Koegel Fontein intrusive

phase altering the surrounding volcanic and/or country rock. These low δ^{18}O rocks were then partially melted during subsequent magmatic activity. Thirdly, low δ^{18}O material formed as in mechanism (two) could have been assimilated by subsequent magmas. The above mechanisms can be distinguished using field relationships and the relationship between radiogenic and stable isotopes.

Low δ^{18}O magmas do not form by direct water–magma interaction (e.g. Taylor, 1974). A finite amount of water is soluble in an epizonal felsic magma (<5%) so that the amount of water which interacts with the magma is to small to cause such low δ^{18}O values (Taylor, 1977). The hydrostatic pressure within the fluid conduits is up to three times lower than the pressure in the magma chamber which is under lithostatic pressure and thus, prevents water from entering the magma (e.g. Taylor, 1977, 1978; Taylor and Sheppard, 1986).

If the low–δ^{18}O magmas formed by (one) the resultant rocks would have similar whole–rock geochemical parameters. Smaller intrusions would reflect localized heterogeneities of the source while larger intrusions would homogenize these variations. This is true for the Koegel Fontein complex especially with respect to radiogenic and stable isotopes (Figure 6.11).

If the low δ^{18}O magmas were formed by the second mechanism, there would be little or no difference between the geochemical properties of the low δ^{18}O rocks and their normal counterparts. Melting of altered, previously erupted or intruded material would probably result in small quantities of low δ^{18}O rocks. This is true for the Koegel Fontein Complex. There is no discernible difference in whole–rock geochemistry between the normal and low δ^{18}O quartz porphyries and the Rietpoort granite. ϵ_{Nd} values are the same within error for the low δ^{18}O quartz porphyries, quartz porphyries and Rietpoort granite. Initial Sr–isotope ratios are different with the low δ^{18}O quartz porphyries having lower initial $^{87}Sr/^{86}Sr$ than the quartz porphyries and the Rietpoort granite (Figure 6.11). Lead–isotopes have no correlation with δ^{18}O and have a wide variation in values. This variation is most likely due to heterogeneities in the source as apposed to post–crystallization processes, as the time elapsed since the intrusion of the complex is too short to have had a major effect on these ratios.

Mechanism (three) would only be distinguishable from mechanism two by single grain analysis such as that done by Bindeman and Valley (2001) for Yellowstone.

6.3.2 The effect of contamination on Koegel Fontein magmas

In order to test assimilation or contamination as a possible mechanism for generating the Koegel Fontein low–δ^{18}O quartz porphyries the amount of contamination needed to lower the

Table 6.3: Average δ^{18}O values and the lowest δ^{18}O values of the possible crustal contaminants. Data summarised from Table 5.3

Rock type	Average whole–rock δ^{18}O (‰)	σ
Namaqua amphibolite	0.8	5.35
Jakkelshoek granite	3.5	3.34
Koegel Fontein bostonites	2.9	3.22
Rooivleitjie granite	4.9	1.18
Koegel Fontein mafic rocks	0.3	3.26
Intermidate plug	-4.1	
Lowest δ^{18}O Jakkelshoek granite	-2.8	
Lowest δ^{18}O bostonite	-2.9	
Lowest δ^{18}O mafic rock	-3.1	

magmatic δ^{18}O by 6.4‰ must be calculated. Table 6.3 shows the most probable contaminants at Koegel Fontein as well as the lowest δ^{18}O values recorded for the bostonites, mafic rocks and Jakkelshoek granite. Few samples of the roof material were taken from the centre of the complex due to poor outcrop. The lowest δ^{18}O sample of Jakkelshoek granite was taken near the intermediate plug which has the lowest δ^{18}O measured at Koegel Fontein. Both the lowest δ^{18}O bostonite and mafic rock samples were collected at the coast about 15km away from the low–δ^{18}O magmas. The values of these rocks and the intermediate plug were included to test the effect of assimilation or contamination of material with negative δ^{18}O values on the magmatic δ^{18}O.

The amount of crustal contamination needed to produce the low–δ^{18}O magmas can be calculated using mass balance in a simple mixing model (e.g. James, 1981; Graham and Harmon, 1983).

$$\delta^{18}O_m = (1 - x)\delta^{18}O^o_m + x.\delta^{18}O_c \tag{6.3}$$

Where $\delta^{18}O^{\circ}{}_m$ and $\delta^{18}O_m$ are the mean oxygen isotope compositions for the original and contaminated magmas respectively. $\delta^{18}O_c$ is the δ^{18}O of the contaminant and x is the mass fraction of oxygen input by the contaminant. The value of $\delta^{18}O^{\circ}{}_m$ was assumed to be the same as either the "normal" δ^{18}O quartz porphyries or the Rietpoort granite, average δ^{18}O = 7.7±0.6

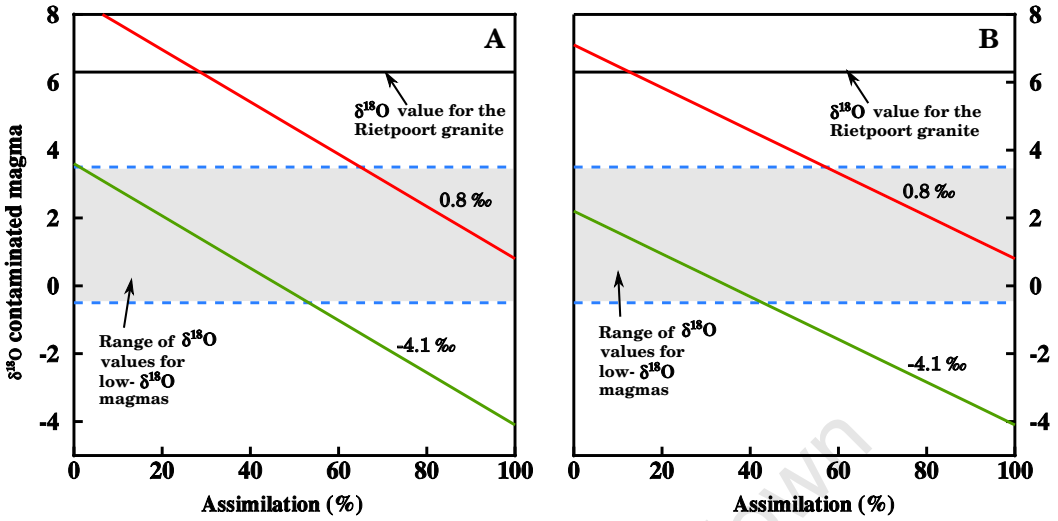

Figure 6.12: Simple mixing mass balance calculations. A. The initial $\delta^{18}O$ of the magma is assumed to be that of the "normal" quartz porphyries, 7.7‰. B. The initial magmatic $\delta^{18}O$ is assumed to be the same as the average value for the Rietpoort granite or 6.3‰ (Rietpoort granite).

and 6.3±0.5‰ respectively. The average $\delta^{18}O$ values of the possible crustal contaminants, the intermediate plug ($\delta^{18}O$ = -4.1‰) and the lowest $\delta^{18}O$ values for the Jakkelshoek granite, bostonites and mafic rocks were used for $\delta^{18}O_c$. Only mixing curves for the highest feasible contaminant and the intermediate plug are shown Figure 6.12.

Figure 6.12 shows assimilation models for a magma with two possible initial $\delta^{18}O$ values. Model A (Figure 6.12A) assumes that the original $\delta^{18}O$ of the magma is that of the "normal" $\delta^{18}O$ quartz porphyries (7.7‰). Model B (Figure 6.12B) assumes that the original $\delta^{18}O$ of the magma is the same as the Rietpoort granite (6.3‰).

To lower the $\delta^{18}O$ of the Rietpoort granite from 7.7‰ to 6.3‰ using a contaminant with a $\delta^{18}O$ of 0.8‰, 10% assimilation would be required. If the assimilant had a $\delta^{18}O$ of -4.1‰ then only be a few % assimilation would be required. The low–$\delta^{18}O$ magmas range from -0.5 to 3.5‰. In order to lower the $\delta^{18}O$ of a magma from 7.7‰ to this range, assuming a contaminant with a $\delta^{18}O$ of 0.8‰, the amount of assimilation would be between 60 and 100%. If the assimalant had a $\delta^{18}O$ of -4.1‰ the amount of assimilation required would be between 0 and 55%.

Assuming that model B is true (Figure 6.12B) than the amount of assimilation required to produce the low–$\delta^{18}O$ magmas would be between 55 and 100%, for a assimilation with a $\delta^{18}O$ of 0.8‰. If material with a $\delta^{18}O$ of -4.1‰ was assimilated then 0 to 45% assimilation would be needed. It is possible that the variation in $\delta^{18}O$ values at Koegel Fontein could be caused

Table 6.4: Initial Sr–isotope ratios for the Rietpoort granite and quartz porphyries.

Sample Number	Rock Type	$^{87}Sr/^{86}Sr_1$
CCK52	Rietpoort granite	0.727190
CCK53	Rietpoort granite	0.725696
CCK55	Rietpoort granite	0.724595
CCK10	Quartz porphyry	0.715504
CDB336	Quartz porphyry	0.720337
CDB388	Quartz porphyry	0.731879
CDB650	Quartz porphyry	0.725212
CN495	Quartz porphyry	0.722665
CCK23	Low–δ^{18}O quartz porphyry	0.709175
CDB580	Low–δ^{18}O quartz porphyry	0.712783
CDB588	Low–δ^{18}O quartz porphyry	0.715800
CDB594	Low–δ^{18}O quartz porphyry	0.716063
CCK2	Grey gneiss	0.726315
CCK27	Augen gneiss	0.909869

by assimilation of hydrothermally altered material.

The variation in initial Sr–isotope ratios seen in the Rietpoort granite and quartz porphyries (Table 6.4) could also be the result of contamination. The amount of assimilation can be calculated using $^{87}Sr/^{86}Sr$ ratios and the mass balance equation from Faure (1986):

$$(^{87}Sr/^{86}Sr)_m = \frac{(^{87}Sr/^{86}Sr)_a Sr_a.f + (^{87}Sr/^{86}Sr)^o_m Sr^o_m(1-f)}{(Sr_a.f + Sr^o_m(1-f))} \tag{6.4}$$

Strontium ratios for the magma and assimilant are represented by $^{87}Sr/^{86}Sr^o_m$ and $^{87}Sr/^{86}Sr_a$ respectively and the weight fraction of material assimilated is denoted by f. The average initial $^{87}Sr/^{86}Sr$ for the syenites (0.7051±8) was used for $^{87}Sr/^{86}Sr^o_m$. The average initial value of the syenite was used for the magmatic value as these rocks appear to be the least contaminated rocks from the Koegel Fontein Complex. Samples of augen gneiss (CCK27) and grey gneiss (CCK2) were used for $^{87}Sr/^{86}Sr_a$. The Sr–isotope values for these country rock samples were calculated for 135Ma (Table 6.4). The results are shown in Figure 6.13.

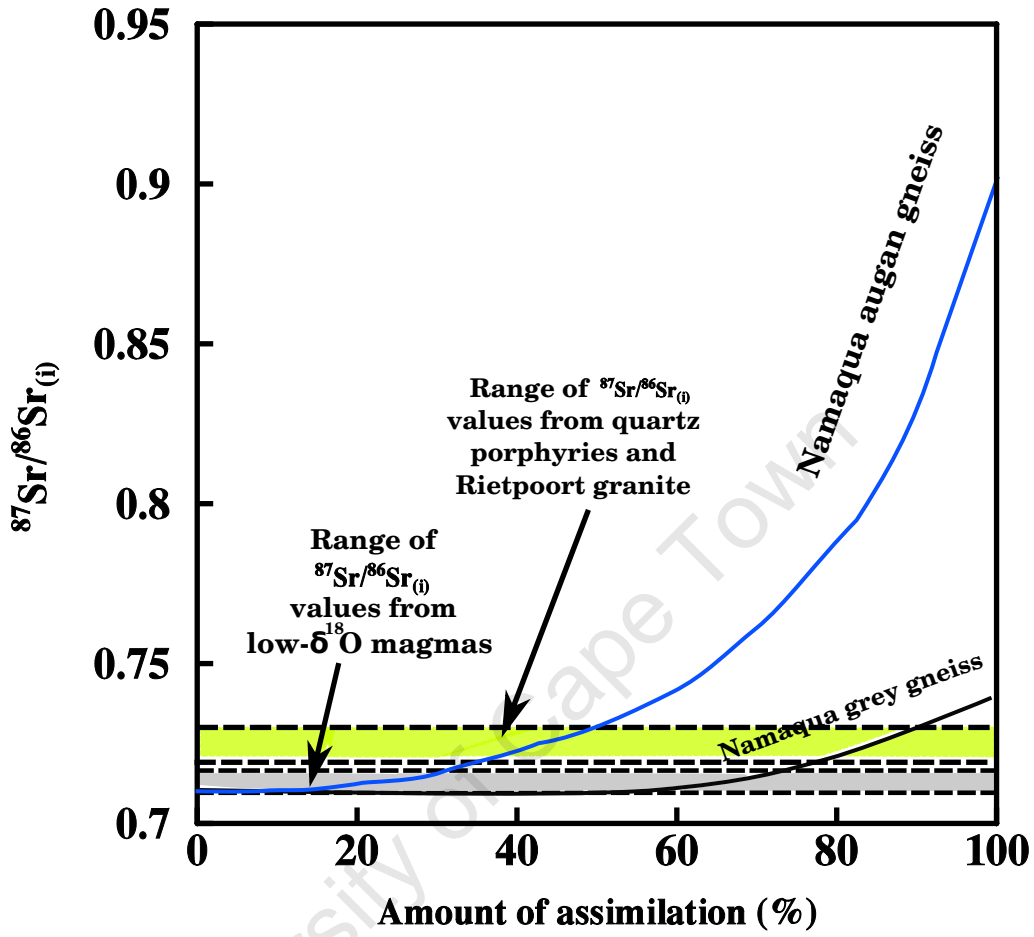

Figure 6.13: Crustal contamination calculated using Sr–isotope mass balance plotted with the range of initial Sr–isotope ratios for the low–δ^{18}O quartz porphyries, quartz porphyries and the Rietpoort granite. Measured $^{87}Sr/^{86}Sr$ values of the two country rock samples were used as possible contaminants assuming that the original $^{87}Sr/^{86}Sr$ ratio was similar to the $^{87}Sr/^{86}Sr_i$ of the syenites.

The Namaqua augen gneiss could be a possible contaminant. The amount of assimilation needed to produce the initial Sr–isotope ratios for the Rietpoort granite and "normal" quartz porphyries would be between 30 and 45%. In order to produce the initial $^{87}Sr/^{86}Sr$ range seen in the low–δ^{18}O quartz porphyries contamination would be between 0 and 30%. The grey gneiss is an unlikely contaminant for the granite and "normal" quartz porphyries as the amount of assimilation required ranges from 80 to 90%. Contamination by the grey gneiss could account for the variation in initial $^{87}Sr/^{86}Sr$ for the low–δ^{18}O quartz porphyries. The amount of assimilation needed would be between 0 and 75%.

However, assimilation of either contaminant requires larger amounts of contamination for the

Rietpoort granite and "normal" quartz porphyries than the low–δ^{18}O quartz porphyries. This is the opposite of the oxygen–isotope model. Field relationships show that the quartz porphyries are older than the Rietpoort granite. This suggests that the low–δ^{18}O quartz porphyries are not inter–caldera melts of hydrothermally altered, early erupted material such as those found at Yellowstone (Boroughs *et al.*, 2005). Trace element geochemistry (Figure 6.1 and 5.9) and Pb–isotopes (Figure 5.15) show that the source region of the Koegel Fontein complex is heterogeneous. It is possible that the O–and Sr–isotope data also reflect crustal heterogeneities. Therefore, the simplest explanation for the generation of the low–δ^{18}O magmas would be emplacement into a region of previously altered rocks.

6.3.3 Summary of the origin of the δ^{18}O magmas

There are three mechanisms for generating low–δ^{18}O magmas: (1) melting or assimilation of pre-existing low–δ^{18}O crust; (2) melting of early erupted material and/or country rock altered by a synchronous hydrothermal system; (3) assimilation of material formed by (2). Oxygen–isotope assimilation models show that larger percentages of assimilation are needed for the low–δ^{18}O magmas than the "normal" quartz porphyries and Rietpoort granite. Strontium–isotope assimilation models indicate that the Rietpoort granite and "normal" quartz porphyries would require more contamination than the low–δ^{18}O quartz porphyries. This suggests that assimilation is an unlikely mechanism for the generation of the low–δ^{18}O magmas.

It has been established by de Beer and Armstrong (1998) that the quartz porphyries and the Rietpoort granite are indistinguishable in age using zircon dating. The quartz porphyries are thought to be the precursor intrusions to the Rietpoort granite as they abut against the granite. This suggests that the low–δ^{18}O quartz porphyries are either a result of melting of early altered material associated with syenite or of older altered material. The variation in REE patterns for the Rietpoort granite and quartz porphyries and Pb–isotopes for all the Koegel Fontein rock types indicate that the source of the Koegel Fontein magmas was heterogeneous. It is possible that the O– and Sr–isotopes are also the result of heterogeneities in the source.

Chapter 7

Conclusions

1. The Koegel Fontein felsic rocks originate from at least two magma series. The Syenites, bostonites and Rooivleitjie granite belong to one whereas the Rietpoort granite and quartz porphyries belong to the other.

2. Trace elements and Pb–isotopes indicate that the source region of the Koegel Fontein complex was heterogeneous. The Rietpoort granite has similar ϵ_{Nd} and initial Sr–isotope values as the Erongo and Spitzkoppe in northern Namibia. Both of the Namibian granites are interpreted as crustal melts which suggest that the Rietpoort granite also formed by crustal melting.

3. At Koegel Fontein there are rocks which achieved low–δ^{18}O values through water–rock interaction with high–temperature fluids and a more limited number of rocks that crystallized from low–δ^{18}O magmas.

4. There were at least two hydrothermal systems at the complex, one centred around the Sandkop syenite and the other around the Rietpoort granite.

5. Meteoric–hydrothermal fluids were responsible for the high–temperature alteration at Koegel Fontein. The δ^{18}O of the fluid was calculated to be -9.9‰ and the δD = -6.9‰. Calculated W/R ratios for the complex are high and range from 0.02–1.39.

6. Meteoric water with δ^{18}O values as low as -9.9‰ are unlikely in the Koegel Fontein area. The complex was at a relatively low latitude, <1000km from the nearest ocean and there is no evidence of high elevation around the complex. Therefore, none of the factors which lower the δ^{18}O of meteoric water were present in the Cretaceous when the Koegel Fontein complex was emplaced.

7. Assimilation models for O–isotopes indicate that the low–δ^{18}O quartz porphyries require the largest amounts of contamination compared to the Rietpoort granite and normal δ^{18}O quartz porphyries. Whereas Sr–isotope assimilation models suggest that the low–δ^{18}O quartz porphyries had the least amount of contamination of the 133Ma Koegel Fontein felsic rocks. The O– and Sr–isotope variations seen at Koegel Fontein may, therefore, be the result of heterogeneities in the Namaqua crust.

8. Low–δ^{18}O magmas were most likely formed as a result of small scale melting of pockets of previously altered crust and represent local heterogeneities in the source region.

9. The "normal" δ^{18}O quartz porphyries have a magmatic δ^{18}O = +7.7±0.6‰ and Erongo and Spitzkoppe have a magmatic δ^{18}O of 10‰. The Rietpoort granite has a magmatic δ^{18}O = 5.9±0.7‰ which is unusually low for a crustal melt. Assuming that the quartz porphyries are the precursor intrusions to the Rietpoort granite, indicates that the δ^{18}O of the Rietpoort granite has been lowered by at least 1.8‰.

10. The Rietpoort granite δ^{18}O was probably lowered by the homogenization of small scale heterogeneities in the Koegel Fontein source region, where the source region interacted with meteoric–hydrothermal fluids prior to melting.

11. Mafic dykes with low–δ^{18}O whole–rock values and xenoliths intrude Namaqua country rocks which have normal δ^{18}O values (+6 to +10‰). This suggests that the hydrothermal alteration synchronous with the emplacement of the complex is not solely responsible for the low–δ^{18}O values measured at Koegel Fontein.

12. The source rocks for the low–δ^{18}O magmas appear to have been altered prior to the intrusion of the Koegel Fontein complex. The low–δ^{18}O magmas are restricted to the centre of the Koegel Fontein Complex, close to the largest shear zone in the area. Their trace element concentrations, Sr– and Pb–isotope values indicate that their source region was heterogeneous. The assimilation models for O– and Sr–isotopes disagree with one another, indicating that assimilation was not responsible for the low–δ^{18}O magmas. Preliminary data for the mafic dykes suggests that the dykes acquired their low–δ^{18}O signal at the source and not by synchronous hydrothermal alteration. These factors suggest that the Koegel Fontein complex intruded a region which had been previously altered by high–temperature fluids.

Chapter 8

Future work

Zircon has a high closure temperature for oxygen diffusion and is very resistant to alteration. Cores of inherited zircons retain their original δ^{18}O. Zircon δ^{18}O studies would be useful in determining the history of the low–δ^{18}O magmas. Similar studies have been done on the low–δ^{18}O magmas at Yellowstone (e.g. **?**Bindeman and Valley, 2001), revealing the history of these rocks, as the zircons have normal–δ^{18}O cores and low–δ^{18}O rims. A similar study could be done on the low–δ^{18}O quartz porphyries at Koegel Fontein to determine their melting history.

Fluid inclusion studies would help to better define the temperature of the hydrothermal fluid. They would also allow the composition of the hydrothermal fluid to be determined. The presence of NaCl and KCl and the pH of the fluid affects how the fluid reacts with feldspar, which is the main constituent of most of the Koegel Fontein rocks. The composition of the fluid and SEM micrographs would help explain how different minerals responded to the hydrothermal alteration.

The intermediate plug has the lowest δ^{18}O values recorded at the Koegel Fontein complex. More detailed sampling, analysis and dating are required to determine whether the plug is related to the Koegel Fontein complex.

The mafic rocks are a diverse group of rocks ranging from tholeiitic basalt to lamprophyre and require a more detailed study. The mineral geochemistry, radiogenic isotopes and the mineral δ^{18}O values need to be analysed. These will also improve the understanding as to how these rocks relate to the felsic rocks of the Koegel Fontein Complex.

A comprehensive dating project would add valuable information to the ages already obtained by de Beer and Armstrong (1998). The bostonite, Rooivleitjie granite and mafic rocks have

not been dated while only one quartz porphyry sample was analysed. Absolute ages, especially zircon ages, would be able to determine the relationship of the low–δ^{18}O magmas to the Rietpoort granite and confirm the differentiation trends seen in the whole–rock geochemistry.

There is a magnetic anomaly at the Koegel Fontein Complex. The whole rock geochemistry did not give any indication as to why this might be present. Therefore, a seismic and/or gravity study needs to be done in order to determine the origin of this anomaly.

References

Balsley, S. D., Gregory, R. T., 1998. Low–δ^{18}O silicic magmas: Why are they so rare? Earth and Planetary Science Letters 162, 123–136.

Bauer, K., Trumbull, R. B., Vietor, T., 2003. Geophysical images and a crustal model of intrusive structures beneath the Messum ring complex, Namibia. Earth and Planetary Science Letters 216, 65–80.

Best, M., G., Christiansen, E., H., 2001. Igneous Petrology. Blackwell Schence, Ltd., Abingdon, Oxon, England.

Bindeman, I. N., 2008. Oxygen isotopes in mantle and crustal magmas as revealed by single crystal analysis. Reviews in Mineralogy and Geochemistry 69, 445–478.

Bindeman, I. N., Valley, J. W., 2000. Formation of low–δ^{18}O rhyolites after caldera collapse at Yellowstone, Wyoming, USA. Geology 28, 719–722.

Bindeman, I. N., Valley, J. W., 2001. Low–δ^{18}O ryholites from Yellowstone: magmatic evolution based on analyses of zircons and individual phenocrysts. Journal of Petrology 42, 1491–1517.

Boroughs, S., Wolff, J., Bonnichsen, B., Godchaux, M., Larson, P., 2005. Large–volume, low–δ^{18}O rhyolites of the Central Snake River Plain, Idaho, USA. Geology 33, 821–824.

Botha, B. J. V., Hodgson, F. D. I., 1976. Karoo dolerites in northwestern Damaraland. Transactions of the Geological Society of South Africa 79, 186–190.

Broad, D. S., Jungslage, E. H. A., McLachlan, I. R., Roux, J., 2006. Offshore Mesozoic basins *in* The Geology of South Africa, Johnson, M. R., Anhaeusser, C. R., Thomas, R. J. (Eds.), Council for Geoscience, Pretoria, South Africa, pp. 553–572.

Candela, P. A., 1997. A review of shallow, ore-related granites: Textures, volatiles, and ore metals. Journal of Petrology 38, 1619–1633.

Coplen, T. B., Kendall, C., Hopple, J., 1983. Comparison of stable isotope reference samples. Nature 302, 236–238.

Cornell, D. H., Thomas, R. J., Moen, H. F. G., Reid, D. L., Moore, J. M., Gibson, R. . L., 2006. The Namaqua–Natal Province *in* The Geology of South Africa, Johnson, M. R., Anhaeusser, C. R., Thomas, R. J. (Eds.), Council for Geoscience, Pretoria, South Africa, pp. 325–379.

Craig, H., 1961. Isotopic variations in meteoric waters. Science 133, 1702–1703.

Criss, R. E., Taylor Jr., H. P., 1986. Meteoric–hydrothermal systems. Reviews in Mineralogy and Geochemistry 16, 373–424.

Dansgaard, W., 1964. Stable isotopes in precipitation. Tellus 16, 436–468.

De Beer, C., In Press. The Geology of the Garies area. Explanation 1:250,000 sheet 3017 Garies. Council for Geoscience, Pretoria, South Africa.

de Beer, C. H., Armstrong, R. A., 1998. Age and tectonic setting of Mesozoic anorogenic complex west of Bitterfontein, Namaqualand, South Africa. In: Abstract volume. Vol. 15. IAVCEI International Volcanological Congress, Cape Town.

de Beer, C. H., Gresse, P. G., Theron, J. N., Almond, J. E., 2002. The geology of the Calvinia area. Explanation of the 1:250 000 sheet 3118 Calvinia. Council for Geoscience, Pretoria, South Africa.

de Beer, J. H., Meyer, R., 1984. Geophysical characteristics of the Namaqua–Natal Belt and its boundaries. South African Journal of Geodynamics 1, 473–494.

Deer, W. A., Howie, R. A., Zussman, J., 1992. Introduction to the rock–forming minerals, 2nd Edition. Pearson Education Ltd.

Diehl, M., 1990. Geology, mineralogy, geochemistry and hydrothermal alteration of the Brandberg alkaline complex, Namibia. Geological Survey Namibia Memoir 10, 1–11.

Eglington, B. M., Harmer, R. E., 1999. GEODATE for Windows version 1: Isotope regression and modeling software. Council for Geoscience Open File Report 1999–0206–0, 51.

Erlank, A. J., Marsh, J. S., Duncan, A. R., Miller, R. M., Hawkesworth, C. J., Betton, P. J., Rex, D. C., 1984. Geochemistry and petrogenesis of the Etendeka Volcanic rocks from SWA/Namibia. Special Publication Geological Society South Africa 13, 195–245.

Ewart, A., Milner, S. C., Armstrong, R. A., Duncan, A. R., 1998a. Etendeka volcanism of the Goboboseb Mountains and Messum Igneous Complex, Namibia. Part i: Geochemical evidence of early Cretaceous Tristan Plume melts and the role of crustal contamination in the Paraná–Etendeka CFB. Journal of Petrology 39, 191–225.

Ewart, A., Milner, S. C., Armstrong, R. A., Duncan, A. R., 1998b. Etendeka volcanism of the Goboboseb Mountains and Messum Igneous Complex, Namibia. Part ii: Voluminous quartz latite volcanism of the Awahab Magma System. Journal of Petrology 39, 227–253.

Faure, G., 1986. Principles of isotope geology, 2nd Edition. John Wiley and Sons.

Fengming, X., Xiang, X., 1994. Two A–type syenite–granite belts in anhui. Chinese Journal of Geochemistry 13, 340–354.

Frindt, S., Trumbull, R. B., Romer, R. L., 2004. Petrogenesis of the Gross Spitzkoppe topaz granite, central western Namibia: a geochemical and Nd–Sr–Pb isotope study. Chemical Geology 206, 43–71.

Frost, B. R., Barnes, C. G., Collins, W. J., Arculus, R. J., Ellis, D. J., Frost, C. D., 2001. A geochemical classification for granitic rocks. Journal of Petrology 42, 2033–2048.

Gallagher, K., Brown, R., 1999. Denudation and uplift at passive margins: The record on the Atlantic Margin of southern Africa. Phil. Trans. Royal Sociehy of London 357, 835–859.

Gibson, S. A., Thompson, R. N., Day, J. A., 2006. Timescales and mechanisms of plume–lithosphere interactions: $^{40}Ar/^{39}Ar$ geochronology and geochemistry of alkaline igneous rocks from the Paraná–Etendeka large igneous province. Earth and Planetary Science Letters 251, 1–17.

Giletti, B. J., 1986. Diffusion effects of oxygen isotope temperatures of slowly cooled igneous and metamorphic rocks. Earth and Planetary Science Letters 77, 218–228.

Giletti, B. J., Yund, R. A., 1984. Oxygen diffusion in quartz. Journal of Geophysical Research 89, 4039–4046.

Graham, C. M., Harmon, R. S., 1983. Stable isotope evidence on the nature of crust–mantle interactions *in* Continental basalts and mantle xenoliths, Shiva Publishing Ltd., Cheshire, UK, pp. 20–45.

Gregory, R. T., Criss, R. E., 1986. Isotopic exchange in open and closed systems. Reviews in Mineralogy and Geochemistry 16, 91–127.

Gregory, R. T., Criss, R. E., Taylor, Jr., H. P., 1989. Oxygen isotope exchange kinetics of mineral pairs in closed and open system applications to problems of hydrothermal alteration of igneous rocks and Precambrian iron formation. Chemical Geology 75, 1–42.

Gresse, P. G., von Veh, M. W., Frimmel, H. E., 2006. Namibian (Neoproterozoic) to Early Cambrian successions *in* The Geology of South Africa, Johnson, M. R., Anhaeusser, C. R., Thomas, R. J. (Eds.), Council for Geoscience, Pretoria, South Africa, pp. 395–20.

Haapala, I., Frindt, S., Kandara, J., 2007. Cretaceous Gross Spitzkoppe and Klein Spitzkoppe stocks in Namibia: Topaz–bearing A–type granites related to continental rifting and mantle plume. Lithos 97, 174–192.

Harris, C., 1995. Oxygen isotope geochemistry of the Mesozoic anorogenic complexes of Damaraland, northwest Namibia: Evidence for crustal contamination and its effect on silica saturation. Contributions to Mineral Petrology 122, 308–321.

Harris, C., Ashwal, L., 2002. The origin of low $\delta^{18}O$ granites and related rocks from the seychelles. Contributions to Mineralogy and Petrology 143, 366–376.

Harris, C., Faure, K., Diamond, R. E., Scheepers, R., 1997. Oxygen and hydrogen isotope geochemistry of S– and I–type granitoids: The Cape Granite Suite, South Africa. Chemical Geology 143, 95–114.

Harris, C., Marsh, J. S., Milner, S. C., 1999. Petrology of the alkaline core of the Messum Igneous Complex, Namibia: evidence for the progressively decreasing effect of crustal contamination. Journal of Petrology 40, 1377–1397.

Harris, C., Smith, H., le Roex, A., 2000. Oxygen isotope composition of phenocrysts from Tristan da Cunha and Gough Island lavas: Variation with fractional crystallization and evidence for assimilation. Contributions to Mineral petrology 138, 164–175.

Harris, C., Whittingham, A. M., C., M. S., Armstrong, R. A., 1990. Oxygen isotope geochemistry of the silicic volcanic rocks of the Etendeka–Paraná province: Source constraints. Geology 18, 1119–1121.

Hart, S., 1984. A large-scale isotope anomaly in the Southern Hemisphere mantle. Nature 309, 753–757.

Irvine, T. N., Baragar, W. R. A., 1971. A guide to the chemical classification of the common volcanic rocks. Canadian Journal of Earth Science 8, 523–548.

Jack, A. M., 1980. The geology of western Namaqualand. Bulletin of the Precambrian Research Unit 29, 173.

James, D. E., 1981. The combined use of oxygen and radiogenic isotopes as indicators of crustal contamination. Annual Review of Earth and Planetary Sciences 9, 311–344.

Jansen, H., 1960. The Geology of the Bitterfontein Area, Cape Province. Council for Geoscience.

Joubert, P., 1971. The regional tectonism of the gneisses of part of Namaqualand. Bulletin of the Precambrian Research Unit 10, 220.

Kounov, A., Viola, G., de Wit, M. J., Andreoli, M., 2008. A mid Cretaceous paleo–Kroo river valley across the Knersvlakte plain (northwestern coast of South Africa): Evidence from apatite fission–track analysis. South African Journal of Geology 111, 409–420.

LaBas, M. J., LaMaitre, R. W., Streckeisen, A., Zanettin, B., 1986. A chemical classification of volcanic rocks based on the total alkali silica diagram. Journal of Petrology 27, 745–750.

Larson, P. B., Taylor, Jr., H. P., 1986. An oxygen isotope study of hydrothermal alteration in the Lake City caldera, San Juan Mountains, Colorado. Journal of Volcanology and Geothermal Research 30, 47–82.

le Roex, A. P., Lanyon, R., 1998. Isotope and trace element geochemistry of the Cretaceous Damaraland lamprophyres and carbonatites, northwestern Namibia: Evidence for plume–lithosphere interactions. Journal of Petrology 39, 1117–1146.

le Roex, A. P., Watkins, R. T., Reid, A. M., 1996. Geochemical evolution of the Okenyenya sub–volcanic ring complex, northwestern Namibia. Geological Magazine 133, 645–670.

Macey, P., Harris, C., 2006. Stable isotope and fluid inclusion evidence for the origin of the Brandberg West area Sn–W vein deposits NW Namibia. Mineralium Depoita 41, 671–690.

Martin, H., Mathias, M., Simpson, E. S., 1960. The Damaraland sub–volcanic ring complexes in South West Africa. Petrographic provinces, Igneous and Metamorphic Rocks, 156–174.

Martinez, I. A., Harris, C., le Roex, A. P., Milner, S. C., 1996. Oxygen isotope evidence for extensive crustal contamination in the Okenyenya igneous complex, Namibia. Geochimica et Cosmochimica Acta 60, 4497–4508.

McIver, J., 1981. Aspects of ultrabasic and basic alkaline intrusive rocks from Bitterfontein, South Africa. Contributions to Mineral petrology 78, 1–11.

Miller, C. F., Mittlefehldt, D. W., 1982. Depletion of light rare earth elements in felsic magmas. Geology 10, 129–133.

Milner, S. C., le Roex, A. P., 1996. Isotope characteristics of the Okenyenya igneous complex, northwestern Namibia: constraints on the composition of the early Tristan Plume and the origin of the EM 1 mantle component. Earth and Planetary Science Letters 141, 277–291.

Milner, S. C., le Roex, A. P., Watkins, R. T., 1993. Rb–Sr age determinations of rocks from the Okenyenya igneous complex, northwestern Namibia. Geological Magazine 130, 335–343.

Mingram, B., Trumbull, R. B., Littman, S., Gerstenberger, H., 2000. A petrogenetic study of anorogenic felsic magmatism in the Cretaceous Paresis ring complex, Namibia: Evidence for mixing of crust and mantle–derived components. Lithos 54, 1–22.

Moore, A. E., Verwoerd, W. J., 1985. The olivine melilitite–"kimberlite"–carbonatite suite of Namaqualand and Bushmanland, South Africa. Transactions of the Geological Society of South Africa 88, 281–294.

Moore, R. O., Gurney, J. J., 1989. Mineral inclusions in diamond from Monastery kimberlite, South Africa *in* Kimberlites and Related Rocks, Special Publication, et al, J. R. (Ed.), Geological Society of Australia, Blackwell, Carlton, pp. 1029–1041.

O'Connor, J. M., le Roex, A. P., 1992. South Atlantic hot spot–plume systems. i: Distribution of volcanism in time and space. Earth and Planetary Science Letters 113, 343–364.

O'Neil, J. R., Tayler, Jr., H. P., 1967. The oxygen isotope and cation exchange chemistry of feldspars. Journal of Geophysics Research 74, 6012–6022.

Patino Dounce, A. E. P., 1997. Generation of metaluminous a–type granites by low–p melting of calc–alkaline granitoids. Geology 25, 743–746.

Peate, D. W., 1997. The Paraná–Etendeka Province *in* Large Igneous Provinces: Continental, Oceanic and Planetary, Union, A. G. (Ed.), Geological Society of Australia, Geophysical Monograph, pp. 217–231.

Peucat, J. J., Vidal, P., Bernard-Griffiths, J., Condie, K. C., 1989. Sr, nd, and pb isotopic systematics in the archean low- to high-grade transition zone of southern india: Syn-accretion vs. post-accretion granulites. The Journal of Geology 97 (5), 537–549.

Porada, H., 1989. Pan–African rifting and orogenesis in southern to equitorial Africa and eastern Brazil. Precambrian Research 44, 103–136.

Reid, D. L., 1979. Total rock Rb–Sr and U–Th–Pb isotopic study of Precambrian metavolcanic rocks in the lower Orange River region, Southern Africa. Earth and Planetary Science Letters 42, 368–378.

Reid, D. L., 1999. Whole–rock radiometric age patterns in the Aggeneys–Gamsberg, central Bushmanland, South Africa. South African Journal of Geology 100, 11–22.

Rietti-Shati, M., Yam, R., Karlen, W., Shemesh, A., 2000. Stable isotope composition of tropical high–altitude fresh–waters on Mt. Kenya, Equatorial East Africa. Chemical Geology 166, 341–350.

Robb, L. J., 1983. Trace elements trends in granites and the distinction between partial melting and crystal fractionation processes: Case studies from two granites in Southern Africa *in* The significance of trace elements in solving petrogenetic problems and controversies, Theophrastus Publications S. A., Athens, Greece, pp. 553–572.

Rogers, A. W., 1911. Geological survey of parts of Van Rynsdorp and Namaqualand Divisions. Annual report of the Geological Commission of the Cape of Good Hope, 7–87.

Romer, R. L., Förster, H. J., Breitkreuz, C., 2001. Intracontinental extensional magmatism with a subduction fingerprint: The late Carboniferous Halle Volcanic Complex (Germany). Contributions to Mineralogy and Petrology 141.

Romer, R. L., Xiao, Y., 2005. Initinal Pb– Sr–Nd–isotopic heterogeneity in a single allanite-epidote crystal: implications of reaction history for the dating of minerals with low parent– to daughter– ratios. Contributions to Mineralogy and Petrology 148, 662–674.

Scotese, 1997. Continental drift PALEOMAP project, 7th Edition. Arlington, Texas USA.

Shand, S. J., 1943. The eruptive rocks, 2nd Edition. John Wiley.

Sharp, Z., 2006. Igneous petrology *in* The Principles of Stable Isotope Geochemistry, Pearson Prentice Hall, Upper Saddle River, NJ 07458, pp. 242–266.

Sheppard, S. M. F., 1986. Characteriszation and isotopic variations in natural waters. Reviews in Mineralogy and Geochemistry 16, 165–183.

Stevenson, C. T. E., Owens, W. H., Hutton, D. H. W., Hood, D. N., Meighan, I. G., 2007. Laccolithic, as opposed to cauldron subsidence, emplacement of the Eastern Mourne pluton, N. Ireland: evidence from anisotropy of magnetic susceptibility. Journal of the Geological Society 164, 99–110.

Sun, S. S., McDonough, W. F., 1989. Chemical and isotopic systematics of oceanic basalts: Implications for mantle composition and processes. Earth and Planetary Science letters 42, 313–345.

Taylor, B. E., Eichelberger, J. C., Westrich, H. R., 1983. Hydrogen isotopic evidence of rhyolitic magma degassing during shallow intrusion and eruption. Nature 306, 541–545.

Taylor, Jr., H. P., 1974. The application of oxygen and hydrogen isotope studies to problems of hydrothermal alteration and ore deposition. Economic Geology 69, 843–883.

Taylor, Jr., H. P., 1977. Water/rock interactions and the origin of water in granitic batholiths: Thirtieth william smith lecture. Journal of the Geological Society of London 133, 509–558.

Taylor, Jr., H. P., 1978. Oxygen and hydrogen isotope studies of plutonic granitic rocks. Earth and Planetary Science letters 38, 177–210.

Taylor, Jr., H. P., Sheppard, S. M. F., 1986. Igneous rocks: I. processes of isotope fractionation and isotope systematics. Reviews in Mineralogy and Geochemistry 16, 227–271.

Thompson, R. N., Gibson, S. A., Dickin, A. P., Smith, P. M., 2001. Early Cretaceous basalt and picrite dykes of the southern Etendeka region, NW Namibia: Windows into the role of the Tristan Mantle Plume in the Paraná–Etendeka magmatism. Journal of Petrology 42, 2049–2081.

Titterington, D. M., Halliday, A. N., 1979. On the fitting of parallel isochrons and the method of maxim likelihood. Chemical Geology 26, 183–195.

Trumbull, R. B., Buhn, B., Romer, R. L., Volker, F., 2003. The petrology of basanite–tephrite intrusions in the Erongo complex and implications for a plume origin of Cretaceous alkaline complexes in Namibia. Journal of Petrology 44, 93–111.

Trumbull, R. B., Harris, C., Frindt, S., Wigand, M., 2004. Source diversity on Cretaceous anorogenic granites from Namibia, O–Nd evidence for mixing of mantle derived magmas with isotopically homogenized orogenic crust and implications for A–type granite genesis. Lithos 73, 21–40.

Trumbull, R. B., Reid, D. L., de Beer, C., van Acken, D., Romer, R. L., 2007. Magmatism and continental breakup at the west margin of Southern Africa: A geochemical comparison of dolerite dikes from northwestern Namibia and the Western Cape. South African Journal of Geology 110 (2), 477–502.

Valley, J. W., Kitchen, N., Kohn, M. J., Niendorf, C. R., Spicuzza, M. J., 1995. UWG–2, a garnet standard for oxygen isotope ratios: Strategies for high precision and accuracy with laser heating. Geochimica et Cosmochimica Acta 59, 5223–5231.

Vennemann, T. W., O'Neil, J, R., 1993. A simple and inexpensive method of hydrogen isotope and water analyses of minerals and rocks based on zinc reagent. Chemical Geology 103, 227–234.

Verwoerd, W. J., de Beer, C. H., 2006. Cretaceous and Tertiary igneous events *in* The Geology of South Africa, Johnson, M. R., Anhaeusser, C. R., Thomas, R. J. (Eds.), Council for Geoscience, Pretoria, South Africa, pp. 573–583.

Watkeys, M., 2006. Gondwana Break–up: A South African perspective *in* The Geology of South Africa, Johnson, M. R., Anhaeusser, C. R., Thomas, R. J. (Eds.), Council for Geoscience, Pretoria, South Africa, pp. 531–539.

Watkins, R. T., McDougall, I., le Roex, A. P., 1994. K–Ar ages of the Brandberg and Okenyenya Igneous Complexes, north–western Namibia. Geol Rundsch 83, 348–356.

Wedepohl, K. H., 1995. The composition of the continental crust. Geochimica et Cosmochimica Acta 57, 1217–1232.

Wei, C. S., Zheng, Y. F., Zhao, Z. F., 2000. Hydrogen and oxygen isotope geochemistry of A–type granites in the continental margins of eastern China. Tectonophysics 328, 205–227.

White, W. M., 2007. Geochemistry: an online–text book. John–Hopkins University Press, Baltimore, Maryland.

William, J. H., 1968. Least–squares fitting of a straight line. Journal of Physics 46, 1845–1847.

York, D., 1969. Least–squares fitting of a straight line with correlated errors. Earth and Planetary Science Letters 5, 320–324.

Appendix A

Table 1: Petrographic descriptions for Koegel Fontein samples

Sample number	Rock type	Mineralogy	Description
CCK3	Bostonite	Quartz, feldspar, biotite, apatite, fluorite, zircon, opaque minerals, chlorite, carbonate minerals, sericite.	Predominantly feldspar which has pervasive alteration, sericite, carbonate minerals and very turbid. It is fine-grained (2–0.5mm) and inequigranular. Biotite is altered to chlorite.
CCK4	Quartz porphyry	Groundmass (80%): quartz, feldspar, biotite, amphibole, zircon, opaque minerals, carbonate minerals, sericite Phenocrysts (20%): quartz, feldspar, biotite.	The groundmass is holocrystaline, fine-grained and inequigranular. There are some quartz-feldspar intergrowths. The graphic texture is usually associated with phenocrysts. Small cavities are also present in the groundmass. Phenocrysts are euhedral to subhedral and often have coronas of fine-grained quartz and feldspar. Some quartz phenocrysts are embayed. Quartz grains are often glomeroporphyritic.
CCK6	Mafic rock	Plagioclase, chlorite, carbonate minerals, epidote, opaque minerals.	The sample is fine-grained. Plagioclase grains are euhedral and have a felted texture. Some feldspar grains are altered to epidote but most appear fresh. Chlorite and carbonate minerals replace round grains which may have been olivine or pyroxene.
CCK7	Quartz porphyry	Groundmass (60%): biotite, quartz, feldspar, carbonate minerals, opaque minerals, zircon, apatite, amphibole, rutile. Phenocrysts (40%): quartz, feldspar, biotite.	The groundmass is medium grained (1–5mm) and inequigranular. Grains tend to be anhydral . There are some quartz-feldspar intergrowths present. Phenocrysts tend to be coarse-grained (>5mm) and discrete grains, although, glomeroporphyritic texture does occur. Some of the feldspar phenocrysts are plagioclase most of which appear to be xenocrysts.
CCK8	Metagranite	Quartz, feldspar, opaque minerals, biotite.	Coarse-grained sample consisting predominantly of quartz. Grain boundaries tend to form 120 degrees terminations. Some evidence of the original magmatic textures is present in the form of graphic texture.

continued . . .

Sample number	Rock type	Mineralogy	Description
CCK9	Gneiss	Alkali feldspar, plagioclase, quartz, carbonate and opaque minerals, zircon, chlorite.	Medium- to coarse-grained, inequigranular. Feldspar grains are often turbid and altered to sericite. Some feldspar grains have a perthitic texture. Grain boundaries tend to be sutured.
CCK10	Quartz porphyry	Groundmass (70%): quartz, feldspar, biotite, zircon Phenocrysts (20%): quartz, feldspar, biotite	The majority of the groundmass is very fine-grained with a fibrous texture indicating rapid cooling. There are some fine-grained minerals (quartz, feldspar and zircon) which can be distinguished. Phenocrysts tend to be quartz and turbid felspar with minor amounts of biotite. Most phenocrysts are discrete grains.
CCK11	Zout River plug	Chlorite, plagioclase, carbonate, epidote, orthopyroxene, opaque minerals.	Medium- to coarse-grained, inequigranular. Most of the orthopyroxene has been altered to chlorite. Orthopyroxene grains have overgrowths of carbonate minerals. Many plagioclase grains have been altered to epidote.
CCK12	Quartz porphyry	Groundmass (60%): Quartz, alkali feldspar, chlorite, amphibole, opaque minerals, zircon. Phenocrysts (40%): quartz, alkali feldspar.	Groundmass is fine grained. There is intergrowths between quartz and feldspar (graphic texture). Grains are quite equigranular and feldspar is turbid. Grain boundaries are sutured. Phenocrysts are coarse grained and some are glomeroporphyritic. Many of the grain boundaries have coronas of fine grained alkali feldspar and quartz. The feldspar is also turbid and in some cases perthitic. Miarolitic cavities.
CCK13	Schist	Quartz, muscovite, biotite, opaque minerals.	Sheared texture. The quartz has wavy extinction and sutured grain boundaries. Some grains have 120 degree grain boundary terminations. The micas have a preferred orientation.
CCK14	Schist	Biotite, quartz, alkali feldspar, opaque minerals, muscovite, zircon.	Sample is foliated. Some quartz grains have been recrystallised and have 120 degree grain boundaries. Quartz has wavy extinction, and the grains that have not been recrystallised have sutured boundaries.
CCK15	Bostonite	Groundmass (98%): alkali feldspar, plagioclase, quartz, biotite, opaque minerals. Phenocrysts (2%): Feldspar.	Groundmass is fine grained. The feldspar grains have a felty texture. Feldspar grains are subhedral, and alkali feldspar grains have simple twinning. Phenocrysts are glomeroporphyritic and turbid.

continued . . .

Sample number	Rock type	Mineralogy	Description
CCK17	Rooivleitjie granite	Alkali feldspar, quartz, zircon, opaque minerals, amphibole, chlorite.	Texture is coarse grained, the rock is predominantly feldspar. Feldspars are perthitic and turbid. Inequigranular with sutured grain boundaries.
CCK18	Syenite	Alkali feldspar, amphibole, biotite, apatite, quartz, zircon, opaque minerals.	Coarse-grained sample, some sample grains have coarse patch perthite. The rock is inequigranular and has sutured grain boundaries. Apatite and zircon grains tend to be euhedral or subhedral.
CCK19	Rietpoort granite	Alkali feldspar, quartz, zircon, amphibole, plagioclase, biotite, cassiderite.	Coarse-grained, inequigranular, and does not have sutured grain boundaries. Graphic texture is present, some alkali feldspar grains have perthitic texture.
CCK20	Gneiss	Feldspar, quartz, amphibole, zircon, opaque minerals, biotite.	Texture is medium to coarse-grained with sutured grain boundaries. There is evidence of shearing, and elongate minerals have a lineation. There is some evidence of recrystallisation, with smaller quartz grains showing 120 degree grain boundaries.
CCK21	Intermediate diatreme	Groundmass (40%): Feldspar Xenocrysts (60%): Quartz, feldspar, chlorite, carbonate, opaque minerals, zircon.	Groundmass is very fine grained and cryptocrystalline. Xenocrysts of augen gneiss and clusters of recrystallised quartzite. The sample is fairly altered, contains lithic and crystal fragments.
CCK22	Gneiss	Feldspar, quartz, zircon, chlorite, sericite, opaque minerals, chlorite.	Texture is medium to coarse-grained with sutured grain boundaries. There are some areas where recrystallisation is evident in the form of 120 degree grain boundaries. There is evidence of shearing.
CCK23	Quartz porphyry	Groundmass (50%): feldspar, quartz, amphibole, biotite, chlorite, zircon, opaque minerals. Phenocrysts (50%): Quartz, feldspar, amphibole, biotite, zircon.	Texture is fine grained, the matrix is equigranular, with no evidence of recrystallisation, the feldspar is slightly turbid, but otherwise the groundmass is relatively fresh. Feldspar phenocrysts are turbid and in some cases poikilitic. The amphibole and biotite tend to be glomeroporphyritic, whereas the feldspar and quartz tend to be discrete grains.

continued ...

Sample number	Rock type	Mineralogy	Description
CCK24	Marble	Carbonate, talc, quartz.	Texture is medium to coarse-grained with sutured grain boundaries. Some grains display 120 degree boundary terminations. Some grains have good cleavage, and many carbonate grains have glide twins. There is evidence of shearing.
CCK25	Schist	Feldspar, quartz, biotite, amphibole, muscovite, opaque minerals, zircon, carbonate, chlorite	A fine to medium grained foliated rock. The majority of grain boundaries are sutured, however some have 120 degree terminations.
CCK26	Bostonite	Feldspar, amphibole, apatite, quartz, fluorite, zircon.	A fine to medium grained rock with a felted texture, apatite and feldspar tend to subhedral. The feldspar is very turbid.
CCK27	Gneiss	Microcline, plagioclase, alkali feldspar, quartz, biotite, muscovite.	The sample has a gneissic texture and is medium to coarse grained. There is evidence of recrystallisation with the smaller grains occurring in patches, all with 120 degree grain boundary terminations. Larger grains tend to have sutured grain boundaries. Some feldspar grains are slightly turbid.
CCK28	Schist	Quartz, feldspar, muscovite, amphibole, biotite, zircon.	The rock is medium to coarse grained. Platey minerals have preferred orientation, and the rock has experienced shearing. Quartz grains have wavy extinction, and the majority of grains have sutured grain boundaries.
CCK30	Gneiss	Feldspar, quartz, muscovite, zircon, opaque minerals, sericite, biotite, opaque minerals, zircon.	Gneissic texture, and inequigranular (0.5-5mm). Feldspar tends to be turbid and altered to sericite. Majority of grains have sutured grain boundaries except where recrystallisation has occurred. Quartz grains tend to have wavy extinction.
CCK31	Bostonite	Feldspar, quartz, sericite, opaque minerals.	Rock is fine grained, inequigranular, and pervasively altered. Feldspar has been altered to sericite.
CCK32	Quartz porphyry	Groundmass (70%): quartz, feldspar, zircon, chlorite, sericite and carbonate minerals, apatite. Phenocrysts (30%): Feldspar, quartz, carbonate.	Groundmass is fine grained and inequigranular, with pervasive alteration in the form of turbid feldspar. The chlorite grains may be the result of altered amphibole due to the shape of the grains. Phenocrysts tend to be glomeroporphyritic, the feldspar grains tend to be highly altered to sericite and carbonate.

continued . . .

Sample number	Rock type	Mineralogy	Description
CCK33	Mafic rock	Plagioclase, chlorite, carbonate minerals, epidote, opaque minerals	A very fine-grained rock (<0.5mm) with a holocrystaline almost glassy groundmass. Larger (<1mm) circular grains of chlorite and carbonate were probably olivine or pyroxene prior to alteration.
CCK34	Schist	Feldspar, biotite, quartz, zircon, muscovite, opaque minerals.	Has a schistose texture. The rock is medium grained. The rock has been sheared and grain boundaries tend to be sutured. Feldspar grains are slightly turbid and some have been altered to sericite.
CCK35	Mafic rock	Plagioclase, clinopyroxene, epidote, chlorite, opaque minerals, orthopyroxene.	Rock is coarse grained, with felted plagioclase, and interstitial clinopyroxene. Epidote is restricted to veins. Some clinopyroxene grains have been altered to chlorite. All grains are highly fractured. Some subhedral grains of orthopyroxene.
CCK36	Mafic rock	Plagioclase, clinopyroxene, chlorite, carbonate minerals, epidote, opaque minerals, biotite, bytownite.	The sample is fine-grained with euhedral to subhedral plagioclase grains. Xenoliths of augen gneiss are abundant as well as xenocrysts of zircon and quartz. Clinopyroxene is mostly altered to chlorite.
CCK37	Mafic rock	Feldspar, clinopyroxene, olivine, chlorite, opaque minerals.	Fine to medium grained. Some clinopyroxenes have been altered to chlorite. Miarolitic cavities. Felted feldspars.
CCK38	Mafic rock	Feldspar, clinopyroxene, chlorite, opaque minerals.	Rock is medium grained, with clinopyroxene which has been altered to chlorite. Quenched texture in the form of fine-grained fibrous 'fans'.
CCK39	Mafic rock	Plagioclase, clinopyroxene, orthopyroxene, amphibole, chlorite, opaque minerals.	Coarse-grained sample with myrmekite texture. Some pyroxene grains have been altered to chlorite, and others have twinning. Amphibole appears to be secondary.
CCK45	Gneiss	Microcline, alkali feldspar, quartz, muscovite, plagioclase, biotite.	The sample has a gneissic texture and is coarse grained. Feldspar tends to be turbid. Grain boundaries are sutured.
CCK46	Gneiss	Quartz, feldspar, microcline, muscovite, biotite, opaque minerals, zircon.	Medium to coarse grained rock with a gneissic texture. Some grains appear sheared. The quartz has wavy extinction. Some feldspar grains are turbid. Grain boundaries tend to be sutured.

continued ...

Sample number	Rock type	Mineralogy	Description
CDB336	Quartz porphyry	Groundmass (95%): quartz, alkali feldspar, biotite, apatite, opaque minerals, carbonate minerals, chlorite Phenocrysts (5%): quartz, alkali feldspar, xenocryst plagioclase.	Very fine-grained groundmass (<0.5mm) which is pervasively altered. The groundmass is about 70% feldspar. Feldspar is turbid and some grains have been altered to carbonate and the chlorite is replacing biotite. Phenocrysts tend to be coarse-grained and occur as separate discrete grains. Feldspar is turbid with reaction rims of fine-grained feldspar and carbonate. Plagioclase xenocrysts are extensively altered to carbonate minerals and epidote.
CDB383	Quartz porphyry	Groundmass (70%): quartz, alkali feldspar, biotite, zircon, opaque minerals, carbonate minerals, chlorite, sericite Phenocrysts (30%): quartz, feldspar.	The groundmass is very fine-grained (<0.5mm). Biotite is replaced by chlorite and has a fibrous appearance. Graphic intergrowths are also present. Feldspar grains are turbid and often altered to sericite or carbonate. Quartz phenocrysts are embayed or have reaction rims. Feldspar grains tend to be turbid.
CDB388	Quartz porphyry	Groundmass (80%): quartz, feldspar, biotite, zircon, spinel, opaque minerals, sericite, chlorite Phenocrysts (20%): quartz, feldspar, biotite.	the groundmass has a graphic texture and is holocrystaline. Grains are inequigranular Phenocrysts can be clustered and often have reaction rims. Quartz grains are sometimes embayed while feldspar grains are turbid. Some biotite grains have 'wavey' extinction and might be xenocrysts
CDB549	Bostonite	Groundmass (98%): feldspar, quartz, zircon, opaque minerals. Phenocrysts (2%): feldspar.	Groundmass is fine to medium grained. Feldspar grains have a felted texture and are turbid and often altered to sericite Phenocrysts are coarse grained and tend to be turbid. There are some xenoliths of country rock present.
CDB555	Bostonite	Phenocrysts (5%): quartz, biotite, amphibole Groundmass (95%): feldspar, quartz, biotite, amphibole, epidote, apatite, chlorite, opaque minerals.	Groundmass is fine grained. Feldspar grains are turbid and form fans indicative of quenching. Amphibole and biotite are often altered to chlorite and epidote is restricted to veins. Phenocrysts are glomeroporphyritic and euhedral.

continued ...

Sample number	Rock type	Mineralogy	Description
CDB564	Quartz porphyry	Groundmass (50%): feldspar, quartz, sercite, biotite, chlorite, carbonate, opaque minerals Phenocrysts (50%): quartz, feldspar.	Groundmass is medium grained and inequigranular. Graphic texture is present. Feldspar grains tend to be turbid or altered to sericite. Biotite is often altered to chlorite. Phenocrysts are glomeroporphyritic. Feldspar grains are turbid and/or altered to sericite and carbonate.
CDB572	Quartz porphyry	Groundmass (60%): feldspar, quartz, zircon, opaque minerals Phenocrysts (40%): feldspar, quartz.	Groundmass is fine grained and equigranular. Feldspar tends to be turbid. Phenocrysts are glomeroporphyritic and some quartz grains are embayed. Feldspar grains are perthitic and turbid.
CDB580	Quartz porphyry	Groundmass (50%): quartz, feldspar, biotite Phenocrysts (50%): quartz, feldspar, sericite.	Groundmass is fine to medium grained with graphic texture. Feldspar grains tend to be turbid. Phenocrysts are glomeroporphrytic. Feldspar grains are turbid and perthitic. Quartz phenocrysts often display a 'high' quartz crystal shape.
CDB581	Quartz porphyry	Groundmass (30%): quartz, feldspar, sericite, zircon, opaque minerals, biotite Xenoliths (70%): quartz, feldspar, biotite, zircon.	Groundmass tends to be fine grained and equigranular. Feldspar grains are altered to sericite. Xenoliths show extensive recrystallisation and are probably Namaqua gneisses.
CDB588	Quartz porphyry	Groundmass (40%): quartz, feldspar, sericite, amphibole, biotite, zircon, opaque minerals Phenocrysts (60%): feldspar, quartz.	Groundmass tends to be fine to medium grained with the feldspar being slightly turbid. The phenocryst feldspar grains are perthitic, turbid and some grains have simple twinning. Phenocrysts are often in clusters and quartz grains can display the 'high' quartz crystal shape.
CDB594	Quartz porphyry	Groundmass (60%): feldspar, quartz, sericite Phenocrysts (40%): feldspar, quartz.	Groundmass is cryptocrystalline and equigranular. Some feldspar grains are altered to sericite. The phenocryst feldspar grains are turbid and can be poikilitic and some grains are altered to sericite. Quartz phenocrysts often display the high quartz crystal shape, and some grains are embayed. Phenocrysts tend to be glomeroporphyritic.

continued . . .

Sample number	Rock type	Mineralogy	Description
CDB650	Quartz porphyry	Groundmass (80%): feldspar, quartz, biotite, zircon, apatite, opaque minerals, epidote, carbonate minerals, chlorite Phenocrysts (20%): quartz, alkali feldspar, biotite, chlorite.	Very fine-grained groundmass (<0.5mm) which is extensively altered to chlorite, carbonate and epidote. All feldspar grains are turbid and biotite tends to be chloritzed. Phenocryst feldspar is turbid with kelyphitic rimes of chlorite and carbonate. Phenocrysts tend to be glomeroporphyritic. Both the phenocrysts and groundmass have graphic intergrowths.
CDB687	Rooivleitjie granite	Feldspar, quartz, amphibole, muscovite, biotite, opaque minerals, chlorite.	Coarse grained and inequigranular. Grain boundaries are sutured. Feldspar grains are perthitic and turbid. Biotite and amphibole are altered to chlorite.
CDB699	Mafic rock	Phenocrysts (5%): Plagioclase, clinopyroxene, olivine, orthopyroxene, biotite Groundmass (95%): plagioclase, clinopyroxene, olivine, orthopyroxene, bytownite.	Phenocrysts are glomeroporphyritic and euhedral to subhedral. Some olivine grains have coronas of bytownite. Groundmass is microcrystalline. Feldspar grains tend to be felted.
CDB703	Syenite	Feldspar, quartz, amphibole, biotite, zircon, apatite, opaque minerals, chlorite.	Coarse grained and inequigranular. Feldspar grains are slightly turbid and display coarse patch perthite. Some chlorite alteration of the amphibole.
CDB719	Micro Syenite	Feldspar, quartz, biotite, apatite, opaque minerals, chlorite.	Medium grained. Feldspar is turbid and has coarse patched perthite and micro perthite. Grain boundaries are sutured and the biotite is altered to chlorite. Feldspar grains also have a felted texture, and some grains display simple twinning.
CDB753	Syenite	Feldspar, quartz, amphibole, biotite, zircon, apatite, opaque minerals, chlorite	Coarse grained and inequigranular. Feldspar grains are slightly turbid and display coarse patch perthite., and some are slightly altered to sericite. Some chlorite alteration of the amphibole. Some biotite grains are embayed. Graphitic texture is present.

continued . . .

Sample number	Rock type	Mineralogy	Description
CDB819	Agerine fenite	Feldspar, quartz, agerine, biotite, opaque minerals.	Fine to medium grained with sutured grain boundaries. The agerine grains tend to occur in clusters and have a preferred orientation. Evidence of re-crystallisation in the form of small grains with 120 degree grain boundaries.
CDB825	Rietpoort granite	Quartz, feldspar, biotite, zircon, opaque minerals.	Coarse grained and inequigranular. Feldspar grains are slightly turbid and there is graphitic texture along their grain boundaries. Feldspar grains also have simple twinning and perthitic texture. Quartz grains tend to show the 'high' quartz crystal shape.
CDB922	Mafic rock	Olivine, clinopyroxene, orthopyroxene, plagioclase, bytownite.	Clinopyroxene grains form long laths. Olivine occurs as euhedral to subhedral crystals. Plagioclase is interstitial. Some bytownite on olivine boarders.
CDB932	Mafic rock	Ti-clinopyroxene, Ti-amphibole, plagioclase, serpentine, olivine.	Titanium clinopyroxene has a pinkish colour in plain polarised light and is subhedral. Pyroxene and olivine occur as discrete grains with interstitial plagioclase. Amphibole tends to form long laths.
CDB953	Mafic rock	Plagioclase, clinopyroxene, olivine, orthopyroxene.	Medium to coarse grained. Plagioclase grains tend to be subhedral. Clinopyroxene grains are subhedral, and often display twinning. Some clinopyroxene and orthopyroxene grains tend to be interstitial. Olivine tends occur as small subhedral grains.
CDB974	Mafic rock	Plagioclase, clinopyroxene, orthopyroxene.	Fine to medium grained. Plagioclase tends to be subhedral, and has a felted texture. Orthopyroxene and clinopyroxene are interstitial.
CDB978	Mafic rock	Plagioclase, clinopyroxene, orthopyroxene.	Medium to coarse grained. Plagioclase grains tend to be subhedral. Clinopyroxene grains are subhedral, and often display twinning. Some clinopyroxene and orthopyroxene grains tend to be interstitial.
CDB1064	Quartz porphyry	Phenocrysts (30%): quartz, feldspar Groundmass (70%): feldspar, quartz, apatite, opaque minerals, biotite.	Groundmass is fine grained and inequigranular and larger grains have graphitic texture. Some feldspar grains are turbid. Phenocryst feldspar is very turbid and some grains display simple twinning. Quartz grains can show a 'high' quartz crystal shape.

continued ...

Sample number	Rock type	Mineralogy	Description
CDB1066	Bostonite	Phenocrysts (20%): quartz, feldspar Groundmass (80%): feldspar, quartz, biotite, chlorite.	Phenocrysts are coarse grained, they tend to have coarse patch perthite. and are turbid. The groundmass is fine grained and inequigranular. Some areas are cryptocrystalline with a fan line texture indicative of quenching. The quenched texture can be associated with the phenocrysts.
CDB1092	Mafic rock	Plagioclase, clinopyroxene, orthopyroxene, opaque minerals.	Coarse grained with subhedral laths of plagioclase and interstitial clinopyroxene. Some clinopyroxene grains have simple twinning.
CDB1101	Mafic rock	Plagioclase, clinopyroxene, orthopyroxene, serpentine, chlorite.	Medium to coarse grained with interstitial clinopyroxene Plagioclase has a cumulus texture. The serpentine grains form clusters which look like pseudocrystals which may have resulted from the complete alteration of olivine.
CDB1105	Mafic rock	Plagioclase, clinopyroxene, orthopyroxene, chlorite, sericite	Medium to coarse grained with interstitial clinopyroxene. Plagioclase has a cumulus texture. The chlorite replaces clinopyroxene. Some plagioclase is altered to sericite.
CDB1126	Mafic rock	Plagioclase, clinopyroxene, olivine, orthopyroxene.	Medium grained rock with cumulus plagioclase and olivine with interstitial clinopyroxene. Some interstitial spaces are filled with cryptocrystalline minerals.
CDB1200	Mafic rock	Plagioclase, clinopyroxene.	Fine to medium grained with some cryptocrystalline interstitial spaces. The feldspar tends to have a felted texture.
CDB1341	Mafic rock	Plagioclase, clinopyroxene, sericite, quartz, orthopyroxene	Coarse grained rock with cumulus plagioclase with interstitial pyroxene. Myrmekite texture is present. Some feldspar grains have been sericitized.
CDB1451	Bostonite	Groundmass (60%): feldspar, amphibole, biotite, quartz, plagioclase, zircon, opaque minerals, chlorite Phenocrysts (40%): plagioclase, alkali feldspar, carbonate minerals, sericite.	Groundmass is fine to medium grained with turbid feldspar. Biotite and amphibole have been altered to chlorite. Graphitic texture is present. Some of the phenocrysts have been altered to carbonate and sericite. Some feldspar have coarse patch perthite. One xenolith is present which shows re-crystallisation with small grains with 120 degree grain boundaries and an alteration rim.

continued . . .

Sample number	Rock type	Mineralogy	Description
CDB1454	Mafic rock	Plagioclase, clinopyroxene, orthopyroxene, biotite, sericite, chlorite, opaque minerals.	Coarse grained rock with cumulus plagioclase and intercumulus pyroxene and biotite. Some feldspar grains have been altered to sericite and some biotite grains have been altered to chlorite.
CDB1459	Mafic rock	Plagioclase, clinopyroxene, orthopyroxene, sericite, chlorite, opaque minerals.	Coarse grained rock with cumulus plagioclase and some cumulus clinopyroxene. The majority of the pyroxene is interstitial. Some clinopyroxene grains have twinning.
CDB1491	Mafic rock	Plagioclase, clinopyroxene, orthopyroxene, sericite.	Medium to coarse grained rock with cumulus plagioclase which has been sericitized. Pyroxene tends to be interstitial and some clinopyroxene displays twinning.
CN495	Quartz porphyry	Groundmass (80%): feldspar, quartz, apatite, zircon, opaque minerals, sericite Phenocrysts (20%): quartz, feldspar, sericite.	Groundmass is fine grained and inequigranular with sutured grain boundaries. Feldspar grains are turbid, while some grains display simple twinning and others have been altered to sericite. Feldspar phenocrysts are turbid and some grains are zoned. Some quartz grains display the 'high' quartz crystal shape.

Appendix B

Table 2: Locations for CCK, CDB and CN samples

Sample number	Rock type	Longitude	Latitude
CCK1	Quartz vein	31 09’ 14.7”	18 02’ 45.0”
CCK2	Gneiss	-	-
CCK3	Bostonite	31 06’35.5”	18 00’35.5”
CCK4	Quartz porphyry	31 05’06.0”	18 02’31.1”
CCK5	Quartz vein	31 06’ 05.2”	18 03’43.9”
CCK6	Tholeiitic mafic rock	31 06’05.0”	18 03’44.4”
CCK7	Quartz porphyry	31 06’06.5”	18 03’44.4”
CCK8	Gneiss	32 06’06.5”	19 03’44.4”
CCK9	Gneiss	33 06’06.5”	20 03’44.4”
CCK10	Quartz porphyry	31 06’12.9”	18 04’55.6”
CCK11	Zout Rivier plug	31 06’05.6”	18 05’11.2”
CCK12	Quartz porphyry	31 06’10.2”	18 03’48.0”
CCK13	Schist	31 05’04.8”	18 02’44.1”
CCK14	Amphibolite	31 05’36.3”	18 00’48.3”
CCK15	Bostonite	31 09’06.5”	17 56’06.6”
CCK16	Quartz vein	31 09’07.7”	17 56’08.9”
CCK17	Rooivleitjie granite	31 09’07.8”	17 55’28.8”
CCK18	Syenite	31 08’58.3”	17 53’56.5”
CCK19	Rietpoort granite	31 05’33.9”	17 57’24.9”
CCK20	Gneiss	31 03’01.5”	17 54’51.5”
CCK21	Intermediate plug	32 03’01.5”	18 54’51.5”
CCK22	Gneiss	31 08’00.1”	17 54’52.9”
CCK23	Quartz porphyry	31 01’25.5”	17 55’36.0”
CCK24	Marble	31 14’08.8”	17 50’20.5”
CCK25	Schist	32 14’08.8”	18 50’20.5”
CCK26	Bostonite	31 11’52.9”	17 47’40.4”
CCK27	Gneiss	32 11’52.9”	18 47’40.4”
CCK28	Schist	33 11’52.9”	19 47’40.4”
CCK29	Quartz vein	34 11’52.9”	20 47’40.4”
CCK30	Gneiss	31 11’30.1”	17 47’35.6”
CCK31	Bostonite	32 11’30.1”	18 47’35.6”
CCK32	Quartz porphyry	31 11’11.9”	17 47’19.3”

continued . . .

Sample number	Rock type	Longitude	Latitude
CCK33	Tholeiitic mafic rock	31 09’50.4”	17 46”05.9”
CCK34	Amphibolite	31 09’24.5”	17 45’47.0”
CCK35	Tholeiitic mafic rock	31 08’08.9”	17 44’40.3”
CCK36	Alkali mafic rock	32 08’08.9”	18 44’40.3”
CCK37	Alkali mafic rock	31 04’34.1”	17 42’49.6”
CCK38	Alkali mafic rock	31 04’21.0”	17 42’46.5”
CCK39	Tholeiitic mafic rock	31 04’28.6”	17 42’46.0”
CCK40	Quartz vein	32 04’28.6”	18 42’46.0”
CCK41	Quartz vein	31 04’32.6”	17 42’47.5”
CCK42	Quartz vein	31 04’42.9”	17 42’54.5”
CCK43	Quartz vein	31 04’50.1”	17 43’00.0”
CCK44	Quartz vein	32 04’50.1”	18 43’00.0”
CCK45	Gneiss	33 04’50.1”	19 43’00.0”
CCK46	Gneiss	31 04’53.6”	17 53’ 05.0”
CCK47	Tholeiitic mafic rock	32 04’53.6”	18 53’ 05.0”
CCK48	Quartz vein	33 04’53.6”	19 53’ 05.0”
CCK49	Quartz vein	31 04’59.4”	17 43’10.2”
CCK50	Quartz vein	31 04’59.3”	17 43’12.3”
CCK51	Rietpoort granite	31 05’48.5”	17 57’51.8”
CCK52	Rietpoort granite	31 04’59.6”	17 56’43.6”
CCK53	Rietpoort granite	31 03’09.5”	17 52’23.0”
CCK54	Gneiss	31 01’36.5”	17 57’02.4”
CCK55	Rietpoort granite	30 59’05.5”	17 59’11.24”
CBD336	Quartz porphyry	-	-
CBD369	Gneiss	31 06’ 48”	18 15’ 53”
CBD383	Quartz porphyry	31 10’ 10”	18 08’ 34”
CBD388	Quartz porphyry	31 10’ 27”	18 09’ 13”
CBD541	Quartz porphyry	31 07’ 50”	18 00’ 40”
CBD544	Bostonite	31 08’ 23”	18 03’ 33”
CBD546	Tholeiitic mafic rock	31 06’ 03”	18 03’ 51”
CBD547	Quartz porphyry	31 06’ 06”	18 03’ 47”
CBD549	Alkali mafic rock	31 06’ 27”	18 04’ 36”
CBD550	Tholeiitic mafic rock	31 07’ 06”	18 05’ 09”
CBD551	Bostonite	31 05’ 27”	18 03’ 38”

continued . . .

Sample number	Rock type	Longitude	Latitude
CBD552	Bostonite	31 05’ 35”	18 02’ 04”
CBD553	Quartz porphyry	31 05’ 32”	18 00’ 23”
CBD555	Bostonite	31 05’ 03”	17 59’ 36”
CBD556	Dolerite	31 05’ 11”	18 00’ 03”
CBD561	Dolerite	31 03’ 16”	18 02’ 53”
CBD562	Dolerite	31 03’ 30”	18 02’ 52”
CBD563	Bostonite	31 05’ 32”	18 03’ 43”
CBD564	Quartz porphyry	31 05’ 23”	18 03’ 55”
CN493	Quartz porphyry	31 02’ 00”	17 57’ 21”
CBD572	Quartz porphyry	31 02’ 00”	17 57’ 21”
CN495	Quartz porphyry	31 06’ 13”	18 03’ 41’
CN496	Dolerite	31 05’ 36”	18 03’ 21’
CBD580	Quartz porphyry	31 00’ 27”	17 56’ 45”
CBD581	Quartz porphyry	30 59’ 23”	17 55’ 57”
CBD582	Quartz porphyry	30 59’ 23”	17 55’ 57”
CBD588	Quartz porphyry	30 59’ 03”	17 54’ 56”
CBD590	Syenite	31 00’ 30”	17 54’ 09”
CBD591	Gneiss	31 00’ 34”	17 54’ 09”
CBD592	Bostonite	31 00’ 19”	17 54’ 06”
CBD593	Quartz porphyry	31 01’ 21”	17 54’ 08”
CBD594	Quartz porphyry	31 00’ 47”	17 53’ 40”
CBD597	Schist	31 01’ 04”	17 56’ 52”
CBD601	Quartz porphyry	31 02’ 33”	17 57’ 08”
CBD602	Quartz porphyry	31 02’ 23”	17 58’ 48”
CBD604	Quartz porphyry	31 02’ 32”	17 55’ 23”
CBD605	Quartz porphyry	31 02’ 58”	17 55’ 39”
CBD606	Bostonite	31 02’ 57”	17 54’ 51”
CBD607	Quartz porphyry	31 01’ 30”	17 53’ 51”
CBD609	Quartz porphyry	31 01’ 18”	17 53’ 17”
CBD611	Quartz porphyry	31 00’ 27”	17 51’ 41”
CBD615	Quartz porphyry	31 01’ 55”	17 52’ 19”
CBD619	Bostonite	31 03’ 10”	17 52’ 13”
CBD633	Quartz porphyry	31 04’ 16”	17 53’ 41”
CBD634	Bostonite	31 03’ 59”	17 53’ 53”

continued . . .

Sample number	Rock type	Longitude	Latitude
CBD639	Quartz porphyry	31 04’ 12”	17 53’ 10”
CBD640	Quartz porphyry	31 04’ 52”	17 53’ 12”
CBD641	Bostonite	31 04’ 39”	17 53’ 37”
CBD645	Bostonite	31 05’ 47”	17 55’ 09”
CBD650	Quartz porphyry	31 11’ 24”	17 47’ 21”
CBD653	Quartz porphyry	31 09’ 33”	17 46’ 06”
CBD678	Bostonite	31 05’ 54”	17 56’ 00”
CBD679	Bostonite	31 06’ 55”	17 58’ 57”
CBD681	Dacite	31 04’ 46”	17 43’ 03”
CBD683	Bostonite	31 09’ 05”	17 56’ 15”
CBD684	Bostonite	31 09’ 37”	17 56’ 36”
CDB607	Quartz porphyry	31 08’ 52”	17 55’ 31”
CBD686	Gneiss	31 09’ 47”	17 55’ 26”
CBD687	Rooivleitjie granite	31 09’ 28”	17 55’ 30”
CDB699	Tholeiitic mafic rock	31 2’54”	19 11’43”
CBD753	Syenite	31 08’ 35”	17 54’ 38”
CBD702	Bostonite	31 08’ 35”	17 54’ 38”
CBD703	Syenite	31 09’ 00”	17 54’ 30”
CBD704	Bostonite	31 09’ 04”	17 54’ 15”
CBD719	Bostonite	31 09’ 04”	17 55’ 42”
CBD752	Rooivleitjie granite	31 09’ 31”	17 55’ 32”
CBD761	Quartz porphyry	31 00’ 52”	17 41’ 21”
CBD764	Bostonite	31 00’ 34”	17 01’ 06”
CBD817	Gneiss	30 59’ 36”	17 54’ 05”
CBD819	Dolerite	30 59’ 53”	17 53’ 57”
CBD822	Tholeiitic mafic rock	30 59’24”	17 55’08”
CBD823	Gneiss	30 57’ 42”	17 54’ 17”
CBD824	Gneiss	30 57’ 42”	17 54’ 17”
CBD825	Rietpoort granite	30 57’ 40”	17 53’ 40”
CBD922	Alkali mafic rock	30 46’13”	17 57’38”
CBD932	Alkali mafic rock	30 45’8”	17 57’11”
CBD953	Tholeiitic mafic rock	30 40’13”	17 54’24”
CBD974	Tholeiitic mafic rock	30 45’8”	17 53’49”
CBD978	Tholeiitic mafic rock	30 43’24”	17 51’47”

continued . . .

Sample number	Rock type	Longitude	Latitude
CBD1064	Quartz porphyry	31 05’ 54”	18 05’ 42”
CBD1066	Bostonite	31 06’ 27”	18 05’ 04”
CBD1092	Zout Rivier plug	30 35’13”	17 27’43”
CBD1101	Zout Rivier plug	30 33’41”	17 24’42”
CBD1105	Zout Rivier plug	30 32’49”	17 24’28”
CBD1126	Zout Rivier plug	30 39’15.6”	18 00’9.4”
CBD1200	Zout Rivier plug	30 36’59.5”	17 45’22.5”
CBD1341	Zout Rivier plug	30 28’25.8”	17 21’54.4”
CBD1454	Tholeiitic mafic rock	30 06’22.5”	18 05’41.3”
CBD1459	Tholeiitic mafic rock	30 15’19.5”	17 52’52.5”
CBD1491	Tholeiitic mafic rock	30 09’10.1”	17 51’21.7”

Appendix C

Table 3: Whole–rock geochemical data analyses done by XRF for all CDB and CN samples. Not Measured (NM), Not Detected (ND)

	CDB217	CDB249	CDB251	CDB267	CDB300	CDB328	CDB329	CDB331	CDB335	CDB336
Rock type	Tholeiitic mafic rock	Alkali mafic rock	Tholeiitic mafic rock	Tholeiitic mafic rock	Tholeiitic mafic rock	Tholeiitic mafic rock	Alkali mafic rock	Alkali mafic rock	Bostonite	Quartz porphyry
SiO_2	49	54	53	50	49	47	43	43	55	62
TiO_2	1.68	2.26	2.32	3.23	2.81	0.89	2.97	2.92	2.18	1.04
Al_2O_3	15	14	14	13	14	16	15	15	12	11
Fe_2O_3	14	13	13	16	15	11	12	11	15	8.88
MnO	0.19	0.16	0.2	0.27	0.18	0.17	0.19	0.17	0.16	0.14
MgO	5.56	2.9	3.36	5.13	3.36	8.08	6.71	5.87	1.4	0.51
CaO	8.65	6.59	7.21	4.96	7.62	11	8.56	7.69	4.72	3.47
Na_2O	2.46	2.34	2.4	0.05	2.35	2.05	3.46	3.21	2.22	1.81
K_2O	1.21	2.61	2.3	0.26	2.12	0.28	3.01	3.32	3.84	4.3
P_2O_5	0.43	0.75	0.65	0.36	0.82	0.13	0.92	0.88	1.04	0.44
H_2O	1.15	1.24	1.21	5.35	1.72	2.02	2.7	1.38	1.64	1.21
CO_2	0.06	0.07	0.05	0.23	0.09	1.31	1.9	4.42	0.07	3.98
Total	99.62	99.75	99.68	100.00	99.03	99.58	99.88	99.70	99.54	99.51
Ba	526	1168	1044	186	927	205	1150	1422	1610	886
Cr	40	39	13	142	23	137	116	54	ND	16
Ga	14	18	18	21	16	14	16	18	19	22
Nb	14	22	19	ND	23	ND	82	77	24	31
Ni	73	26	29	71	47	129	73	47	10	ND

continued . . .

	CDB217	CDB249	CDB251	CDB267	CDB300	CDB328	CDB329	CDB331	CDB335	CDB336
Rock type	Tholeiitic mafic rock	Alkali mafic rock	Tholeiitic mafic rock	Tholeiitic mafic rock	Tholeiitic mafic rock	Tholeiitic mafic rock	Alkali mafic rock	Alkali mafic rock	Bostonite	Quartz porphyry
Rb	21	50	42	ND	61	35	63	70	88	133
Sr	344	341	376	197	337	229	1098	1294	202	149
V	249	240	286	435	329	226	227	214	100	40
Y	39	59	55	60	65	24	23	22	82	106
Zn	101	138	127	140	141	83	168	81	238	162
Zr	171	333	297	226	305	95	263	260	459	564

	CDB339	CDB349	CDB353	CDB383	CDB387	CDB388	CDB390	CDB415	CDB484	CDB489
Rock type	Tholeiitic mafic rock	Tholeiitic mafic rock	Tholeiitic mafic rock	Quartz porphyry	Tholeiitic mafic rock	Quartz porphyry	Tholeiitic mafic rock	Tholeiitic mafic rock	Alkali mafic rock	Tholeiitic mafic rock
SiO_2	40	51	51	75	42	76	46	52	42	49
TiO_2	2.99	3.04	3.42	0.13	2.3	0.06	2.29	2.76	2.48	1.59
Al_2O_3	13	13	13	12	12	13	14	13	14	15
Fe_2O_3	14	16	16	2.44	13	0.98	12	14	11	13
MnO	0.14	0.22	0.25	0.01	0.17	0.02	0.17	0.21	0.19	0.21
MgO	9.12	4.38	3.13	0.03	9.31	0.05	6.27	3.87	5.96	5.41
CaO	7.43	7.54	5.57	0.31	9.49	0.07	7.03	7.38	9.29	8.04
Na_2O	1.41	2.07	2.79	2.37	2.27	2.8	2.71	2.41	2.69	1.91
K_2O	1.37	1.44	1.53	5.19	0.98	5.05	3.11	1.4	1.89	1.55
P_2O_5	0.65	0.37	0.37	0.1	0.42	0.03	0.79	0.24	0.68	0.32
H_2O	5.62	1.25	2.92	1.32	2.72	1.17	1.93	1.81	3.37	2.93

continued . . .

	CDB339	CDB349	CDB353	CDB383	CDB387	CDB388	CDB390	CDB415	CDB484	CDB489
Rock type	Tholeiitic mafic rock	Tholeiitic mafic rock	Tholeiitic mafic rock	Quartz porphyry	Tholeiitic mafic rock	Quartz porphyry	Tholeiitic mafic rock	Tholeiitic mafic rock	Alkali mafic rock	Tholeiitic mafic rock
CO_2	4.22	0.25	0.71	0.38	4.5	0.32	3.91	0.27	5.8	0.66
Total	99.78	100.58	99.55	99.57	99.93	99.72	99.54	99.35	100.10	99.61
Ba	1290	NM	419	66	248	218	540	390	390	517
Cr	163	NM	37	13	284	20	126	25	183	19
Ga	16	NM	17	22	16	29	16	16	17	17
Nb	56	NM	16	224	26	180	50	16	51	13
Ni	159	NM	22	14	304	11	117	29	160	60
Rb	54	NM	68	529	27	749	122	45	42	51
Sr	495	NM	156	44	505	21	937	180	717	336
V	223	NM	601	ND	195	ND	129	500	152	253
Y	19	NM	37	212	19	105	33	41	25	44
Zn	100	NM	114	70	85	46	82	108	82	131
Zr	268	NM	172	387	130	233	254	173	240	193

	CDB500	CDB509	CDB510	CDB511	CDB513	CDB514	CDB518	CDB526	CDB530	CDB536
Rock type	Tholeiitic mafic rocks	Alkali mafic rock	Tholeiitic mafic rock	Tholeiitic mafic rock	Tholeiittic mafic rock	Tholeiitic mafic rock	Bostonite	Alkali mafic rock	Alkali mafic rock	Tholeiitic mafic rock
SiO2	42	42	46	44	52	51	56	40	43	42
TiO2	2.34	3.38	3.1	3.2	1.04	2.43	1.94	2.83	2.76	2
Al2O3	13	13	13	13	14	13	15	13	14	13
Fe2O3	13	11	15	15	11	15	11	14	13	14

continued . . .

	CDB500	CDB509	CDB510	CDB511	CDB513	CDB514	CDB518	CDB526	CDB530	CDB536
Rock type	Tholeiitic mafic rocks	Alkali mafic rock	Tholeiitic mafic rock	Tholeiitic mafic rock	Tholeiittic mafic rock	Tholeiitic mafic rock	Bostonite	Alkali mafic rock	Alkali mafic rock	Tholeiitic mafic rock
MnO	0.19	0.17	0.21	0.21	0.18	0.21	0.17	0.16	0.16	0.18
MgO	9.22	8.3	2.25	2.96	6.62	3.57	1.87	8.79	6.53	7.36
CaO	11	10	9.14	8.44	9.04	7.33	5.74	8.75	10	9.55
Na2O	1.69	1.45	1.88	1.78	2.22	2.4	3.19	1.82	2.55	2.08
K2O	0.76	4.49	1.73	1.45	1.5	2.06	3.1	1.84	1.32	0.78
P2O5	0.47	1.27	0.84	0.81	0.13	0.68	1.14	0.5	0.48	0.49
H2O	3.99	2.92	2	3.83	1.51	1.25	1.11	2.78	3	2.22
CO2	2.62	1.77	4.65	4.48	0.05	0.07	0.21	6.77	2.98	6.77
Total	99.84	99.37	99.76	99.57	99.33	99.29	99.77	99.96	99.65	100.64
Ba	248	4642	696	601	1017	868	993	580	341	NM
Cr	364	288	ND	ND	51	15	ND	171	228	NM
Ga	14	14	17	18	14	17	18	17	17	NM
Nb	38	105	24	26	ND	21	37	35	30	NM
Ni	298	122	34	36	63	33	15	209	153	NM
Rb	ND	183	29	23	67	40	56	58	29	NM
Sr	470	1180	374	382	251	327	473	681	515	NM
V	205	240	263	300	283	290	126	224	216	NM
Y	19	40	67	61	22	60	70	21	20	NM
Zn	80	96	143	136	72	126	275	456	166	NM
Zr	186	260	306	303	98	294	436	168	144	NM

	CDB541	CDB544	CDB546	CDB547	CDB550	CDB551	CDB552	CDB553	CDB555	CDB556
Rock type	Quartz porphyry	Bostonite	Tholeiitic mafic rocks	Quartz porphyry	Tholeiitic mafic rocks	Bostonite	Bostonite	Quartz porphyry	Bostonite	Bostonite
SiO_2	73	59	48	61	50	67	65	72	69	56
TiO_2	0.15	1.72	1.59	1.34	2.36	0.18	0.22	0.3	0.33	2
Al_2O_3	15	15	15	14	13	16	18	12	13	13
Fe_2O_3	0.67	8.4	13	9.09	15	4.11	2.44	4.58	5.12	12
MnO	0.01	0.23	0.19	0.15	0.2	0.02	0.07	0.03	0.07	0.21
MgO	0.09	0.85	6.14	1.1	3.51	0.15	0.11	0.09	0.8	1.74
CaO	0.06	1.69	8.93	4.15	7.29	0.13	0.32	0.7	1.84	4.69
Na_2O	5.49	3.83	2.12	2.76	1.87	5.27	5.71	2.07	2.11	3.01
K_2O	3.83	4.94	1.04	4.14	1.93	4.55	5.72	5.94	5.9	3.72
P_2O_5	0.04	1.06	0.43	0.52	0.69	0.08	0.19	0.03	0.06	1.22
H_2O	1.02	2.1	1.83	1.25	1.44	1.67	1.34	1.13	0.75	1.2
CO_2	0.06	0.13	0.68	0.47	2.1	0.11	0.25	0.23	0.18	0.05
Total	99.60	99.39	99.71	99.51	99.39	99.58	99.52	99.52	99.34	99.41
Ba	254	983	452	1119	813	103	104	386	116	1134
Cr	18	13	118	ND	22	14	12	15	28	12
Ga	15	24	18	20	19	32	12	21	30	19
Nb	356	84	9	51	17	380	332	132	153	52
Ni	ND	12	105	10	26	12	ND	12	28	ND
Rb	217	158	45	116	48	253	232	336	360	96
Sr	54	260	367	247	378	82	160	36	44	468

continued . . .

	CDB541	CDB544	CDB546	CDB547	CDB550	CDB551	CDB552	CDB553	CDB555	CDB556
Rock type	Quartz porphyry	Bostonite	Tholeiitic mafic rocks	Quartz porphyry	Tholeiitic mafic rocks	Bostonite	Bostonite	Quartz porphyry	Bostonite	Bostonite
V	ND	75	256	86	302	ND	ND	10	39	120
Y	110	81	38	72	60	161	65	175	268	88
Zn	24	179	111	254	151	176	84	103	234	139
Zr	761	754	177	549	327	1155	1153	681	497	601

	CDB561	CDB562	CDB563	CDB565	CDB570	CDB572	CDB580	CDB582	CDB588	CDB592
Rock type	Bostonite	Bostonite	Bostonite	Alkali mafic rocks	Tholeiitic mafic rock	Quartz porphyry	Quartz porphyry	Quartz porphyry	Quartz porphyry	Bostonite
SiO_2	51	49	69	44	45	75	76	74	76	64
TiO_2	2.64	2.63	0.14	2.72	2.39	0.15	0.17	0.16	0.17	0.72
Al_2O_3	14	14	15	14	15	12	12	13	12	16
Fe_2O_3	14	15	3.54	8.96	12	2.47	1.84	3.03	2.55	4.55
MnO	0.09	0.26	0.11	0.2	0.15	0.03	0.02	0.04	0.03	0.03
MgO	2.42	2.61	0.03	5.81	7.09	0.04	0.03	0.09	0.03	0.19
CaO	2.93	4.52	0.64	7.75	11	0.88	0.7	0.81	0.49	0.26
Na_2O	2.11	3.11	5.01	3.75	2.61	2.85	2.51	2.19	2.53	4.41
K_2O	3.77	3.5	4.62	5.07	1.4	5.59	5.66	6.11	5.43	6.48
P_2O_5	1.98	1.86	0.02	0.9	0.77	0.02	0.02	0.02	0.02	0.2
H_2O	4.02	2.19	0.96	1.65	1.93	0.42	0.58	0.67	0.64	1.3
CO_2	0.08	0.74	0.07	4.79	0.13	0.17	0.08	0.09	0.1	0.78
Total	99.30 99.51 99.26 99.67	99.22	99.66	99.56	99.58	99.79	99.54			

continued . . .

	CDB561	CDB562	CDB563	CDB565	CDB570	CDB572	CDB580	CDB582	CDB588	CDB592
Rock type	Bostonite	Bostonite	Bostonite	Alkali mafic rocks	Tholeiitic mafic rock	Quartz porphyry	Quartz porphyry	Quartz porphyry	Quartz porphyry	Bostonite
Ba	1473	1162	73	1119	1162	239	328	405	314	1051
Cr	9	ND	16	ND	ND	22	20	17	19	15
Ga	22	18	35	20	18	18	17	25	18	17
Nb	69	62	498	51	62	109	62	109	95	98
Ni	11	13	11	10	13	15	10	15	ND	ND
Rb	115	71	345	116	71	339	347	373	295	299
Sr	709	561	24	247	561	54	46	165	42	294
V	115	103	ND	86	103	ND	ND	ND	9	10
Y	89	87	170	72	87	190	154	260	74	75
Zn	224	183	232	254	183	69	55	182	94	140
Zr	571	483	1012	549	483	314	326	347	335	1056

	CDB593	CDB594	CDB601	CDB602	CDB604	CDB605	CDB607	CDB609	CDB611	CDB615
Rock type	Quartz porphyry	Quartz porphyry	Quartz porphyry	Quartz porphyry	Quartz porphyry	Quartz porphyry	Quartz porphyry	Quartz porphyry	Quartz porphyry	Quartz porphyry
SiO_2	75	77	72	77	74	61	76	75	75	75
TiO_2	0.14	0.1	0.34	0.12	0.19	0.04	0.14	0.15	0.36	0.14
Al_2O_3	12	12	13	13	13	20	12	12	12	12
Fe_2O_3	3.04	1.72	4.2	1.45	3.16	4.67	1.99	2.95	3.75	2.95
MnO	0.02	0.01	0.03	ND	0.04	0.17	0.02	0.04	0.05	0.04
MgO	0.01	ND	0.03	0.04	0.04	0.02	ND	ND	0.45	0.01

continued . . .

	CDB593	CDB594	CDB601	CDB602	CDB604	CDB605	CDB607	CDB609	CDB611	CDB615
Rock type	Quartz porphyry	Quartz porphyry	Quartz porphyry	Quartz porphyry	Quartz porphyry	Quartz porphyry	Quartz porphyry	Quartz porphyry	Quartz porphyry	Quartz porphyry
CaO	0.28	0.33	0.83	0.32	0.74	0.7	0.27	0.41	1.87	0.34
Na_2O	2.83	3.03	2.9	4.88	2.3	5.41	2.93	2.81	0.9	2.56
K_2O	5	4.84	5.41	2.31	5.75	6.55	4.95	4.67	3.9	5.23
P_2O_5	ND	0.02	0.05	0.02	0.02	0.02	0.02	0.02	0.12	0.02
H_2O	0.75	0.52	0.61	0.84	0.78	0.76	1.01	0.89	1.1	0.77
CO_2	0.24	0.09	0.08	0.37	0.07	0.12	0.34	0.18	0.04	0.11
Total	99.70	99.76	99.55	99.64	99.51	99.38	99.47	99.34	99.75	99.23
Ba	ND	29	442	39	22	137	ND	ND	266	ND
Cr	15	20	17	18	21	14	20	18	24	19
Ga	27	24	17	16	29	21	24	32	14	30
Nb	313	140	86	389	153	214	321	300	12	316
Ni	ND	11	12	11	18	10	14	18	10	19
Rb	484	400	210	234	353	444	506	456	372	532
Sr	30	20	52	48	30	163	40	40	84	33
V	ND	ND	ND	13	ND	ND	ND	ND	12	ND
Y	81	122	95	107	346	55	144	298	60	407
Zn	250	38	121	159	243	357	88	287	75	282
Zr	886	264	717	1176	579	2284	881	856	320	873

	CDB619	CDB633	CDB634	CDB639	CDB641	CDB645	CDB650	CDB653	CDB678	CDB681
Rock type	Bostonite	Quartz porphyry	Bostonite	Quartz porphyry	Bostonite	Bostonite	Quartz porphyry	Quartz porphyry	Bostonite	Bostonite
SiO_2	77	73	66	73	65	66	71	79	70	56
TiO_2	0.07	0.27	0.24	0.28	0.3	0.24	0.56	0.08	0.13	2.01
Al_2O_3	12	12	16	12	17	16	12	11	15	14
Fe_2O_3	1.47	4.4	4.69	4.67	4.86	4.39	6.9	1.75	2.99	11
MnO	0.01	0.06	0.1	0.07	0.08	0.07	0.06	0.02	0.07	0.11
MgO	ND	0.11	0.02	0.18	0.02	ND	0.34	0.12	0.12	2.05
CaO	0.59	1.36	0.83	1.73	0.89	0.84	0.2	0.24	0.85	2.76
Na_2O	3.36	1.88	6.04	1.5	5.76	5.88	1.09	ND	5.2	2.18
K_2O	4.07	5.72	4.93	5.23	5.49	5.05	5.77	5	3.49	4.64
P_2O_5	0.01	0.03	0.02	0.03	0.04	0.02	0.15	0.02	0.02	1.34
H_2O	0.52	0.64	0.46	0.78	0.49	0.42	1.82	1.59	1.05	2.35
CO_2	0.15	0.09	0.06	0.04	0.08	0.09	0.07	0.09	0.08	0.09
Total	99.73	99.59	99.63	99.52	99.28	99.17	99.56	99.64	99.01	99.23
Ba	127	63	73	68	53	59	803	142	55	1441
Cr	11	21	18	22	16	18	18	16	17	16
Ga	29	23	35	24	25	25	15	30	45	21
Nb	266	152	326	149	255	301	37	183	555	48
Ni	ND	18	ND	17	13	ND	12	16	14	11
Rb	331	364	261	321	203	236	253	508	252	206
Sr	74	49	25	93	71	45	83	20	66	321

continued . . .

	CDB619	CDB633	CDB634	CDB639	CDB641	CDB645	CDB650	CDB653	CDB678	CDB681
Rock type	Bostonite	Quartz porphyry	Bostonite	Quartz porphyry	Bostonite	Bostonite	Quartz porphyry	Quartz porphyry	Bostonite	Bostonite
V	ND	ND	ND	11	ND	ND	13	ND	ND	138
Y	80	263	103	268	201	161	141	195	367	87
Zn	152	124	175	209	139	169	156	66	252	161
Zr	325	610	592	643	1494	1330	920	258	1195	677

	CDB683	CDB684	CDB687	CDB699	CDB702	CDB703	CDB704	CDB716	CDB719	CDB752
Rock type	Bostonite	Bostonite	Rooivleitjie granite	Tholeiitic mafic rock	Bostonite	Syenite	Bostonite	Bostonite	Bostonite	Rooivleitjie granite
SiO_2	61	69	75	51	61	60	66	65	74	74
TiO_2	0.88	0.18	0.08	1.59	0.81	0.75	0.32	0.27	0.09	0.09
Al_2O_3	17	15	13	13	17	18	18	16	13	13
Fe_2O_3	5.24	2.5	2.11	15	5.89	5.35	1.91	5.1	2.6	3
MnO	0.1	0.19	0.03	0.22	0.15	0.15	0.01	0.06	0.04	0.04
MgO	0.58	0.13	0.01	5.18	0.65	0.62	ND	0.08	0.02	0.02
CaO	0.71	0.05	0.05	9.46	2.16	2.3	0.57	0.19	0.08	0.08
Na_2O	4.25	4	4.04	2.29	5.11	5.09	5.5	5.65	4.31	4
K_2O	7.27	6.41	4.52	0.78	5.5	5.61	6.1	5.26	4.49	4
P_2O_5	0.34	0.06	ND	0.24	0.32	0.29	0.08	0.04	ND	ND
H_2O	1.42	0.98	0.67	0.74	0.7	0.86	0.92	1.02	0.76	0.76
CO_2	0.13	0.07	0.07	0.05	0.06	0.42	0.25	0.2	0.14	NM
Total	99.47	99.11	99.50	99.72	99.32	99.43	99.53	99.20	99.38	99.25

continued . . .

	CDB683	CDB684	CDB687	CDB699	CDB702	CDB703	CDB704	CDB716	CDB719	CDB752
Rock type	Bostonite	Bostonite	Rooivleitjie granite	Tholeiitic mafic rock	Bostonite	Syenite	Bostonite	Bostonite	Bostonite	Rooivleitjie granite
Ba	875	223	89	219	1957	1423	152	230	224	164
Cr	11	15	18	114	12	16	13	21	16	15
Ga	28	59	29	21	25	19	25	25	37	34
Nb	89	465	703	8	114	103	234	101	346	516
Ni	ND	10	10	52	ND	ND	ND	14	ND	12
Rb	172	469	649	24	121	111	184	371	456	684
Sr	127	36	9	174	315	439	96	21	23	13
V	ND	ND	ND	334	12	ND	ND	ND	ND	ND
Y	33	134	32	36	63	49	79	321	100	30
Zn	240	1642	82	118	149	137	27	221	99	132
Zr	309	933	597	142	613	983	1993	689	1777	595

	CDB753	CDB761	CDB764	CDB822	CDB825	CDB922	CDB932	CDB953	CDB974	CDB978
Rock type	Syenite	Quartz porphyry	Bostonite	Tholeiitic mafic rock	Rietpoort granite	Alkali mafic rock	Alkali mafic rock	Tholeiitic mafic rock	Tholeiitic mafic rock	Tholeiitic mafic rock
SiO_2	61	72	56	51	76	37	35	53	53	52
TiO_2	0.64	0.29	1.84	2.43	0.22	5.49	7.04	1.24	1.14	1.07
Al_2O_3	18	12	12	13	12	7.3	8.92	13	14	14
Fe_2O_3	4.59	4.34	13	15	2.13	17	19	13	11	12
MnO	0.12	0.05	0.17	0.17	0.03	0.19	0.24	0.21	0.17	0.19
MgO	0.56	0.42	1.74	3.45	0.06	13	7.31	5.09	6.15	6.34

continued . . .

	CDB753	CDB761	CDB764	CDB822	CDB825	CDB922	CDB932	CDB953	CDB974	CDB978
Rock type	Syenite	Quartz porphyry	Bostonite	Tholeiitic mafic rock	Rietpoort granite	Alkali mafic rock	Alkali mafic rock	Tholeiitic mafic rock	Tholeiitic mafic rock	Tholeiitic mafic rock
CaO	1.87	0.13	5.79	7.4	0.52	12	14	8.7	10	9.83
Na_2O	5.19	0.58	1.84	1.94	2.27	1.55	1.96	2.28	1.86	2.16
K_2O	5.55	7.76	2.78	1.96	6.03	1.16	1.14	1.2	0.74	0.86
P_2O_5	0.25	0.04	0.75	0.7	0.02	1.46	1.39	0.17	0.14	0.13
H_2O	0.86	1.41	1.37	0.93	0.59	2.84	2.63	1.21	1.61	1.35
CO_2	0.17	0.13	1.65	0.09	0.08	0.06	0.16	0.04	0.06	0.06
Total	99.48	99.28	99.35	98.74	99.71	99.16	99.02	99.67	99.74	99.71
Ba	1442	NM	1049	863	387	844	553	232	371	199
Cr	13	NM	29	28	19	449	97	61	58	60
Ga	23	NM	18	19	18	14	10	22	20	18
Nb	90	NM	18	21	45	146	241	8	6	7
Ni	ND	NM	22	22	11	160	40	47	61	59
Rb	121	NM	73	76	284	64	73	42	39	29
Sr	470	NM	230	396	33	1582	1451	179	268	214
V	ND	NM	130	312	ND	282	327	353	332	301
Y	47	NM	78	65	110	26	27	32	23	24
Zn	105	NM	156	100	72	143	149	105	96	86
Zr	610	NM	421	343	314	634	1160	131	118	106

	CDB1064	CDB1066	CDB1092	CDB1101	CDB1105	CDB1126	CDB1200	CDB1341	CDB1454	CDB1459
Rock type	Quartz porphyry	Bostonite	Zout Rivier Plug	Zout River Plug	Zout River Plug	Zout River Plug	Zout River Plug	Zout River Plug	Tholeiitic mafic rock	Tholeiitic mafic rock
SiO_2	70	73	53	50	51	53	53	51	52	48
TiO_2	0.48	0.26	1.25	1.08	1.21	2.4	1.21	1.08	1.32	2.59
Al_2O_3	12	13	13	14	14	12	14	14	13	13
Fe_2O_3	5.9	2.09	13	12	13	16	12	12	13	15
MnO	0.11	0.04	0.19	0.2	0.21	0.22	0.19	0.2	0.19	0.22
MgO	0.13	0.21	5.01	7.19	6.73	2.78	5.84	7.37	6.11	6.37
CaO	1.03	0.36	8.82	10	10	6.85	10	11	8.88	10
Na_2O	1.79	4.25	2.24	1.74	1.64	2.12	1.89	1.58	1.94	2.03
K_2O	5.91	3.84	1.15	0.57	0.41	1.9	0.69	0.55	1.04	0.46
P_2O_5	0.09	0.06	0.17	0.09	0.11	0.34	0.15	0.09	0.16	0.26
H_2O	1.44	1.5	1.26	1.93	1.47	1.19	1.22	1.3	1.37	1.43
CO_2	0.66	1	0.04	0.44	0.43	0.28	0.04	0.44	0.16	0.1
Total	99.56	99.59	99.71	99.64	99.55	99.32	99.67	99.65	99.78	99.45
Ba	1104	194	258	119	103	341	273	226	246	80
Cr	21	15	64	89	76	33	61	86	43	163
Ga	18	16	19	19	18	21	21	18	22	24
Nb	63	246	8	3	3	16	7	4	5	11
Ni	18	13	50	47	38	17	56	45	49	80
Rb	195	222	40	83	11	81	69	20	43	25
Sr	147	30	176	103	102	148	328	105	203	189

continued . . .

	CDB1064	CDB1066	CDB1092	CDB1101	CDB1105	CDB1126	CDB1200	CDB1341	CDB1454	CDB1459
Rock type	Quartz porphyry	Bostonite	Zout Rivier Plug	Zout River Plug	Zout River Plug	Zout River Plug	Zout River Plug	Zout River Plug	Tholeiitic mafic rock	Tholeiitic mafic rock
V	ND	12	353	322	330	520	332	316	346	399
Y	102	136	32	25	26	53	25	24	26	39
Zn	158	52	103	89	98	138	94	87	100	118
Zr	815	655	136	76	85	214	128	76	130	170

	CDB1491	CN495
Rock type	Tholeiitic mafic rocks	Quartz porphyry
SiO_2	47	72
TiO_2	2.44	0.33
Al_2O_3	13	13
Fe_2O_3	15	4.07
MnO	0.21	0.03
MgO	6.33	0.09
CaO	10	0.6
Na_2O	3.27	2.85
K_2O	0.41	5.25
P_2O_5	0.25	0.09
H_2O	1.49	1.31
CO_2	0.08	0.1
Total	99.27	99.47
Ba	73	457
Cr	162	16
Ga	20	18
Nb	10	189
Ni	82	13
Rb	26	322
Sr	172	64
V	385	11
Y	36	164
Zn	117	110
Zr	157	524

Table 4: Whole–rock trace element analyses done by ICP–MS for all CDB and CN samples. Not Measured (NM), Not Detected (ND)

	CDB217	CDB249	CDB251	CDB267	CDB300	CDB328	CDB329	CDB331	CDB335	CDB336
Rock type	Tholeiitic mafic rock	Alkali mafic rock	Tholeiitic mafic rock	Tholeiitic mafic rock	Tholeiitic mafic rock	Tholeiitic mafic rock	Alkali mafic rock	Alkali mafic rock	Bostonite	Quartz porphyry
Y	38	NM	53	NM	61	23	23	NM	NM	91
La	29	NM	47	NM	52	12	87	NM	NM	96
Ce	63	NM	100	NM	120	25	164	NM	NM	201
Pr	7.6	NM	13	NM	14	2.8	18	NM	NM	23
Nd	32	NM	51	NM	61	13	62	NM	NM	96
Sm	6.8	NM	10	NM	12	3	9.6	NM	NM	19
Eu	2	NM	2.9	NM	3	0.99	2.8	NM	NM	2.9
Gd	7.3	NM	11	NM	13	3.7	8	NM	NM	19
Tb	1.3	NM	1.8	NM	2	0.69	1.2	NM	NM	2.9
Dy	7.2	NM	10	NM	12	4.2	5.4	NM	NM	19
Ho	1.4	NM	1.9	NM	2.2	0.87	0.88	NM	NM	3.6
Er	4.6	NM	6.3	NM	7.4	2.8	2.4	NM	NM	12
Tm	0.68	NM	0.92	NM	1.1	0.43	0.35	NM	NM	1.8
Yb	4.5	NM	6	NM	6.9	2.8	2.1	NM	NM	11
Lu	0.65	NM	0.88	NM	1	0.41	0.29	NM	NM	1.6
Li	13	NM	35	NM	7.83	13	24	NM	NM	19
Rb	25	NM	48	NM	72	37	68	NM	NM	144
Sr	361	NM	402	NM	363	233	1354	NM	NM	146

continued . . .

Sample number	CDB217	CDB249	CDB251	CDB267	CDB300	CDB328	CDB329	CDB331	CDB335	CDB336
Rock type	Tholeiitic mafic rock	Alkali mafic rock	Tholeiitic mafic rock	Tholeiitic mafic rock	Tholeiitic mafic rock	Tholeiitic mafic rock	Alkali mafic rock	Alkali mafic rock	Bostonite	Quartz porphyry
Nb	13	NM	19	NM	24	4.08	82	NM	NM	37
Mo	1.08	NM	1.72	NM	2.3	0.56	3.45	NM	NM	4.21
Cd	0.15	NM	0.19	NM	0.14	0.12	0.12	NM	NM	0.27
Sn	1.23	NM	1.74	NM	2.06	0.56	1.73	NM	NM	3.45
Cs	0.83	NM	0.97	NM	21	55	21	NM	NM	0.69
Hf	4.15	NM	7.17	NM	7.6	2.14	5.45	NM	NM	12
Pb	5.82	NM	9.44	NM	9.9	2.48	7.23	NM	NM	25
Bi	0.01	NM	0.01	NM	0.01	0	0.01	NM	NM	0.02
Th	2.11	NM	3.48	NM	4.26	0.88	7.6	NM	NM	14
U	0.46	NM	0.7	NM	0.9	0.14	1.9	NM	NM	2.57
Sc	36	NM	37	NM	37	37	21	NM	NM	20
Cr	34	NM	14	NM	23	124	108	NM	NM	6
Co	46	NM	41	NM	40	48	38	NM	NM	10
Ni	59	NM	20	NM	33	114	56	NM	NM	2.64
Cu	40	NM	18	NM	31	54	25	NM	NM	4.27
Zn	112	NM	138	NM	155	78	90	NM	NM	158
Ga	19	NM	21	NM	22	16	18	NM	NM	23
Sb	0	NM	0.02	NM	0.03	0	0.04	NM	NM	0.14
Tl	0.18	NM	0.25	NM	0.59	0.57	0.21	NM	NM	NM

Sample number	CDB339	CDB349	CDB353	CDB383	CDB387	CDB388	CDB390	CDB415	CDB484	CDB489
Rock type	Tholeiitic mafic rock	Tholeiitic mafic rock	Tholeiitic mafic rock	Quartz porphyry	Tholeiitic mafic rock	Quartz porphyry	Tholeiitic mafic rock	Tholeiitic mafic rock	Alkali mafic rock	Tholeiitic mafic rock
Y	NM	NM	36	175	NM	70	NM	39	NM	40
La	NM	NM	24	139	NM	7.9	NM	22	NM	26
Ce	NM	NM	51	215	NM	29	NM	47	NM	55
Pr	NM	NM	6.6	23	NM	1.4	NM	5.9	NM	7
Nd	NM	NM	28	75	NM	5.9	NM	25	NM	30
Sm	NM	NM	6.5	15	NM	1.7	NM	6	NM	6.7
Eu	NM	NM	2	0.24	NM	0.04	NM	2.2	NM	1.9
Gd	NM	NM	7.2	17	NM	3.1	NM	6.9	NM	7.4
Tb	NM	NM	1.3	3.4	NM	1.1	NM	1.3	NM	1.3
Dy	NM	NM	7.1	26	NM	9.9	NM	7.2	NM	7.5
Ho	NM	NM	1.4	6.1	NM	2.5	NM	1.5	NM	1.5
Er	NM	NM	4.3	22	NM	9.6	NM	4.6	NM	4.8
Tm	NM	NM	0.62	3.4	NM	1.8	NM	0.66	NM	0.72
Yb	NM	NM	4.1	23	NM	16	NM	4.5	NM	4.7
Lu	NM	NM	0.6	3	NM	2.1	NM	0.65	NM	0.68
Li	NM	NM	34	13	NM	36	NM	17	NM	26
Rb	NM	NM	76	514	NM	773	NM	50	NM	55
Sr	NM	NM	167	39	NM	20	NM	184	NM	340
Nb	NM	NM	15	228	NM	205	NM	13	NM	9.73
Mo	NM	NM	0.95	4.83	NM	2.25	NM	0.98	NM	1.46

continued . . .

Sample number	CDB339	CDB349	CDB353	CDB383	CDB387	CDB388	CDB390	CDB415	CDB484	CDB489
Rock type	Tholeiitic mafic rock	Tholeiitic mafic rock	Tholeiitic mafic rock	Quartz porphyry	Tholeiitic mafic rock	Quartz porphyry	Tholeiitic mafic rock	Tholeiitic mafic rock	Alkali mafic rock	Tholeiitic mafic rock
Cd	NM	NM	0.15	0.04	NM	ND	NM	0.17	NM	0.17
Sn	NM	NM	1.88	6.31	NM	26	NM	2.21	NM	1.32
Cs	NM	NM	1.31	1.64	NM	3.28	NM	1.94	NM	1.31
Hf	NM	NM	4.44	8.92	NM	9.87	NM	4.63	NM	3.49
Pb	NM	NM	6.83	39	NM	25	NM	7.6	NM	8.5
Bi	NM	NM	0.04	0.07	NM	0.43	NM	0.02	NM	0
Th	NM	NM	5.34	60	NM	60	NM	5.82	NM	1.69
U	NM	NM	1.37	14	NM	9.47	NM	1.44	NM	0.42
Sc	NM	NM	42	1.34	NM	0.91	NM	45	NM	34
Cr	NM	NM	31	6.3	NM	7.57	NM	21	NM	18
Co	NM	NM	44	0.32	NM	0.46	NM	39	NM	43
Ni	NM	NM	9.99	3.2	NM	3.5	NM	19	NM	44
Cu	NM	NM	10	3	NM	2.37	NM	28	NM	28
Zn	NM	NM	126	67	NM	46	NM	118	NM	138
Ga	NM	NM	20	31	NM	40	NM	20	NM	19
Sb	NM	NM	0.17	0.21	NM	0.14	NM	0.08	NM	0.05
Tl	NM	NM	0.51	2.36	NM	NM	NM	0.3	NM	0.41

Sample number	CDB500	CDB509	CDB510	CDB511	CDB513	CDB514	CDB518	CDB526	CDB530	CDB536
Rock type	Tholeiitic mafic rocks	Alkali mafic rock	Tholeiitic mafic rock	Tholeiitic mafic rock	Tholeiittic mafic rock	Tholeiitic mafic rock	Bostonite	Alkali mafic rock	Alkali mafic rock	Tholeiitic mafic rock
Y	NM	NM	NM	NM	21	NM	65	NM	NM	NM
La	NM	NM	NM	NM	13	NM	78	NM	NM	NM
Ce	NM	NM	NM	NM	28	NM	172	NM	NM	NM
Pr	NM	NM	NM	NM	3.4	NM	21	NM	NM	NM
Nd	NM	NM	NM	NM	15	NM	86	NM	NM	NM
Sm	NM	NM	NM	NM	3.6	NM	17	NM	NM	NM
Eu	NM	NM	NM	NM	1.1	NM	3.7	NM	NM	NM
Gd	NM	NM	NM	NM	4	NM	16	NM	NM	NM
Tb	NM	NM	NM	NM	0.78	NM	2.5	NM	NM	NM
Dy	NM	NM	NM	NM	4.1	NM	14	NM	NM	NM
Ho	NM	NM	NM	NM	0.77	NM	2.6	NM	NM	NM
Er	NM	NM	NM	NM	2.4	NM	7.7	NM	NM	NM
Tm	NM	NM	NM	NM	0.32	NM	1.2	NM	NM	NM
Yb	NM	NM	NM	NM	2.3	NM	7.2	NM	NM	NM
Lu	NM	NM	NM	NM	0.33	NM	1	NM	NM	NM
Li	NM	NM	NM	NM	18	NM	19	NM	NM	NM
Rb	NM	NM	NM	NM	72	NM	62	NM	NM	NM
Sr	NM	NM	NM	NM	262	NM	492	NM	NM	NM
Nb	NM	NM	NM	NM	5.94	NM	39	NM	NM	NM
Mo	NM	NM	NM	NM	0.49	NM	3.73	NM	NM	NM

continued . . .

Sample number	CDB500	CDB509	CDB510	CDB511	CDB513	CDB514	CDB518	CDB526	CDB530	CDB536
Rock type	Tholeiitic mafic rocks	Alkali mafic rock	Tholeiitic mafic rock	Tholeiitic mafic rock	Tholeiittic mafic rock	Tholeiitic mafic rock	Bostonite	Alkali mafic rock	Alkali mafic rock	Tholeiitic mafic rock
Cd	NM	NM	NM	NM	0.09	NM	0.2	NM	NM	NM
Sn	NM	NM	NM	NM	1.02	NM	2.87	NM	NM	NM
Cs	NM	NM	NM	NM	0.83	NM	0.51	NM	NM	NM
Hf	NM	NM	NM	NM	2.47	NM	10	NM	NM	NM
Pb	NM	NM	NM	NM	4.46	NM	13	NM	NM	NM
Bi	NM	NM	NM	NM	0.02	NM	0.01	NM	NM	NM
Th	NM	NM	NM	NM	3.14	NM	5.16	NM	NM	NM
U	NM	NM	NM	NM	0.66	NM	1.33	NM	NM	NM
Sc	NM	NM	NM	NM	40	NM	20	NM	NM	NM
Cr	NM	NM	NM	NM	44	NM	6.52	NM	NM	NM
Co	NM	NM	NM	NM	42	NM	17	NM	NM	NM
Ni	NM	NM	NM	NM	50	NM	6.89	NM	NM	NM
Cu	NM	NM	NM	NM	87	NM	12	NM	NM	NM
Zn	NM	NM	NM	NM	75	NM	130	NM	NM	NM
Ga	NM	NM	NM	NM	16	NM	22	NM	NM	NM
Sb	NM	NM	NM	NM	0.01	NM	0.05	NM	NM	NM
Tl	NM	NM	NM	NM	0.4	NM	0.35	NM	NM	NM

Sample number	CDB541	CDB544	CDB546	CDB547	CDB550	CDB551	CDB552	CDB553	CDB555	CDB556
Rock type	Quartz porphyry	Bostonite	Tholeiitic mafic rocks	Quartz porphyry	Tholeiitic mafic rocks	Bostonite	Bostonite	Quartz porphyry	Bostonite	Bostonite
Y	80	NM	NM	64	NM	101	53	132	226	NM
La	113	NM	NM	89	NM	205	186	87	316	NM
Ce	221	NM	NM	176	NM	349	347	282	594	NM
Pr	24	NM	NM	21	NM	44	34	24	71	NM
Nd	76	NM	NM	80	NM	141	97	87	253	NM
Sm	14	NM	NM	15	NM	25	15	18	46	NM
Eu	0.41	NM	NM	2.8	NM	0.46	1.2	1	1.1	NM
Gd	13	NM	NM	14	NM	21	11	18	44	NM
Tb	2.3	NM	NM	2.2	NM	3.5	1.7	3.4	7.2	NM
Dy	14	NM	NM	13	NM	22	10	24	44	NM
Ho	2.9	NM	NM	2.6	NM	4.2	2.1	5	8.5	NM
Er	9.5	NM	NM	7.8	NM	13	6.4	18	27	NM
Tm	1.6	NM	NM	1.2	NM	2	1.2	2.8	4.2	NM
Yb	9.9	NM	NM	7.5	NM	13	6.9	19	27	NM
Lu	1.5	NM	NM	1.1	NM	1.7	1.1	2.6	3.4	NM
Li	7.75	NM	NM	28	NM	30	3.91	8.94	25	NM
Rb	156	NM	NM	123	NM	196	156	310	323	NM
Sr	50	NM	NM	253	NM	76	120	33	38	NM
Nb	362	NM	NM	50	NM	381	351	132	157	NM
Mo	1.17	NM	NM	3.51	NM	1.68	0.73	0.99	8.23	NM

continued . . .

Sample number	CDB541	CDB544	CDB546	CDB547	CDB550	CDB551	CDB552	CDB553	CDB555	CDB556
Rock type	Quartz porphyry	Bostonite	Tholeiitic mafic rocks	Quartz porphyry	Tholeiitic mafic rocks	Bostonite	Bostonite	Quartz porphyry	Bostonite	Bostonite
Cd	0.02	NM	NM	0.32	NM	0.04	0.11	0.09	0.54	NM
Sn	15	NM	NM	2.35	NM	11	6.27	6.68	8.57	NM
Cs	0.49	NM	NM	1.5	NM	2.33	0.58	0.8	1.28	NM
Hf	20	NM	NM	11	NM	30	25	15	10	NM
Pb	12	NM	NM	26	NM	17	29	34	63	NM
Bi	0.08	NM	NM	0.03	NM	0.07	0.09	0.04	0.06	NM
Th	58	NM	NM	13	NM	54	33	45	56	NM
U	11	NM	NM	2.17	NM	12	7.78	6.82	9.79	NM
Sc	2.22	NM	NM	19	NM	2.74	5.67	3.39	6.63	NM
Cr	5.66	NM	NM	5.27	NM	3.85	2.74	6	15	NM
Co	0.53	NM	NM	13	NM	2.14	1.35	0.6	6.72	NM
Ni	4	NM	NM	4.43	NM	5.09	2.26	3.92	16	NM
Cu	2.98	NM	NM	8.36	NM	2.17	1.28	4.02	15	NM
Zn	22	NM	NM	140	NM	155	80	93	213	NM
Ga	28	NM	NM	20	NM	47	28	27	32	NM
Sb	0.34	NM	NM	0.12	NM	0.23	0.29	0.11	0.14	NM
Tl	1.45	NM	NM	0.77	NM	0.87	NM	1.82	1.91	NM

Sample number	CDB561	CDB562	CDB563	CDB565	CDB570	CDB572	CDB580	CDB582	CDB588	CDB592
Rock type	Bostonite	Bostonite	Bostonite	Alkali mafic rocks	Tholeiitic mafic rock	Quartz porphyry	Quartz porphyry	Quartz porphyry	Quartz porphyry	Bostonite
Y	NM	NM	NM	NM	24	NM	128	NM	59	NM
La	NM	NM	NM	NM	45	NM	171	NM	35	NM
Ce	NM	NM	NM	NM	89	NM	343	NM	77	NM
Pr	NM	NM	NM	NM	10	NM	39	NM	7.8	NM
Nd	NM	NM	NM	NM	40	NM	133	NM	26	NM
Sm	NM	NM	NM	NM	7.6	NM	24	NM	5	NM
Eu	NM	NM	NM	NM	2.4	NM	0.79	NM	0.54	NM
Gd	NM	NM	NM	NM	7.1	NM	23	NM	5.6	NM
Tb	NM	NM	NM	NM	1.1	NM	3.6	NM	1.2	NM
Dy	NM	NM	NM	NM	5.2	NM	24	NM	9.9	NM
Ho	NM	NM	NM	NM	0.89	NM	4.4	NM	2.4	NM
Er	NM	NM	NM	NM	2.5	NM	15	NM	9.1	NM
Tm	NM	NM	NM	NM	0.36	NM	2.4	NM	1.6	NM
Yb	NM	NM	NM	NM	2	NM	15	NM	10	NM
Lu	NM	NM	NM	NM	0.27	NM	1.9	NM	1.5	NM
Li	NM	NM	NM	NM	39	NM	13	NM	6.45	NM
Rb	NM	NM	NM	NM	72	NM	342	NM	284	NM
Sr	NM	NM	NM	NM	722	NM	43	NM	41	NM
Nb	NM	NM	NM	NM	52	NM	73	NM	101	NM
Mo	NM	NM	NM	NM	2.2	NM	11	NM	4.31	NM

continued . . .

Sample number	CDB561	CDB562	CDB563	CDB565	CDB570	CDB572	CDB580	CDB582	CDB588	CDB592
Rock type	Bostonite	Bostonite	Bostonite	Alkali mafic rocks	Tholeiitic mafic rock	Quartz porphyry	Quartz porphyry	Quartz porphyry	Quartz porphyry	Bostonite
Cd	NM	NM	NM	NM	0.13	NM	0.12	NM	ND	NM
Sn	NM	NM	NM	NM	1.97	NM	4.98	NM	6.91	NM
Cs	NM	NM	NM	NM	8.72	NM	1.18	NM	1.01	NM
Hf	NM	NM	NM	NM	1.71	NM	6.82	NM	7.89	NM
Pb	NM	NM	NM	NM	6.98	NM	34	NM	38	NM
Bi	NM	NM	NM	NM	0.04	NM	0.03	NM	0.3	NM
Th	NM	NM	NM	NM	3.75	NM	38	NM	36	NM
U	NM	NM	NM	NM	1.31	NM	8.23	NM	8.36	NM
Sc	NM	NM	NM	NM	19	NM	3.9	NM	2.72	NM
Cr	NM	NM	NM	NM	261	NM	6.72	NM	9.3	NM
Co	NM	NM	NM	NM	46	NM	0.61	NM	0.76	NM
Ni	NM	NM	NM	NM	168	NM	2.64	NM	4.02	NM
Cu	NM	NM	NM	NM	46	NM	3.15	NM	5.33	NM
Zn	NM	NM	NM	NM	107	NM	59	NM	93	NM
Ga	NM	NM	NM	NM	20	NM	23	NM	26	NM
Sb	NM	NM	NM	NM	0.04	NM	0.21	NM	0.1	NM
Tl	NM	NM	NM	NM	0.62	NM	NM	NM	NM	NM

Sample number	CDB593	CDB594	CDB601	CDB602	CDB604	CDB605	CDB607	CDB609	CDB611	CDB615
Rock type	Quartz porphyry	Quartz porphyry	Quartz porphyry	Quartz porphyry	Quartz porphyry	Quartz porphyry	Quartz porphyry	Quartz porphyry	Quartz porphyry	Quartz porphyry
Y	NM	84	73	NM	284	NM	93	NM	NM	339
La	NM	28	113	NM	295	NM	86	NM	NM	191
Ce	NM	51	226	NM	579	NM	160	NM	NM	371
Pr	NM	6.4	28	NM	69	NM	19	NM	NM	44
Nd	NM	23	101	NM	254	NM	67	NM	NM	154
Sm	NM	6	18	NM	52	NM	16	NM	NM	34
Eu	NM	0.13	1.8	NM	0.37	NM	0.42	NM	NM	0.64
Gd	NM	8	16	NM	55	NM	16	NM	NM	38
Tb	NM	1.8	2.6	NM	8.4	NM	2.7	NM	NM	7.1
Dy	NM	15	15	NM	57	NM	16	NM	NM	45
Ho	NM	3.3	3	NM	11	NM	2.9	NM	NM	9.2
Er	NM	12	8.9	NM	32	NM	8.5	NM	NM	28
Tm	NM	2	1.5	NM	4.6	NM	1.4	NM	NM	4.2
Yb	NM	14	9	NM	28	NM	9	NM	NM	26
Lu	NM	1.8	1.4	NM	3.4	NM	1.3	NM	NM	3.1
Li	NM	4.54	4.94	NM	17	NM	15	NM	NM	50
Rb	NM	387	196	NM	342	NM	462	NM	NM	460
Sr	NM	17	47	NM	27	NM	37	NM	NM	28
Nb	NM	155	85	NM	169	NM	323	NM	NM	328
Mo	NM	20	7.4	NM	14	NM	1.65	NM	NM	1.7

continued . . .

Sample number	CDB593	CDB594	CDB601	CDB602	CDB604	CDB605	CDB607	CDB609	CDB611	CDB615
Rock type	Quartz porphyry	Quartz porphyry	Quartz porphyry	Quartz porphyry	Quartz porphyry	Quartz porphyry	Quartz porphyry	Quartz porphyry	Quartz porphyry	Quartz porphyry
Cd	NM	0.05	0.18	NM	0.69	NM	0.04	NM	NM	0.12
Sn	NM	6.27	4.52	NM	14	NM	6.42	NM	NM	24
Cs	NM	0.78	1.15	NM	0.49	NM	0.78	NM	NM	1.22
Hf	NM	9.72	2.21	NM	7.29	NM	5.7	NM	NM	8.76
Pb	NM	31	29	NM	49	NM	25	NM	NM	44
Bi	NM	0.13	0.02	NM	0.1	NM	0.55	NM	NM	0.2
Th	NM	52	19	NM	43	NM	53	NM	NM	51
U	NM	16	4.68	NM	11	NM	15	NM	NM	19
Sc	NM	1.17	3.31	NM	1.05	NM	0.4	NM	NM	0.43
Cr	NM	8.98	6.56	NM	9.08	NM	7.47	NM	NM	7.69
Co	NM	0.63	1.07	NM	0.27	NM	0.28	NM	NM	0.21
Ni	NM	3.46	3.56	NM	3.74	NM	3.07	NM	NM	3.14
Cu	NM	2.72	5.81	NM	11	NM	7.86	NM	NM	5.03
Zn	NM	38	110	NM	228	NM	80	NM	NM	249
Ga	NM	28	25	NM	33	NM	41	NM	NM	43
Sb	NM	0.12	0.21	NM	0.18	NM	0.08	NM	NM	0.1
Tl	NM	NM	1.08	NM	1.93	NM	2.64	NM	NM	2.47

Sample number	CDB619	CDB633	CDB634	CDB639	CDB641	CDB645	CDB650	CDB653	CDB678	CDB681
Rock type	Bostonite	Quartz porphyry	Bostonite	Quartz porphyry	Bostonite	Bostonite	Quartz porphyry	Quartz porphyry	Bostonite	Bostonite
Y	NM	232	89	218	NM	NM	78	NM	314	NM
La	NM	321	259	341	NM	NM	104	NM	278	NM
Ce	NM	632	459	645	NM	NM	171	NM	608	NM
Pr	NM	74	49	75	NM	NM	26	NM	76	NM
Nd	NM	263	158	274	NM	NM	102	NM	268	NM
Sm	NM	47	25	48	NM	NM	19	NM	54	NM
Eu	NM	1.4	0.37	1.5	NM	NM	2.2	NM	0.49	NM
Gd	NM	46	21	46	NM	NM	18	NM	48	NM
Tb	NM	7.3	3.2	7.5	NM	NM	2.9	NM	8	NM
Dy	NM	45	19	44	NM	NM	17	NM	42	NM
Ho	NM	8.8	3.4	8.5	NM	NM	3.5	NM	7.2	NM
Er	NM	28	10	26	NM	NM	10	NM	20	NM
Tm	NM	4.3	1.8	4	NM	NM	1.6	NM	3.1	NM
Yb	NM	27	11	27	NM	NM	10	NM	18	NM
Lu	NM	3.5	1.6	3.4	NM	NM	1.6	NM	2.1	NM
Li	NM	16	1.75	31	NM	NM	33	NM	14	NM
Rb	NM	341	241	321	NM	NM	274	NM	190	NM
Sr	NM	44	22	90	NM	NM	78	NM	62	NM
Nb	NM	164	338	167	NM	NM	48	NM	554	NM
Mo	NM	3.47	5.43	3.59	NM	NM	2.84	NM	1.05	NM

continued . . .

Sample number	CDB619	CDB633	CDB634	CDB639	CDB641	CDB645	CDB650	CDB653	CDB678	CDB681
Rock type	Bostonite	Quartz porphyry	Bostonite	Quartz porphyry	Bostonite	Bostonite	Quartz porphyry	Quartz porphyry	Bostonite	Bostonite
Cd	NM	0.15	0.23	0.18	NM	NM	0.03	NM	0.11	NM
Sn	NM	5.61	12	12	NM	NM	3.2	NM	18	NM
Cs	NM	1.4	0.32	1.54	NM	NM	0.66	NM	0.54	NM
Hf	NM	2.26	2.63	15	NM	NM	19	NM	6.75	NM
Pb	NM	34	19	87	NM	NM	36	NM	8.56	NM
Bi	NM	0.09	0.04	0.1	NM	NM	0.09	NM	0.06	NM
Th	NM	58	42	55	NM	NM	20	NM	51	NM
U	NM	5.79	9.85	5.79	NM	NM	3.47	NM	11	NM
Sc	NM	2.96	2.34	3.72	NM	NM	11	NM	0.52	NM
Cr	NM	9.25	6.25	12	NM	NM	6.05	NM	6.14	NM
Co	NM	1	0.51	1.18	NM	NM	2.67	NM	0.5	NM
Ni	NM	4.64	3.32	6.23	NM	NM	3.53	NM	2.81	NM
Cu	NM	5.2	3.87	9.31	NM	NM	13	NM	4.69	NM
Zn	NM	112	159	192	NM	NM	149	NM	229	NM
Ga	NM	32	41	33	NM	NM	25	NM	64	NM
Sb	NM	0.29	0.24	0.57	NM	NM	0.2	NM	0.27	NM
Tl	NM	1.93	0.5	1.88	NM	NM	NM	NM	0.98	NM

Sample number	CDB683	CDB684	CDB687	CDB699	CDB702	CDB703	CDB704	CDB716	CDB719	CDB752
Rock type	Bostonite	Bostonite	Rooivleitjie granite	Tholeiitic mafic rock	Bostonite	Syenite	Bostonite	Bostonite	Bostonite	Rooivleitjie granite
Y	25	102	14	NM	55	43	61	NM	69	15
La	88	309	14	NM	137	93	124	NM	121	18
Ce	167	536	19	NM	258	185	325	NM	195	29
Pr	20	56	2	NM	27	20	38	NM	24	2.7
Nd	73	168	5.1	NM	97	80	132	NM	80	7.1
Sm	12	27	1	NM	17	14	23	NM	14	1.4
Eu	3.3	0.53	0	NM	3.9	3.6	0.84	NM	24	0.01
Gd	9.2	23	1	NM	15	12	18	NM	12	1.3
Tb	1.4	3.5	0.21	NM	0	1.9	2.7	NM	2.2	0.24
Dy	6.5	21	2.1	NM	12	9.5	16	NM	14	2.2
Ho	1.1	3.9	0.59	NM	2.2	2	3.1	NM	3.2	0.64
Er	3	13	2.4	NM	6.5	5.2	8.1	NM	10	2.4
Tm	0.46	2.1	0.47	NM	0.99	0.73	1.2	NM	1.7	0.47
Yb	2.8	15	4.6	NM	6.1	4.9	7.3	NM	14	4.8
Lu	0.38	1.9	0.68	NM	0.91	0.71	1	NM	2	0.71
Li	14	8.21	140	NM	8.21	21	1.25	NM	2.41	192
Rb	166	399	620	NM	124	102	171	NM	449	700
Sr	120	33	6.96	NM	317	453	91	NM	21	11
Nb	91	476	642	NM	121	98	249	NM	344	539
Mo	4.34	39	1.78	NM	7.72	3.44	18	NM	13	1.36

continued . . .

Sample number	CDB683	CDB684	CDB687	CDB699	CDB702	CDB703	CDB704	CDB716	CDB719	CDB752
Rock type	Bostonite	Bostonite	Rooivleitjie granite	Tholeiitic mafic rock	Bostonite	Syenite	Bostonite	Bostonite	Bostonite	Rooivleitjie granite
Cd	0.1	0.74	0.14	NM	0.27	0.1	0.1	NM	0.19	0.16
Sn	2.62	12	3.9	NM	5.32	4.21	8.13	NM	40	5.13
Cs	1.53	0.78	2.3	NM	1.07	1.07	0.32	NM	5.67	3.33
Hf	5.03	27	9.92	NM	3.41	2.43	3.21	NM	26	11
Pb	30	1287	9.24	NM	26	17	15	NM	10	5.04
Bi	0.04	0.12	0.28	NM	0.02	0.03	0.22	NM	0.18	0.27
Th	7.94	72	32	NM	15	16	33	NM	46	27
U	1.77	13	10.12	NM	3.33	2.63	3.36	NM	8.47	6.76
Sc	14	2.7	0.61	NM	11	7.87	3.11	NM	3.17	0.62
Cr	3.5	5.06	8.14	NM	4.02	4.81	5.52	NM	4.58	6.7
Co	1.19	0.57	0.32	NM	1.3	2.15	0.5	NM	0.84	0.41
Ni	2.39	2.47	3.33	NM	1.7	2.42	3.84	NM	2.25	2.71
Cu	2.94	11	2.92	NM	1.36	105	3.79	NM	4.3	3.01
Zn	207	1461	79	NM	133	173	27	NM	86	123
Ga	25	33	50	NM	27	28	47	NM	46	51
Sb	0.22	1.29	0.14	NM	0.2	0.21	0.33	NM	0.47	0.16
Tl	0.7	2.58	1.08	NM	0.3	NM	NM	NM	1.59	1.23

Sample number	CDB753	CDB761	CDB764	CDB822	CDB825	CDB922	CDB932	CDB953	CDB974	CDB978
Rock type	Syenite	Quartz porphyry	Bostonite	Tholeiitic mafic rock	Rietpoort granite	Alkali mafic rock	Alkali mafic rock	Tholeiitic mafic rock	Tholeiitic mafic rock	Tholeiitic mafic rock
Y	38	245	NM	NM	77	25	25	28	22	20
La	105	302	NM	NM	112	81.2	72.3	16.6	15.1	12.9
Ce	193	591	NM	NM	214	183.6	173	37.5	34.6	30
Pr	20	73	NM	NM	27	22.1	21.6	4.7	4.27	3.72
Nd	70	281	NM	NM	97	85.6	86.1	19.1	17.5	15.3
Sm	11	52	NM	NM	18	15.2	16.05	4.71	4.21	3.77
Eu	3.4	1	NM	NM	0.82	4.4	4.7	1.41	1.28	1.18
Gd	9.6	51	NM	NM	17	12.2	13.2	5.38	4.51	4.13
Tb	1.5	8.5	NM	NM	2.7	1.57	1.67	0.88	0.71	0.65
Dy	7.9	49	NM	NM	16	6.55	6.93	5.48	4.36	3.94
Ho	1.6	9.6	NM	NM	3	1.03	1.08	1.13	0.85	0.79
Er	4.6	30	NM	NM	8.9	2.33	2.37	3.3	2.43	2.2
Tm	0.71	4.6	NM	NM	1.5	0.27	0.26	0.47	0.34	0.31
Yb	4.6	30	NM	NM	8.7	1.61	1.58	3.23	2.2	2.16
Lu	0.68	3.9	NM	NM	1.3	0.2	0.2	0.47	0.34	0.31
Li	NM	29	NM	NM	25	5.8	4.4	16	10	13
Rb	NM	352	NM	NM	282	47	45	46	47	38
Sr	NM	17	NM	NM	30	1553	1431	175	264	210
Nb	NM	114	NM	NM	48	132	221	8.9	7	6.3
Mo	NM	4.37	NM	NM	3.36	NM	NM	NM	NM	NM

continued . . .

Sample number	CDB753	CDB761	CDB764	CDB822	CDB825	CDB922	CDB932	CDB953	CDB974	CDB978
Rock type	Syenite	Quartz porphyry	Bostonite	Tholeiitic mafic rock	Rietpoort granite	Alkali mafic rock	Alkali mafic rock	Tholeiitic mafic rock	Tholeiitic mafic rock	Tholeiitic mafic rock
Cd	NM	0.36	NM	NM	0.08	NM	NM	NM	NM	NM
Sn	NM	11	NM	NM	4.42	3.1	4.9	1.7	1.1	1.1
Cs	NM	0.34	NM	NM	1.77	1.3	0.4	1.1	2.8	1.2
Hf	NM	20	NM	NM	4.98	NM	NM	NM	NM	NM
Pb	NM	63	NM	NM	37	1.3	1.4	7.2	5.8	5
Bi	NM	0.05	NM	NM	0.09	NM	NM	NM	NM	NM
Th	NM	41	NM	NM	24	7.5	4.1	4.5	3.2	2.8
U	NM	7.02	NM	NM	4.62	5.9	4.4	1.1	0.77	0.64
Sc	NM	3.16	NM	NM	4.81	22	28	42	41	40
Cr	NM	8.12	NM	NM	7.56	NM	NM	NM	NM	NM
Co	NM	0.52	NM	NM	0.82	65	51	44	50	47
Ni	NM	3.86	NM	NM	3.34	149	38	42	59	52
Cu	NM	5.59	NM	NM	3.57	56	84	150	123	125
Zn	NM	196	NM	NM	66.27	NM	NM	NM	NM	NM
Ga	NM	30	NM	NM	19	22	29	20	19	19
Sb	NM	0.18	NM	NM	0.09	NM	NM	NM	NM	NM
Tl	NM	2.26	NM	NM	1.61	NM	NM	NM	NM	NM

Sample number	CDB1064	CDB1066	CDB1092	CDB1101	CDB1105	CDB1126	CDB1200	CDB1341	CDB1454	CDB1459
Rock type	Quartz porphyry	Bostonite	Zout Rivier Plug	Zout River Plug	Zout River Plug	Zout River Plug	Zout River Plug	Zout River Plug	Tholeiitic mafic rock	Tholeiitic mafic rock
Y	NM	NM	29	21	24	NM	23	21	24	35
La	NM	NM	17	6.4	7.3	NM	16.1	6.42	16	12.3
Ce	NM	NM	38.6	15.6	17.8	NM	36.7	15.7	36.8	32.5
Pr	NM	NM	4.76	2.11	2.4	NM	4.58	2.08	4.64	4.59
Nd	NM	NM	19.8	9.4	10.7	NM	18.7	9.26	19	21.4
Sm	NM	NM	4.8	2.78	3.15	NM	4.33	2.72	4.62	6.26
Eu	NM	NM	1.43	0.94	1.04	NM	1.33	0.99	1.36	2
Gd	NM	NM	5.56	3.61	4.1	NM	4.75	3.56	5.13	7.19
Tb	NM	NM	0.91	0.62	0.7	NM	0.774	0.59	0.826	1.17
Dy	NM	NM	5.57	3.96	4.46	NM	4.56	3.98	4.9	7.13
Ho	NM	NM	1.15	0.84	0.94	NM	0.91	0.84	0.972	1.41
Er	NM	NM	3.18	2.39	2.72	NM	2.6	2.43	2.61	3.82
Tm	NM	NM	0.48	0.35	0.4	NM	0.37	0.351	0.387	0.568
Yb	NM	NM	3.3	2.43	2.79	NM	2.38	2.38	2.7	3.73
Lu	NM	NM	0.49	0.36	0.4	NM	0.36	0.353	0.395	0.534
Li	NM	NM	15	46	13	NM	6	8.2	15	16
Rb	NM	NM	44	91	22	NM	76	29	39	30
Sr	NM	NM	172	98	101	NM	316	103	195	182
Nb	NM	NM	9.2	4	4.6	NM	7.6	4	8.1	11
Mo	NM	NM	NM	NM	NM	NM	NM	NM	NM	NM

continued . . .

Sample number	CDB1064	CDB1066	CDB1092	CDB1101	CDB1105	CDB1126	CDB1200	CDB1341	CDB1454	CDB1459
Rock type	Quartz porphyry	Bostonite	Zout Rivier Plug	Zout River Plug	Zout River Plug	Zout River Plug	Zout River Plug	Zout River Plug	Tholeiitic mafic rock	Tholeiitic mafic rock
Cd	NM	NM	NM	NM	NM	NM	NM	NM	NM	NM
Sn	NM	NM	1.7	0.9	1	NM	1.2	1	1.2	1.6
Cs	NM	NM	1.1	0.5	0.5	NM	7.6	0.6	0.8	1.1
Hf	NM	NM	NM	NM	NM	NM	NM	NM	NM	NM
Pb	NM	NM	7.2	3.5	3.9	NM	6.2	3.3	6	1.9
Bi	NM	NM	NM	NM	NM	NM	NM	NM	NM	NM
Th	NM	NM	4.5	1.5	1.8	NM	3.6	1.5	3.6	1.7
U	NM	NM	1.1	0.44	0.51	NM	0.83	0.44	0.84	0.48
Sc	NM	NM	41	44	46	NM	38	44	41	42
Cr	NM	NM	NM	NM	NM	NM	NM	NM	NM	NM
Co	NM	NM	46	50	50	NM	50	51	50	51
Ni	NM	NM	42	41	37	NM	50	41	45	77
Cu	NM	NM	156	91	87	NM	125	94	144	162
Zn	NM	NM	NM	NM	NM	NM	NM	NM	NM	NM
Ga	NM	NM	20	18	17	NM	19	17	19	21
Sb	NM	NM	NM	NM	NM	NM	NM	NM	NM	NM
Tl	NM	NM	NM	NM	NM	NM	NM	NM	NM	NM

Sample number	CDB1491	CN495
Rock type	Tholeiitic mafic rocks	Quartz porphyry
Y	34	133
La	11.7	118
Ce	31	228
Pr	4.38	22
Nd	20.7	74
Sm	5.82	14
Eu	1.88	0.72
Gd	7	16
Tb	1.14	3
Dy	6.85	22
Ho	1.38	4.5
Er	3.6	16
Tm	0.53	2.5
Yb	3.62	18
Lu	0.516	2.3
Li	14	15
Rb	29	329
Sr	170	61
Nb	11	207
Mo	NM	3.67
Cd	NM	0.02
Sn	1.6	6.48
Cs	0.8	1.04
Hf	NM	8.2
Pb	1.8	25
Bi	NM	0.02
Th	1.6	48
U	0.43	7.78
Sc	41	4.85
Cr	NM	7.26
Co	50	2.49

continued . . .

Sample number	CDB1491	CN495
Rock type	Tholeiitic mafic rocks	Quartz porphyry
Ni	79	5.03
Cu	160	2.45
Zn	NM	110
Ga	21	28
Sb	NM	0.11
Tl	NM	NM